Optimization of sensitivity to disease-associated cortical metabolic abnormality by evidence-based quantification of in vivo proton magnetic resonance spectroscopy data from 3 Tesla and 7 Tesla

Kelley M. Swanberg

Submitted in partial fulfillment of the
requirements for the degree of
Doctor of Philosophy
under the Executive Committee
of the Graduate School of Arts and Sciences

COLUMBIA UNIVERSITY

2022

Abstract

Optimization of sensitivity to disease-associated cortical metabolic abnormality by evidence-based quantification of in vivo proton magnetic resonance spectroscopy data from 3 Tesla and 7 Tesla

Kelley M. Swanberg

In vivo proton magnetic resonance spectroscopy (^{1}H MRS) is the only method available to measure small-molecule metabolites in living human tissue, including the brain, without ionizing radiation or invasive medical procedures. Despite its attendant potential for supporting clinical diagnostics in a range of neurological and psychiatric conditions, the metabolite concentration estimates produced by ^{1}H-MRS experiments, and therefore their sensitivity and specificity to any particular biological phenomenon under study, are readily distorted by a number of confounds. These include but are not limited to static and radiofrequency field characteristics, signal relaxation dynamics, macromolecule and lipid contributions to the spectral baseline, spectral fitting artifacts, and other uncontrolled idiosyncrasies of ^{1}H-MRS data acquisition, processing, and quantification.

Using ^{1}H-MRS data obtained via 3-Tesla and 7-Tesla magnetic resonance (MR) scanners from healthy controls, individuals with progressive and relapsing-remitting multiple sclerosis (MS), and individuals with post-traumatic stress disorder (PTSD) and/or major depressive disorder (MDD), this work therefore aims to build and apply a framework for quantifying and thereby reducing such confounds introduced to ^{1}H-MRS estimates of in vivo metabolite concentrations at the steps of data processing and quantification, with an ultimate aim to maximizing the potential of ^{1}H MRS for supporting sensitive and specific clinical diagnosis of neurological or psychiatric disease. The steps examined include spectral quantification by linear combination modeling (Chapter 2), absolute quantification by internal concentration referencing (Chapter 3), and cross-sectional statistical analysis of results (Chapters 4 and 5).

Chapter 2 designs and implements a graphical user interface (GUI)-supported validation pipeline for measuring how data quality, spectral baseline, and baseline model affect the precision and accuracy of ^{1}H-MR spectral quantification by linear combination modeling. This validation pipeline is then used to show that spectral data quality indices signal to noise ratio (SNR) and full width at half maximum (FWHM) interact with spectral baseline to influence not only the precision but also the accuracy of resultant metabolite concentration estimates, with fit residuals poorly indicative of true fit error and spectral baselines modeled as regularized cubic splines not significantly outperformed by those employing simulated macromolecules. A novel method for extending the commonly used spectral quantification precision estimate Cramér-Rao Lower Bound (CRLB) to incorporate considerations of continuous and piecewise polynomial baseline shapes is therefore presented, tested, and similarly integrated into a GUI-supported toolkit to improve the correspondence between estimated CRLB and metabolite fit error variability when this now empirically justified approach to spectral baseline modeling is used.

In Chapter 3, age- and disease-associated differences in transverse (T_2) water signal relaxation measured at 7 Tesla in the prefrontal cortex of individuals with progressive (N=21) relative to relapsing-remitting (N=26) or no (N=25) multiple sclerosis are shown to influence absolute quantification of metabolite concentrations by internal referencing to water.

In Chapter 4, these findings from Chapters 2 and 3 are used to justify an evidence-based ^{1}H-MR spectral processing and quantification protocol that focuses optimization efforts on baseline modeling approach and references metabolite concentration estimates to internal creatine instead of water. When this protocol is applied to 7-Tesla prefrontal cortex ^{1}H-MR spectra from the aforementioned multiple sclerosis and control cohorts, it supports metabolite concentration

estimates that, in the absence of any additional supporting data, inform supervised-learning-enabled identification of progressive multiple sclerosis at nearly 80% held-out validation sensitivity and specificity.

Finally, in Chapter 5, the same processing, quantification, and machine-learning pipeline employed in Aim 3 is independently applied to a new set of 7-Tesla prefrontal cortex ^{1}H-MRS raw data from an entirely different cohort of individuals with (N=20) and without (N=18) PTSD and/or comorbid or primary MDD. Here the processing, quantification, and statistics procedures designed using lessons in Chapters 2 and 3 and optimized for classifying multiple sclerosis phenotype in Chapter 4 generalize directly to metabolite-only classification of PTSD and/or MDD with sensitivity and specificity similarly near to or greater than 80%. In both Chapters 4 and 5, supervised learning avoids dimensionally reducing metabolite feature sets in order to pinpoint the specific metabolites most informative for identifying each disease group.

Taken together, these findings justify the potential and continued development of ^{1}H MRS, at least as applied in the human brain and especially as supported by multivariate approaches including supervised learning, as an auxiliary or mainstay of clinical diagnostics for neurological or psychiatric disease.

Table of Contents

List of Charts, Graphs, Illustrations

Acknowledgements

A special word of gratitude to my advisor Dr. Christoph Juchem, in particular for the uncommon generosity of time, patience, and intellectual independence offered throughout my academically and professionally formative years in the various iterations of his research group, consistently an honor to work within. Appreciation is also due to various other laboratory colleagues, notable among them Dr. Martin Gajdošík, Mr. Yun Shang, and especially Dr. Sebastian Theilenberg, for constructive and collaborative engagement in the day-to-day workings of a team with whom it has been a privilege to learn and grow; thanks are also due to other laboratory members and alumni over the years for the lively and enjoyable community and conversations they inspired throughout our brief time together. A note of appreciation, as well, to several very able undergraduate mentees, especially Mr. Leonardo Campos and Mr. Abhinav V. Kurada, who began their time in the laboratory with little knowledge of magnetic resonance (MR), much less in vivo MR spectroscopy, and ended it with significant contributions to several works, in particular implementation of brain tissue segmentation and early machine-learning pipelines for the cross-sectional multiple sclerosis study, also employed in the generalization to post-traumatic stress disorder and major depressive disorder (A.V. Kurada), and spectral data processing for the investigation of post-traumatic stress disorder and major depressive disorder (L. Campos) noted in this dissertation's Related Publications list.

Additional thanks are offered to my dissertation committee, including chair Dr. Elisa Konofagou, sponsor Dr. Christoph Juchem, and members Dr. Lawrence Kegeles, Dr. Joshua Jacobs, and Dr. John Thomas Vaughan, for their time and energy spent reviewing this work in both written and verbally defended forms.

A particular acknowledgement is due to Dr. Hetty Prinsen of the Yale School of Medicine

Department of Radiology and Biomedical Imaging, who served as an inspiring and attentive mentor in my first year at the laboratory. Special acknowledgement and gratitude are also accorded to Dr. Jodi Weinstein of Stony Brook University and Dr. Rebecca Feldman of the University of British Columbia for enriching mentorship, guidance, and friendship over the years. Thank you as well to Columbia MR Research Center colleagues Dr. Jia Guo, Ms. Kay Chioma Igwe, Mr. Jochen Weber, Dr. David Gultekin, and Dr. Ray Lee for many stimulating and useful discussions, and, to Drs. Gultekin and Lee, also for responsive administration of MR platform resources integral to this work; to Ms. Kathleen Durkin, Ms. Karen Evans, and Ms. Helen Cen for uncommonly efficacious handling of numerous managerial affairs integral to this research; and to Ms. Yvette Strong of the Yale Center for Clinical Investigation for impressive skill and extraordinary commitment in recruiting many of the volunteers, also due a large share of deep gratitude, from whom the data presented in this dissertation have been acquired.

Thank you to the colleagues who showed some extra kindness and professional consideration to a new research associate in an uncertain novel environment: Dr. Robert K. Fulbright and Dr. David Pitt of the Yale School of Medicine Departments of Radiology and Biomedical Imaging and Neurology, respectively; Mr. Stephen Dashnaw of the Columbia School of Physicians and Surgeons Department of Radiology; and Dr. Lawrence Kegeles of the New York Psychiatric Institute; in addition to, again, my own advisor Dr. Christoph Juchem and first mentor Dr. Hetty Prinsen.

It bears additional note that parts of this work were supported by the National Multiple Sclerosis Society (NMSS) grant In Vivo Metabolomics of Oxidative Stress with 7 Tesla Magnetic Resonance Spectroscopy (RG 5319), by the VA National Center for PTSD Clinical Neurosciences Division, by the National Institute of Mental Health via award R01MH112668, and by the Yale

Center for Clinical Investigation, and falls within the purview of Yale Medical School Human Investigation Committee protocols 1501015145, 1305011972, 1402013497 and 1308012549 as well as Columbia University Institutional Review Board protocols AAQ9641, AAQ9795, and AAAR7598. This work was furthermore made possible by CTSA Grant Number UL1 TR000142 from the National Center for Advancing Translational Science (NCATS), components of the National Institutes of Health (NIH), and the NIH Roadmap for Medical Research. Its contents are solely the responsibility of the authors and do not necessarily represent the official view of the NIH. This work was performed in part at the Zuckerman Mind Brain Behavior Institute MRI Platform, a shared resource and Columbia MR Research Center site.

For the last several years the persistent emotional challenges of life in Manhattan and of science as a vocation have been rendered far more tractable by a group of tragically unfiltered and terminally irreverent friends. Thank you, friends, in particular Mr. Gus Carlock, Mr. David Szybilski, Mr. Matt Wetherbee, Ms. Shoshanna Benjamin, Mr. Kai Pak, Mr. Ben Lavon, and Dr. Eva X. Devience, for gracing my doctoral life with jokes that now cannot be unheard, emergency cross-town fish heists, and frequent dramatic declarations that there are four lights. Thank you to Ms. Terrie Barnewolt Swanberg for support and care, particularly during the fearsome uncertainty of the ongoing pandemic, as well as to the late Ms. Mary Lou Gauwitz Barnewolt and to Ms. Sharon Barnewolt Keller for wisdom, presence, and perspective. Deep appreciation is similarly owed to Mr. Yang Jae-Taek, Ms. Kim Eunok, Mr. Eunsuk Yang, and Mr. Hongsuk Tom Yang for abiding courage, gratitude, and peace sustained by years of imprinted compassion and modeled aspirations. Thank you, finally, to Dr. Michael Chapman for continuing to serve as a role model of fearless intellectual honesty and unapologetic zeal for life's many wild adventures, and to Ms. Xinyuan Qi Meng, whose painstakingly crafted 长寿面 are evidently still working.

Dedication

To the teachers who inspired wonder, patience, and trust in reason at a most critical age, including Ms. Linda Rachner, Ms. Julie Pekar, Mr. Paul Pocius, Dr. Dave DeVol, and many others.

Integrated and Related Publications

Parts of this dissertation document, including text, figures, figure captions, and other materials, have been directly reproduced, with publisher permissions where applicable, from my own contributions to the following previously published or unpublished works:

Original research papers

Swanberg, K.M., Landheer, K., Gajdošík, M., Treacy, M.S., and C. Juchem. Effect of regularized spline baseline knot and smoothing parameters on macromolecule prediction and metabolite quantification by in vivo proton magnetic resonance spectroscopy. Manuscript in preparation.

Swanberg, K.M.*, Kurada, A.V.*, Prinsen, H. and C. Juchem. Multiple sclerosis diagnosis and phenotype identification by multivariate classification of in vivo frontal cortex metabolite profiles. Submitted to *Scientific Reports*.

Swanberg, K.M.*, Prinsen, H.*, Destefano, K., Bailey, M., Pitt, D., Fulbright, R.K., and C. Juchem. In vivo evidence of differential frontal cortex metabolism in progressive and relapsing-remitting multiple sclerosis. *NMR Biomed* 34(11):e4590.

Swanberg, K.M., Prinsen, H., Coman, D., Rothman, D.L., de Graaf, R.A., and C. Juchem. In vivo quantification of glutathione T_2 in the human brain at 7 Tesla. *J Magn Reson* 290: 1-11. 2018.

* Shared first authorship

Review papers

Swanberg, K.M., L. Campos, C.G. Abdallah, and C. Juchem. Proton magnetic resonance spectroscopy in post-traumatic stress disorder: Updated systematic review and meta-analysis. Manuscript in preparation.

Swanberg, K.M., Landheer, K., Pitt, D., and C. Juchem. Quantifying the metabolic signature of multiple sclerosis by in vivo proton magnetic resonance spectroscopy: Current challenges and future outlook in the translation from signal to biomarker. *Front Neurol* 10: 1173. 2019.

International conference abstracts

Swanberg, K.M., H. Prinsen, C. Averill, L. Campos, A.V. Kurada, J.H. Krystal, I.L. Petrakis, L.A. Averill, C.G. Abdallah, and C. Juchem. Abnormal glutamate metabolism in prefrontal cortex of post-traumatic stress disorder linked to comorbidity with major depression. Submitted to *Proc Int Soc Magn Reson Med* 2022.

Swanberg, K.M., M. Gajdošík, K. Landheer, and C. Juchem. Computation of Cramér-Rao

Lower Bounds (CRLB) for spectral baseline shapes. *Proc Int Soc Magn Reson Med* 2021, 2010.

Swanberg, K.M., Landheer, K., Gajdošík, M., Treacy, M.S., and C. Juchem. Hunting the perfect spline: Baseline handling for accurate macromolecule estimation and metabolite quantification by in vivo ^{1}H MRS. *Proc Int Soc Magn Reson Med* 2020, 2856.

Swanberg, K.M., Prinsen, H., and C. Juchem. Spectral quality differentially affects apparent metabolite concentrations as estimated by linear combination modeling of in vivo magnetic resonance spectroscopy data at 7 Tesla. *Proc Int Soc Magn Reson Med* 2019, 4237.

Swanberg, K.M., Prinsen, H., Kurada, A.V., Fulbright, R.K., Pitt, D., Destefano, K., Bailey, M., and C. Juchem. Towards in vivo neurochemical profiling of multiple sclerosis with MR spectroscopy at 7 Tesla: Apparent increase in frontal cortex water T_2 in aged individuals with progressive multiple sclerosis stabilizes in biexponential model constrained by tissue partial volumes. *Proc Int Soc Magn Reson Med* 2018, 0161.

Swanberg, K.M., Prinsen, H., Destefano, K., Bailey, M., Pitt, D., Fulbright, R.K., and C. Juchem. Towards in vivo neurochemical profiling of multiple sclerosis with MR spectroscopy at 7 Tesla: Cross-sectional assessment of frontal-cortex glutathione, GABA, and glutamate in individuals with relapsing-remitting and progressive multiple sclerosis. *Proc Int Soc Magn Reson Med* 2017, 2970.

Swanberg, K.M., Prinsen, H., Coman, D., Rothman, D.L., de Graaf, R.A., and C. Juchem. In vivo quantification of glutathione T_2 in the human brain at 7 Tesla using echo time extension with variable refocusing selectivity and symmetry. *Proc Int Soc Magn Reson Med* 2017, 3000.

Additional related efforts have contributed to the following works not directly presented in either text or figure form here:

Original research papers

Gajdošík, M., Landheer, K., Swanberg, K.M., and C. Juchem. INSPECTOR: Magnetic resonance spectroscopy software for user-friendly data inspection, processing, simulation and analysis. Manuscript in review at *Scientific Reports*.

Gajdošík, M., Landheer, K., Adlparvar, F., Swanberg, K.M., Madelin, G., Juchem, C. and I.I. Kirov. Hippocampal single-voxel MR spectroscopy with long echo time at 3 Tesla. *NMR Biomed* e4538.

Landheer, K., Swanberg, K.M., and Juchem, C. (2019). Magnetic Resonance Spectrum Simulator (MARSS), a novel software package for fast and computationally efficient basis set simulation. *NMR Biomed* e4129.

Review papers

Campos, L., K.M. Swanberg, and C. Juchem. Evidence-based metabolic profiling with single-voxel proton magnetic resonance spectroscopy: A complete beginner's guide to spectral data quality assessment, processing, and quantification. Manuscript in preparation.

Landheer, K., Schulte, R.F., Treacy, M., Swanberg, K.M., and C. Juchem. Theoretical description of modern ^{1}H in Vivo magnetic resonance spectroscopic pulse sequences. *JMRI* 2020 Apr; 51(4):1008-1029.

International conference abstracts

Campos, L., K.M. Swanberg, M. Gajdošík, K. Landheer, and C. Juchem. Complex fitting of 1H-MR spectra improves quantification precision independent of SNR and noise correlation. Submitted to *Proc Int Soc Magn Reson Med* 2022.

Gajdošík, M., K. Landheer, K.M. Swanberg, L.S. Kegeles, C. de la Fuente-Sandoval, D.C. Shungu, and C. Juchem. The effects of basis sets on the analysis of in vivo brain MRS data obtained with standard PRESS sequences. *Proc Int Soc Magn Reson Med* 2021, 2013.

Gajdošík, M., K. Landheer, K.M. Swanberg, F. Adlparvar, G. Madelin, W. Bogner, C. Juchem, and I.I. Kirov. Hippocampal single-voxel MR spectroscopy with long echo time at 3 Tesla. *Proc Int Soc Magn Reson Med* 2021, 2230.

Kurada, A.V., Swanberg, K.M., Prinsen, H., and C. Juchem. Diagnosis of multiple sclerosis subtype through machine learning analysis of frontal cortex metabolite profiles. *Proc Int Soc Magn Reson Med* 2019, 4871.

Landheer, K., Swanberg, K.M., and C. Juchem. Magnetic Resonance Spectrum Simulator (MARSS): Software for fast and reliable simulation of spin systems. *Proc Int Soc Magn Reson Med* 2019, 2289.

Abbreviations

^{1}H MRS	proton magnetic resonance spectroscopy
5HT	5-hydroxytryptamine; serotonin
$5HT_{1B}R$	5-hydroxytryptamine receptor 1B
ACC	anterior cingulate cortex
ACTH	adrenocorticotropic hormone
AlloP	allopregnanolone
Asc	ascorbate
Asp	aspartate
AUD	alcohol use disorder
AUROC	area under the receiver operating characteristic
AVLT	auditory verbal learning test
AVP	arginine vasopressin
BOLD	blood-oxygen-level-dependent
CAPS	Clinician-Administered PTSD Scale
CB_1R	cannabinoid receptor 1
CI	confidence interval
COSY	COrrelated SpectroscopY
CRH	corticotropin-releasing hormone
CRLB	Cramér-Rao Lower Bound
CSF	cerebrospinal fluid
CV	coefficient of variation
dACC	dorsal anterior cingulate cortex
DSM	Diagnostic and Statistical Manual
EAE	experimental autoimmune encephalomyelitis
EDSS	expanded disability status scale
EMG	electromyography
FFT	Fast Fourier Transform
FLAIR	fluid-attenuated inversion recovery
fMRI	functional magnetic resonance imaging
FWHM	full width at half maximum
GABA	γ-aminobutyric acid
$GABA_AR$	GABA receptor A
Gln	glutamine
Glu	glutamate
Glx	glutamate + glutamine
GSH	γ-L-Glutamyl-L-cysteinylglycine, glutathione
HC	healthy control; trauma-unmatched control
HLA	human leukocyte antigen
ISI	Insomnia Severity Index
JDE	*J*-difference editing
KNN	k-nearest neighbors
LCM	linear combination modeling
LOOCV	leave-one-out cross-validation
MADRS	Montgomery-Åsberg Depression Rating Scale
MAG	myelin-associated glycoprotein
MBP	myelin basic protein
MDD	major depressive disorder
MEGA-sLASER	MEscher-GArwood semi-Localization by Adiabatic SElective Refocusing

$mGluR_5$	metabotropic glutamate receptor 5
MHC	major histocompatibility complex
mIns	myoinositol
MOG	myelin oligodendrocyte glycoprotein
mPFC	medial prefrontal cortex
MRI	magnetic resonance imaging
MRSI	magnetic resonance spectroscopic imaging
MS	multiple sclerosis
NMO	neuromyelitis optica
NPY	neuropeptide Y
OFC	orbitofrontal cortex
OPC	oligodendrocyte precursor cell
PCL	post-traumatic stress disorder checklist
PET	positron emission tomography
PFC	prefrontal cortex
PI	permutation importance
PLP	proteolipid protein
P-MS	progressive multiple sclerosis
PTSD	post-traumatic stress disorder
rACC	rostral anterior cingulate cortex
ROC	receiver operating characteristic
ROS	reactive oxygen species
RR-MS	relapsing-remitting multiple sclerosis
S1P	sphingosine-1-phosphate
SARS	severe acute respiratory syndrome
sIns	scylloinositol
sLASER	semi-Localization by Adiabatic SElective Refocusing
SNR	signal to noise ratio
SPS	single prolonged stress
SSRI	selective serotonin reuptake inhibitor
STEAM	STimulated Echo Acquisition Mode
SVD	small-vessel disease; alternatively, singular value decomposition
SVM	support-vector machine
TSH	thyroid-stimulating hormone
QDA	quadratic discriminant analysis
T_1	longitudinal (spin-lattice) relaxation time constant
T_2	transverse (spin-spin) relaxation time constant
T_E	echo time
T_{Eext}	echo-time extension
T_I	inversion time
T_M	mixing time
T_R	repetition time
Taur	taurine
tCho	total choline (choline + phosphocholine + glycerophosphocholine)
tCr	total creatine (creatine + phosphocreatine)
TEC	trauma-exposed control
tNAA	total N-acetyl aspartate (N-acetyl aspartate + N-acetyl aspartylglutamate)
USFDA	United States Food and Drug Administration
VC	veteran control

Chapter 1: Overview

1.1. Motivation: The unfulfilled clinical promise of ^{1}H MRS. In vivo magnetic resonance spectroscopy (MRS) is a method that can estimate the concentrations of select small molecules in living tissue by using electromagnetic waves in a strong magnetic field to manipulate and monitor the spin behavior of certain atomic nuclei within them. Since Felix Bloch of Stanford University performed in 1946 what is now considered to be the first in vivo MRS measurement, of the protons in his finger [2], the method has developed considerably, now enabling the routine and noninvasive assessment of multiple small-molecule metabolites in tissues like the human skeletal muscle [3], liver [4, 5], brain [6], heart [7], breast [8], bone [9], prostate [10], kidney [11], and, more recently, the spinal cord [12].

While any atomic nucleus with odd mass number or odd atomic number and even mass number—in other words, an odd number of protons, neutrons, or both (and therefore odd integral or half-integral spin **I**)—exhibits a dipole moment in a magnetic field that can be measured in an MRS experiment [13], only those elements that naturally comprise some significant portion of living biomatter, such as ^{1}H, ^{23}Na, ^{31}P, and sometimes ^{13}C [14], or that can be safely administered to a living organism, like ^{15}N, ^{17}O, ^{13}C, and ^{19}F, can be usefully measured in vivo. Among these, the most abundant in the human body is the hydrogen nucleus (^{1}H or proton), rendering ^{1}H MRS, with its close cousin magnetic resonance imaging (MRI) of MR-visible water protons, one of the most common variants used in investigations pertaining to human biology.

Despite the diagnostic potential suggested by the range of organs to which spectroscopy has been applied to noninvasively investigate in vivo metabolism in the laboratory, its clinical utility remains limited. The reimbursable clinical use of magnetic resonance spectroscopy is still largely confined to glioma differentiation [15], in part due to still-inadequate knowledge

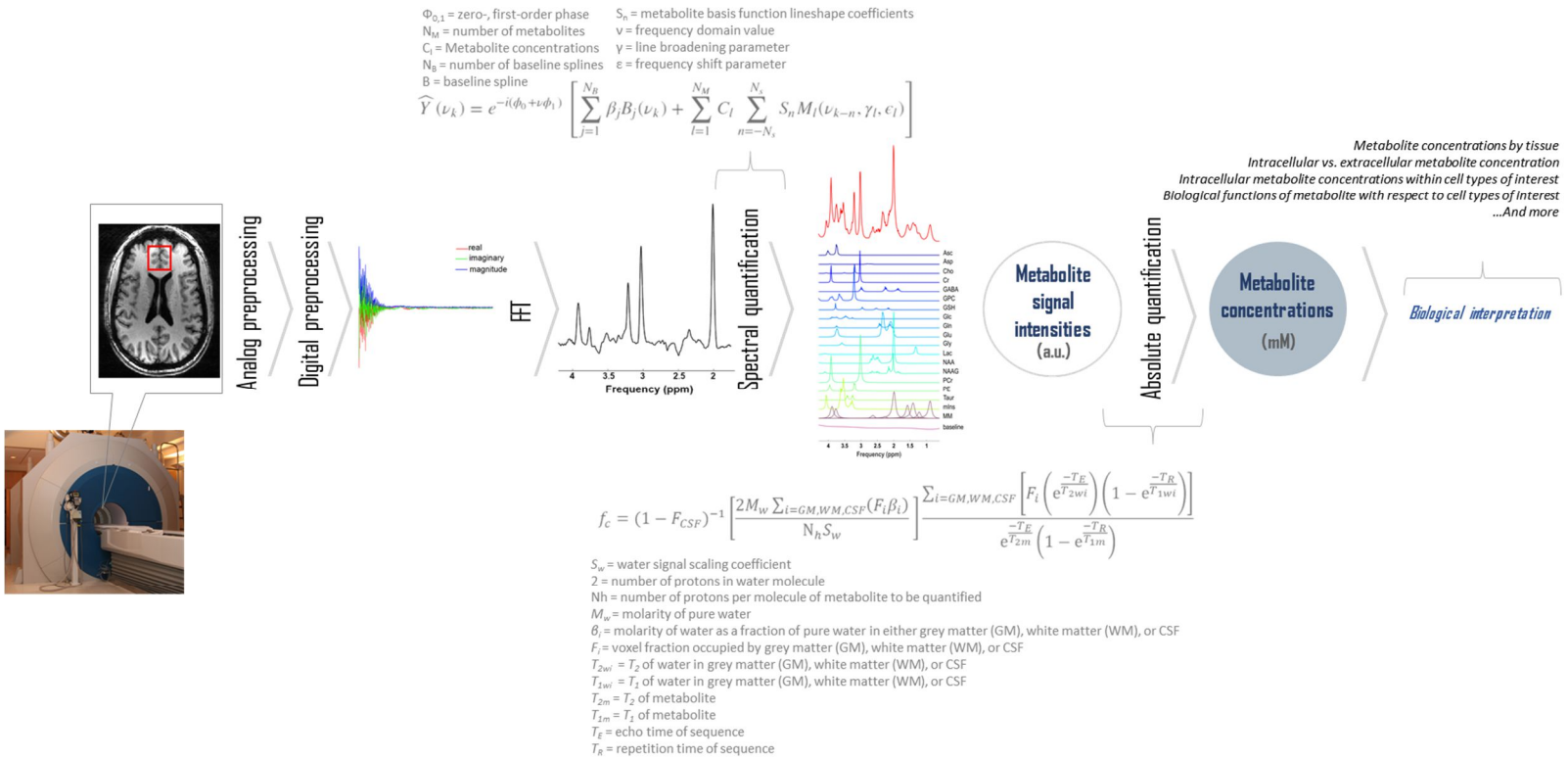

Figure 1.1. Many error-prone processing steps are required to translate from proton signal to metabolite concentration in a proton MR spectroscopy (^{1}H MRS) experiment. Protons (hydrogen nuclei ^{1}H) in the sample induce analog voltage oscillations in radiofrequency receive hardware that are amplified, demodulated into two orthogonal sinusoids, filtered, and sampled into a complex, discretized time-domain free induction decay (FID) signal. Multiple such digital signals representing measurements taken from the same experiment are then corrected for phase distortions, frequency- and phase-aligned with each other over repetition and receive channel, and averaged. At some point during or after alignment, the data are Fourier transformed from time domain into a frequency-domain spectrum, where signals from individual populations of protons become separated according to differing frequencies of the voltage oscillations that they induce, equivalent to the frequencies at which their magnetization vectors oscillate in the scanner (Larmor frequency ω), themselves a function of gyromagnetic ratio γ, the ratio between the magnetic moment of a particle system (i.e., atomic nucleus) and its angular momentum as determined by spin, and the magnetic field B to which they are exposed. Protons from different compounds are shielded from the scanner magnetic field (B_0) differently (encompassed here within ΔB), by the electrons around them. This causes them to precess and therefore induce receive hardware signals at slightly different frequencies from each other. Protons living in different molecules thus manifest as distinct amplitude peaks along disparate locations in the frequency domain. When compared to a standard, this difference is called chemical shift, and it is what makes spectroscopy possible. A process called spectral quantification can help to unpack these disparate but overlapping signals at different chemical shifts and estimate relative concentrations, in arbitrary units (a.u.), of the small-molecule metabolites to which they belong. Translating from these arbitrary units to physically meaningful concentrations takes a few extra steps with additional prior knowledge, a process called absolute quantification. Inconsistencies or errors in any step of this pipeline can degrade the precision and/or accuracy of the metabolite concentration estimates that constitute its endpoint. ppm: parts per million, a measure of nuclear precession frequency scaled by B_0 field strength to enable universal comparisons of proton spectra across scanners.

regarding the complex relationships among disease states and the limited collection of small molecules into which this method provides a window. Its applications in biomedical research, however, are extensive, in large part as a result of its safety and ability to assess tissue biochemistry within the context of living humans. ^{1}H MRS, like MRI, is classified as only moderate risk by the United States Food and Drug Administration (USFDA) [16], approved for clinical use up through magnetic field strengths of 7 Tesla as of 2017 [17], and constrained by no absolute legal limit on the number of scans that can be administered to an individual over time. These features, combined with the persistent difficulty of generating animal disease models with high predictive, face, and construct validity, as well as the dearth of other tools for noninvasively querying human tissue biochemistry in vivo, render ^{1}H MRS a potentially useful avenue for developing novel disease diagnostics and therapies.

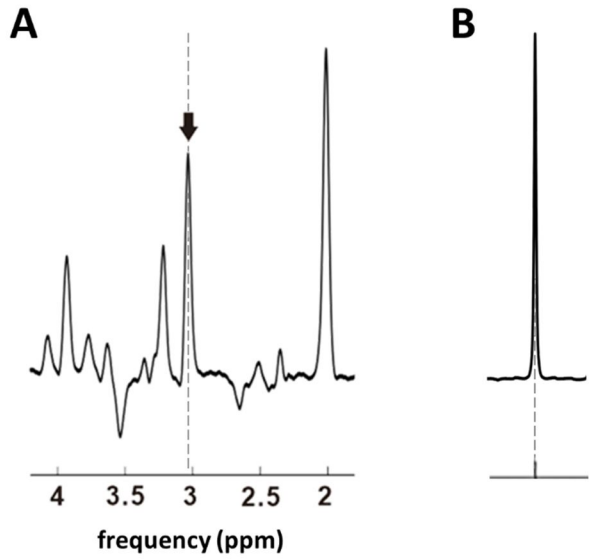

Figure 1.2. Resonance-specific, extra-concentration variables including but not limited to proton number contribute to metabolite signal amplitudes in the spectral output of a ^{1}H-MRS experiment. A. For example, three methyl protons underlie the contribution of creatine to the 3.03-ppm singlet (arrow) of this spectral output to an in vivo ^{1}H-MRS experiment localized to an occipital cortex voxel. B. By contrast, two protons underlie the contribution of water to a signal of nonetheless similar appearance to that of the 3.03-ppm creatine resonance. These and other resonance-specific differences in the relationship between concentration and signal intensity must be accounted for in metabolite quantification procedures using ^{1}H-MRS data.

Rendering this potential a reality still awaits, however, either the continued refinement of techniques, e.g., improved pulse sequences and quality assurance techniques, to maximize the precision with which one can measure one or two metabolic smoking guns for a particular disease, or the development of newer approaches, e.g., machine learning, to uncover reproducible patterns of subtle disease effects on several metabolites. Most likely, the

successful development of clinically useful diagnostic biomarkers from ^{1}H-MRS data will represent a combination of the two efforts. Spectroscopic data inputs to disease classifiers may be normalized, dimensionally reduced, or otherwise transformed into uninterpretable arbitrary units and therefore do not need to represent physically accurate measurements of absolute molar concentrations to be clinically useful. Even metabolite signals in arbitrary units, however, must be enable classification schemes that are both sensitive and reproducible. Increased between-subject variance from the variable influence of extra-concentration factors like relaxation, discussed in greater detail below and especially in Chapter 3, may complicate the parcellation of a many-dimensional matrix of metabolite signals into distinct disease groups; on the other hand, increased between-group variance in metabolite signals on the basis of a confound that may not be generalizable to every sequence, such as diffusion weighting, can enable the development of a seemingly sensitive classifier but obstruct the usefulness of its broad application to clinical decision-making.

Translating the temporal shifts in MR scanner receive hardware voltage induced by radiofrequency waves emitted by protons in the ^{1}H-MRS sample under study into physically meaningful localized concentrations of particular small molecules is a complicated and multi-step process (Figure 1.1). Spectroscopic quantification can, as such, encompass multiple sources of increased between-subject variance or spurious between-group variance, from unrepresentative or mismatched subject sampling, unconsidered effects of spectral acquisition and processing techniques, and faulty evidentiary support for conversion factors used to translate between signal intensity and usable concentration values. While these potential confounds to metabolite quantification by ^{1}H MRS, including voxel grey-white matter composition, atrophy index, diffusion weighting, metabolite T_1 and T_2, and other MR-visible differences in tissue physiology

may, when characterized and controlled, serve as useful biomarkers in their own right for disease diagnosis, the present dissertation focuses on characterizing and thereby minimizing their influence on the utility of ^{1}H MRS as a measure of small molecules that may additionally serve as a window to the metabolic pathophysiology underlying the clinical manifestation of neurological disease.

1.2. From proton magnetic resonance spectral signal to physically meaningful metabolite concentration. A non-optical process, a ^{1}H magnetic resonance experiment produces raw data outputs that do not directly represent the densities of protons in each spectral (for MRS), spatial (for MRI), or both (for magnetic resonance spectroscopic imaging or MRSI) region of the sample in the scanner. The spectroscopy or imaging data obtained instead themselves constitute an inverse Fourier transform or Fourier transform as samples in either time domain or k-space, respectively, of the spectral or spatial information desired. The inverse Fourier transform (typically implemented as an inverse Fast Fourier Transform or FFT) of discretized k-space data acquired from a slice-specific 2D imaging experiment therefore yields a visual map of proton signal intensities across a 2D spatial matrix of voxels comprising the single slice measured in the scan. Analogously, Fourier transform of preprocessed (amplified, demodulated, filtered, and sampled) time-domain free induction decay (FID) data acquired from a single-voxel (volumetric pixel, the often cubic, or at least rectangular prismatic, region of spins excited for measurement) spectroscopy scan yields a spectrum of signals associated with select hydrogen nuclei of certain small-molecule metabolites dispersed along a single frequency dimension. In the more complex case of a slice-specific 2D magnetic resonance spectroscopic imaging scan, inverse Fourier transform yields a 2D spatial matrix of FID datasets, each analogous to those that might be

obtained by single-voxel spectroscopy.

Following FID decomposition by Fourier transform, the intensity of each signal, or resonance, of the frequency-domain spectrum obtained by a ^{1}H-MR spectroscopy experiment does not itself represent the concentration of any particular metabolite (Figure 1.2). Each resonance instead reflects the degree of voltage oscillation induced in radiofrequency receive-coil hardware by a population of hydrogen nuclei whose location along the frequency axis depends on the chemical environment in which it resides. Different nuclei experience different intensities of so-called electron shielding from the B_0 magnetic field of the scanner as a result of differing electronegativities of the other elements to which they are bonded. This nucleus-specific variability in electron shielding thereby differentially alters the effective magnetic field experienced by each species. Higher electron probability densities near the hydrogen nucleus result in greater electron shielding and proportional reductions of the effective magnetic field that it inhabits. This effective field, in turn, affects the angular frequency at which the net magnetic moment of a nuclear dipole gyrates or "precesses" about the scanner magnetic field, according to a relationship called the Larmor equation[1]:

$$\omega = -\gamma(\mathbf{B_0} + \Delta\mathbf{B}) \tag{1}$$

in which ω is the angular "Larmor" frequency of precession, γ is the gyromagnetic ratio in rad/T of the nucleus in question, $\mathbf{B_0}$ is the magnetic field vector imposed by the scanner bore, and $\Delta\mathbf{B}$, a crucial term that enables spectroscopic differentiation of disparate metabolite nuclei, represents

[1] The Larmor equation is named for Irish physicist Joseph Larmor, who did not consider its potential applications to the as-yet nonexistent domain of empirical in vivo nuclear magnetic resonance spectroscopy when he published its mathematical basis in 1897. He instead derived it within the context of electrons following studies of Zeeman splitting, or partitioning in the optical spectral emissions of charged particles in the presence of magnetic fields ([18] N. Tubridy and C. S. McKinstry, "Neuroradiological history: Sir Joseph Larmor and the basis of MRI physics," *Neuroradiology,* vol. 42, no. 11, pp. 852-5, Nov 2000. [Online]. Available: http://www.ncbi.nlm.nih.gov/pubmed/11151696.).

the relative contribution of electron shielding to the effective magnetism experienced by a nucleus [13]. Consequently, distinct hydrogen nuclei present in the same molecule may or may not resonate at multiple different points along the spectrum, or "chemical shifts," according to the electronic milieu in which they reside. For example, while the two protons of water both bond to the same oxygen molecule and thus both contribute to the same single peak ("singlet") at 4.65 ppm (parts per million, which is a unit of frequency that divides out the effect of field strength on the Larmor frequency of a resonance, thereby creating a frequency scale that is identical across different MR scanners), the CH_3, CH_2, and NH protons of creatine constitute entirely different peaks at 3.03, 3.91, and 6.65 ppm, respectively. As a result, the signal intensities of some resonances may be increased relative to others not directly because they necessarily represent metabolites of higher concentrations but because they represent metabolites with more protons at that particular chemical shift in the spectrum, which is as also attributable to the numbers of protons in the moiety in question as it is to the concentration of the compound(s) that this moiety represents. As shown in Figure 1.1 and discussed elsewhere in this dissertation, this factor is just one of the many extra-concentration variables contributing to nuclear signal magnitudes in ^{1}H MRS.

That disparate protons in different compounds resonate at diverse Larmor frequencies as described by their relative chemical shifts is the physical property that makes metabolite quantification by ^{1}H MRS possible, but this chemical-shift-induced separation along the frequency axis of a spectrum is often subtle. Even at a 7-Tesla B_0 field strength, the highest currently approved by the USFDA for clinical use in humans [17], for which spectral dispersion of Larmor frequencies is highest among all clinical scanners due to the higher-magnitude $\mathbf{B_0}$ term on the right side of Equation (1) enabling a larger dynamic range of possible Larmor frequencies ω over all metabolites of interest on the left, separation of proton signals along the frequency domain by

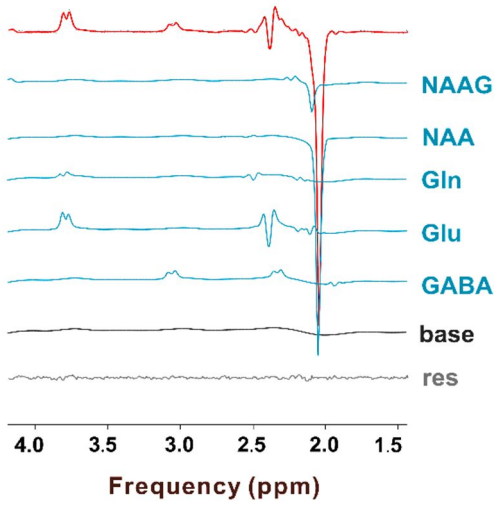

Figure 1.3. Spectral data comprise overlapping signals from multiple metabolites and can be decomposed using prior knowledge of metabolite signal shapes. Above is a spectral data set (top line; light grey) decomposed into component metabolites by linear combination modeling of basis set functions representing each (blue) plus an underlying baseline ("base"; black) of low-frequency oscillations, in this case modeled by smoothed cubic splines. The residual ("res"; grey) demonstrates the difference between the data and the final model (red). These data were obtained from a MEGA-sLASER (T_E 72 ms; T_R 3 s) sequence with *J*-difference editing for GABA (3.01-ppm $^4CH_2$ resonance; editing on the 1.89-ppm $^3CH_2$ resonance) from a 27-cc voxel in the medial prefrontal cortex. The spectrum was acquired as 4096 complex points and cut to 1024 complex points for fitting. NAAG: N-acetylaspartylglutamate; NAA: N-acetyl aspartate; Gln: glutamine; Glu: glutamate; ppm: parts per million. Displayed as appears in Swanberg, Prinsen et al., *NMR Biomed* 2021; 34(11): e4590.

chemical shift is incomplete. This overlap among signals from different metabolites can range from being a source of measurement uncertainty, as in the case of glutamate and glutamine at 7 Tesla, to being an ineluctable confound that necessitates the use of dedicated pulse sequences for signal isolation, as in the case of glutathione (GSH) or GABA and its overlapping creatine resonance, to even rendering confident estimation of some metabolites as isolated from others close to impossible without even higher field strengths or further specialized methods, as in the separation of creatine (Cr) and phosphocreatine (PCr) via typically visualized resonances between 0 and 4.5 ppm.

Not only do proton magnetic resonance spectra exhibit overlap among signals from different metabolites, but even those acquired via the simplest conventional single-voxel localization techniques also demonstrate a number of other visual elements extraneous to the metabolites generally under study. These include but are not limited to residual water signal left unspoiled by imperfect water suppression during spectral acquisition, lipid signatures both native and external to the voxel at hand, resonances from proton moieties within the context of large, complicated, and difficult-to-model macromolecule signals, spurious echoes from incompletely crushed coherence pathways

excited by the pulse sequence, lineshape distortions due to nonlinear gradients and uncorrected eddy currents, antisymmetric artifacts from uncorrected eddy currents, and thermal noise from physiological and hardware sources. In the case of spectra acquired by *J*-difference editing [19], one of the methods by which certain metabolite signals might be extricated from the overlapping spectral background, the story is further complicated by errors potentially introduced by inappropriate alignment of the two spectral conditions—editing pulse-on and editing pulse-off—that are subtracted to produce the so-called difference spectrum put to final analysis. For this reason, unraveling a spectrum into its component metabolite signatures to determine their relative signal amplitudes, a step called spectral quantification, is not a straightforward endeavor even if one temporarily puts aside the equally complicated next question of then associating those metabolite signal amplitudes with physically meaningful concentration values. Currently the most accepted approach to this complex problem is linear combination modeling, or the construction of a similarly complex picture of the data under analysis by weighting and transforming a series of expected metabolite signal shapes (called basis set functions), the underlying baseline, and any other signal or artifact in the data except thermal noise, such that when these components are all summed, they exhibit a residual, or difference from the actual data, of pointwise Gaussian distribution and minimal magnitude or norm (Figure 1.3). One commonly employed modeling framework can be summarized as follows, as originally published in 1993 [20]:

$$\hat{Y}(\nu_k) = e^{-i\varphi_0}\left[\sum_{l=1}^{N_M} C_l\, FFT\left(e^{-(\gamma_l + i\in_l)t} m_l(t)\right)\right] + \sum_{i=1}^{N_B} ß_j B_j\,(\nu_k) \qquad (2)$$

In this equation ν_k describes the discretized precession frequency domain and $\hat{Y}(\nu_k)$ describes the final reconstruction of spectral data, defined over these frequency domain values, as expressed by

the linear combination model on the right. This spectral model comprises a linear combination of two major components: the metabolite basis functions (left sum) and a baseline designed to capture additional smooth lineshapes in the data not encompassed by the metabolite functions (right sum). Additional mathematical descriptions of first-order (frequency-dependent) phase and metabolite signal lineshape effects have been omitted here in Equation (2) because they are not routinely applied in our work; another notable difference from the original formulation is that the phasing term is applied only to the metabolites here and not also the baseline.

In the metabolite basis term (left sum), N_M describes the number of metabolite basis functions included in the model, FFT is of course the Fast Fourier Transform, $e^{-\gamma_l t}$ is an exponential decay term that convolves the frequency-domain spectrum with a Lorentzian shape of full width at half-maximum proportional to $(\pi\gamma_l)^{-1}$, and $e^{-i\varepsilon_l t}$ is a frequency shift term that, when applied in time domain, offsets the frequency-domain spectrum by a value proportional to angular frequency ε_l. Of utmost importance in the first term of this model is the vector C_l, describing scaling factors applied to each metabolite described by its respective time-domain representation (plus transformations applied as described here)—indeed the result in which one is most interested when attempting to estimate in vivo metabolite concentrations by ^{1}H MRS. $e^{-i\varphi_0}$ describes a zero-order (frequency-independent) phase of radian value φ_0 applied to all metabolite bases equally.

Here the baseline term (right sum) is rendered as a summation of cubic splines, but it should be clarified that this is but one, albeit among the most flexible, approaches to model the smoothed shapes of a metabolite spectrum, influenced by residual water, macromolecules and lipids, and other factors, which will be discussed further in Chapter 2, not encompassed by the metabolite terms on the left. Here N_B describes the number of spline terms used to develop the model, $B_j(\nu_k)$ the spline basis shapes themselves as functions of discretized frequency-domain value ν_k, and β_j

the respective weights on each such term.

Chapter 2 of this dissertation explains the ways in which this linear combination modeling approach to spectral quantification can be influenced by data quality and especially the technique for modeling and optimizing the summed vector of frequency-domain baseline terms $\beta_j B_j(\nu_k)$, and develops and applies novel methods for systematically observing and quantifiably expressing these errors to enable their evidence-based correction.

Even when spectral quantification can successfully decompose a metabolite spectral dataset into its component parts scaled by accurate and precise coefficients C_l, a number of steps needs to be taken in order to convert these unitless relative weights to physically interpretable (milli)molar units. Experiment-specific factors like scanner field strength, resistive load on the resonance circuits established by the radiofrequency coil hardware, and the gain on signal receiver sensitivity can dial up or down the relative signal obtainable by a particular scanning session [21]. In this way, the metabolite signal intensities acquired by ^{1}H MRS are not directly comparable from one scan to another, and even less so from one research center to another. In addition, the signals of individual metabolite moieties within the same acquisition can vary relative to each other for reasons like, as already mentioned, differing proton numbers, in addition to, as will be discussed, disparate T_1 and T_2 signal relaxation. As a result of variables such as these, absolute metabolite quantification by ^{1}H MRS can be a complex and an open-ended process even once the prior step of spectral quantification has been completed, and multiple potential routes exist for achieving it. Namely, the translation of ^{1}H-MRS data from institutional units of metabolite signal intensity to absolute units of concentration typically involves comparing signal intensity with the intensity of an external or internal quantification reference of known (in the case of an external reference) or

independently estimable (in the case of an internal reference) concentration.[2]

Because referencing concentrations to an external source requires the additional effort of preparing and scanning solutions of a reference metabolite or metabolites that also appear(s) in the spectrum under study, as well as additional consideration of possible differences in coil load and $B_{0,1}$ fields between this phantom and the in vivo voxel from which metabolite concentrations are being investigated, internal referencing is a popular method for calculating absolute from arbitrary metabolite concentrations in proton magnetic resonance spectroscopy [21, 24]. Internal concentration referencing depends on accurately estimating the concentration of a reference compound that is present in the same voxel as the scanned metabolite to be referenced. This compound must be measurable by the same ^{1}H-MRS sequence as the metabolite(s) in question—indeed, it may itself comprise a component of the spectral output thereof—but also possess a concentration that is estimable by another means independent of this sequence. By thus linking the measurement of ^{1}H-MRS signal intensity with an estimation of absolute concentration, an internal reference facilitates the easy calculation of a conversion factor that can then be applied, with proper corrections for potential differences in proton number, relaxation, and other resonance-specific confounds, to the ^{1}H-MRS signal intensities of other metabolites to yield absolute concentration values. One such representation of the considerations behind a conversion factor built from internal reference signals can be expressed mathematically as follows, for an internal reference based on water in the voxel under study:

[2] Injecting a synthetic signal from a transmitting radiofrequency coil separate from that used for nuclear spin handling can provide a means, first applied in [22] L. Barantin, A. Le Pape, and S. Akoka, "A new method for absolute quantitation of MRS metabolites," *Magn Reson Med,* vol. 38, no. 2, pp. 179-82, Aug 1997. [Online]. Available: http://www.ncbi.nlm.nih.gov/pubmed/9256094., to correct for the influences of various scan-specific hardware conditions like receiver gain and coil loading on intensities of the signals obtained through an MRS experiment. This method can thus also be used as a concentration-free external reference for metabolite quantification. A deep treatment of this class of quantification methods is, however, beyond the scope of this dissertation. For more information on the use of synthetic signals as external quantification references for in vitro and in vivo magnetic resonance spectroscopy, please refer to [23] K. Mehr, B. John, D. Russell, and D. Avizonis, "Electronic referencing techniques for quantitative NMR: pitfalls and how to avoid them using amplitude-corrected referencing through signal injection," *Anal Chem,* vol. 80, no. 21, pp. 8320-3, Nov 1 2008, doi: 10.1021/ac800865c.

$$f_c = (1 - F_{CSF})^{-1} \left[\frac{2M_w \sum_{i=GM,WM,CSF}(F_i \beta_i)}{\mathrm{N}_h S_w} \right] \frac{\sum_{i=GM,WM,CSF} \left[F_i \left(\mathrm{e}^{\frac{-T_E}{T_{2wi}}} \right) \left(1 - \mathrm{e}^{\frac{-T_R}{T_{1wi}}} \right) \right]}{\mathrm{e}^{\frac{-T_E}{T_{2m}}} \left(1 - \mathrm{e}^{\frac{-T_R}{T_{1m}}} \right)} \quad (3)$$

This equation expresses the derivation of conversion factor f_c to be applied to a metabolite of arbitrary scaling a.u. as expressed by C_l in Equation (2) to obtain an estimate in mM units for that metabolite. It can be broken further into two elements: the first (leftmost fraction on right side) takes the ratio between the estimated concentration of water in the voxel and its observed a.u. scaling (here expressed as water signal S_w, equivalent to C_l for water in Equation (2)) while controlling for differences in proton number in the water and metabolite moieties from which these C_l were obtained; the second (rightmost fraction on right side) controls for relaxation differences, explained below, between water and the metabolite in question. Here '2' represents the number of protons in the ~4.67-ppm H_2O signal, M_w the molarity of pure water, β_i the molarity of water as a fraction of pure water in either grey matter (GM), white

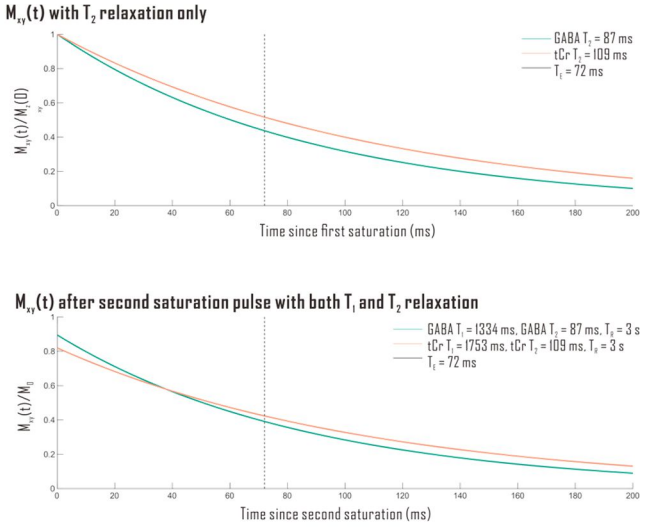

Figure 1.4. Apparent metabolite concentrations derived from ^{1}H MR spectral quantification can be affected by extra-concentration factors like T_1 and T_2 relaxation. The magnitude of longitudinal magnetization (M_z) representing metabolite signal available for excitation and measurement in a ^{1}H MRS experiment is determined in part by T_1 or spin-lattice relaxation, which can differ not only by metabolite but also by nuclear moiety, as a function of sequence repetition time T_R, the duration between sequence excitation. Following radiofrequency (RF) excitation of available longitudinal magnetization, the magnitude of signal available upon acquisition (M_{xy}) is also affected in part by T_2 relaxation as a function of sequence echo time T_E, the duration between excitation and acquisition (top panel). In reality, both factors can influence available metabolite signal within the context of an experiment (bottom panel). Simulation T_R 3 s, T_E 72 ms; metabolite T_1 and T_2 derived from literature values for MEGA-sLASER of GABA at 7 T [1]. tCr: total creatine.

matter (WM), or cerebrospinal fluid (CSF) as obtained from the literature or by experimentation, F_i the voxel fraction occupied by each of these three tissue types, N_h the number of protons represented by the metabolite signal being scaled as a companion to '2' in the numerator, and S_w, as mentioned, the a.u. signal for water. T_{2wi} and T_{1wi} are the T_2 and T_1 relaxation constants, respectively, of water for the sequence employed, as obtained from the literature or by experimentation, in either grey matter, white matter, or cerebrospinal fluid, while T_{2m} and T_{1m} are the same constants for the metabolite being quantified. Please note that the application of these latter values is not broken into individual tissue types to reflect the continued, though slowly ameliorating, lack of such detailed information for compounds other than water.

As already mentioned, using an internal concentration reference avoids the potentially confounding influences of local differences in transmit radiofrequency field strength and resultant transverse magnetization available for measurement, signal receive gain, and magnetic susceptibility that can plague corrections based on use of an external reference compound measured at a different location in the scanner bore from the metabolites under investigation [13]. In other words, such variables as these that are accepted to equivalently affect the amplitudes of all metabolites in a spectrum are likely to be adequately controlled by the internal referencing approach.

The variables that appear in Equation (3), by contrast, have been shown to affect different metabolites in different ways. For example, the signal intensity of each resonance along a spectrum decays in a unique manner directly with the period between proton dipole excitation by radiofrequency emission and subsequent dipole measurement within one ^{1}H-MRS sequence repetition (echo time or T_E), described by the transverse decay constant T_2:

$$M_{xy}(t) = M_{xy}(0)e^{\frac{-t}{T_2}} \quad (4)$$

where $M_{xy}(t)$ represents the transverse component of the net magnetic dipole of the nuclei under study following the RF pulse (with t=0 at pulse cessation). Signal intensities also vary inversely with the period between one ^{1}H-MRS sequence repetition and the next (repetition time or T_R), described by the longitudinal relaxation constant T_1 [13]:

$$M_z(t) = M_0 + (M_z(0) - M_0)e^{\frac{-t}{T_1}} \quad (5)$$

where $M_z(t)$ represents the longitudinal component of the net magnetic dipole of the nuclei under study, with time t the duration since the last RF pulse excitation (with t=0 at pulse cessation), and M_0 represents the net magnetization (considered to be entirely longitudinal, parallel with the scanner B_0 field) at thermal equilibrium.

To complicate matters even further, the weightings imposed by influences like T_2 and T_1 relaxation on signal amplitude may themselves change with some disease states [25, 26]. This means that they sometimes require independent correction, or at least consideration, for each experimental cohort in any cross-sectional comparison of ^{1}H-MRS-measured absolute metabolite concentrations between groups that may exhibit differential pathological conditions. Failing to do so may allow metabolite signals to be erroneously weighted by these variables, confounding apparent concentrations estimated by MRS depending on sequence T_R and T_E (Figure 1.4).

Translating relative concentrations into absolute ones is therefore also a complicated task involving a multitude of analytic steps that currently rest on varying degrees of evidentiary support. Chapter 3 of this dissertation discusses how the internal concentration referencing method of

achieving this step, called absolute quantification, can be confounded by disease-specific physiological conditions that can be observed and corrected even though this has not always been the case in the existing ^{1}H MRS literature.

1.3. The promise of ^{1}H MRS as a source of diagnostic biomarkers: Progressive multiple sclerosis as a case application. Multiple sclerosis (MS) is the most common neurological disorder among young people in the world. With a global prevalence of over 2 million [27], multiple sclerosis has been calculated, based on information from fifteen states in North America and Europe, to cost the global economy an average of $41,000 per patient per year [28], or an estimated annual 9 billion Euro to the European Union alone [29], in addition to immeasurable personal loss in duration and quality of life.

The disease is a chronic autoimmune and neurodegenerative condition that involves immune attacks on central nervous tissue, particularly on the myelin sheaths that insulate neuronal axons. In about 85% of cases, these attacks follow a relapsing-remitting course. This so-called relapsing-remitting multiple sclerosis phenotype manifests as relapses of neurological symptoms including paresthesias, gait and balance difficulties, and visual and cognitive disturbances, concomitant with gadolinium contrast-enhancing inflammatory lesions, typically in the white matter of the brain, including the optic nerve and brainstem, or the spinal cord [30]. Relapses are followed over weeks to months by partial or even largely complete remissions of symptoms and MR-visible damage. Mechanisms of structural and functional recovery may include remyelination [31], axonal redistribution of ion channels [32], and reorganization of functional networks [33], though remyelination in particular has been shown to attenuate in long-standing demyelinated lesions [30, 31].

In the remaining 15% of individuals diagnosed with multiple sclerosis, the disease will manifest as the so-called primary progressive variant. This phenotype is marked by steady functional decline alongside central nervous tissue atrophy, especially in grey matter [34], particularly subcortical [35], with a relative but not necessarily complete absence of temporally punctuated and spatially focal inflammatory white-matter lesions [36].

It has been considered in the past that 50-80% of individuals with relapsing-remitting multiple sclerosis would eventually transition from the relapsing-remitting phase into a progressive stage termed secondary progression [37, 38], though lower estimates of 15-30% have been more recently claimed [39]. Secondary progressive multiple sclerosis resembles primary progression in many aspects relative to the relapsing-remitting expression of disease, including advanced age of onset [37], the predominance of chronic inactive versus active white-matter lesions [40] as well as cortical versus active white-matter lesions [40], increased cortical demyelination [41], more extensive white-matter demyelination [41], increased presence of "smoldering" or slowly expanding demyelinating lesions [42], infiltration of lesions by plasma cells [42], increased evidence of diffuse microglial activation and axonal transection in normal-appearing tissue [40], reduced lesional expression of superoxide synthesis enzyme [43], enhanced rates of functional decline [44], and unresponsiveness to disease-modifying therapies demonstrated efficacious for relapsing-remitting multiple sclerosis [45]. The human leukocyte antigen-DRB15 allele, which has been associated with multiple sclerosis of all phenotypes [46], has been shown to similarly decrease the age of disease onset in both secondary and primary progressive cases [37, 47]. In other ways, however, secondary progression differs from primary progression: tertiary lymphoid-like B-lymphocyte follicles in the sulcal meninges are more likely present [48-50]; its prevalence, like that of relapsing-remitting multiple sclerosis, skews more female [51]; focal lesion load is

higher [52, 53]; small MR-visible lesions may constitute a smaller proportion of total lesions [54]; the prevalence of remyelinating lesions is lower [55]; the development of new lesions over time is more frequent [56]; associated human leukocyte antigen (HLA) polymorphisms are potentially different [57, 58]; and perivascular cuffing and parenchymal infiltration by lymphocytes are potentially greater [59] in secondary progression.

This body of largely non-^{1}H-MRS research suggests that the underlying biochemical manifestations of progressive multiple sclerosis differ both from relapsing-remitting multiple sclerosis and also from each other. Indeed, one complicating factor in our path to a working model of multiple sclerosis is the pathophysiological and resultant clinical heterogeneity of the disease. This lack of complete understanding about the distinctions between relapsing-remitting and progressive MS is evidenced by the fact that disease-modifying therapies demonstrated efficacious for slowing the course of relapsing-remitting disease have had minimal effect on progressive forms [60]. This may be due in part to the fact that currently available disease-modifying therapies target cells and pathways in the peripheral immune system, while progressive MS pathophysiology may instead involve the central nervous immune system or neurodegenerative processes downstream to loss of glioneuronal homeostasis [61]. Indeed, clinical symptoms reportedly worsen during secondary progressive MS despite MRI lesion burden, which suggests that processes other than acute inflammation and its immediate effects are of importance in progressive MS for brain atrophy and functional decline [62]. Given that, as mentioned, a significant proportion of multiple sclerosis patients exhibit either secondary or primary progression, the comparative lack of efficacious therapies for the progressive phenotype exerts significant influence on the present course of multiple sclerosis clinical care. A more complete understanding of the mechanistic differences between relapsing-remitting and progressive forms of MS will inform more useful

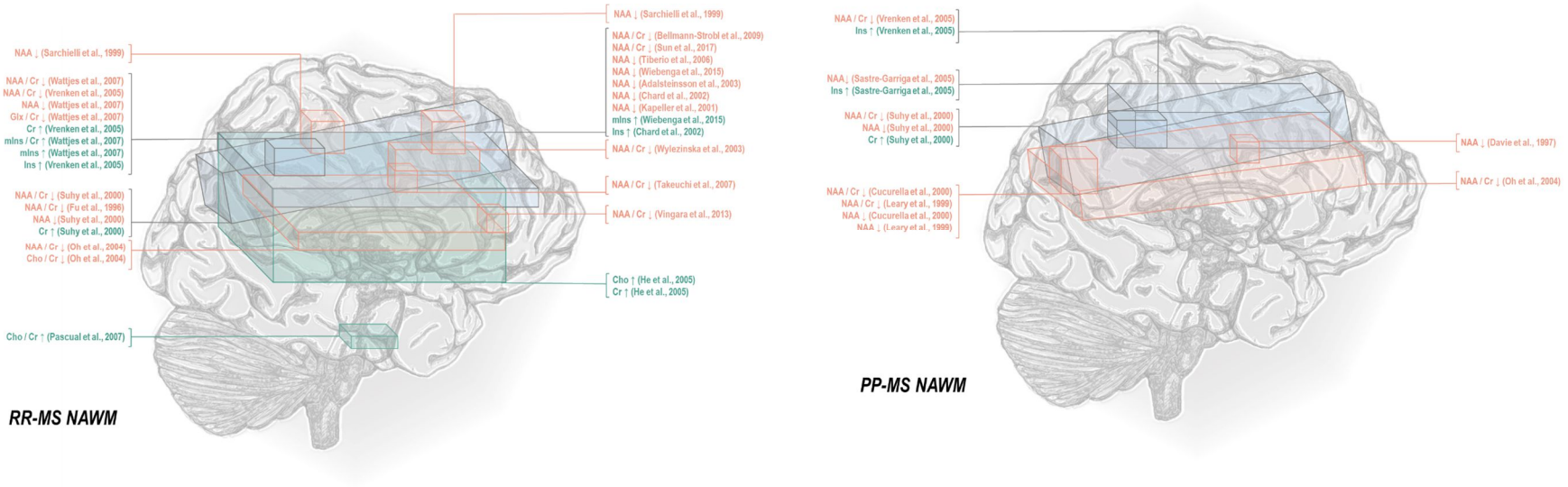

Figure 1.5. Multiple sclerosis subtype-related metabolic abnormalities measurable by ^{1}H MRS appear to lack specificity to disease phenotype. Even when studies are constrained to those assessing normal-appearing white matter (NAWM), the most extensively studied brain tissue type in ^{1}H MRS or ^{1}H MRS imaging (MRSI) research on multiple sclerosis (MS), patterns of abnormality center on decreased total N-acetyl aspartate (NAA) and increased inositols (Ins) and perhaps total creatine (Cr) regardless of MS subtype. RR-MS: relapsing-remitting multiple sclerosis; PP-MS: primary progressive multiple sclerosis; Cho: total choline; Glx: glutamate + glutamine; mIns: myoinositol. Figures adapted from Swanberg, Landheer, Pitt, and Juchem, *Front Neurol.* 2019; 10: 1173.

routes of development for novel therapies.

In addition to hampering therapeutic development, which is not the primary focus of the present dissertation, our incomplete understanding of the metabolic mechanisms underlying multiple sclerosis has additionally obstructed the discovery of clear biomarkers for disease diagnosis, which currently relies on the multifactorial synthesis of symptom self-report, neurological evaluation, imaging for central nervous lesions, and sometimes assay of cerebrospinal fluid for the presence of oligoclonal bands or immunoglobulin G [63]. Under this clinical paradigm, misdiagnosis of multiple sclerosis is not uncommon [64]: One survey of over one hundred neurologists found, for example, that 95% of respondents had dealt in the past year with at least one patient whom they believed had been misdiagnosed with the disease [65]. Conversely, the cost of misdiagnosing an individual with multiple sclerosis is high, as it has been argued that early therapeutic intervention is important for delaying the onset of permanent disability and what is perhaps the preventable shift to comparatively untreatable progressive illness in patients of relapsing-remitting multiple sclerosis [66]. Uncertainty surrounds not only initial identification but also phenotypic classification of multiple sclerosis, especially during the transition from relapsing to progressive manifestation, for which a mean duration of diagnostic uncertainty as high as three years has previously been calculated [67]. While recent revisions to the MacDonald diagnostic criteria [30] as applied to magnetic resonance imaging, particularly T_1-weighted MR imaging sequences that can demonstrate local abnormalities in blood-brain barrier permeability to injectable gadolinium contrast indicative of inflammatory lesion activity and T_2-weighted fluid-attenuated inversion recovery (FLAIR) imaging that can indicate lesions of some age, have improved diagnostic accuracy for new multiple sclerosis cases, specificity remains low [68].

Despite continued shortcomings of current imaging-supported diagnostic pipelines in

identifying multiple sclerosis, magnetic resonance techniques in general are attractive as potential diagnostic tools. Magnetic resonance is noninvasive and safe, facilitating its repeated use for not only initial identification of disease state but also for continued monitoring of treatment and transition between phenotypes. In part for these reasons, "advanced" magnetic resonance techniques, including magnetic transfer imaging [69, 70], diffusion tensor imaging [71], and proton magnetic resonance spectroscopy [24] have been explored for their potential use in multiple sclerosis prognosis, disease progression, or diagnosis [72].

Among these, ^{1}H MRS is unique in its ability to simultaneously query concentrations of several small-molecule metabolites in one or more regions of interest. This is particularly advantageous for diagnosing a disease like multiple sclerosis, associated to some degree of reproducibility with abnormalities in multiple spectroscopy-visible metabolites, including N-acetyl aspartate, choline, myoinositol, glutamate, glutathione, GABA, and potentially common spectroscopy quantification reference creatine, as will be discussed further in Chapter 4 of this dissertation.

Despite this potential array of metabolic disease markers, and in contrast to the litany of non-^{1}H-MRS findings, enumerated above, suggestive of profound biochemical differences among relapsing-remitting, secondary progressive, and primary progressive multiple sclerosis, the subtype-specific metabolic abnormalities so far observed by the ^{1}H-MRS literature have proven much less distinctive. In over thirty years of ^{1}H-MRS research on multiple sclerosis, the most replicated takeaway appears to be that cortical N-acetyl aspartate in either or both grey and white matter drops with all three major phenotypes (Figure 1.5).

In addition to not associating particularly with any multiple sclerosis subtype, this result is also not specific to multiple sclerosis more generally, having similarly been found in diabetes

mellitus cortex [73], lupus grey and white matter [74], and HIV basal ganglia [75], among other neurological and psychiatric conditions, including post-traumatic stress disorder (PTSD) as discussed below. Moreover, among conditions demonstrating lesion activity on magnetic resonance imaging for which ^{1}H MRS might serve as an auxiliary toward differential diagnosis, N-acetyl aspartate has similarly been reported to decrease in, among others, acute disseminated encephalomyelitis lesions [76] and lesioned tissue in patients with cerebral small vessel disease (SVD) [77]. Along the same lines, one classification analysis of demyelinating lesions and gliomas based on N-acetyl aspartate alone incorrectly classified every demyelinating lesion, even while it demonstrated higher-than-chance accuracy in differentiating among glioma types [78]. One notable exception to the low specificity of N-acetyl aspartate reductions to multiple sclerosis may be in the differentiation between multiple sclerosis and neuromyelitis optica (NMO), as NMO has demonstrated increased N-acetyl aspartate concentration relative to multiple sclerosis while not differing from control in white matter [79], recapitulating a previous report of normalcy in both white and grey matter [80]. Additionally, a limited number of studies comparing multiple sclerosis subtypes have reported evidence suggesting greater decreases in N-acetyl aspartate in secondary progressive than relapsing-remitting white matter [81-85]. Despite these counterexamples, taken together, the state of the current literature suggests that even the most reproduced finding of metabolic abnormality in the ^{1}H-MRS literature on multiple sclerosis is currently not widely applicable as a diagnostic biomarker.

In addition to being nonspecific to multiple sclerosis, previously observed multiple-sclerosis-associated reductions of N-acetyl aspartate appear to lack a sufficiently replicable effect size for application to rule-based diagnostics of single individuals. In other words, even this effect, the most robust across the ^{1}H-MRS literature on multiple sclerosis, is subtle and not always

recapitulated. Among 64 publications reporting comparisons with control in this metric for individuals with unspecified or mixed, relapsing-remitting, or progressive phenotypes in voxels that were not predominantly lesions, we found that 22 publications did not reject the null hypothesis for comparisons in at least one tissue type, and 11 reported only null results, for creatine-referenced N-acetyl aspartate (Table 1.1 [24]).

Among those studies reporting significant between-group effects of disease on creatine-referenced N-acetyl aspartate, the largest effect size from a fixed-effects model [86] of studies conducted on individuals with various multiple sclerosis phenotypes was for comparisons involving progressive MS cohorts (including mixed or unspecified progressive, secondary progressive, and primary progressive), with a standardized mean difference (Hedges' g) of -1.50 in 25 comparisons over 16 publications reporting group sizes, means, and labeled standard deviations or errors for internal-creatine-referenced N-acetyl aspartate as measured by ^{1}H MRS in voxels that were not predominantly lesions (Figure 1.6). This effect size is comparable to the standardized mean differences between secondary progressive cohorts and control, also reported as Hedges' *g*, found by Caramanos and colleagues [87] for absolute total N-acetyl aspartate concentrations reported in comparisons over studies on normal-appearing white matter (g = -0.96, N = 7, p = 0.039) and normal-appearing grey matter (g = -1.29, N = 4, p = 0.0522); our estimate is likely slightly larger than these published values due to its inclusion of studies examining primary progressive patients as well as white-matter voxels containing some lesioned tissue.

In contrast to this broad range of findings, ^{1}H-MRS detection of 2-hydroxyglutarate for brain tumor characterization, a rare category of ^{1}H-MRS clinical applications for which insurance reimbursement is sometimes considered [15], has previously demonstrated in at least one analysis all-or-nothing association with the presence of isocitrate dehydrogenase mutation status in gliomas

References	MS	Tissue	Effect	References	MS	Tissue	Effect
Aboul-Enein et al. (80)	SP	NAWM	↓ in MS	Pan et al. (54)	R	mixed	↓ in MS
Aboul-Enein et al. (80)	R	NAWM	NS	Parry et al. (74)	R	mixed	↓ in MS
Anik et al. (41)	M	WM	↓ in MS	Pascual et al. (141)	R	NAWM	NS
Anik et al. (41)	M	NAWM	↓ in MS	Pelletier et al. (85)	PP	mixed, supratentorial	↓ in MS
Arnold et al. (47)	M	mixed	↓ in MS	Pelletier et al. (85)	PP	mixed, excluding central	↓ in MS
Bagory et al. (84)	SP	mixed	↓ in MS	Pelletier et al. (85)	PP	mixed, central	↓ in MS
Bagory et al. (84)	PP	mixed	↓ in MS	Pelletier et al. (85)	SP	mixed, supratentorial	↓ in MS
Bagory et al. (84)	R	mixed	NS	Pelletier et al. (85)	SP	mixed, excluding central	↓ in MS
Bellmann-Strobl et al. (65)	R	NAWM	↓ in MS	Pelletier et al. (85)	SP	mixed, central	↓ in MS
Brass et al. (43)	M	NAWM	↓ in MS	Pelletier et al. (85)	R	mixed, supratentorial	NS
Caramanos et al. (83)	SP	GM	↓ in MS	Pelletier et al. (85)	R	mixed, excluding central	NS
Caramanos et al. (83)	R	GM	NS	Pelletier et al. (85)	R	mixed, central	NS
Casanova et al. (204)	R	NAWM, peduncles	NS	Pelletier et al. (89)	PP	mixed	↓ in MS
Casanova et al. (204)	R	NAWM, pons	NS	Pokryszko-Dragan et al. (63)	R	mixed	↓ in MS
Cucurella et al. (78)	SP	NAWM	NS	Pokryszko-Dragan et al. (63)	R	WM	↓ in MS
Cucurella et al. (78)	PP	NAWM	↓ in MS	Reddy et al. (59)	R	WM	↓ in MS*
Davie et al. (24)	M	NAWM	↓ in MS	Rooney et al. (37)	M	NAWM	↓ in MS
De Stefano et al. (86)	RP	mixed	↓ in MS*	Ruiz-Peña et al. (143)	R	NAWM	NS
De Stefano et al. (36)	M	WM	↓ in MS	Sarchielli et al. (53)	R	NAWM	NS
De Stefano et al. (36)	R	WM	↓ in MS	Sarchielli et al. (88)	SP	mixed	↓ in MS
De Stefano et al. (36)	SP	WM	↓ in MS	Siger-Zajdel et al. (44)	M_{sp}	NAWM	↓ in MS
De Stefano et al. (72)	R	mixed	↓ in MS	Siger-Zajdel et al. (44)	M_f	NAWM	↓ in MS
De Stefano et al. (61)	R	WM	↓ in MS	Staffen et al. (58)	R	mixed	↓ in MS
D'Haeseleer et al. (42)	M	NAWM	↓ in MS	Staffen et al. (58)	R_{nl}	NAWM	NS
Duan et al. (64)	R	WM	↓ in MS	Staffen et al. (58)	R_l	WM	↓ in MS
Fu et al. (52)	SP	NAWM	↓ in MS	Steen et al. (81)	P	NAWM	↓ in MS
Fu et al. (52)	R	NAWM	↓ in MS	Steen et al. (39)	M	NAWM	↓ in MS
Fu et al. (60)	SP	WM	↓ in MS	Suhy et al. (50)	PP	NAWM	↓ in MS
Fu et al. (60)	R	WM	↓ in MS	Suhy et al. (50)	R	NAWM	↓ in MS
Hannoun et al. (62)	SP	WM	↓ in MS	Sun et al. (68)	R	NAWM, frontal	↓ in MS
Hannoun et al. (62)	PP	WM	↓ in MS	Sun et al. (68)	R	NAWM, parietal	↓ in MS
Hannoun et al. (62)	R	WM	↓ in MS	Sun et al. (68)	R	NAWM, parietal-occipital	↓ in MS
Husted et al. (30)	M	NAWM	↓ in MS	Takeuchi et al. (51)	R	NAWM	↓ in MS
Kimura et al. (32)	M	NAWM	NS	Tartaglia et al. (25)	M	NAWM	↓ in MS
Leary et al. (82)	PP	NAWM	↓ in MS	Tedeschi et al. (34)	M	NAWM	↓ in MS
Maffei et al. (76)	R	spine	↓ in MS*	Téllez et al. (75)	R_{nf}	mixed, lentiform nucleus	↓ in MS
Maffei et al. (76)	SP	spine	NS*	Téllez et al. (75)	R_{nf}	WM, frontal	NS
Mathiesen et al. (144)	R	GM	NS	Téllez et al. (75)	R_{lf}	mixed, lentiform nucleus	NS
Mathiesen et al. (144)	R	mixed	NS	Téllez et al. (75)	R_{lf}	WM, frontal	NS
Mathiesen et al. (144)	R	NAWM	NS	Tourbah et al. (40)	M	NAWM	↓ in MS
Matthews et al. (55)	M	NAWM	NS	Tourbah et al. (46)	M	NAWM	↓ in MS
Matthews et al. (71)	SP	mixed	↓ in MS	Tourbah et al. (46)	R	NAWM	NS
Matthews et al. (71)	R	mixed	↓ in MS	Tourbah et al. (46)	SP	NAWM	↓ in MS
Narayanan et al. (73)	SP	mixed	↓ in MS	Tourbah et al. (79)	R	NAWM	NS
Narayanan et al. (73)	R	mixed	↓ in MS	Tourbah et al. (79)	SP	NAWM	↓ in MS
Narayana et al. (87)	PP	mixed	↓ in MS	van Walderveen et al. (22)	M	NAWM	↓ in MS
Obert et al. (172)	SP	NAWM	NS	Vingara et al. (48)	R	NAWM	↓ in MS
Obert et al. (172)	R	NAWM	NS	Vrenken et al. (69)	PP	NAWM	↓ in MS
Oguz et al. (148)	R	NAWM	NS	Vrenken et al. (69)	SP	NAWM	↓ in MS
Oh et al. (45)	M	NAWM	↓ in MS	Vrenken et al. (69)	R	NAWM	↓ in MS
Oh et al. (45)	PP	NAWM	↓ in MS	Wattjes et al. (67)	R	NAWM	↓ in MS
Oh et al. (66)	SP	NAWM, c.c.	↓ in MS	Wood et al. (38)	M	NAWM	↓ in MS
Oh et al. (66)	SP	NAWM, central	↓ in MS	Wu et al. (145)	R	mixed	NS
Oh et al. (66)	SP	NAWM, not c.c.	NS	Wylezinska et al. (70)	R	GM	↓ in MS
Oh et al. (66)	R	NAWM, c.c.	↓ in MS	Wylezinska et al. (70)	R	NAWM	↓ in MS
Oh et al. (66)	R	NAWM, central	NS	Yetkin et al. (56)	R	NAWM	NS
Oh et al. (66)	R	NAWM, not c.c.	NS	Zaini et al. (57)	R_{nf}	WM	↓ in MS
Pan et al. (54)	R	GM	↓ in MS	Zaini et al. (57)	R_{lf}	WM	↓ in MS
Pan et al. (54)	R	WM	↓ in MS				

*Single-subject MS case report.
MS: multiple sclerosis; P: progressive; SP: secondary progressive; PP: primary progressive; R: relapsing-remitting; M: mixed or unspecified MS phenotype(s); c.c.: corpus callosum; M_{sp}: sporadic MS; M_f: familial MS; R_{nl}: relapsing-remitting with no lesions in region of interest; R_l: relapsing-remitting with lesions in region of interest; R_{nf}: relapsing-remitting with any or high fatigue; R_{lf}: relapsing-remitting with no or low fatigue.

Table 1.1. Multiple sclerosis-associated reductions in N-acetyl aspartate are not always consistently replicated across the ^{1}H-MRS literature. Table displayed as appears in Swanberg, Landheer, Pitt, and Juchem, *Front Neurol.* 2019; 10: 1173.

[88], supporting, according to a 2018 meta-analysis of fourteen studies, a pooled sensitivity of 95% [89]. Even this application of ^{1}H MRS, however, is suboptimal for patients whose tumors have already undergone resection or radiotherapy and still not considered definitive in the absence of a biopsy [90].

In a recent survey of the in vivo proton magnetic resonance spectroscopy community, "inconsistent or unreliable data quality/reproducibility" was weighted most heavily as the largest practical barrier to the wider clinical application of MRS [91]. Evidence-based standards for generating reliable—precise, accurate, reproducible, and replicable—metabolite concentration estimates via ^{1}H MRS, as explored and developed in Chapters 2 and 3 of this dissertation, thus represent a

welcome point of research for improving the sensitivity and specificity of potential biomarkers derived from ^{1}H MRS, not just for multiple sclerosis diagnosis but for a variety of clinical applications.

Also promising to multiple sclerosis diagnostics may be the determination of a potential disease-specific signature of subtle alterations in many metabolites. While one aforementioned study boasted a 100% failure rate at acute demyelinating lesion identification when it employed a predictive algorithm built using linear discriminant analysis of N-acetyl aspartate concentration alone, the inclusion of additional inputs from choline, creatine, lactate, and lipids enabled a 100% cross-validation accuracy for demyelinating lesions and 99% cross-validation accuracy over the whole sample of lesions, glioblastomas, and astrocytomas [78]. Similarly, analysis over multiple inputs has demonstrated superior accuracy over single-feature metrics in efforts to use patient demographics and existing magnetic resonance images to predict second attacks in clinically isolated syndrome [92]. The addition of metabolite ratios among N-acetyl aspartate, choline, and creatine as measured by ^{1}H MRS has slightly increased F_1 score in linear discriminant analyses using age, disease duration, lesion load, and expanded disability status scale (EDSS) score to distinguish between clinically isolated syndrome and relapse-onset multiple sclerosis, between relapsing-remitting and primary progressive multiple sclerosis, and between relapsing-remitting and secondary progressive multiple sclerosis [93]. With a continued explosion of free software libraries and packages enabling the straightforward implementation of a varied zoo of iterative classification and learning algorithms, like scikit-learn [94], PyTorch [95], TensorFlow [96], and others in Python and a number of packages in R [97], the influence of such approaches is likely to grow in coming years [98].

In the case of analysis pipelines that output intuitively interpretable models, like decision

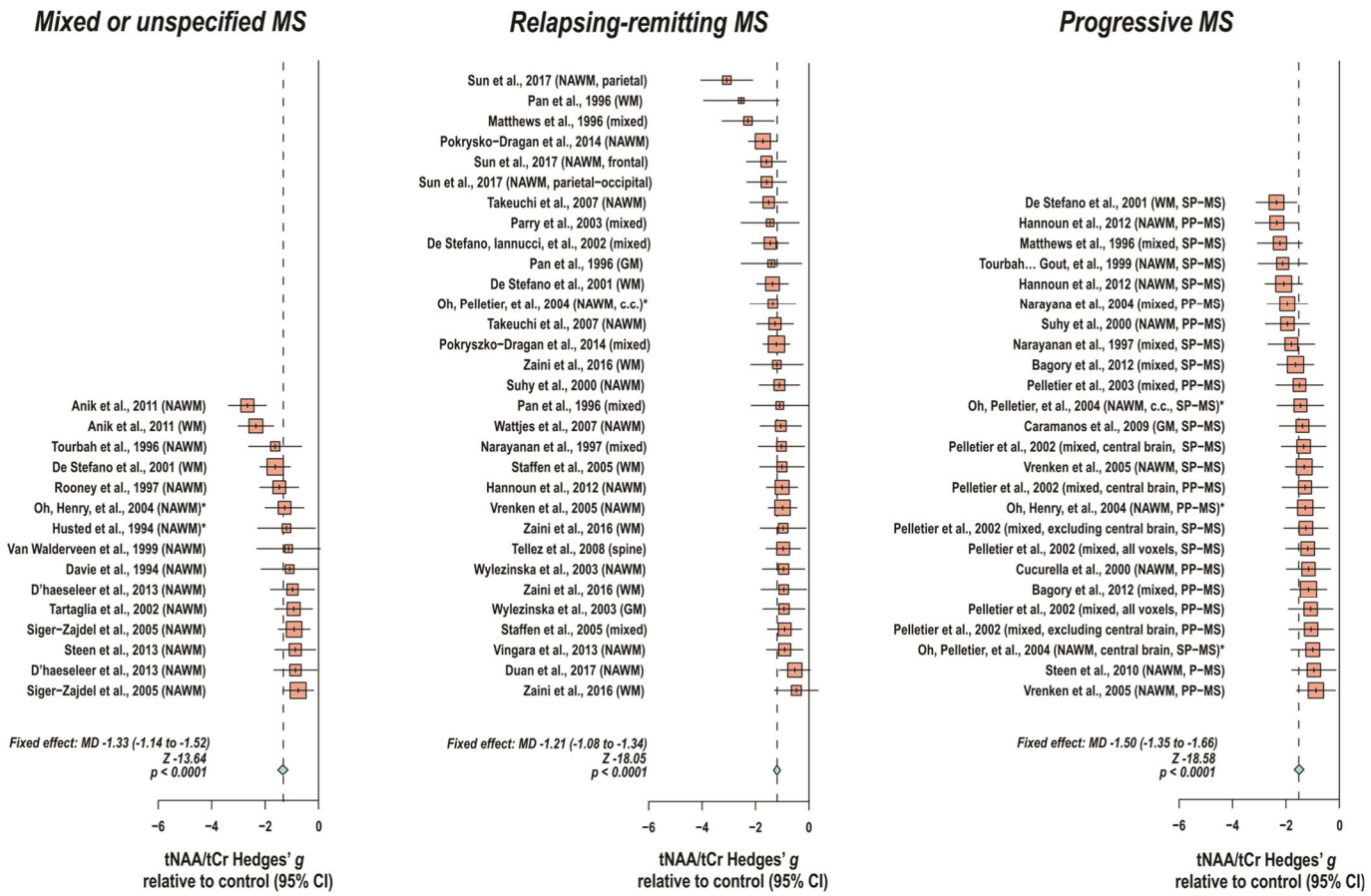

Figure 1.6. Effect sizes for disease state by multiple sclerosis phenotype in creatine-referenced N-acetyl aspartate as measured by ^{1}H MRS. Among 64 publications reporting comparisons with control in proton magnetic resonance spectroscopy (^{1}H-MRS), N-acetyl aspartate referenced to creatine for individuals with unspecified or mixed, relapsing-remitting, or progressive MS phenotypes in non-lesion voxels, 22 publications did not reject the null hypothesis for comparisons in at least one tissue type (Table 1.1). Among those reporting significant between-group effects of disease on this parameter, the largest effect size from meta-analysis of studies conducted on individuals with various MS phenotypes was for comparisons involving progressive MS cohorts (including unspecified progressive, secondary progressive, and primary progressive), with a standardized mean difference (Hedges' *g*) of -1.50 in 25 comparisons over 16 publications reporting group sizes, means, and labeled standard deviations or errors for this metabolite in voxels that were not predominantly lesions. *Standard deviations calculated from group sizes and standard errors as described in table source paper. MD: standardized mean difference, reported as Hedges' *g*; CI: Confidence interval; NAWM: normal-appearing white matter; WM: white matter; GM: grey matter; SP-MS: secondary progressive multiple sclerosis; PP-MS: primary progressive multiple sclerosis; c.c.: corpus callosum. Displayed as appears in Swanberg, Landheer, Pitt, and Juchem, *Front Neurol.* 2019; 10: 1173.

trees built on untransformed metabolite ratios, or classifiers that can be otherwise queried to determine the relative importance of particular features [99], some classification algorithms can not only offer practically useful diagnostic tools but also provide novel insights about the physiology of multiple sclerosis and reshape priorities regarding the metabolic targets of future investigations thereof. As with any analysis, however, the accuracy and generalizability of even the most sophisticated classifier depends on the precision and replicability, respectively, of its inputs. A systematically shorter T_2 in white-matter metabolite resonances comprising the creatine signal of multiple sclerosis patients relative to control may, for example, enable a classifier to identify patients on the basis of higher apparent concentrations of creatine-referenced choline acquired from a long-T_E scan. Regardless of the potentially even perfect cross-validation accuracy achievable by this classifier, because its inputs are artefactually based on creatine T_2, which disproportionately affects those metabolite signals referenced to creatine and acquired at long echo time, and not on molecular concentrations, which are theoretically invariant to such sequence parameters, such a classifier could not be confidently generalized until the source of the original between-group difference—creatine T_2 and not choline concentration—were appreciated with precision and subsequent clinical applications limited accordingly.

Chapter 4 of this dissertation attempts to apply both lines of methodological improvement to ^{1}H MRS, including a) optimized data processing and analysis based on empirical validation of spectral quantification and absolute quantification pipelines developed in Chapters 2 and 3, respectively, to maximize the reliability of individual metabolite concentration estimates derived via ^{1}H MRS, and b) employment of multivariate statistical procedures including discriminant analysis and machine learning to maximize the probability of discovering the most useful patterns they may exhibit. This chapter thereby seeks to demonstrate the unique niche that ^{1}H MRS has to

fill in furthering our ability to differentiate between progressive and relapsing-remitting multiple sclerosis, particularly how group differences in frontal cortex metabolites, including glutamate, GABA, and possibly glutathione, described first by general linear models applied to one empirically optimized metabolite concentration estimate at a time, can be further informed by multivariate modeling and supervised learning methods that simultaneously consider concentration estimates of all small-molecule compounds assessed by a ^{1}H-MRS dataset. Specifically, our findings are employed in the service of developing a clinically transferable model for supporting rapid and accurate differentiation of progressive from relapsing-remitting multiple sclerosis using data-driven machine-learning techniques that use as inputs only the brain metabolite concentrations obtained by single-voxel 7-Tesla ^{1}H MRS of the prefrontal cortex.

1.4. The promise of ^{1}H MRS as a source of diagnostic biomarkers: Extension to post-traumatic stress disorder. Post-traumatic stress disorder (PTSD) is a condition wherein experience of a traumatic event induces chronic emotional dysregulation that can disrupt functional participation in society. The 2012 economic toll of PTSD care was estimated at $300 million within the United States Department of Defense alone [100], a figure not considering its many comorbidities, including increased risk of suicide and of cardiorespiratory, gastrointestinal, immune, and additional psychiatric diagnoses [101]. Though the lifetime prevalence of PTSD in some communities is estimated up to 1 in 12 [101], diagnosis, and related treatment, continues to rely on the subjective and potentially slow evaluation of symptoms that must persist over several weeks [102]. The continued reliance on symptom-based diagnosis of PTSD is due in part to an incomplete understanding of its neurobiological manifestations, particularly the metabolic changes in central nervous system pathways affected by the condition [103]. The only method currently

available for safely and noninvasively researching these changes by measuring local tissue metabolism in living humans is ^{1}H MRS.

Preliminary ^{1}H-MRS research indicates that the pattern of cortical metabolic abnormalities associated with PTSD is subtle and complex [104]. Most prior research has focused on the hippocampus and/or the anterior cingulate cortex, two structures in the brain thought to be implicated in the encoding of memory, including emotional memories like learned fear [105]. Additional studies have also examined the metabolic signatures of PTSD in the insula or temporal cortex more generally, basal ganglia, the parieto-occipital or parietal cortex, and the prefrontal cortex not only including and but also beyond the anterior cingulate [105]. As with multiple sclerosis, the most pervasive MR spectroscopy-visible abnormality, if any, observed in post-traumatic stress disorder has been decreased N-acetyl aspartate, as will be further discussed in Chapter 5 of this dissertation.

Given that PTSD has thus been associated with abnormalities in multiple metabolites measurable by ^{1}H MRS, its ^{1}H-MRS-visible disease signature is potentially therefore best characterized using data-driven multivariate techniques like machine learning. Few applications of such approaches to interpreting the complexity of brain metabolic changes in PTSD have, however, been published, in part due to the dearth of studies simultaneously assessing a broad range of disease-relevant metabolites in the same participants. Chapters 2 through 4 describe the optimization of ^{1}H-MRS processing and quantification methods that together with a reproducibility-validated data acquisition pipeline [106] have enabled for the first time the reliable simultaneous in vivo measurement of three such compounds implicated in PTSD pathophysiology: excitatory neurotransmitter glutamate, inhibitory neurotransmitter γ-amino-butyric acid (GABA), and antioxidant glutathione (GSH). Coupled with the measurement of five other small molecules

(choline, creatine, myoinositol, N-acetyl aspartate, and glutamine) each also implicated in various neurological conditions [107], these ^{1}H-MRS data acquisitions may thus uniquely enable data-driven metabolomics-level analysis to support more efficient and objective diagnosis of PTSD.

We hypothesize that, as in multiple sclerosis, the local metabolic alterations in brain tissue associated with PTSD can be exploited to enable the sensitive and specific identification of this disease state. Chapter 5 of this dissertation describes the generalized application of data analysis methods developed in Chapters 2 through 4 to a comprehensive cross-sectional investigation of PTSD frontal cortex tissue metabolism using ^{1}H MRS, both with and without consideration of common psychiatric comorbidity major depressive disorder (MDD). These findings are employed in the service of developing, similarly to Chapter 4, a model for supporting rapid and accurate diagnosis of psychiatric disease using data-driven machine-learning techniques that distinguish patients from control based on solely brain metabolite concentrations obtained via single-voxel ^{1}H MRS.

Chapter 2: Spectral Quantification.

Effects of spectral quality, baseline, and baseline model on accuracy and precision of metabolite concentrations estimated by linear combination model fitting of simulated basis functions to in vivo ^{1}H MR spectra

Despite recent efforts toward evidence-based standardization in spectral acquisition, processing, and quantification, the field of in vivo proton magnetic resonance spectroscopy continues to lack data-driven quality control standards. This circumstance may impede the development of ^{1}H-MRS-derived diagnostic biomarkers by contributing to biologically uninformative variability in metabolite concentration estimates both within and between participant cohorts providing spectral data sets. Quality control standards can be informed by systematically quantifying the effects of spectral data quality on metabolite quantification so that educated judgments about quantification approaches can be made in light of expected error. To this end, we develop a batch simulation and spectral quantification by linear combination modeling pipeline to assess the influences of two common and easily quantified measures of spectral quality, spectral line width and signal-to-noise ratio, on both simulated and experimentally derived in vivo resonances from twenty-one metabolites measured by short-echo-time localization by STimulated Echo Acquisition Mode (STEAM) and *J*-difference editing (JDE) for glutathione and GABA at 7 Tesla. We show that spectral quality exerts distinct effects on apparent concentrations of different metabolites, underlining the importance of explicit quality analyses in studies employing in vivo magnetic resonance spectroscopy, especially cross-sectional investigations of physiologically distinct groups. We then investigate the effect of experimental spectral baselines on the relationship between spectral quality and spectral quantification error and demonstrate that in the presence of baseline shapes such as would be expected from an in vivo spectroscopy acquisition, inadequate baseline modeling can interact with suboptimal spectral quality to introduce not only zero-centered but rather systematic errors, i.e. affect not only the precision but also the accuracy of metabolite

scaling estimates derived by spectral quantification via linear combination modeling. We therefore develop and implement a method for including complex regularized cubic spline baselines with user-defined smoothing coefficients and knot spacing intervals in our linear combination model framework and then use it to assess the influence of various baseline models, including simulated macromolecules and the aforementioned complex regularized cubic splines of various smoothing and knot spacing definitions, on metabolite quantification precision and accuracy against known measured or simulated standards within the context of metabolite spectra with in vivo baseline profiles. We conclude that complex regularized cubic splines of some smoothness and knot interval definitions are not necessarily outperformed by baselines of simulated macromolecules in either macromolecule or metabolite prediction accuracy, but quantification pipelines employing prior knowledge from metabolite-nulled acquisitions, though not feasible in all experiment types, exhibited superior metabolite fit accuracy among all baseline models tested. Finally, we design and implement a method for estimating spectral linear combination modeling parameter precision via the Cramér-Rao Lower Bound in not only metabolites but also baseline shapes in situations for which ground truth is not available to assess the accuracy and precision of a spectral quantification approach, such as for experiments conducted in vivo, and validate this implementation to demonstrate its prediction of error standard deviations on modeled spectral baseline coefficients as well as its improvement of Cramér-Rao Lower Bound prediction of error standard deviations on metabolite concentration estimates.

2.1 Introduction

In vivo magnetic resonance spectroscopy currently lacks data-driven quality control standards, the development of which can be informed by characterizing the effects of spectral quality on

metabolite quantification. We assess the influences of spectral line width and signal-to-noise ratio on both simulated and experimentally derived in vivo resonances from twenty-one metabolites measured by short-echo-time STEAM and *J*-difference editing for glutathione and GABA at 7 Tesla. We show that spectral quality exerts distinct effects on apparent concentrations of different metabolites, underlining the importance of explicit quality analysis in studies employing in vivo magnetic resonance spectroscopy, especially cross-sectional investigations of physiologically distinct groups. Additionally, we establish that inappropriately modeled spectral baselines can confound metabolite concentration estimates by in vivo ^{1}H MRS even while contributing to visually reasonable fits.

Despite the strong influence of baseline handling on metabolite quantification error as demonstrated in Section 2, the systematic optimization of spectral quantification pipelines, including baseline modeling, continues nonetheless to be impeded by an under-utilization of validation methods both physically meaningful and involving perfect prior knowledge. We therefore address the extant need for evidence-based spectral baseline handling by combining the practical utility of in vivo data with the prior knowledge enabled by simulated standards. We use this paradigm to compare various baseline models for macromolecule characterization and metabolite quantification accuracy, and the degree to which these two meaningful outcomes of spectral quantification are reflected in visible fit residuals.

Finally, we propose the validation of a method to work toward estimating fit errors in the absence of a gold standard as in the simulation paradigm used in Sections 2 and 3, i.e., within the context of practical experiments. While Cramér-Rao Lower Bounds are widely applied to this end, as a proxy for variance about the true value of a model input, it is well accepted that calculating this parameter in the absence of baseline terms does not adequately capture error. It has been

previously argued, however, that spectral baselines cannot be adequately represented by analytical functions and therefore do not support the calculation of Cramér-Rao Lower Bounds [13]. In this work we investigate the implications of this phenomenon by treating baselines as overlapping piecewise polynomial shapes akin to metabolite basis functions and show that calculating amplitude Cramér-Rao Lower Bounds on baseline terms in this manner is in fact a feasible step toward full characterization of linear combination model error, though further work representing a more radical departure from convention may be needed to bridge this metric of precision to the systematic fit inaccuracies that the Cramér-Rao Lower Bound does not capture.

2.2 Characterizing the effects of spectral quality parameters signal to noise ratio, spectral full width at half maximum, and baseline artifacts on precision and accuracy of spectral quantification by linear combination modeling

2.2.1. Motivation

The in vivo magnetic resonance spectroscopy (^{1}H-MRS) field needs data-driven quality control standards [91]. Such standards can be informed by quantifying the effects of spectral quality, including full width at half maximum (FWHM; frequency width of a resonance at the ordinate point halfway between baseline and apex) and signal-to-noise ratio (SNR; a prominent singlet amplitude normalized by noise intensity standard deviation) on metabolite quantification.

Understanding the numerical influences of spectral quality on metabolite quantification informs both quality control and experimental integrity. Brain water or metabolite spectral FWHM has demonstrated increases in multiple sclerosis [108], Wilson's disease [109], and normal maturation [110]. Additionally, any cohort who might compromise magnetic field homogeneity by increased motion between shim optimization and signal acquisition, like children, may also exhibit

broader lines. It is important to determine how this may influence metabolite quantification by ^{1}H-MRS. Some previous work has addressed this question with simulation experiments [111-113], but these findings are not generalizable to higher field strengths or to metabolite signals isolated by spectral editing.

Glutathione (GSH) is an antioxidant synthesized in neurons and glia [114], while γ-amino butyric acid (GABA) is an inhibitory neurotransmitter and potential immunomodulator [115] and glutamate the central nervous system's predominating excitatory neurotransmitter. All three compounds play key mechanistic roles in neurological health and disease. Reduced peak amplitude and complex line shapes due to *J*-coupling-induced signal splitting, plus spectral overlap with both each other and nearby resonances like creatine, complicate the spectroscopic quantification of these molecules, predicting its strong influence by spectral quality.

To facilitate data-driven quality assessment for ^{1}H-MRS experimental planning and interpretation, we applied linear combination modeling and quantification error analysis to 25,250 simulated and measured MEGA-sLASER and STEAM spectra based on previously published sequences at 7 Tesla [106] and calculated the effects of spectral quality measures FWHM and SNR on the quantification error of these three metabolites, plus common concentration references total creatine and N-acetyl aspartate (NAA) and additional molecule of interest excitatory neurotransmitter glutamate.

2.2.2. Methods

Experimental paradigm. We analyzed the error of linear combination model fits to proton spectra of varying complexity to examine how FWHM and SNR affect apparent metabolite concentration

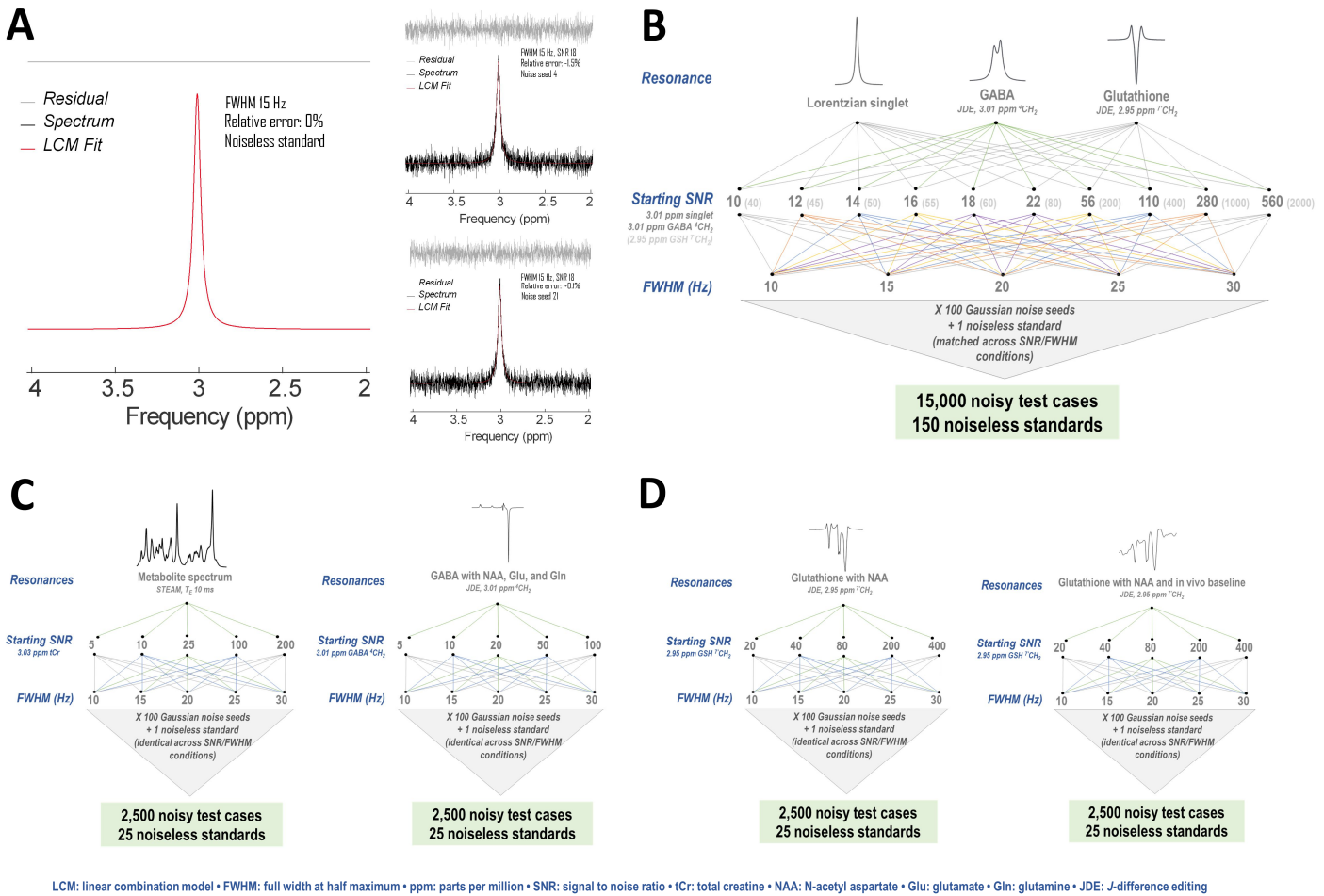

Figure 2.1. Spectral quantification precision and error characterization simulation parameters. We analyzed spectral quality effects on A) fit accuracy, or the error of quantified concentration relative to that of a noiseless standard at the same line width and signal amplitude conditions, of linear combination model fits to B) single resonances (Lorentzian singlets and *J*-difference spectra of 2.95-ppm glutathione $^{7}CH_2$ and 3.01-ppm GABA $^{4}CH_2$); C) overlapping resonances (GABA with co-edited molecules or a STEAM spectrum including 21 metabolites) resembling in vivo concentration ratios; or D) overlapping resonances with in vivo baselines (glutathione plus co-edited N-acetyl aspartate with and without a baseline derived from an identical sequence in the frontal cortex of 7 volunteers). Displayed as appears in Swanberg et al. *Proc ISMRM* 2019, 4237.

as quantified by in vivo ^{1}H-MRS at 7 T. Spectral quantification by linear combination modeling exploited functionality from INSPECTOR; additional scripting was implemented in MATLAB (Mathworks, Natick, MA, USA) to enable batch simulation and fitting (Figures 2.1, 2.2). Quantification errors were calculated relative to apparent concentrations output by perfect model fits to noiseless spectra at each FWHM and signal amplitude combination (Figure 2.1A).

Condition 1 comprised fits at 5 FWHM, 10 starting signal amplitudes, and 100 Gaussian noise patterns, based on a simulated Lorentzian singlet at 3.01 ppm, or GSH or GABA difference resonances from MEGA-sLASER experiments (T_E = 72 ms) with *J*-difference editing (glutathione 4.56 ppm; GABA 1.89 ppm) [116] simulated using SpinWizard [117] (Figure 2.1B). Actual concentration was kept constant across FWHM. Noise patterns were matched across signal amplitude and line width conditions for each resonance; noise amplitude remained constant within each experiment. Condition 2 consisted of fits at 5 FWHM and 5 starting signal amplitudes, also with 100 Gaussian noise patterns, based on GSH or GABA difference spectra plus co-edited resonances (NAA or NAA, glutamate, and glutamine, respectively), or full metabolite spectra (STEAM, T_E =10 ms) including twenty-one metabolites, in approximately physiological ratios (Figure 2.1C). Condition 3 repeated GSH *J*-difference spectral fits with an in vivo baseline averaged from fit residuals to similar acquisitions in the frontal cortex of healthy adults (N = 7; 4 female; age 41 ± 7 y.o.). This enabled the calculation of quantification error under spectral conditions resembling those seen in vivo against a perfect standard without noise or baseline (Figure 2.1D).

In vivo spectral acquisition. Acquisitions were accomplished at Yale University's Magnetic Resonance Research Center (MRRC) as described previously [106], on a 7 Tesla head-only MR

scanner (Agilent Technologies, Santa Clara, CA) with a 298.1-MHz DirectDrive proton spectrometer, custom actively shielded gradients (Magnex Scientific, Oxford, UK), and an 8-channel transmit-receive head coil. Sequences were controlled via VnmrJ software, version 2.3A (Varian, Santa Clara, CA). In vivo data were acquired with the prior approval of and in accordance with standards set forth by the Yale School of Medicine Human Investigation Committee for human subjects research.

Placement of a 3-cm isotropic voxel at midline of frontal cortex was effected with reference to scans by a custom-written T_1-weighted inversion-recovery anatomical imaging sequence (field of view 20 x 22 x 78 cm, matrix size 256 x 256 x 39, echo time T_E 6 ms, repetition time T_R 3 s, inversion time T_I 1 s). Up through third-order spherical-harmonics B_0 shims were

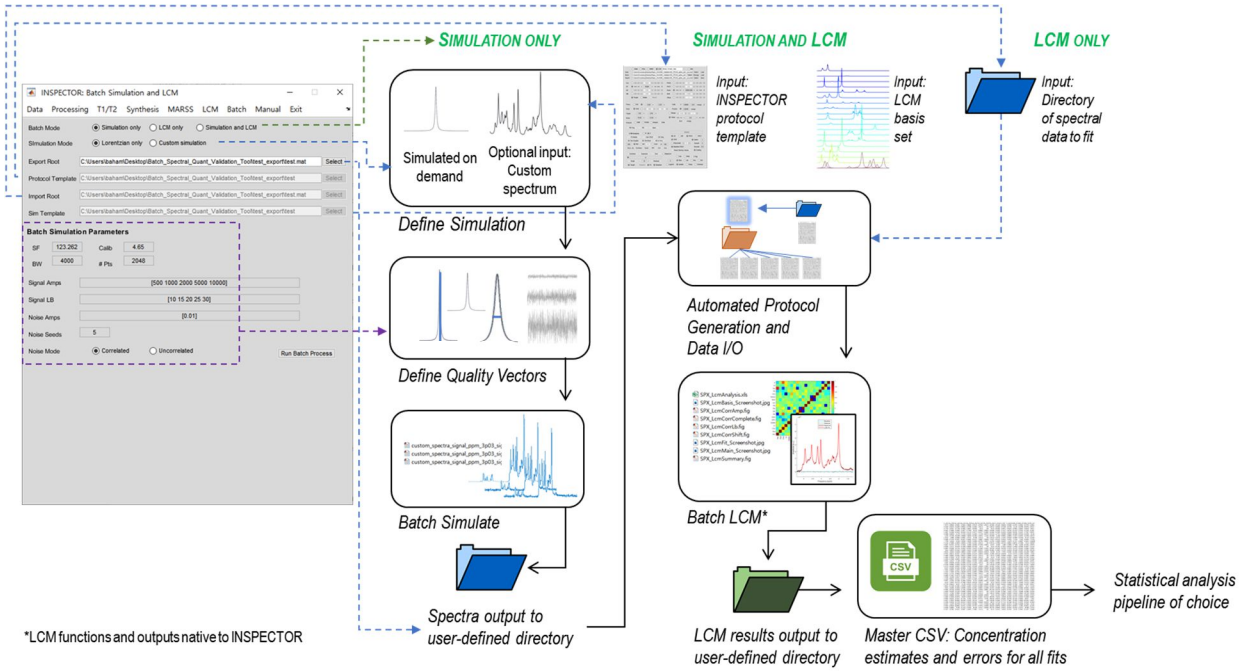

Figure 2.2. The spectroscopy quantification validation toolkit developed in this chapter was further made available for user-friendly employment by others within the INSPECTOR framework. This batch simulation and linear combination modeling (LCM) framework, enabling spectral quantification validation pipelines such as that presented in Figures 2.1, 2.8, and 2.13, have now been implemented into the INSPECTOR user interface to enable less experienced users to perform either mass spectral data simulation, linear combination modeling, or both using either Lorentzian functions simulated on-demand (as in Figure 2.1A) or custom spectra imported as INSPECTOR-readable .mat files (as in the other simulation and modeling pipelines presented here). SF: spectral frequency; Calib: frequency calibration parameter as ppm definition for water; BW: bandwidth; Amps: amplitudes; LB: Lorentzian broadening.

applied according to calculations on gradient-echo images at five T_E (FOV 22 x 22 x 6 cm, matrix size 126 x 64 x 20, T_E 3.8, 4.0, 4.3, 5.3, and 6.8 ms, T_R 1.3 s) in laboratory-developed software B0DETOX, and B_1 phase shimming was calculated by laboratory-developed software IMAGO.

Glutathione spectra were acquired via Mescher-GArwood semi-Localization by Adiabatic Selective Refocusing (MEGA-sLASER; T_E 72 ms, T_R 3 s, number of repetitions N_R 128) with *J*-difference editing at the 4.56-ppm ^{7}CH for isolation of the scalar-coupled $^{7'}CH_2$ moiety at 2.95 ppm. Edit-on scans were interleaved with edit-off conditions for which the *J*-difference editing pulse was placed with a 5 kHz offset to avoid interference with metabolic signals. Water suppression was achieved with Chemical Shift Selective pulses (CHESS), and water-unsuppressed references were acquired in order to correct metabolite scans for eddy currents by the Klose method [118].

In vivo spectral processing. Spectra were acquired at 4096 complex points. Individual traces were eddy-current-corrected as described and phase- and frequency-aligned over coil channels and repetitions in a *J*-difference-editing-condition-specific manner. Coil combination was performed according to averaging weighted by receive sensitivity [119]. The preprocessed averaged spectrum from each editing condition was aligned with the other using zero-order phase, frequency shift, Lorentzian line broadening, amplitude scaling, and polynomial baseline correction over a frequency interval not including moieties expected to receive influence by *J*-difference-editing; the resultant difference spectrum from each case was employed in linear combination model fits for glutathione and co-edited N-acetyl aspartate.

In vivo spectral linear combination model fitting. Linear combination modeling was applied in

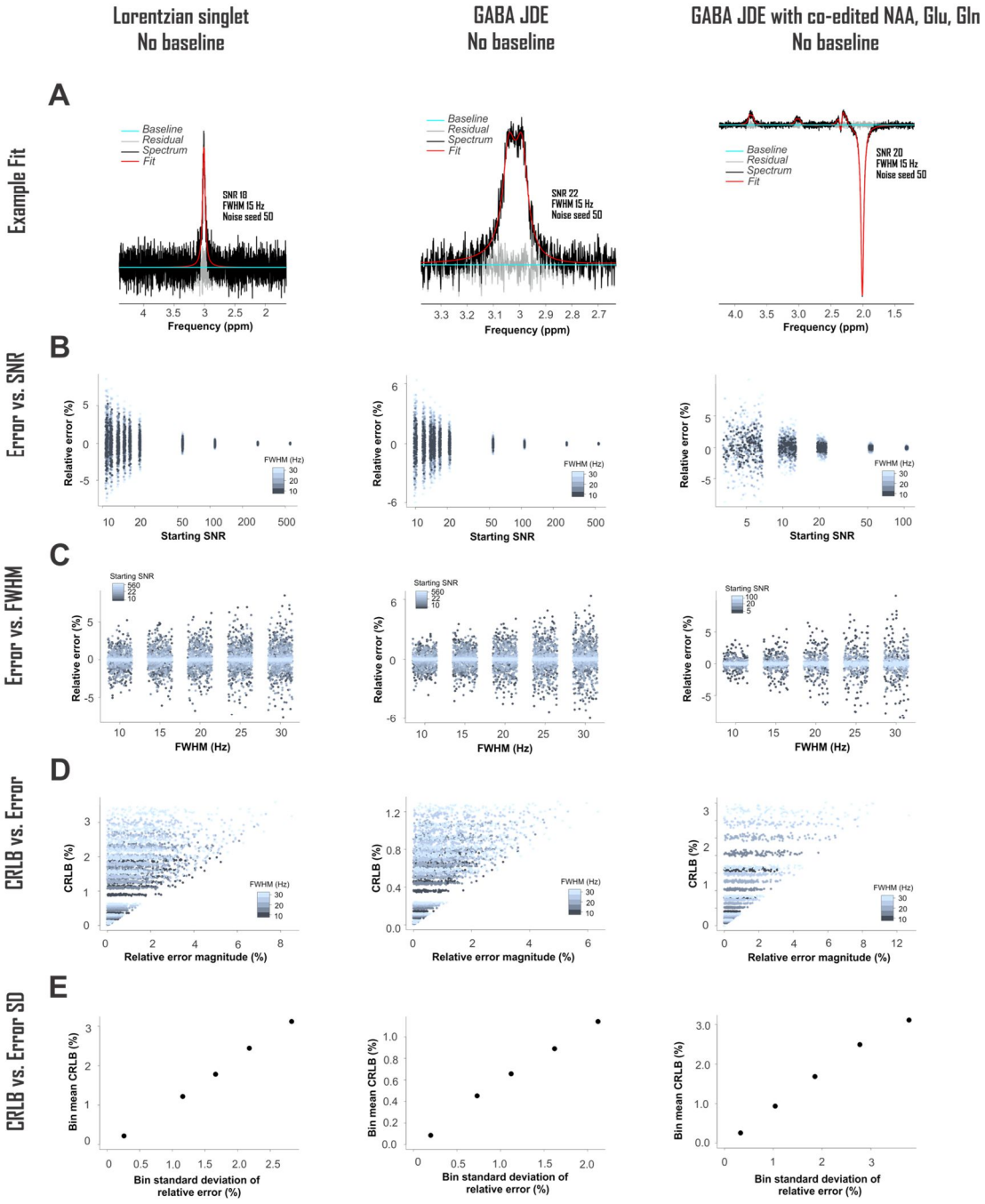

Figure 2.3. Error changes predictably with signal-to-noise ratio and line width in linear combination model fits of single resonances or GABA *J*-difference spectra with overlap. Linear combination model fit (A) error decreases with signal-to-noise ratio (SNR) (B) and increases with full width at half maximum (FWHM) (C) in Lorentzian singlets or GABA spectra with *J*-difference editing (JDE) to isolate the 3.01-ppm $^{4}CH_2$. Amplitude Cramér-Rao Lower Bounds (CRLB) exhibit positive relationships with quantification error magnitude (D), with regular influence by FWHM, and positive relationships with quantification error standard deviation (SD) (E). NAA: N-acetyl aspartate; Glu: glutamate; Gln: glutamine. Displayed as appears in Swanberg et al. *Proc ISMRM* 2019, 4237.

laboratory-written MATLAB-based spectral processing and quantification toolkit INSPECTOR (http://innovation.columbia.edu/technologies/cu17130_inspector) [120] on preprocessed glutathione difference spectra from 7 control participants using sequence-specific bases for glutathione and N-acetyl aspartate density-matrix simulated in SpinWizard and a first-order polynomial baseline. Residuals were extracted, and fit baselines were removed. They were then summed with each other to produce an in vivo-like baseline applied to the third set of spectral simulations previously described as Condition 3.

Error and statistical analysis. The precision of fit parameter estimates, including metabolite signal amplitudes, was reported as Cramér-Rao Lower Bounds within INSPECTOR, using the Fisher information matrix plus transformation to account for linearly dependent parameter vectors as previously explicated [121]. Calculations of relative fit errors, group statistics thereof, and data visualization were performed in R (v. 3.4.4; R Foundation for Statistical Computing, Vienna, Austria).

2.2.3. Results and Discussion

Fit error standard deviation decreased with SNR (Figures 2.3, 2.4B) and increased with FWHM (Figures 2.3, 2.4C) in all fits of singlets, GABA, and GSH and varied positively with metabolite amplitude Cramér-Rao Lower Bound (CRLB) (Figures 2.3, 2.4D-E). In vivo baseline conditions introduced systematic asymmetry into quantification errors expected from linear combination model fits plus linear baseline to GSH *J*-difference spectra (Figures 2.4B, C), and glutamate fit errors exhibited greater influence by spectral quality than those of total creatine or NAA (Figure

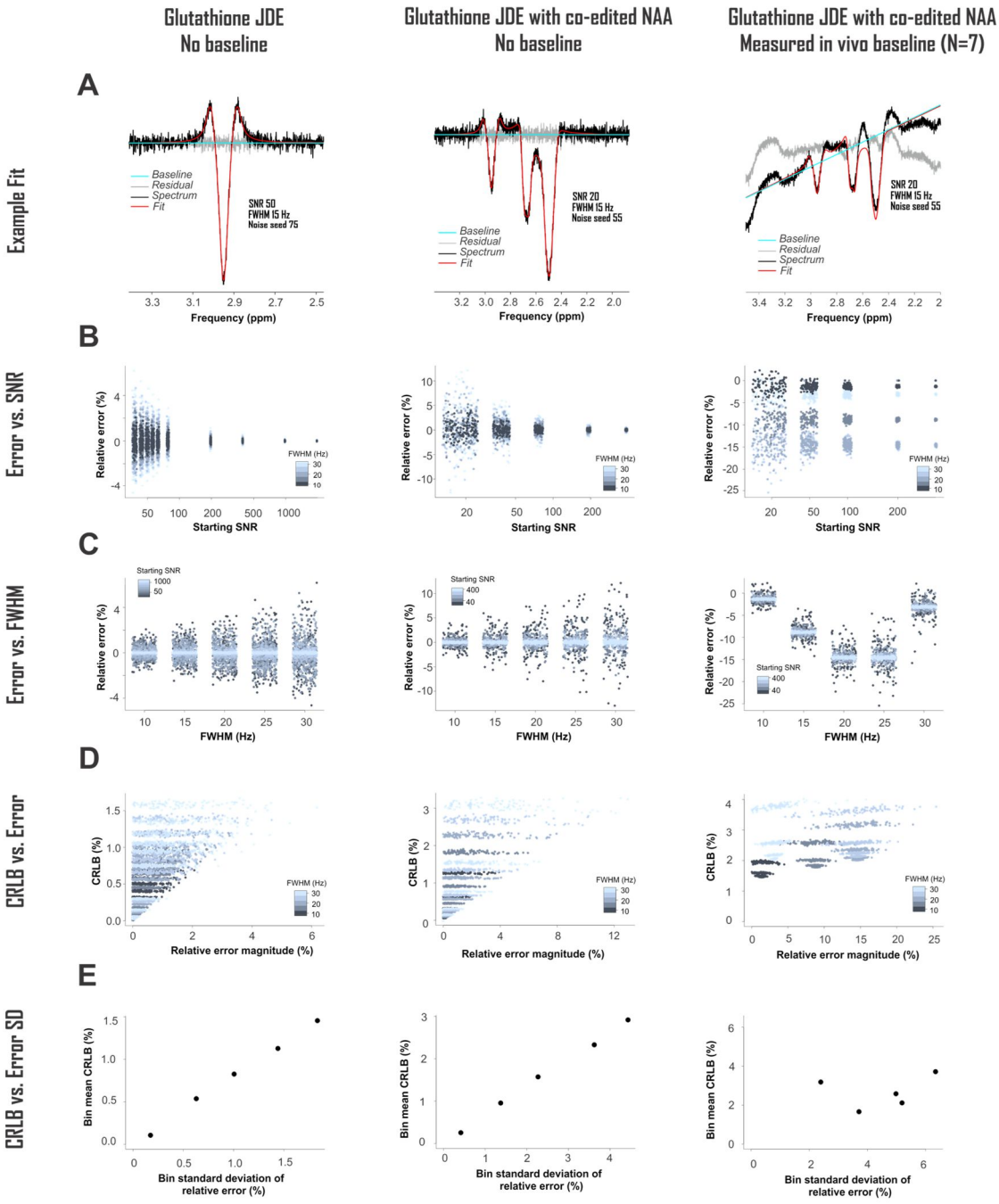

Figure 2.4. In vivo baseline conditions introduce systematic asymmetry to quantification errors expected from linear combination model fits of glutathione *J*-difference spectra. Linear combination model fit (A) error decreases with signal-to-noise ratio (SNR) (B) and increases with full width at half maximum (FWHM) (C), and its magnitude and standard deviation associate positively with Cramér-Rao Lower Bound (CRLB) (D, E), in glutathione (GSH) spectra with *J*-difference editing (JDE) to isolate the 2.95-ppm $^{7}CH_2$. Including a spectral baseline averaged from in vivo JDE acquisitions in the human frontal cortex (N=7) introduces asymmetries into fit errors and their relationships with spectral quality. NAA: N-acetyl aspartate. Displayed as appears in Swanberg et al. *Proc ISMRM* 2019, 4237.

2.5). Underestimation of actual fit errors by reported CRLB varied with fit frequency range and baseline complexity (Figure 2.6). SNR and FWHM predictably affect the standard deviation of quantification errors expected from linear combination model fitting of isolated and overlapping singlet, *J*-difference-edited, and unedited metabolite resonances. Complex baseline shapes may introduce systematic quantification errors that could influence conclusions based on comparisons of groups exhibiting disparate spectral quality. These results motivate further work on the effects of fitting algorithms, particularly baseline modeling routines, on conditions exhibiting such systematic errors here. All told, the relationship between spectral quality and fit error differs by metabolite, arguing against the use of one-size-fits-all quality control thresholds for in vivo ^{1}H-MRS experiments.

2.2.4. Limitations and Conclusions

These findings demonstrate that spectral quantification errors on proton magnetic resonance spectra in the absence of a baseline, i.e., within a perfect linear combination model completely encapsulated by the employed basis set with differences introduced solely by Gaussian noise, are expected as in theory to exhibit zero-centered distributions for which variance increases in a predictable and simulable manner with decreasing spectral quality, at least as measured by commonly applied data quality metrics signal to noise ratio (SNR) and spectral full width at half maximum (FWHM). Against such a context Cramér-Rao Lower Bounds are, as dictated by theory, additionally expected to predict the lower bound of standard deviations on estimated fit parameters, a phenomenon that we also observed in our data. With the addition of a summed series of fit residuals from in vivo data as a complicated in vivo-like baseline, however, both simple relationships were disrupted: zero-centered variance in precision with changes in spectral quality

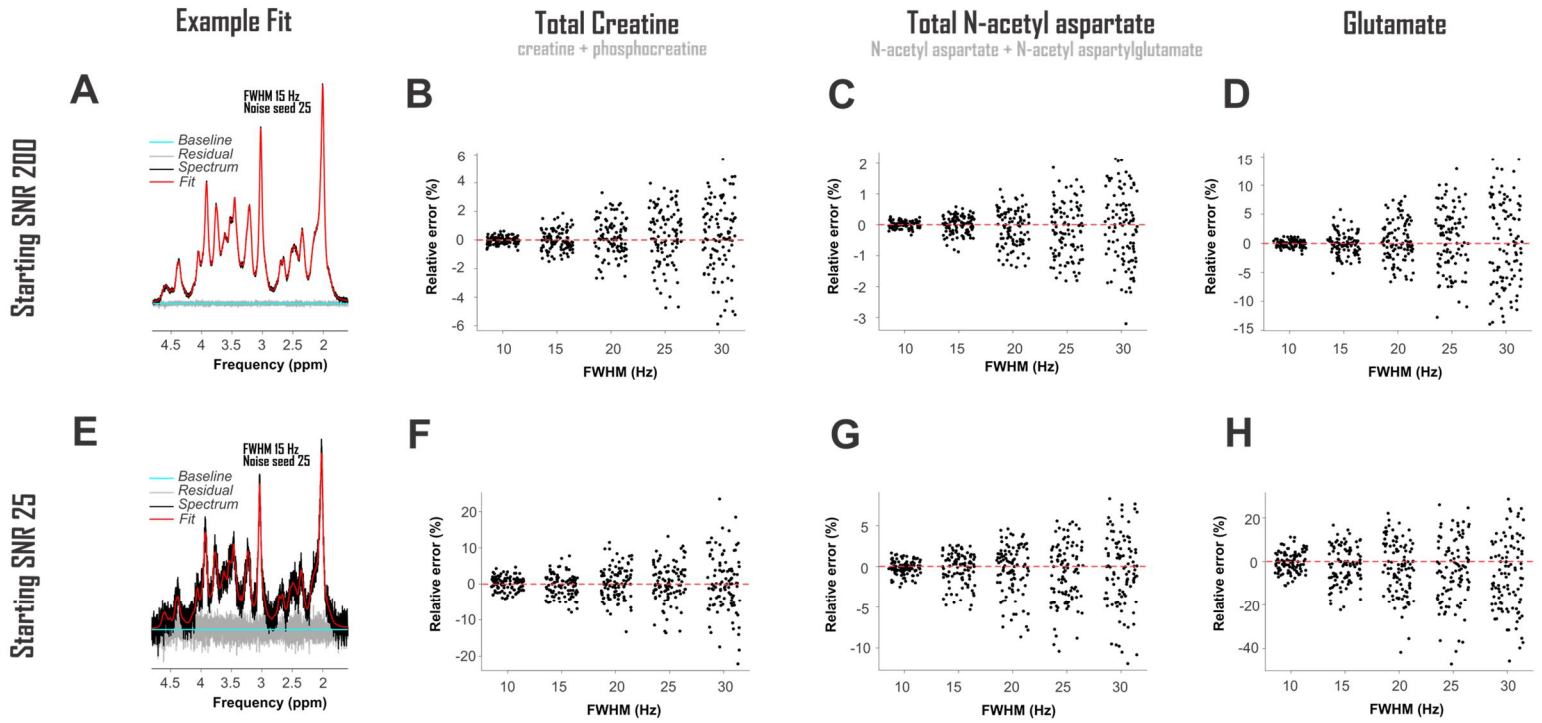

Figure 2.5. Linear combination model fit errors for total creatine, N-acetyl aspartate, and glutamate as measured by STEAM exhibit distinct relationships with spectral quality. Linear combination model fit errors exhibit differential sensitivity to spectral quality depending on the metabolite quantified, with glutamate quantification accuracy exhibiting higher sensitivity to full width at half maximum (FWHM) than that of either total creatine or NAA. With the 100 noise patterns applied here, glutamate also exhibited the strongest tendency among the three metabolites to systematic underestimation, especially at high FWHM and low signal-to-noise ratio (SNR). Displayed as appears in Swanberg et al. *Proc ISMRM* 2019, 4237.

became systematic loss of accuracy, and the linear association between Cramér-Rao Lower Bound and parameter standard deviation was broken. It therefore appears that baseline modeling technique contributes as substantially as, or more substantially than, spectral SNR and FWHM to the error inherent in metabolite concentration estimates derived by linear combination modeling, It also appears that the utility of the Cramér-Rao Lower Bound as a proxy for the lower bound of metabolite fit error standard deviations is affected by the relationship between spectral baselines in the data and linear combination modeling thereof. Further work along these two directions is therefore demanded and will be presented in the succeeding two sections.

2.3 Characterizing the influence of regularized cubic spline baseline inputs to linear combination model on precision and accuracy of spectral quantification

2.3.1. Motivation

It has been previously demonstrated in both Section 2 and by others that spectral quality interacts with insufficient baseline models to introduce systematic errors to apparent concentrations of metabolites quantified by ^{1}H MRS [113, 122]. While exceptions employing exactly scaled metabolite resonances combined with directly measured in vivo baselines exist [123], previous investigations into baseline model accuracy resemble the ongoing hunt for evidence-based ^{1}H MRS quantification guidelines at large in demanding but largely lacking validation methods both maximally meaningful and perfectly reliable [122, 124]. Spectroscopy on phantoms with known metabolite concentrations can enable quantification error measurement against a reasonably precise standard [125], but they do not reflect biologically realistic baseline conditions even if some gel preparations might approach in vivo-like spectral quality. Analyses of variances and/or means across brain regions [125], time points [106, 126], subjects [127, 128], or data centers [129]

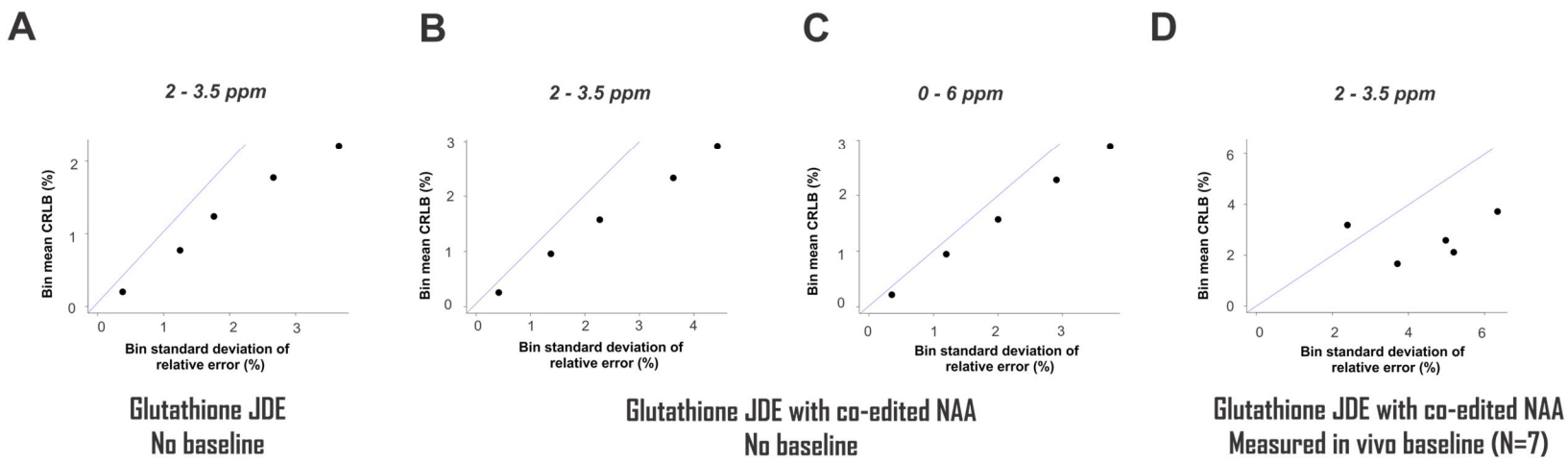

Figure 2.6. Underestimation of fit error standard deviation by Cramér-Rao Lower Bound is exacerbated by insufficient fit range and complicated baseline shapes. As evidenced by the greater deviation from identity (depicted as a blue line) of the relationship between Cramér-Rao Lower Bound (CRLB) and quantification error standard deviation, reported CRLB represents actual fit error more poorly when fits exhibit an insufficient frequency range for determining the spectral baseline (C to B) and inadequate information about complicated baseline shapes (B to D) in linear combination modeling of glutathione (GSH) with *J*-difference editing (JDE) to isolate the 2.95-ppm $^{7}CH_2$. NAA: N-acetyl aspartate. Adapted from Swanberg et al., *Proc ISMRM* 2019, 4237.

exhibit superior biological relevance to phantoms, but they lack known concentration standards. Both approaches involve acquisition error introduced even before quantification.

We address this extant need for evidence-based justification of baseline modeling approaches by using two validation pipelines that together combine the practical utility of in vivo data with the prior knowledge enabled by simulated standards. We use this paradigm to establish the influence of multiple baseline models, including splines with as-yet unexamined combinations of smoothing parameters and absolute knot intervals (Figure 2.7), direct fitting of macromolecule basis functions, and the previously endorsed subtraction of metabolite-nulled acquisitions [130], on macromolecule characterization and/or metabolite quantification accuracy of single-voxel short-echo time sLASER acquisitions in the healthy human cortex.

2.3.2. Methods

Experimental paradigm. Precision and accuracy of macromolecule and metabolite concentration estimation were assessed in two analysis pipelines for three classes of baseline model. The first class exploited novel spline baseline functionality written into INSPECTOR for the purpose of this analysis (details below) at sixteen different user-defined combinations of knot interval and smoothing coefficient λ. The second employed a basis set of macromolecules simulated for the pulse sequence at hand, similar to previous work [131]. The third subtracted corresponding metabolite-nulled acquisitions before spectral fitting with offsets (Figure 2.8A).

First, to examine macromolecule prediction precision and accuracy, we employed complex linear combination model (LCM) fits to in vivo metabolite spectra and compared generated baselines with corresponding metabolite-nulled acquisitions (Figure 2.8). LCM in INSPECTOR employed a 15-metabolite basis (Figure 2.8C) plus a complex cubic spline baseline

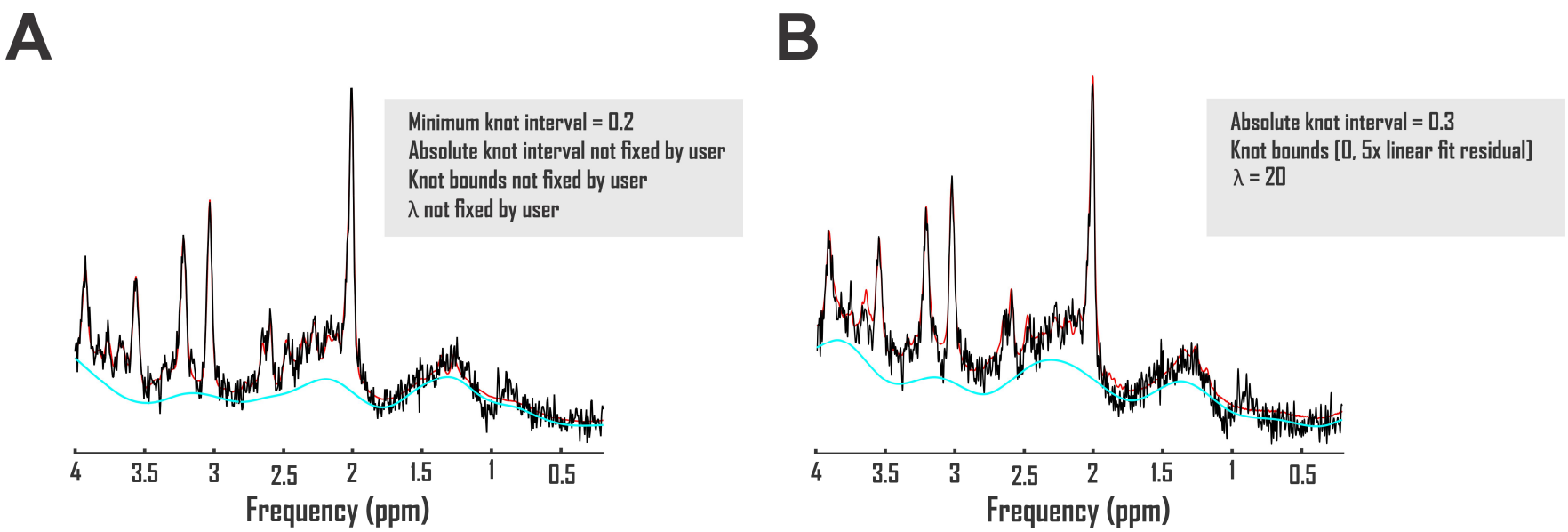

Figure 2.7. While ^{1}H MRS spectral baselines modeled by cubic splines are in wide use, their explicit optimization for particular experiment types is understudied. Cubic splines are commonly used in spectral fitting to account for in vivo baselines, as here with white matter test data acquired at 2 T (STEAM; T_E = 20 ms) from linear combination modeling program LCModel (A). Tools for their explicit definition and optimization, as developed in this chapter and here applied to analysis of the same test data in INSPECTOR (B), have been, however, lacking. Adapted from Swanberg et al., *Proc ISMRM* 2020, 2856.

that entered the optimization according to

$$B_k(\nu)+\lambda\|B''_k(\nu)\| \quad (6)$$

where $B_k(\nu)$ is the series of cubic splines expressed over fit frequency range ν and defined over evenly spaced knots of least-squares optimized ordinate, and λ a constant weight on the cost function thereof, as per previous work [20]. Knots were bound from 0 to 500% of offset-only baseline fit residuals. Fit baselines were compared with metabolite-nulled spectra from the same voxels cleaned of potential residual N-acetyl aspartate, creatine, and choline singlets by subtracting LCM fits. The integrated real differences between measured and modeled baselines were calculated over metabolite fit range 0.5-4.2 ppm (Figure 2.8D).

Second, to examine metabolite quantification precision and accuracy, the same models were used to fit an in vivo-like sLASER spectrum of known metabolite scaling and a sample cleaned prefrontal cortex macromolecule baseline from the previously described data set, with ten predefined patterns of additional Gaussian noise generating low SNR (55 from the 2.01-ppm N-acetyl aspartate $^2CH_3$). Relative errors of fit results were calculated against known metabolite scalings (Figure 2.8E) and compared among baseline models. Details of spectral data acquisition, processing, and quantification are provided below.

In vivo spectral acquisition. Data were acquired as described previously [131]. Briefly, scans were performed on a 3 Tesla clinical MR scanner (MAGNETOM Prisma, Siemens, Erlangen, Germany) and a 32-channel receive-only head coil (Siemens, Erlangen, Germany) at the Zuckerman Mind, Brain, and Behavior Institute within the Columbia University Magnetic Resonance Research Center (CMRRC). In vivo data were acquired in ten volunteers (five female; 23 ± S.D. 5 y.o.) with

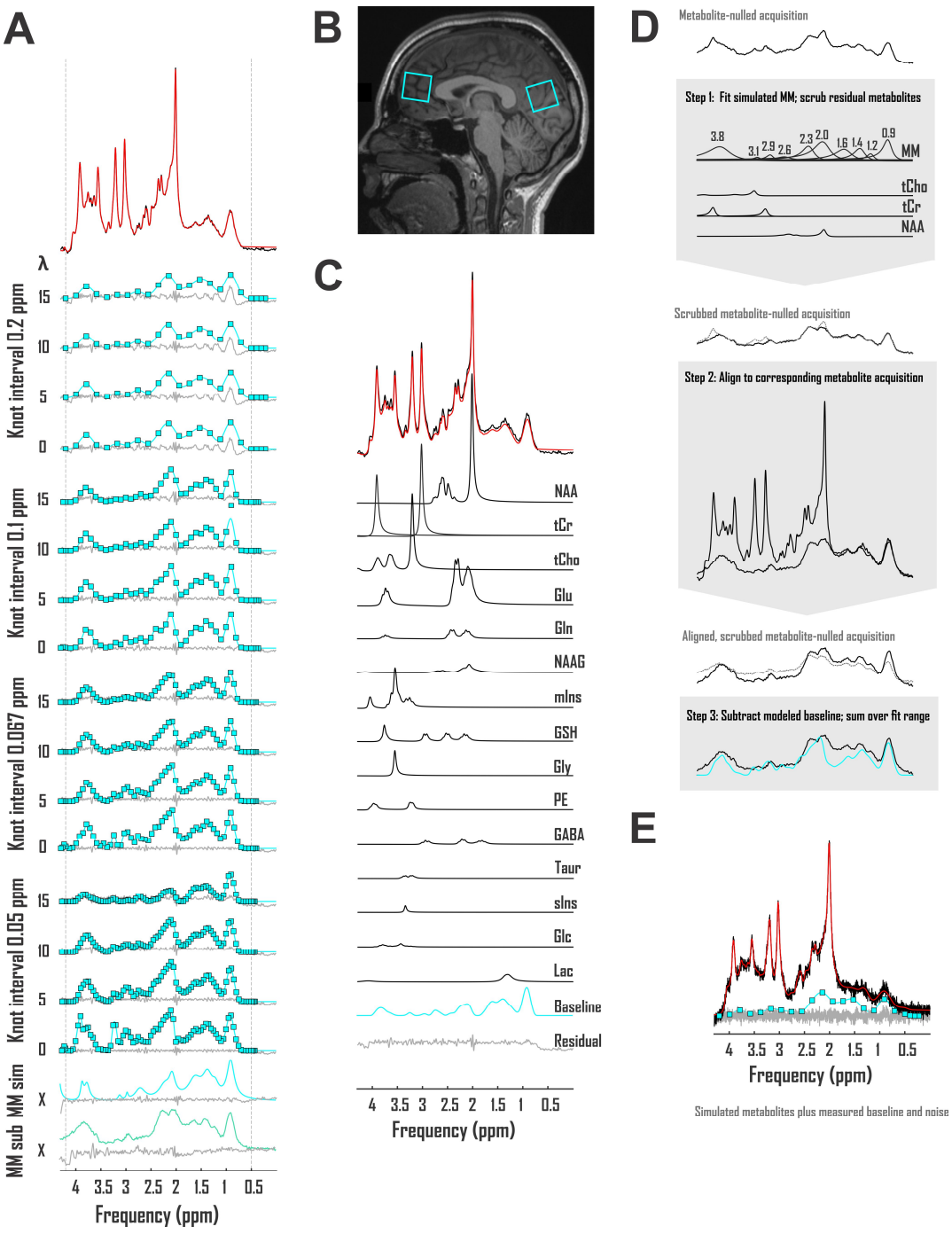

Figure 2.8. Experimental design for baseline handling fit quality, macromolecule prediction accuracy, and metabolite quantification precision and accuracy characterization. Cubic splines, simulated macromolecules (MM sim), or subtracted metabolite-nulled spectra (MM sub) handled frontal and occipital cortex 3 T sLASER (T_E = 20.1 ms) spectral baselines in 10 adults (B). Linear combination modeling (C) determined knot ordinates and signal scaling. Baseline model comparison to corresponding metabolite-nulled acquisitions assessed macromolecule prediction accuracy (D); fits to simulated metabolites of predefined scaling summed with a frontal cortex metabolite-nulled spectrum assessed metabolite fit accuracy (E). Displayed as appears in Swanberg et al., *Proc ISMRM* 2020, 2856.

the prior approval of and in accordance with standards set forth by the Columbia University Institutional Review Board for human subjects research.

Placement of a 2.5- to 3-cm isotropic voxel at midline of frontal or occipital cortex was effected with reference to scans by a T_1-weighted MPRAGE (field of view 25.6 x 25.6 x 19.2 cm, matrix size 256 x 256 x 192, echo time T_E 2.26 ms, repetition time T_R 2.3 s, inversion time T_I 0.9 s). Up through second-order spherical-harmonics B_0 shims were applied according to calculations on gradient-echo images at three T_E (FOV 19.72 x 21.76 x 7.2 cm, matrix size 58 x 64 x 24, T_E 2.46, 4.61, 7.09 ms, ms, T_R 0.231 s) in laboratory-developed software B0DETOX.

Metabolite spectra were acquired via semi-Localization by Adiabatic Selective Refocusing (sLASER; T_E 20.1 ms, T_R 2 s, number of repetitions N_R 128). Water suppression was achieved with a seven-pulse VAriable Pulse and Optimized Relaxation (VAPOR) module with sequence-optimized crushers [132] and 16-step phase cycling [133]. Water-unsuppressed references were acquired in order to correct metabolite scans for eddy currents by the Klose method [118]. Corresponding metabolite-nulled spectra were acquired via an identical sequence with a double inversion-recovery preparation (T_{I1} 920 ms, T_{I2} 330 ms) for metabolite nullification.

In vivo spectral processing. Spectra were acquired at 2048 complex points. Individual traces were eddy-current-corrected as described previously and phase- and frequency-aligned over coil channels and repetitions. Residual water was removed using Hankel singular value decomposition. Resultant preprocessed spectra were employed in linear combination model fits.

Because T_1 differences among metabolites were expected to engender their high but still incomplete nullification by the double inversion-recovery preparation of this sequence,

metabolite-nulled spectra used in the macromolecule subtraction condition of baseline handling (below) as well as for comparison with modeled baselines were further preprocessed via removal of residual metabolite singlets obtained by linear combination model fitting as detailed in 2.2.4. Metabolite-nulled spectra were otherwise preprocessed identically to metabolite spectra except that following averaging and scrubbing for residual metabolites these data sets were also aligned by frequency calibration, zero-order phasing, scaling, Lorentzian line broadening, and zero-order polynomial (offset) to corresponding metabolite spectra to maximize correspondence between the two for further processing and comparison (Figure 2.8D).

In vivo spectral linear combination model fitting. Linear combination modeling was applied in laboratory-written MATLAB-based spectral processing and quantification toolkit INSPECTOR on preprocessed metabolite and metabolite-nulled spectra sequence-specific basis functions density-matrix simulated in laboratory-written MARSS software [134]. Spectral basis sets for metabolite fits included N-acetyl aspartate, total choline (choline and glycerophosphocholine), creatine, glutamate, glutamine, N-acetyl aspartylglutamate, myoinositol, glutathione, glycine, phosphorylethanolamine, GABA, taurine, scylloinositol, glucose, and lactate. Basis resonances for creatine were split between those with and without the 3.91-ppm singlet to account for potential T_1-weighted variability in signal amplitudes; resultant amplitudes on each basis function were averaged to give the arbitrary-unit scaling for total creatine. Metabolite fits allowed global zero-order phasing and basis function-specific frequency shifting, Lorentzian line broadening, and scaling with one of eighteen different baseline handling techniques, including sixteen regularized cubic splines (knot intervals 0.05, 0.067, 0.1, or 0.2 ppm; smoothing lambda 0, 5, 10, or 15), inclusion of simulated macromolecules in linear combination model basis sets as Gaussian peaks

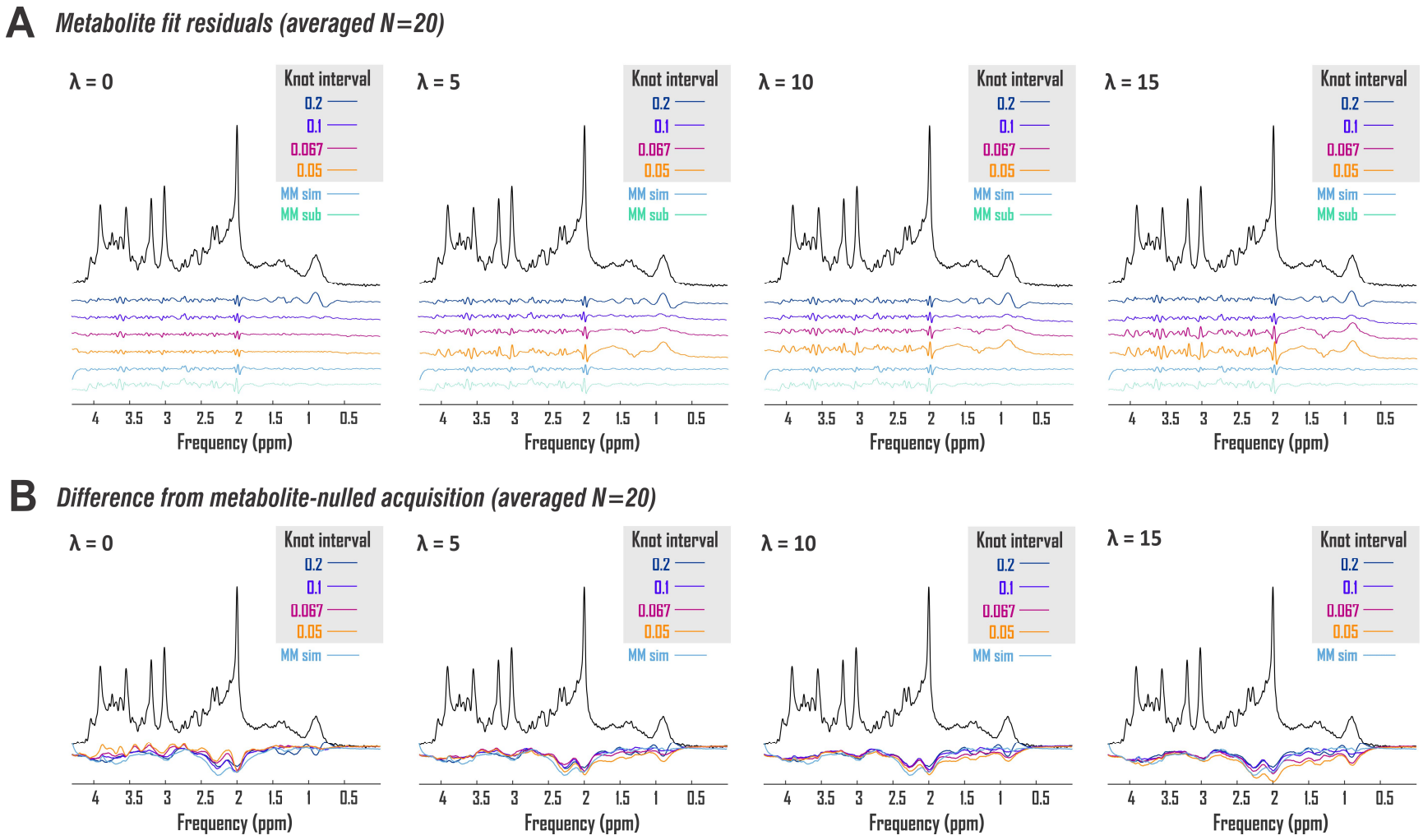

Figure 2.9. Spline baseline model effects on fit residuals and prediction of corresponding metabolite-nulled spectral lineshapes. Accounting for macromolecule signals in the baseline using simulated resonances yields generally smaller residuals (A) but does not resemble corresponding metabolite-nulled acquisitions better than splines, particularly below the 2.01-ppm N-acetyl aspartate peak (B). Correspondingly, the most flexible spline baseline definitions (low smoothing λ and high number of knot points per frequency interval) yielded smaller residuals without commensurate improvement in baseline prediction accuracy. Displayed as appears in Swanberg et al., *Proc ISMRM* 2020, 2856.

at defined chemical shifts (0.9, 1.2, 1.4, 1.6, 2.0, 2.3, 2.6, 2.9, 3.1, and 3.8 ppm), and direct subtraction of preprocessed, scrubbed, and aligned metabolite-nulled acquisitions from the same experiment and voxel. Scrubbing of residual singlets from metabolite-nulled spectra was achieved by linear combination modeling with a basis set of the aforementioned Gaussians for macromolecule shapes plus singlets expected for N-acetyl aspartate, total choline, and creatine (Figure 2.8D). Fitting was achieved as for metabolite spectra except that macromolecule basis functions were accorded wider signal-specific margins than metabolite singlets for not only Lorentzian but also Gaussian lineshape broadening.

Error and statistical analysis. Calculations of relative fit errors and data visualization were performed in R (v. 3.4.4; R Foundation for Statistical Computing, Vienna, Austria). Hypothesis testing was conducted by two-tailed independent t-test assuming heteroscedasticity with uncorrected α=0.05.

2.3.3. Results and Discussion

Spline fit residuals generally exceeded those using other baseline models, increasing with λ (Figure 2.9A). Modeled baseline differences from corresponding metabolite-nulled acquisitions were, however, greater than suggested by fit residuals, especially for simulated macromolecule baselines (Figure 2.9B). This corresponded to mean overestimations of key metabolites, more pronounced in fits with simulated macromolecules than splines for total creatine (15.3±73.5% vs. 0.98±88.5%; $t(12)=5.34$, $p<0.001$) and glutamate + glutamine (34.1±95.3% vs. 0.5±481.2%; $t(17)=9.96$, $p<0.001$), while systematic metabolite underestimations were observed in fits to noisy data that first subtracted fitted metabolite-nulled acquisitions, which nevertheless demonstrated reduced

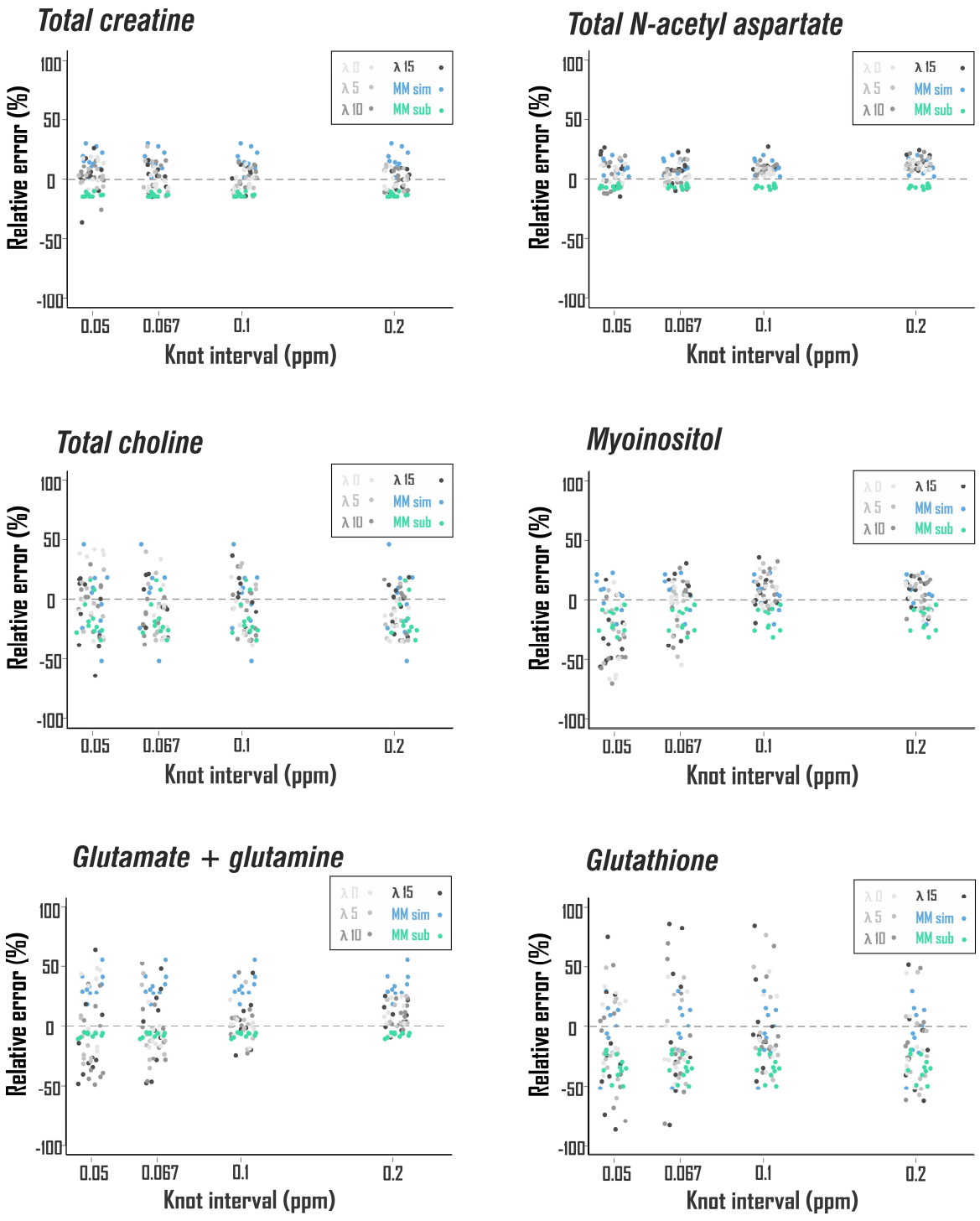

Figure 2.10. Effect of baseline model on systematic metabolite fit errors of noisy simulated spectra with in vivo baselines. Simulating macromolecules (MM sim) to account for spectral fit baselines did not outperform splines to avoid overestimation of key metabolites like N-acetyl aspartate, creatine, and glutamate + glutamine. Subtracting aligned, scaled metabolite-nulled acquisitions (MM sub) prior to fitting also yielded systematic errors, namely underestimation, in quantifying these key metabolites. Notably, glutathione yields particularly error-prone and unreliable fits in this non-edited localization sequence, as expected. Displayed as appears in Swanberg et al., *Proc ISMRM* 2020, 2856.

variability and greater proximity to zero error than models employing simulated macromolecule baselines for key metabolites total creatine and glutamate + glutamine (Figure 2.10).

Among linear combination models employing regularized cubic splines for baseline handling, both λ and frequency interval between subsequent knot points appeared to exhibit a significant effect on metabolite quantification accuracy. For example, for commonly assessed metabolite total N-acetyl aspartate, systematic overestimation of concentration was larger in those models using the most flexible baseline fits (λ 0 or 5) than those using stiffer baseline models (λ 10 or 15) (9.0±88.7% vs. 5.9±43.4%; $t(156)=2.477$, $p<0.05$). Similarly, greater overestimation of total N-acetyl aspartate was also seen with regularized cubic spline baseline models using the widest two knot intervals than those employing the most narrow two (10.8±28.0% vs. 4.1±86.0%; $t(138)=5.895$, $p<0.001$) (Figure 2.10).

Combining the utility of in vivo measurements with the perfect knowledge of simulated gold standards, we show that baselines of simulated macromolecules do not necessarily outperform splines in either macromolecule or metabolite prediction accuracy. We additionally demonstrate that for at least some metabolites, quantification pipelines employing prior knowledge from metabolite-nulled acquisitions appeared to exhibit superior spectral quantification accuracy and precision to those using baselines with simulated macromolecules. Finally, we observed that all three classes of baseline model—spline, simulated, and subtracted—when taken as a whole exhibited some degree of systematic quantification error against noisy data with in vivo baselines. Notably, our observation of N-acetyl aspartate overestimation by splines with fewer knots agrees with previous analysis of low-SNR data despite differing acquisition and validation paradigms [113].

2.3.4. Limitations and Conclusions

The batch spectral simulation and quantification paradigm presented herein constitutes a novel approach to combining the ground truth of simulated spectra with the in vivo generalizability of measured macromolecule baselines. Via this setup we report some key insights into the effects of baseline modeling strategy on expected spectral quantification precision and, importantly, accuracy for several key metabolites within the context of short-T_E sLASER proton ^{1}H-MRS acquisitions in the human cortex. First, replicating a finding first reported in Section 1 with the transformation of zero-centered loss of precision to systematic loss of accuracy in *J*-difference-edited spectra without and with in vivo like baselines and attendant modeling thereof, we continued to observe persistent systematic errors in metabolite quantification accuracy, not just variability in metabolite quantification precision, in linear combination model fits to in vivo like simulated spectral standards involving in vivo measured baseline resonances as nuisance signals. Second, spectral fit residuals are poor indicators of a linear combination model's accuracy in representing the various features of a spectral data set, as those models with the smallest visible residuals did not performed visibly better in macromolecule prediction or metabolite quantification; in fact, for the case of at least one metabolite total N-acetyl aspartate, the most flexible baselines yielding the smallest residuals demonstrated exacerbated concentration overestimates relative to those stiffer baselines yielding larger and more structured fit residuals. Third, direct numerical modeling of baseline resonances via regularized cubic splines is not necessarily outperformed in metabolite quantification accuracy by more commonly accepted approaches accounting for macromolecule resonances in the spectral baseline by simulating or subtracting them.

It is important, however, to contextualize these findings within the single field strength and pulse sequence plus protocol employed in this series of simulations and be wary of

generalizing too readily to other field strengths and acquisition schemes. The expected spectral appearance of many metabolites may change, sometimes dramatically, with acquisition sequence and input parameters like T_E, rendering specific conclusions about the degree of systematic metabolite over-or underestimation expected for a particular baseline modeling approach within the presently reported paradigm difficult to apply with confidence to all experimental situations. Furthermore, expected T_1-based macromolecule amplitude differences between metabolite-inclusive and -nulled acquisitions limit the usefulness of comparison between modeled spectra and these measured acquisitions: Namely, the macromolecule baselines underlying a real short-T_E sequence are expected to exhibit slightly different resonance-specific relative amplitude weightings from those added to these simulated spectral standards, further changing the specific effects of individual baselines on the individual metabolite quantification errors expected for certain modeling approaches. For assessing spectral fit errors (at least with regard to precision around a certain mean which may or may not be itself accurate), the linear, if not identity, association between the standard deviation of error in relative metabolite concentration estimates, not available for experiments lacking known ground truth, and Cramér-Rao Lower Bound, calculated from a linear combination model's Fisher information matrix available regardless of the presence of a known ground truth, becomes paramount. Since this relationship was demonstrated in Section 1 to break in the presence of spectral baselines, work toward restoring the accuracy of the Cramér-Rao Lower Bound even in in vivo spectra involving underlying baseline signals (i.e., nearly all of them) demanding consideration by the models used to quantify them.

Even with these caveats, however, taken together, our findings underline both the feasibility of and critical need for various baseline handling approaches within different spectral quantification pipelines to be informed by rigorous validation against meaningful but well

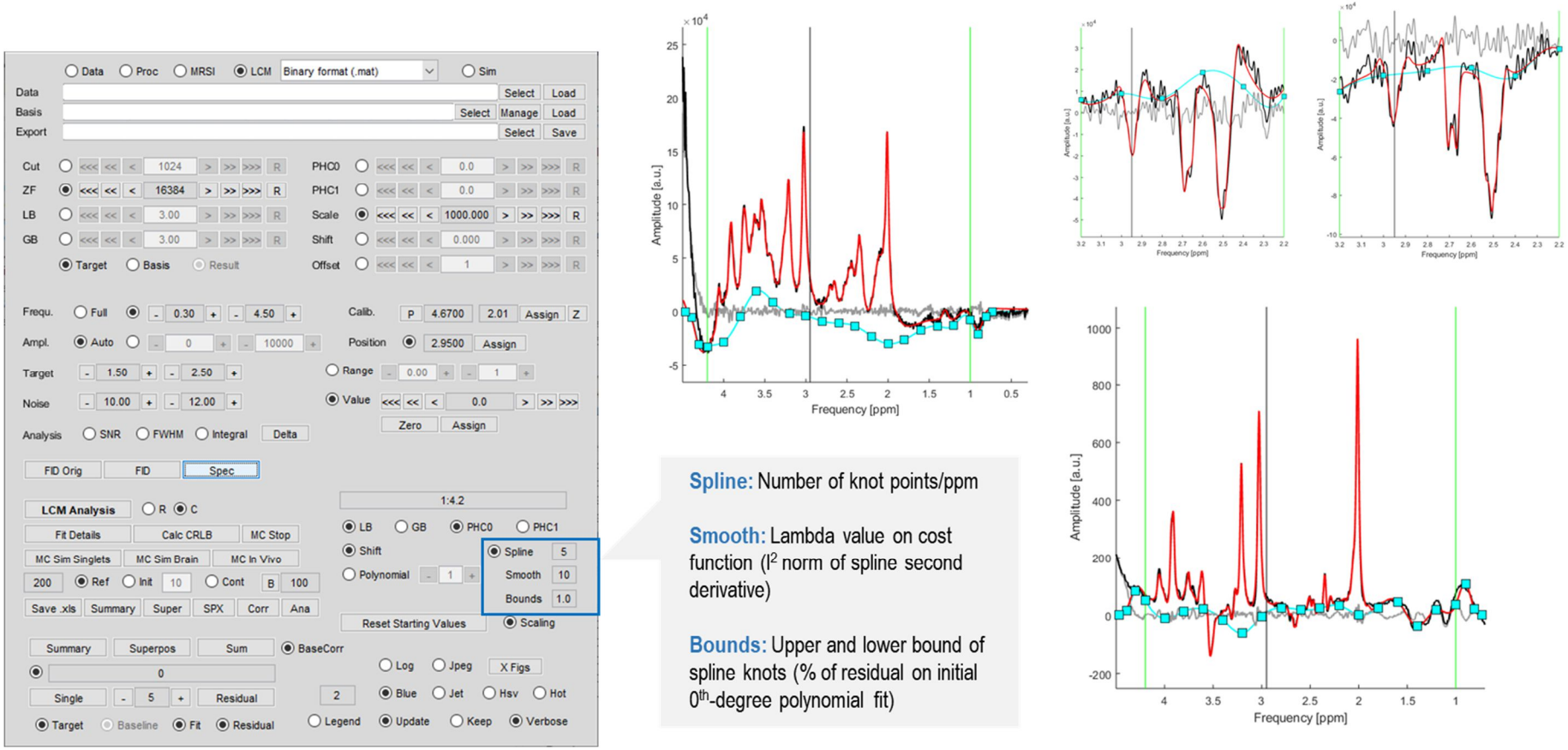

Figure 2.11. The user-defined regularized cubic spline baseline handling procedure designed and developed in this chapter was implemented for user-friendly employment by others into the INSPECTOR framework. Within this functionality, built as an extension upon existing procedures for handling non-piecewise polynomial baselines, users can define the spectral frequency interval between cubic spline knot points, the linear weighting λ on regularization term defined according to the norm of baseline second derivative as in Equation 6, and symmetric bounds on calculated knot ordinates as percent of initial linear-baseline fit residuals.

characterized standards, especially for in vivo experiments that cannot be corrected by subtraction of dedicated metabolite-nulled acquisitions. In this section we have not only presented the results for such a pipeline but also implemented the transparent and user-defined baseline handling functions necessary for executing it into spectral processing analysis freeware toolkit INSPECTOR to enable its wider application in the field at large (Figure 2.11).

4 Calculation and performance validation of analytic Cramér-Rao Lower Bounds for spline baseline shapes

2.4.1. Motivation

Recent efforts have been made toward standardizing, among other practices, the acquisition [91, 135, 136], analysis [137], and reporting [138] of proton MRS data. Many questions remain, however, about what standards should be applied to a number of details important to spectral quantification, including optimal numerical fit algorithms, whether and how to use postprocessing corrections for residual water or deviations from Lorentzian lineshape, and the best approach for modeling spectral baselines under imperfect prior knowledge. Building understanding of the conditionally optimal solutions for each of these outstanding questions requires reliable measurement of quantification errors yielded by each, particularly those applied to in vivo experimentation that lack ground truth for comparison. Since the rise of spectral quantification by linear combination models built upon prior knowledge functions [139] the Cramér-Rao Lower Bound (CRLB) [121, 140] has been historically used for this purpose. To correctly represent the lowest bound of standard deviation on estimated metabolite concentrations (absolute) or concentration error (scaled), CRLB must be calculated from an information matrix that represents a complete fit model [140]; in line with this, previous results suggest that metabolite amplitude

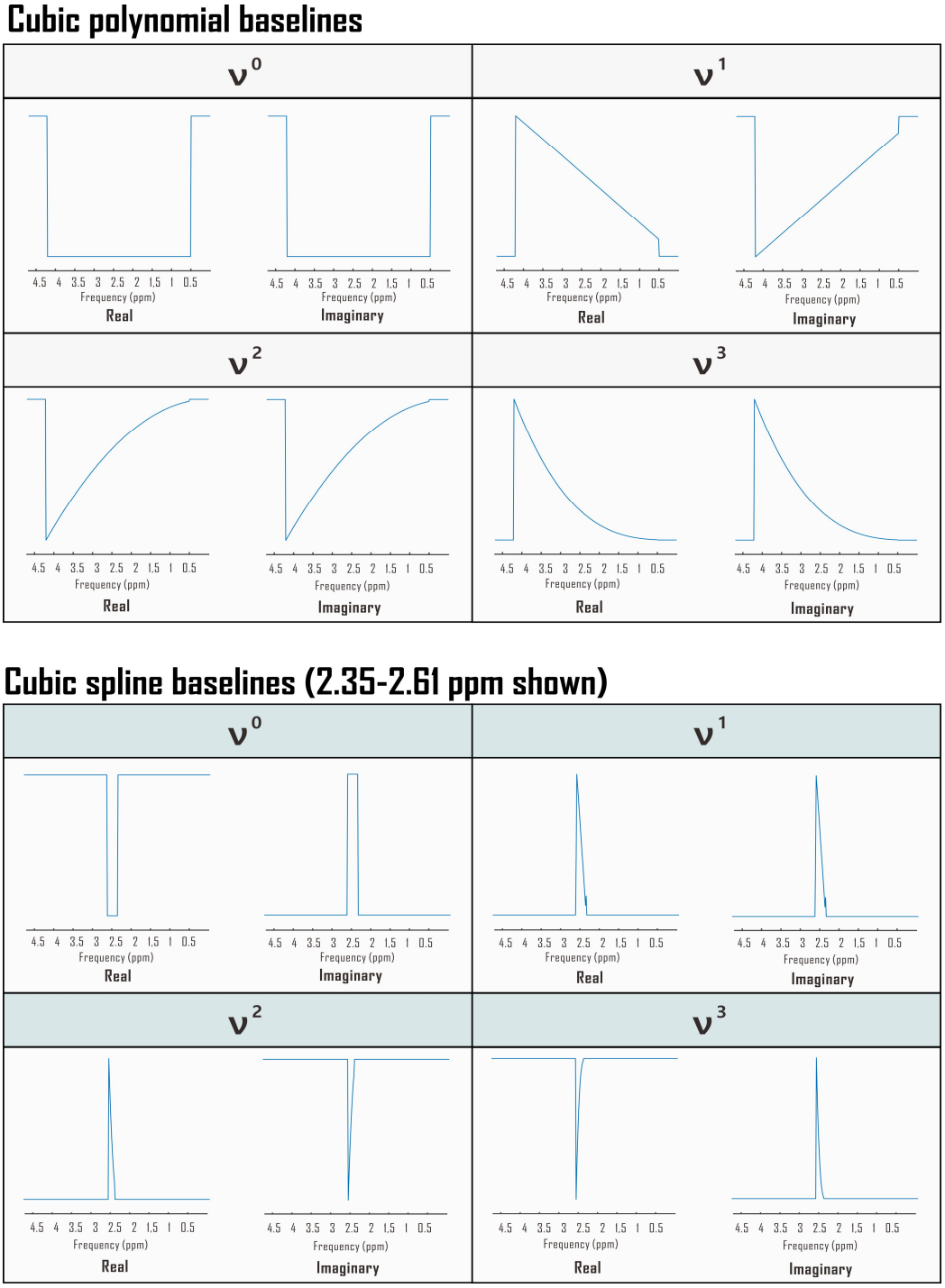

Figure 2.12. Partial derivatives of linear combination model with respect to complex baseline shapes for Fisher information matrix calculation. Shown here are the Fourier transforms of example real and imaginary polynomial and spline baseline components incorporated into the Fisher information matrix used to estimate Cramér-Rao Lower Bounds (CRLB) for linear combination model fits to simulated in vivo sLASER (T_E 20.1 ms) metabolite proton spectra. Each shape is scaled by its corresponding polynomial coefficient for direct calculation of relative CRLBs. ppm: parts per million. Displayed as appears in Swanberg et al., *Proc ISMRM* 2021, 2010.

CRLB are significantly affected by the presence of baseline accommodations in their calculation [141-144].

It has been argued that spectral baselines cannot be represented by analytical functions [13], preventing their inclusion in the Fisher information matrix. Given some measure of uncertainty surrounding the physical-chemical properties of characterized spin systems, however, the difference in the integrity of prior knowledge underpinning spectral baseline and metabolite lineshapes is a matter of degree and not a binary state. It is therefore important to empirically address the practical implications of this theoretical argument, because including baseline terms in a linear combination model and consequently Cramér-Rao Lower Bound calculations affects both metabolite CRLB as mentioned and metabolite quantification accuracy [113, 122, 145].

In this work we treat baselines as overlapping piecewise polynomial shapes akin to metabolite basis functions in order to include them in the Fisher information matrix for calculation of CRLBs on their amplitudes. We thereby assess the degree to which these and metabolite amplitude CRLBs represent the standard deviations of corresponding parameter estimates in fully determined spectral fits including heavily overlapping polynomial or spline baselines.

2.4.2. Methods

CRLB for linear combination model parameters were calculated by inversion of the fit Fisher information matrix, with

$$F = \frac{1}{\sigma^2}\Re(P^T D^H D P) \tag{7}$$

where σ is the standard deviation of 1-ppm interval of noise, D is the matrix of model partial

derivatives w.r.t. each model fit parameter for which CRLB are calculated, and P is the prior knowledge matrix collapsing linear dependence in D [121]. Baseline CRLB were estimated by entering their partial derivatives into D as the inverse Fourier transforms of either full or piecewise polynomial shapes. Piecewise spline polynomials were smoothed for CRLB calculation to mitigate jump discontinuities from zero within the spectral fit range and consequent time-domain Gibbs' ringing artifacts (Figure 2.12). Validation analyses employed a MARSS [134]-simulated sLASER (T_E = 20.1 ms, T_R 2 s, N_R 128) metabolite spectrum acquired on a 3 T MAGNETOM Prisma (Siemens Healthineers, Erlangen, Germany) (Figure 2.13) line-broadened 6 Hz, frequency-shifted, and scaled including a cubic polynomial baseline to an analogous prefrontal cortex (PFC) acquisition [131].

Simulated complex cubic polynomial or complex smoothed cubic spline baselines calculated as presented in Section 2 were derived from LCM fits to the in vivo alignment reference following measured macromolecule subtraction; spline knot interval and smoothing λ were optimized for minimum between-subjects tNAA/tCr coefficient of variation across LCM fits to PFC spectra from 10 healthy adults (5 female, 23 ± S.D. 5 y.o., <27 cm^3 cubic voxels) similar to and including the alignment reference [131] (Figure 2.14).

This preprocessed simulated brain spectrum was summed with either the polynomial (Analysis I) or spline (Analysis II) baseline and then scaled to ten linearly spaced SNR from 18 to 180 (signal from 3.03-ppm creatine). The same 50 complex Gaussian noise patterns were then added to each SNR group, with noiseless references retained for relative error calculation, for 510 simulated spectra per analysis. Spectral quantification by LCM, including baseline modeling and CRLB calculations, was then performed on these simulated spectra by scripting in INSPECTOR. Calculations of fit errors, group statistics, and Bonferroni (N=10)-corrected Shapiro-Wilk analyses

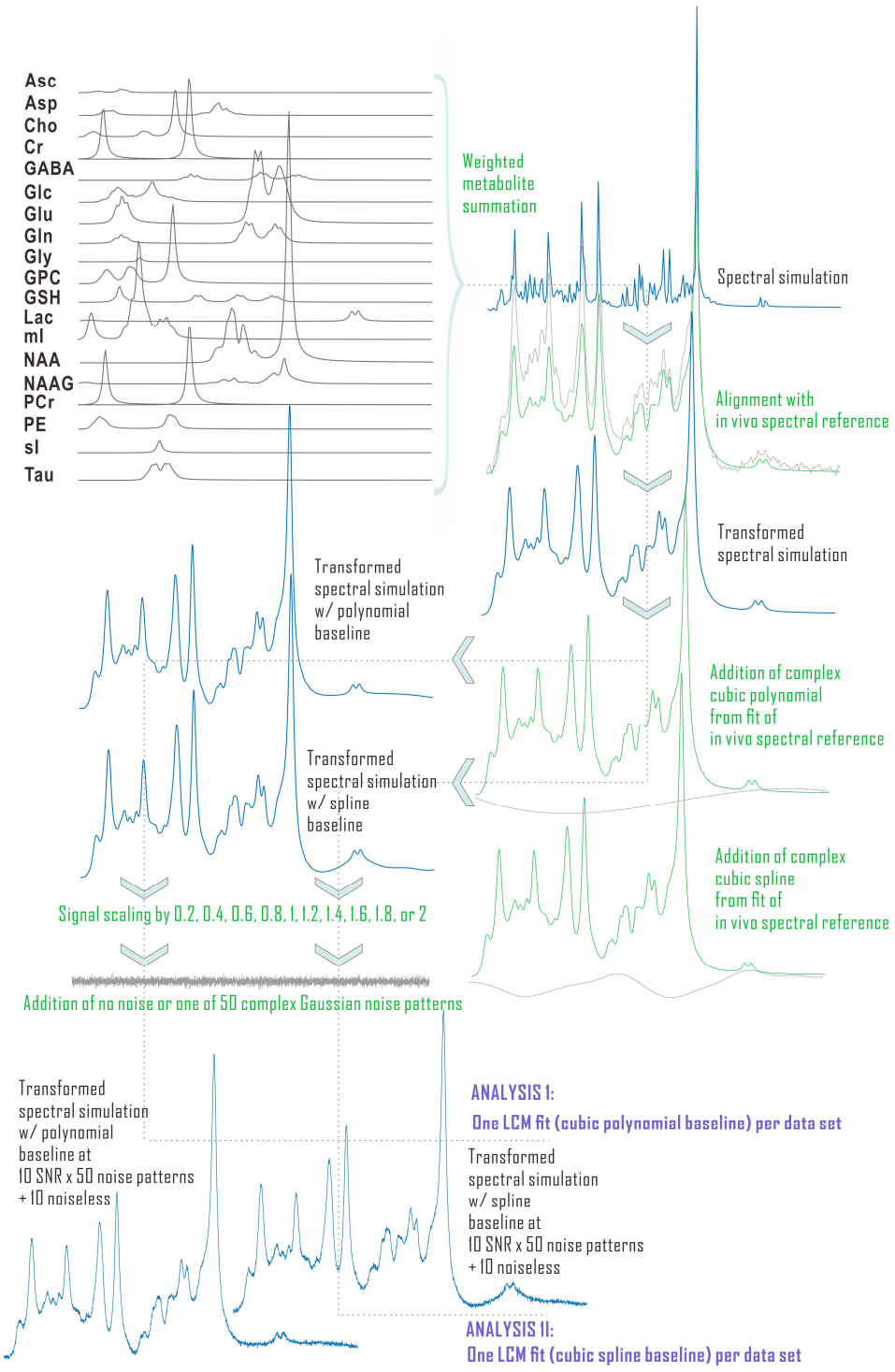

Figure 2.13. Numerical pipeline for validating metabolite and baseline amplitude Cramér-Rao Lower Bounds against observed distributions of estimated fit parameters. Noisy (500 per analysis) simulated metabolite spectra with known polynomial or spline baselines were generated to compare calculated baseline CRLBs with standard deviations of baseline parameters obtained by linear combination model fitting. Noiseless fits (10 per analysis) were used as standards for estimates of fit parameter error. LCM: linear combination model. Adapted from Swanberg et al., *Proc ISMRM* 2021, 2010.

for normality of observed fit parameter distributions were performed in R (v. 3.4.4; R Foundation for Statistical Computing, Vienna, Austria).

2.4.3. Results and Discussion

In Analysis I, CRLB for complex polynomial baseline shapes demonstrated linear relationships with standard deviations of parameter difference from noiseless fits, both values normalized to actual fit coefficients (Figure 2.15). Baseline handling by splines with knot interval 0.25 and smoothing lambda 5 supported the lowest coefficients of variation in tNAA/tCr (Figure 2.14); these inputs were thus used to constitute the modeled spline baseline standard against which spline fit errors and CRLB were measured. Like single polynomial shapes, in Analysis II CRLB for complex piecewise polynomials within splines also demonstrated linear relationships with coefficient errors against those of noiseless fits, though some deviations from identity were observed (Figure 2.15). Including either polynomial or spline baseline shapes in the Fisher information matrix improved correspondence between calculated CRLBs and observed standard deviations of metabolite fit amplitudes (Figure 2.16).

Taken together, these results demonstrate the following:

- Cramér-Rao Lower Bounds calculated on baseline shapes analogously to metabolite bases can estimate fit amplitude standard deviations on polynomials and inform those for piecewise smoothed splines, despite the fact that for the latter the standard deviation of observed fit amplitudes is expected to be constrained by smoothing and neighboring pieces

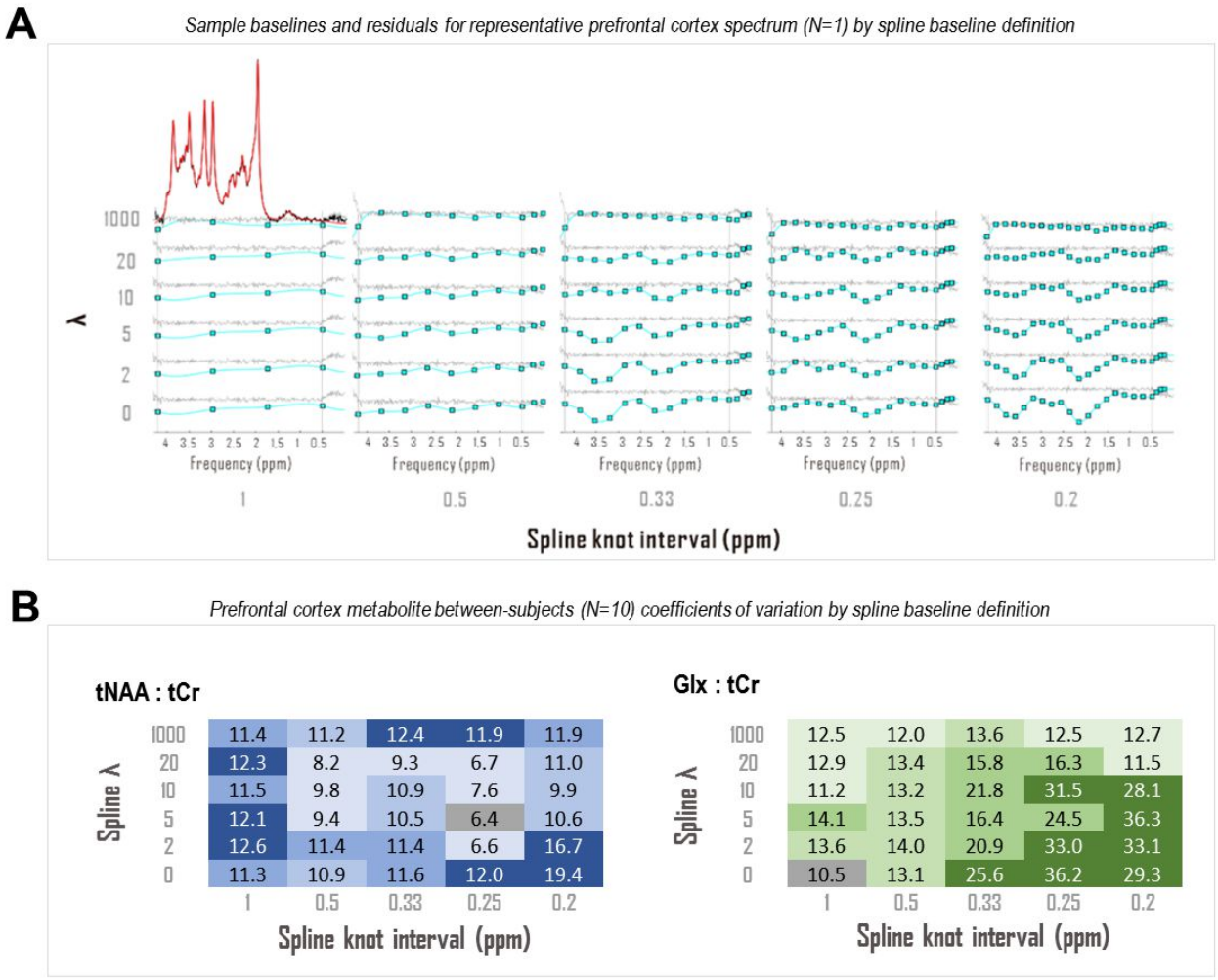

Figure 2.14. Simulated spline baseline optimization. To create an in vivo-like simulated spline baseline, macromolecule-subtracted prefrontal cortex sLASER (T_E 20.1 ms, T_R 2 s, N_R 128, ≤27 cm^3 cubic voxels) spectra (N=10; 5 female, 23 ± S.D. 5 y.o.) were fit with metabolite bases and various splines (A), with splines yielding minimum between-subjects coefficient of variation (CV) boxed in grey (B). Note that multitudinous baseline definitions contribute to visually similar residuals despite divergent CVs. tNAA: total N-acetyl aspartate; tCr: total creatine; Glx: glutamate + glutamine; ppm: parts per million. Displayed as appears in Swanberg et al., *Proc ISMRM* 2021, 2010.

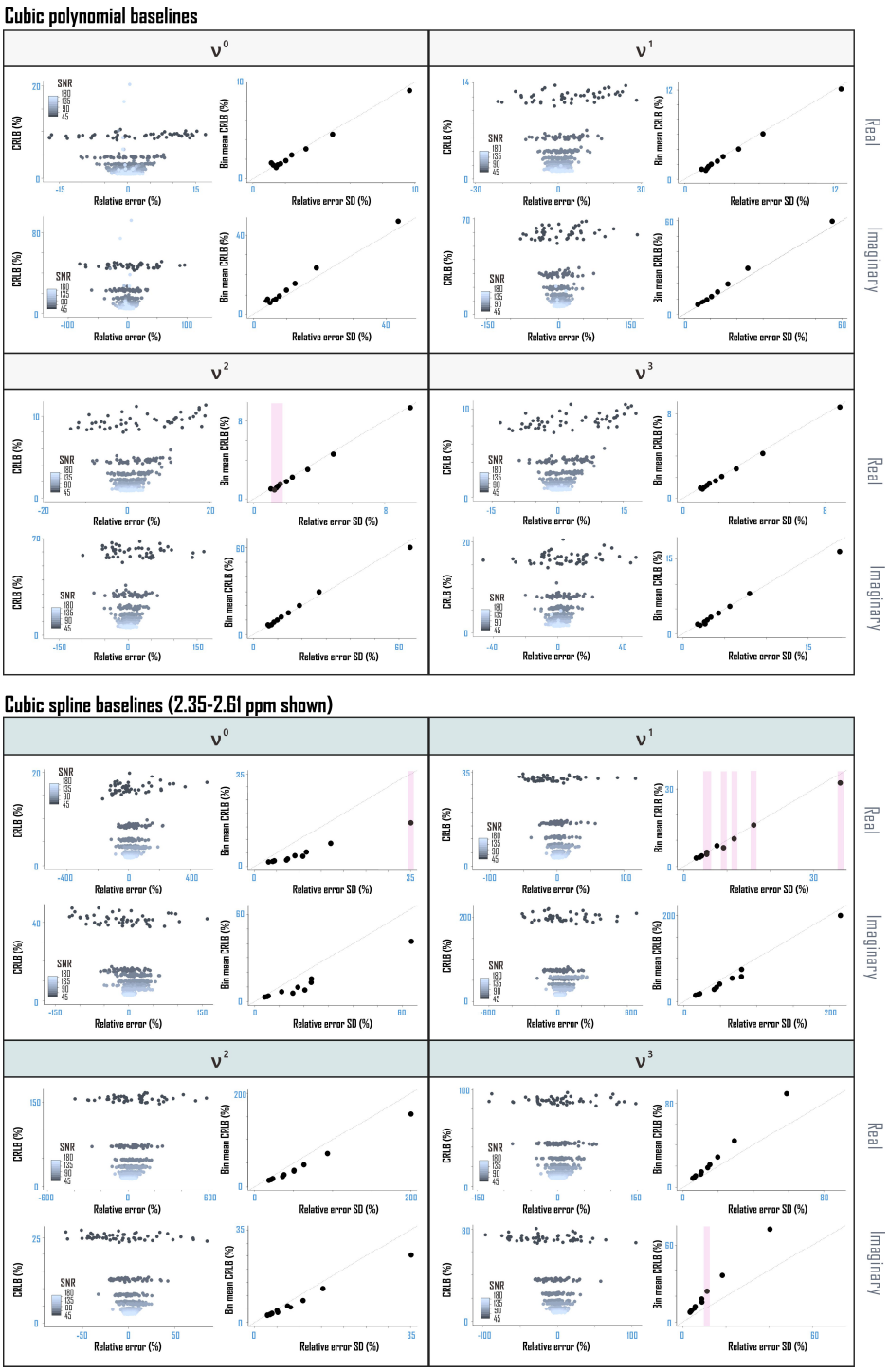

Figure 2.15. Baseline amplitude Cramér-Rao Lower Bounds (CRLB) closely resemble standard deviations of fit amplitude estimates. Relative CRLB and amplitude estimate standard deviations (S.D.) by SNR are normalized to the same noiseless fit standards. For maximum correspondence with Figure 2.16, spline results are for an interval near N-acetyl aspartate and glutamate. Non-normal distributions (pink), for which S.D. may not be an appropriate measure of parameter variability, were found more often for spline than polynomial baseline fit amplitudes. ppm: parts per million. Displayed as appears in Swanberg et al., *Proc ISMRM* 2021, 2010.

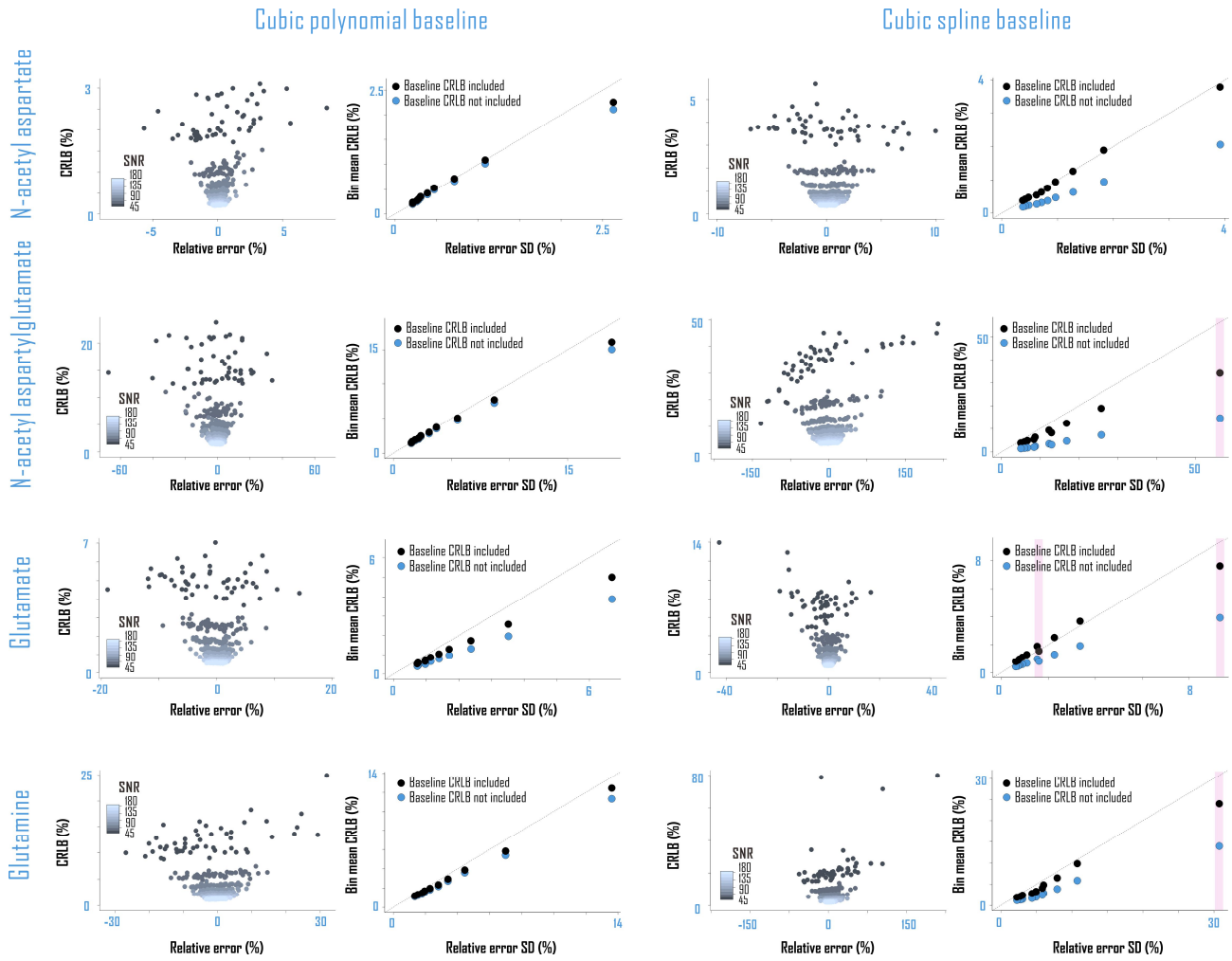

Figure 2.16. Baseline Cramér-Rao Lower Bounds (CRLB) improved metabolite CRLB accuracy. Calculating amplitude CRLBs for polynomial or spline baselines directly from the Fisher information matrix improved correspondence between metabolite amplitude CRLBs and parameter estimate standard deviations (S.D.) by SNR (before=blue; after=black). Correspondent with Figure 2.15, non-normal distributions (pink), for which S.D. may not be an appropriate measure of parameter variability, were observed more often for fits using spline than polynomial baselines. ppm: parts per million. Displayed as appears in Swanberg et al., *Proc ISMRM* 2021, 2010.

in a manner not represented in the straightforward calculation of CRLBs from the Fisher information matrix.

- Incorporating either polynomial or spline baseline shape information directly into the Fisher information matrix can improve the correspondence between calculated CRLBs and observed standard deviations of metabolite fit amplitudes.

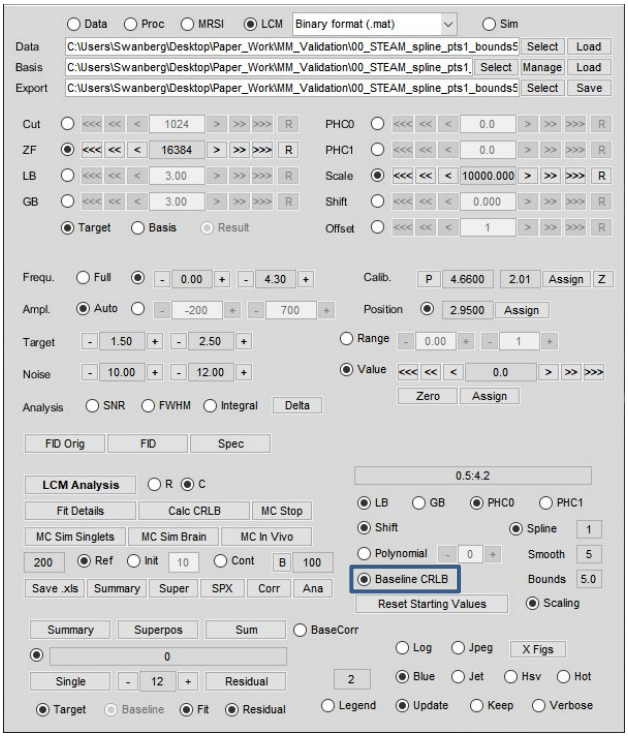

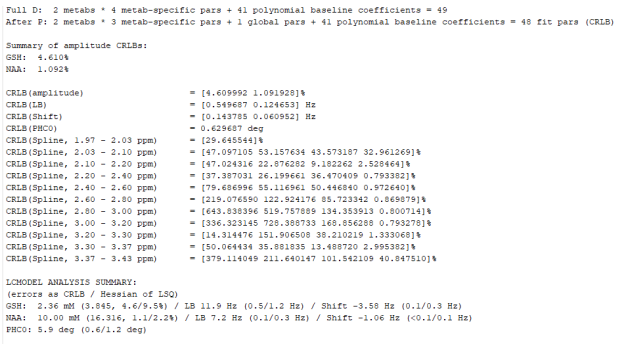

Figure 2.17. The incorporation of polynomial and piecewise cubic spline baseline shapes into Cramér-Rao Lower Bound calculations for linear combination model fits as designed, developed, and tested in this chapter was written as an extension of the INSPECTOR framework. This functionality provides separate CRLB for each polynomial degree within a spectral baseline shape (piecewise by frequency-dependent knot points for cubic splines) and, in addition to tracking linearly with baseline polynomial coefficient error standard deviations as shown in Figure 2.15, also improves correspondence between metabolite CRLB and amplitude estimate error standard deviations as shown in Figure 2.16.

Our implementation of this foundation for characterizing the precision of spectral baseline parameter estimates via Cramér-Rao Lower Bounds enables further systematic elaboration thereof. These include modifications accounting for expected disruptions to parameter estimate normality by model constraints, i.e., on the knots of piecewise splines by neighboring pieces, as well as investigations into the degree to which baseline CRLBs calculated in this manner can further improve CRLB estimates for metabolite amplitudes in cases of greater uncertainty regarding

baseline models for the spectral data sets at hand, i.e., in vivo.

2.4.4. Limitations and Conclusions

Here we demonstrate a novel method for extending the calculation of Cramér-Rao Lower Bounds for metabolite concentration estimates derived from linear combination models of proton spectral data to analogous "concentration" estimates of polynomial coefficients modeling baseline shapes as either continuous single polynomials or piecewise regularized cubic splines using the spline baseline handling functionality developed in Section 2. We then use the batch metabolite spectral simulation and linear combination modeling scheme developed in Section 1 to demonstrate that this method of extending the Fisher information matrix to account not only for metabolite bases but also a set of "bases" describing continuous or piecewise polynomial baseline shapes yields baseline CRLB for spectral baseline polynomial coefficients that track with actual error standard deviations on these estimates in spectra involving known ground-truth simulated baseline function with known coefficients. More importantly, including these baseline CRLB terms in the Fisher information matrix also improves the correspondence between metabolite CRLB and actual fit error standard deviations shown both here and originally in Section 1 to be disturbed by the presence of a spectral baseline.

While this work therefore represents a step forward in the implementation and use of CRLB as measurements of spectral quantification precision, the validity of CRLB themselves as a proxy for fit error continues to suffer some important limitations. First, CRLB represent at best the lower bound of expected standard deviations of a linear combination model fit around a particular center value and do not provide information on the accuracy of that value itself. Because an important prerequisite for their use is that the model employed in spectral quantification is a

complete representation of all the signals that might be present in a given spectrum, it is rightfully assumed that any errors incurred by this model would be due only to Gaussian noise and therefore center on zero systematic deviance from the ground truth. In Sections 1 and 2 of this chapter, however, we have already demonstrated that errors on metabolite concentration estimates derived from spectra involving in vivo-like baselines are not zero-centered but themselves centered on a nonzero mean. This is not surprising given that in these cases the linear combination model is not complete as expected for the appropriate use of CRLB as a proxy for error—rather, the models differ from the data in ways, particularly baseline handling versus the actual baselines at hand, other than simply pointwise Gaussian noise exhibited by the latter. The present dissertation, which focuses in this section on the improvement of CRLB themselves within their limited framework as opposed to a more comprehensive alternative to CRLB for estimating not only zero-centered (on precision) but also systematic (on accuracy) error on spectral data sets without a ground truth, does not offer a solution for this beyond emphasizing the importance of attempting to maximize the realism and generalizability of in vivo like ground-truth standards around which non-CRLB-based error calculation frameworks like the one developed here can be centered.

Within this limited CRLB framework, the present work does present a way to measurably improve the accuracy of metabolite CRLB estimates by including consideration of baseline modeling technique within their calculation, itself reported as dedicated CRLB for each degree value of each polynomial piece. This manner of parsing baseline CRLB, while directly analogous to those for amplitudes on metabolite basis shapes, also provides a roughly linear estimate of baseline modeling precision, but one that nonetheless fails to approach the identity relation in many cases. The CRLB assumes unconstrained Gaussian (normal) error of a calculated model around a ground truth. The piecewise spline coefficients generated by a linear combination model, however,

are heavily constrained by those of neighboring pieces, which may have contributed to the overestimation by baseline CRLB of the supposed lower bound of error on baseline coefficients that we observed for baselines comprising piecewise (spline) but not continuous polynomials. The non-Gaussian error distribution of baseline coefficients predicted by these constraints was confirmed by Shapiro-Wilk test demonstrating non-normality among a number of spline but not continuous polynomial coefficients calculated by linear combination model fits.

Rendering a baseline model as a series of CRLB rather than a single index of error also suffers the same problem of easy interpretability that does providing a single CRLB for each of multiple metabolites key to a given in vivo spectroscopy experiment: Which, if any, single error value is the most crucial endpoint on which to optimize? As for sometimes mutually contradictory trends in metabolite CRLB for a given acquisition scheme, priorities may be most appropriately defined in a metabolite-specific manner, in which case the baseline pieces closest to resonances for that metabolite may be the most viable endpoints for optimization of experimental parameters like T_E. But in situations where generally high precision on prediction of a single baseline may be demanded, as in the use of splines to attempt modeling of an entire measured metabolite-nulled macromolecule spectrum, this approach to baseline CRLB does not provide a unitary measure for the entire baseline at the level of the Fisher information matrix, allowing only for post hoc composites (like summation or averaging) thereof.

Continued work on this novel paradigm for spectral baseline CRLB calculations have at hand, then, the following questions: First, how can the correspondence between CRLB and actual lower bounds of fit error standard deviations for spline baseline coefficients be further improved or at least quantitatively understood even beyond what we have demonstrated here? Second, how can CRLB for multiple baseline coefficients be best combined into a composite measure

sometimes more applicable than interval- and coefficient-specific error estimates for optimizing particular spectral acquisition schemes? Finally, and most crucially, what might exist as a viable alternative to the Cramér-Rao Lower Bound that accommodates the potential for non-zero-centered or systematic deviations from ground truth as well as differently constrained non-Gaussian distributions around that systematic center?

2.5 General summary and conclusions

In this chapter, we set out to address the following questions: What are the effects of spectral quality and baseline on the accuracy and precision of metabolite concentrations estimated by linear combination model fitting of simulated basis functions to in vivo 1H-MR spectra? In turn, how do some parameters that define cubic spline models used to account for in vivo spectral baselines affect quantification accuracy and precision, and how can we improve the precision of these baseline models be better estimated for in vivo experiments involving complicated baselines and models thereof?

Taken together, our findings suggest that under conditions of no spectral baseline, full width at half maximum and signal-to-noise ratio influence zero-centered errors in spectral quantification. In the presence of an in vivo-like baseline, however, these metrics of spectral quality influence not only precision in spectral quantification but also introduce what can be significant systematic errors. Flexibly optimized regularized spline baseline modeling does not necessarily underperform macromolecule simulations in ^{1}H-MRS metabolite quantification precision when a priori standards of comparison are available, and Cramér-Rao Lower Bounds may be employed as a proxy for not only metabolite quantification but also baseline modeling precision when such standards are not available.

Chapter 3: Absolute Quantification.

Influence of differential T_2 relaxation on internal ^{1}H-MRS concentration referencing by water in relapsing-remitting and progressive multiple sclerosis normal-appearing frontal cortex

Tissue water is a common internal reference used for translating from relative metabolite concentrations resultant from spectral quantification of in vivo proton magnetic resonance spectroscopy (^{1}H MRS) data into absolute concentration values that describe physical reality. The usefulness of water as an internal reference depends, however, on the validity of assumptions made about the uniformity of its key properties across individuals, or, alternatively, on detailed knowledge of differences among them. One such property is transverse or spin-spin relaxation constant T_2, which governs the rate at which nuclear spins phased by a radiofrequency pulse applied in a magnetic resonance experiment dephase in part as a result of interactions among them. Here we investigate potential influences on water-referenced metabolite quantification at 7 Tesla by differences in frontal cortex water T_2 in individuals with relapsing-remitting, progressive, and no multiple sclerosis as a case study of disease effects on metabolite concentration quantification in groups for which internal referencing by water may itself be influenced by disease. Water T_2 differed among disease groups in monoexponential models of spin-spin relaxation, exhibiting the highest values in progressive multiple sclerosis only when analyses were not controlled for between-group differences in age. Groupwise T_2 did not differ in biexponential models of spin-spin relaxation constrained by tissue composition and cerebrospinal fluid (CSF) partial volumes, suggesting that monoexponential T_2 differences reflected disparate proportions of water in tissue and CSF rather than differential behavior within them. Our results suggest stability of water T_2 within frontal cortex tissue and CSF with multiple sclerosis only as long as disease or age-related changes in voxel composition are accounted for and emphasize the superiority of metabolite

quantification with group-specific T_2 values when voxel composition may differ if water is to be used as an internal concentration reference for absolute metabolite quantification by ^{1}H MRS.

3.1 Motivation

Following the decomposition of an ^{1}H MRS data set into relative weights on metabolite component parts by spectral quantification, discussed in detail in Chapter 2, these relative results are translated into physically meaningful concentration units in a process called absolute quantification. Tissue water is a common internal reference for this step of ^{1}H MRS processing and analysis [21]. The usefulness of water as an internal reference depends, however, on the validity of assumptions made about the uniformity of its key properties across individuals, or, alternatively, on detailed knowledge of differences among them, as shown previously in Equation 3 of Chapter 1. For example, water-to-metabolite signal ratios are commonly corrected without explicit examination of group-specific transverse relaxation time constant T_2 [106, 146-148]. But multiple lines of evidence suggest that this practice may not always, so to speak, hold water. Age [149] and brain irradiation [150], for instance, may lengthen cortex water T_2 while preserving or reducing cortical N-acetyl aspartate and creatine T_2 [150, 151]. Such evidence reinforces the notion that T_2 values used in metabolite quantification should empirically consider the physical characteristics of populations under study with a minimum of generalized assumptions made over what in reality may constitute a diversity of heterogeneous cases.

One such population for which special consideration of group-specific T_2 values may be warranted is individuals with multiple sclerosis (MS), an autoimmune disorder that damages the central nervous system. To enable accurate water-referenced quantification of ^{1}H-MRS visible metabolites in individuals with relapsing-remitting (RR-MS), progressive (P-MS), and no MS, we

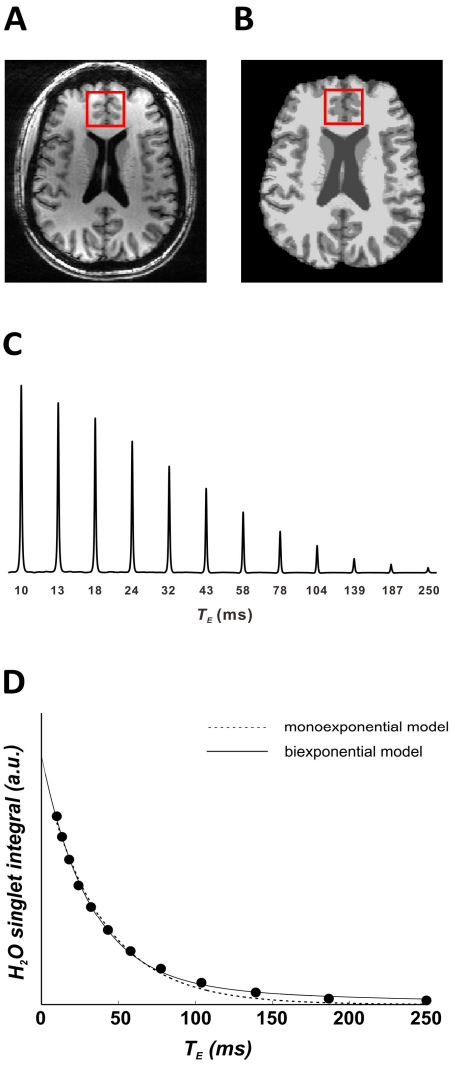

Figure 3.1. Water T_2 was assessed at 7 T using signal acquired in a frontal cortex mixed-tissue voxel with a variable-echo-time STEAM array. A) Skull stripping and automated segmentation of T_1-weighted images enabled the calculation of B) grey matter, white matter, and cerebrospinal fluid partial volumes for use in biexponential transverse decay modeling. C) Fully relaxed water-unsuppressed signal was acquired at twelve echo times via STEAM. Real singlets from interleaved acquisitions (T_E = 10, 250… 43, 58 ms) have been reordered to depict transverse decay. D) Trust-region-reflective least-squares fitting to signal integrals at each of these echo times calculated T_2 by monoexponential and partial-volume-constrained biexponential models. T_E: echo time. Adapted from Swanberg et al., *Proc ISMRM* 2018, 0161.

therefore assess potential differences in frontal cortex water T_2 relaxivity, both in bulk and within tissue- and cerebrospinal fluid (CSF)-specific compartments, to then provide estimates of potential downstream effects of group-specific water T_2 on metabolite concentration estimates referenced to internal water in the event that this variable were not explicitly considered.

3.2 Methods

In vivo acquisition. Data were acquired according to a similar protocol as that outlined in Section 2.2. 2. Briefly, acquisitions were accomplished at the Yale University MRRC as described previously [106], on a 7-Tesla head-only MR scanner (Agilent Technologies, Santa Clara, CA) with a 298.1-MHz DirectDrive proton spectrometer, custom actively shielded gradients (Magnex Scientific, Oxford, UK) and an 8-channel transmit-receive head coil. Sequences were controlled via VnmrJ software, version 2.3A (Varian, Santa Clara, CA). In vivo data were acquired with the prior approval of and in accordance with standards set forth by the Yale

	Non-MS control (N = 25)	RR-MS (N = 22)	P-MS (N = 21)
Age (years)	43 ± 15 *(52 ± 10.)*	46 ± 13 *(51 ± 11)*	55 ± 8 *(55 ± 7.9)*
GM partial volume (%)	47 ± 4.1 *(46 ± 3.7)*	45 ± 5.6 *(45 ± 5.5)*	41 ± 7.3** *(41 ± 7.3)*
WM partial volume (%)	41 ± 7.2 *(40. ± 6.4)*	41 ± 8.9 *(42 ± 8.1)*	40. ± 9.4 *(40. ± 9.4)*
CSF partial volume (%)	12 ± 6.2 *(14 ± 6.6)*	13 ± 5.9 *(13 ± 5.5)*	19 ± 9.5* *(19 ± 9.5)*
Monoexponential H_2O T_2 (ms)	44 ± 3.9 *(44 ± 3.9)*	45 ± 6.0 *(46 ± 6.1)*	49 ± 8.4* *(49 ± 8.4)*
Tissue compartment H_2O T_2 (ms)	31 ± 3.4 *(30. ± 3.4)*	30. ± 3.1 *(30. ± 2.5)*	28 ± 4.4 *(28 ± 4.4)*
CSF compartment H_2O T_2 (ms)	173 ± 56 *(155 ± 44)*	175 ± 62 *(188 ± 61)*	158 ± 45 *(158 ± 45)*

Results reported as means ± standard deviations. Age-matched group statistics in parentheses. * $p < 0.05$; ** $p < 0.01$. RR-MS: relapsing-remitting MS; P-MS: progressive MS.

Table 3.1. Medial prefrontal cortex voxel partial volumes and water T_2 in individuals with relapsing-remitting, progressive, and no multiple sclerosis. Displayed as appears in Swanberg et al., *Proc ISMRM* 2018, 0161.

School of Medicine Human Investigation Committee for human subjects research.

Placement of a 3-cm isotropic voxel at midline of frontal cortex was achieved with reference to scans by a custom-written T_1-weighted inversion-recovery anatomical imaging sequence (field of view 20 x 22 x 78 cm, matrix size 256 x 256 x 39, echo time T_E 6 ms, repetition time T_R 3 s, inversion time T_I 1 s). Up through third-order spherical-harmonics B_0 shims were applied according to calculations on gradient-echo images at five T_E (FOV 22 x 22 x 6 cm, matrix size 126 x 64 x 20, T_E 3.8, 4.0, 4.3, 5.3, and 6.8 ms, T_R 1.3 s) using laboratory-developed software B0DETOX, and B_1 phase shimming was calculated by laboratory-developed software IMAGO.

Scan routines were employed on twenty-five (12 female; 43±15 y.o.) controls without multiple sclerosis, twenty-six (18 female; 44±13 y.o.) participants with relapsing-remitting multiple sclerosis, and twenty-one (12 female; 55±8 y.o.) participants with progressive multiple sclerosis. Specifically in this analysis, water T_2 from the 27-cc cubic prefrontal cortex voxel was

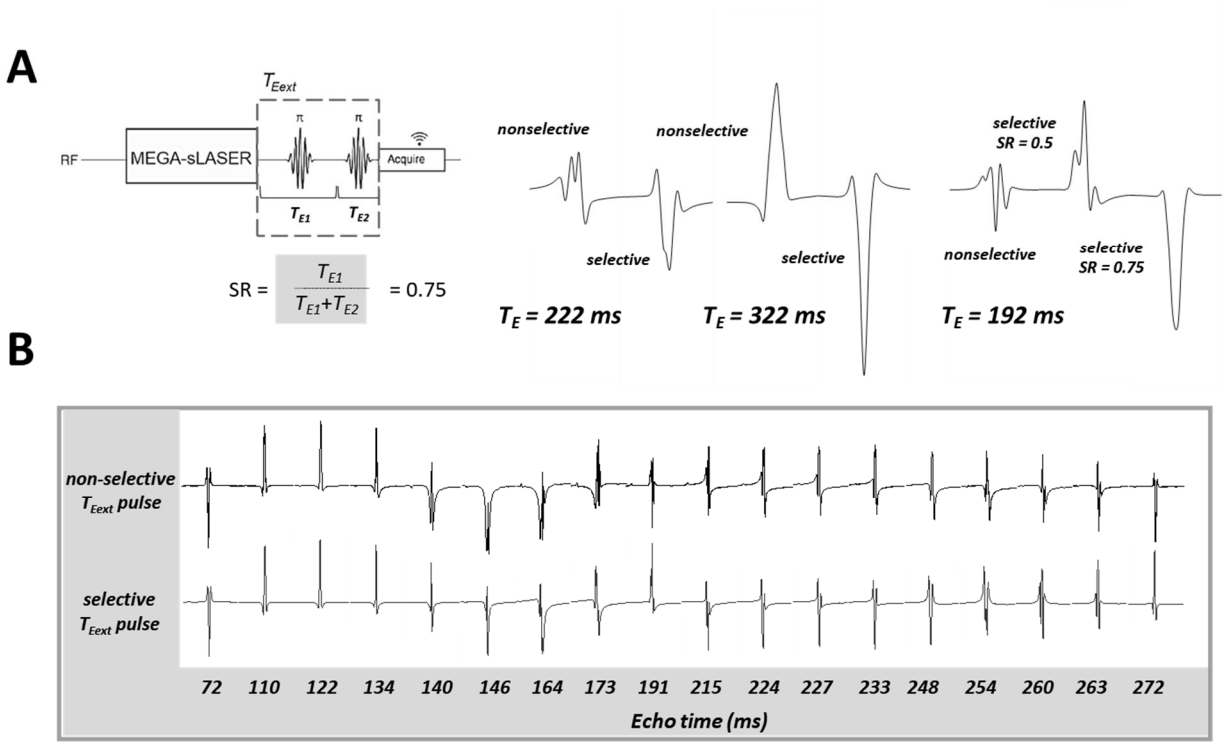

Figure 3.2. Glutathione signal evolution changes as a function of echo time extension (T_{Eext}) pulse timing symmetry and frequency selectivity. A) Visual schema of pulse sequence parameter echo time symmetry. A pair of adiabatic echo time extension pulses with variable intervening time intervals (T_{E1}, T_{E2}) followed a semi-Localization by Adiabatic SElective Refocusing (sLASER) sequence with a MEscher-GArwood (MEGA) module used to edit the glutathione ^{7}CH at 4.56 ppm for measurement of its *J*-coupled $^{7}CH_2$ signal at 2.95 ppm. B) Within this acquisition paradigm the amplitude and distinctiveness of glutathione signal at multiple time points can vary considerably with editing pulse frequency selectivity and inter-pulse interval symmetry ratio (SR). B) Density-matrix simulations of the T_E-extended MEGA-sLASER pulse sequence demonstrate that the evolution of *J*-difference-edited glutathione signal shape with echo time differs with T_{Eext} pulse pair frequency selectivity, yielding a high variety of distinctive quantification challenges for a phantom containing this metabolite. Note that the minimum simulated echo time extension reflects timing limitations imposed by T_{Eext} pulse length in the selective T_{Eext} condition. Displayed as appears in Swanberg et al., *JMR* 2018; 290: 1-11.

examined with a STEAM (T_M 50 ms, T_R 15 s) array with one repetition each of 12 interleaved echo times (T_E) from 10 to 250 ms (Figure 3.1B).

Spectral processing and analysis. Spectra from this protocol were acquired to 8192 complex points. Signals from individual receive channels were corrected for eddy currents using water-unsuppressed references [118], phase- and frequency-aligned, and averaged with weighting by

receive channel sensitivities [119]. Summed metabolite spectra were zero-order phased but not truncated, zero-filled, or line-broadened before direct quantification or alignment between summed editing conditions for difference spectrum calculation, as applicable. Spectral processing was achieved, and real peaks integrated from baseline, using INSPECTOR.

Phantom assessment of spectral processing and quantification procedures. Spectral acquisition, processing, and quantification procedures were tested against two phantoms of known metabolite concentration examined using the same data processing approaches as applied elsewhere in this chapter, as well as spectral quantification via linear combination modeling of simulated basis sets as employed in Chapters 2, 4, and 5.

First, short-echo-time sLASER measurement (T_E = 10 ms; T_R = 2 s; N_R = 128) of glutamate was conducted on a 3 Tesla clinical MR scanner (MAGNETOM Prisma, Siemens, Erlangen, Germany) at the Zuckerman Mind, Brain, and Behavior Institute within the Columbia University Magnetic Resonance Research Center (CMRRC) in an externally prepared aqueous phantom reported to contain 12.5 mM glutamate, 3 mM choline for concentration referencing, and additional other compounds for unrelated test purposes, including 5 mM glycine, 10 mM GABA, 7.5 mM myoinositol, 10 mM creatine, and 12.5 mM N-acetyl aspartate, aspartate, and acetate in an unspecified ratio. Quantification of glutamate concentration estimates from short-T_E sLASER spectra proceeded as per processing and linear combination modeling procedures reported in Chapter 2 and as described previously, applying a flat zero-order polynomial baseline (offset) [145].

Second, MEscher-GArwood (MEGA) *J*-difference-edited semi-Localization by Adiabatic SElective Refocusing (sLASER) measurement (T_E = 72, 109, 117, 127, 192, 222, 282, 322 ms; T_R = 3 s; N_R = 64-128 each edit-on and edit-off per T_E) resembling the acquisition schemes for

glutathione and GABA employed elsewhere in this dissertation were applied on the same 7-Tesla hardware as described in the present chapter as well as in a previous publication of this work [116] to measure metabolite concentrations in an aqueous phantom containing 5 mM glutathione and 5 mM N-acetyl aspartate at physiological temperature and pH. A glutathione phantom was chosen for this challenge because the strongly and weakly coupled ABX-like spin system of glutathione engenders signal shapes that can vary greatly with sequence parameters like echo time and the pulses used to define it (Figure 3.2), enabling a more demanding and comprehensive test set of validation spectra than metabolites with less complex quantum-mechanical properties.

Under these conditions, two endpoints of the phantom metabolite concentration estimation pipeline were evaluated. First, the visual correspondence between basis functions density-matrix-simulated in SpinWizard as described previously in Chapter 2 and measured signal line shapes for glutathione and N-acetyl aspartate was qualitatively assessed in the phantom containing non-overlapping glutathione and N-acetyl signal shapes. Second, the numerical correspondence between measured and predefined relative concentrations of glutamate to choline in the glutamate phantom at a single short echo time, and then glutathione to N-acetyl aspartate in the glutathione phantom at the additional challenges imposed by multiple echo times, were quantitively assessed. Because T_2 differences between glutathione and N-acetyl aspartate were expected to substantially influence the error of the latter results, the effect of echo time on error was also investigated, as reported in a previous publication of this work [116].

Water T_2 estimation. Water T_2 was estimated by trust-region-reflective least-squares curve fitting to signal integral values at each T_E according to:

$$M_{T_E} = M_0 e^{-\frac{T_E}{T_2}} \quad (8)$$

where *M* represents water signal integral. To account for disparate proportions of water protons in tissue versus CSF compartments by voxel composition differences, we then applied a biexponential model:

$$M_{T_E} = M_0 \left(\chi_t e^{-\frac{T_E}{T_{2t}}} + \chi_f e^{-\frac{T_E}{T_{2f}}} \right) \quad (9)$$

with tissue (white matter plus grey matter) T_{2t} and CSF T_{2f}. Variables χ_t and χ_f represent compartmental water fractions in tissue and CSF, respectively, as:

$$\chi_{t/f} = \frac{PV_{t/f}[H_2O]_{t/f}}{PV_{gm}[H_2O]_{gm} + PV_{wm}[H_2O]_{wm} + PV_{csf}[H_2O]_{csf}} \quad (10)$$

where PV_{gm}, PV_{wm}, and PV_{csf} are voxel partial volumes of grey matter, white matter, and CSF, respectively, calculated by custom MATLAB software using T_1-weighted images skull-stripped and segmented as detailed below (Figure 3.1A). The variables $[H2O]_{gm/wm/csf}$ denote published tissue water concentration estimates [147, 152].

Image segmentation. T_1-weighted images were skull-stripped using the Brain Extraction Tool in FSL [153]. BrainSuite (v16a1, http://brainsuite.org/) was applied for bias field correction and partial volume segmentation into grey matter, white matter, and cerebrospinal fluid. Bias field correction calculated tissue intensity mean and noise variance globally across the image; these

were used to build a parametric tissue model including a bias field coefficient. Fits of this model against histograms of small image regions were used to calculate local bias field values over a rough grid smoothed using cubic splines; division by the estimated field achieved correction. This segmentation algorithm employed maximum a posteriori classification on a model of voxel intensity values assuming Gaussian density distributions of either one or two tissue types and a spatial model weighting the relative probabilities of tissue distributions in neighboring voxels [154]. After a composite mask was created for each of the three tissue types, extraction of partial volume statistics in the spectroscopy voxel was achieved in custom MATLAB (v2013b, The Mathworks, Natick, MA) package IMAGO.

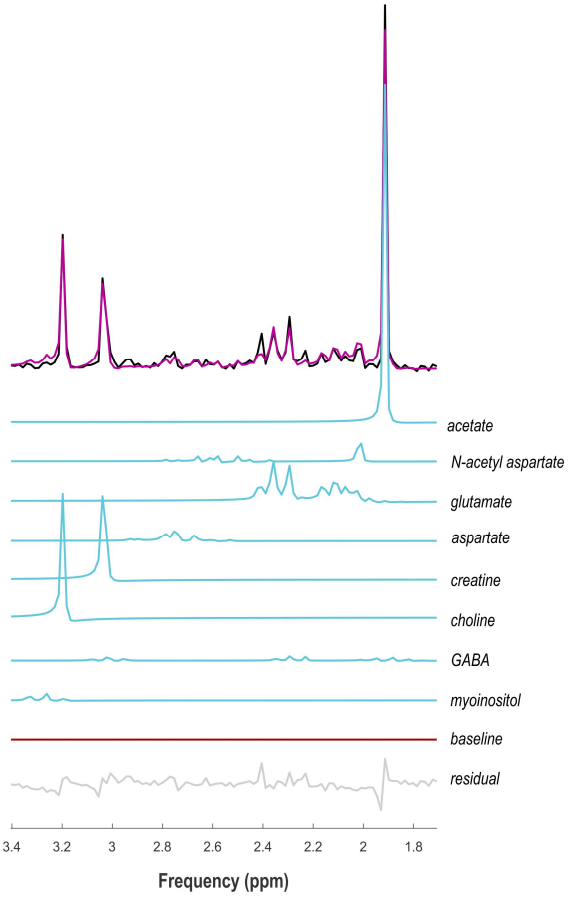

Figure 3.3. Glutamate was measured in an aqueous metabolite phantom to test absolute concentration estimation procedures against a physical sample of predefined composition. An externally prepared aqueous metabolite phantom was employed as a target for short-T_E sLASER (T_E = 20.1 ms, T_R = 2 s) acquisitions at 3 Tesla. Spectral processing and metabolite quantification by linear combination modeling of simulated basis functions were applied according to procedures described in Chapter 2, and glutamate was referenced to a predefined 3 mM choline. ppm: parts per million.

Statistical analysis. Group differences were assessed in SPSS 20 (IBM, Armonk, NY) with $\alpha = 0.05$, with parametric statistics applied only in the case of within-group normality as suggested by prior Shapiro-Wilkes analysis. Age-controlled analyses included only participants over 35 years old.

3.3 Results and Discussion

Linear combination model fitting of simulated basis functions for choline, creatine, glutamate, N-acetyl aspartate, GABA, myoinositol, aspartate, and acetate to corresponding resonances in the mixed-metabolite glutamate phantom yielded a glutamate concentration estimate of 12.98 mM when referenced to a predefined choline concentration of 3 mM, which falls within 5% of the predefined glutamate concentration of 12.5 mM (Figure 3.3).

While glutathione signal shapes demonstrated a high degree of temperature dependence (Figure 3.4), at physiological temperature and pH MEGA-sLASER measurement of aqueous phantom contents yielded glutathione and co-edited N-acetyl aspartate difference spectra that corresponded with those observed following density-matrix simulation or in vivo measurement at all investigated echo times (Figure 3.5).

The glutathione concentration calculated from prior knowledge of N-acetyl aspartate concentrations and the ratio between signal amplitudes of *J*-difference edited GSH and unedited spectral N-acetyl aspartate of a phantom containing 5 mM of each metabolite was 4.7 ± 2.0 mM as averaged over the first two measured T_E, which falls within 5% of the expected value of 5 mM GSH. As would be expected for increased unreliability of quantification of low-signal metabolites at the lower SNR conditions of higher T_E

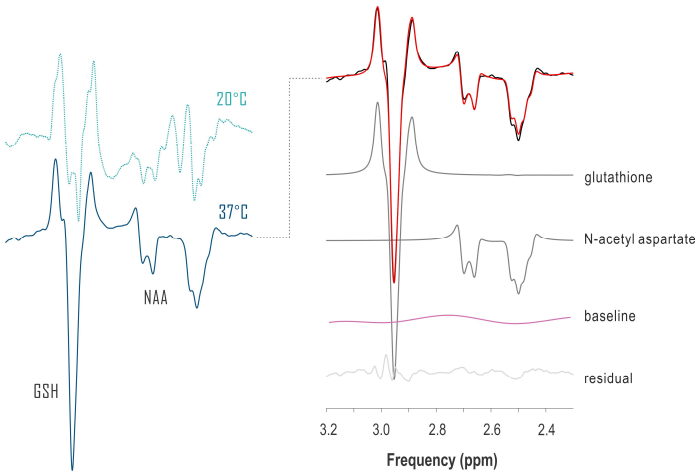

Figure 3.4. Coupled spin system glutathione exhibits temperature-dependent signal shapes. Glutathione possesses a coupled spin system that is expected to demonstrate lineshape alterations with pH and temperature (left), necessitating the use of phantom preparations at in vivo like conditions for quantification by linear combination modeling of full density-matrix simulations. LB: line broadening; ZF: zero-filling.

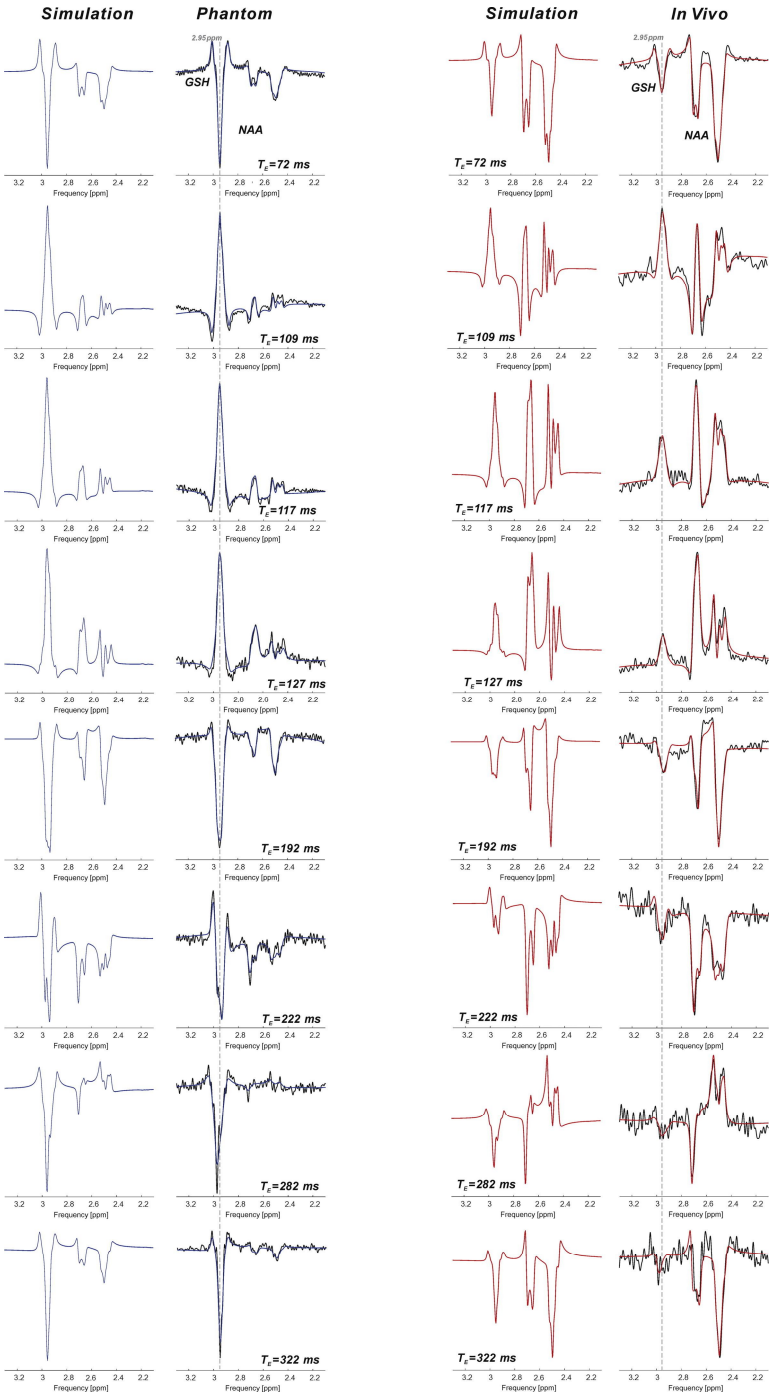

Figure 3.5. Consistency of signals among simulations, phantom experiments, and in vivo experiments across all echo times was observed for 7-Tesla proton spectroscopic measurement of complex spin system glutathione. Density matrix simulations of J-difference-edited GSH and co-edited NAA difference spectra demonstrated high visual accordance with spectral data obtained from both phantom and in vivo experiments. The left column displays the simulated basis set scaled to a phantom ratio of 1:1 GSH: NAA. The middle right column shows the same basis set scaled to an in vivo ratio of approximately 1:5. This correspondence translated to reasonable fits by simulated basis functions to experimental data at all echo times. Phantom data are displayed with no additional line broadening; in vivo data have been Lorentzian line-broadened 2 Hz. GSH = glutathione; NAA = N-acetyl aspartate; T_E = echo time; ppm = parts per million. Displayed as appears in Swanberg et al., *JMR* 290: 1-11.

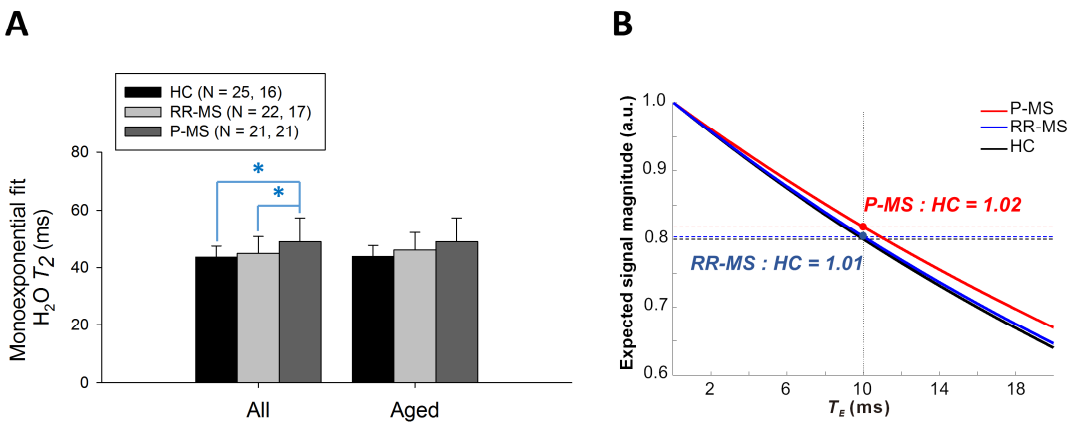

Figure 3.6. Higher T_2 in aged progressive multiple sclerosis participants than control causes water signal overestimation without correction. A) Kruskal-Wallis test demonstrated a significant between-group effect on monoexponential water T_2 (7.772, p = 0.021), with Mann-Whitney test demonstrating increases in P-MS relative to control (2.724, p = 0.006) and RR-MS (2.041, p = 0.041). Aged groups showed no significant difference. B) Uniformly applying control T_2 values would induce 2% overestimation of water signal in the progressive MS group at T_E = 10 ms. * $p < 0.05$. P-MS: progressive multiple sclerosis; RR-MS: relapsing-remitting multiple sclerosis; HC: non-MS control. Adapted from Swanberg et al., *Proc ISMRM* 2018, 0161.

as well as quantification of a metabolite with shorter T_2 than that of its reference NAA, this ratio decreased with the addition of concentrations calculated at each longer T_E to reach a final average of 4.2 ± 0.9 mM across all arrayed echo times, differing by over 15% from the expected 5 mM at echo times much higher than that employed for glutathione quantification in subsequent sections of this work. Notably, in contrast with these systematic errors in quantification accuracy, reported Cramér-Rao Lower Bounds for quantification precision of both glutathione and N-acetyl aspartate remained stable (within 1%) for all echo times.

Taken together, these phantom results provide a measure of empirical verification for both the density-matrix simulation procedures as well as spectral processing and quantification methodologies employed in this work, as applied against the challenges posed by both glutamate resonances within the context of multiple additional metabolites measured using short-echo-time

localization without spectral editing as well as the complex, low-amplitude, and temperature- and T_E-dependent signal shapes of spin system glutathione estimated via spectral editing of the same type of localization scheme.

T_2 models for water in vivo yielded visually satisfactory fits in all participants. Four RR-MS cases with outlying CSF T_2 were excluded from analysis. Kruskal-Wallis test demonstrated a significant group effect on water T_2 (7.772, $p = 0.021$); Mann-Whitney test demonstrated increases in P-MS relative to control (2.724, $p = 0.006$) and RR-MS (2.041, $p = 0.041$) (Figure 3.6A). Uniform application of control T_2 to water signal quantification would overestimate P-MS water concentration by 2% at $T_E = 10$ ms (Figure 3.6B).

Similar analysis demonstrated a group effect on grey (7.745, $p = 0.021$) but not white matter partial volumes, with lower grey matter in P-MS relative to control (-2.746, $p = 0.006$); an effect was also found in CSF (6.266, $p = 0.044$), higher in P-MS than control (2.327, $p = 0.020$) (Figure 3.7A). Between-group differences in voxel composition disappeared upon controlling for age in the manner described in 3.2 (Figure 3.7B).

Groupwise T_2 differences disappeared with biexponential modeling (Figure 3.8A) and became marginally significant ($0.05 < p < 0.1$) upon controlling for age in the manner described in 3.2 (Figure 3.8B).

Taken together, these results suggest a systematic difference in the water T_2 of otherwise normal-appearing frontal cortex brain tissue in individuals with progressive multiple sclerosis relative to relapsing-remitting multiple sclerosis or control. Even at this experiment's low echo time of 10 ms, this increase in progressive multiple sclerosis water T_2 observed across the voxel when modeled as a unitary compartment exhibiting only monoexponential time-domain signal decay would engender substantial (up to 2%) underestimation of metabolite concentrations in the

progressive multiple sclerosis relative to the other experimental groups if a one-size-fits-all T_2 value were used instead.

The disappearance of between-group T_2 differences either when the voxel was modeled as two compartments exhibiting biexponential decay, or when between-group differences in age were explicitly controlled, further suggests that correction of monoexponential T_2 disparities could be achieved by controlling for differential effects of voxel composition (i.e., employing uniform fluid and tissue compartment T_2s for all groups but accounting for greater CSF relative to tissue partial volumes in the progressive multiple sclerosis group) or of age (i.e., employing the same base T_2 for all groups but selectively age-matching the progressive multiple sclerosis group) on group-specific T_2 values in the event that individual T_2 could not be measured for this cohort. Any correction, however, carries with it the potential for introduction of additional error, underlining the potential risk of employing internal

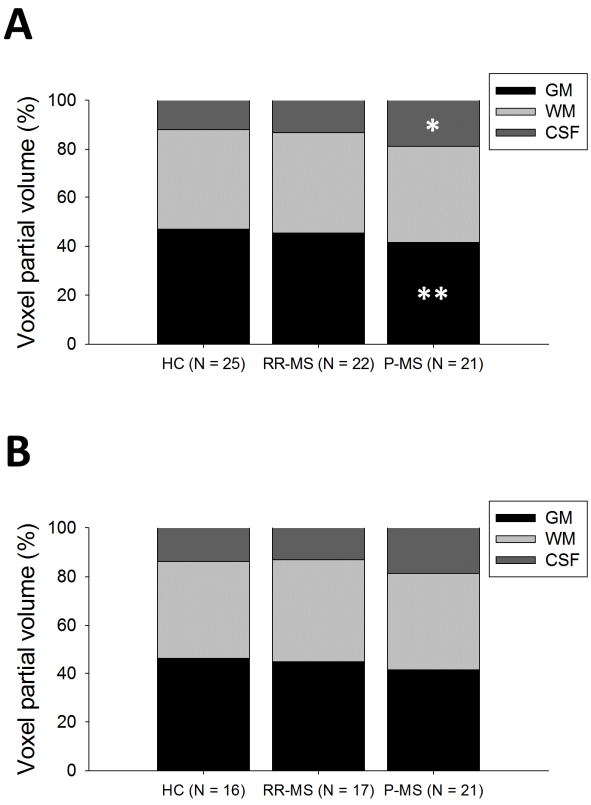

Figure 3.7. Aged progressive multiple sclerosis participants exhibited different voxel partial volumes from control. A) Kruskal-Wallis test showed a between-group effect on grey (7.745, $p = 0.021$) but not white matter partial volumes, with lower grey matter in P-MS relative to control (-2.746, $p = 0.006$) as well as on CSF partial volume (6.266, $p = 0.044$), higher in P-MS than control (2.327, $p = 0.020$). B) Aged groups showed no significant differences. ** $p < 0.01$; * $p < 0.05$. P-MS: progressive multiple sclerosis; RR-MS: relapsing-remitting multiple sclerosis; HC: non-MS control; GM, WM: grey, white matter; CSF: cerebrospinal fluid. Adapted from Swanberg et al., *Proc ISMRM* 2018, 0161.

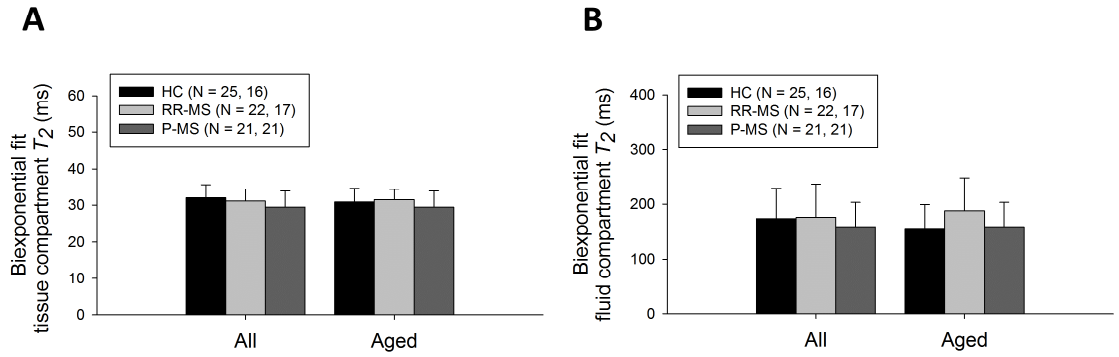

Figure 3.8. Figure 4. Biexponential model fits to water signal decay curves yielded comparable tissue and free fluid compartment T_2 across control, relapsing-remitting, and progressive multiple sclerosis groups. When decay curve models included two exponential terms, each weighted by coefficients constrained by proportions of water concentration calculated from voxel partial volumes of tissue (grey and white matter) and CSF, both tissue (A) and free fluid compartment (B) T_2 values remained stable across both general and aged groups. HC: non-MS control; RR-MS: relapsing-remitting multiple sclerosis; P-MS: progressive multiple sclerosis. Adapted from Swanberg et al., *Proc ISMRM* 2018, 0161.

water referencing for absolute quantification of metabolite estimates by ^{1}H MRS in this progressive multiple sclerosis cohort.

3.4 Limitations and Conclusions

Frontal cortex water T_2 differences in aged individuals with progressive multiple sclerosis disappeared when considering disparate voxel composition in a biexponential model constrained by tissue and CSF partial volumes and when matching group ages. These results suggest that water T_2 within tissue and CSF remains stable with multiple sclerosis disease state and emphasize the superiority of metabolite quantification with group- or voxel-specific T_2 values when voxel composition may differ, as recently implemented [155]. Further refinement to voxel compartment-specific T_2 estimates may be achieved by empirically controlling for potential MS-related differences in tissue water concentration, here assumed equivalent across groups. Finally, that our results notably demonstrated stability in tissue compartment T_2 with multiple sclerosis disease

state suggests similar stability in predominantly tissue-bound metabolite T_2, but this is a question that begs continued empirical investigation.

Notably, significant loss of statistical power was incurred by the age-matching method employed in this analysis. While age-controlling T_2 values by compensation via a linear regression coefficient calculated on the control cohort as performed in Chapters 4 and 5 may address age differences while retaining statistical power to isolate multiple sclerosis disease effects of water T_2, the overall conclusion of the present chapter would not change: Despite the generalized use of single water T_2 across different experimental cohorts to conduct absolute quantification of metabolite concentration estimates by ^{1}H MRS we have observed at least one instance wherein not considering group-specific water T_2 values would have introduced systematic errors into the results.

3.5. General Summary and Conclusions

In this chapter, we set out to address the following question: Does differential T_2 relaxation in relapsing-remitting and progressive multiple sclerosis normal-appearing frontal cortex affect internal ^{1}H-MRS concentration referencing by water?

Taken together, our findings suggest that individuals with progressive multiple sclerosis exhibit increased frontal cortex water T_2 relative to control associated with age-related changes in tissue composition that may influence metabolite concentration estimates referenced to internal water. We have previously shown that evidence-based T_2 corrections can significantly affect metabolite concentration estimates, especially those derived from measurements at long echo time [116]. Correction for these findings of disease effect on water T_2 demonstrated similar influence on metabolite concentrations estimated via referencing to water.

Chapter 4: Statistical Analysis.

In vivo evidence of differential frontal cortex concentrations of glutathione, GABA, and glutamate in progressive and relapsing-remitting multiple sclerosis and multivariate classification of progressive and relapsing-remitting multiple sclerosis via ^{1}H-MRS-measured frontal cortex metabolites

Autoimmune demyelinating condition multiple sclerosis is a heterogeneous disease of which the diagnosis continues to depend on a combination of reported symptoms, clinical evaluation, magnetic resonance imaging, and sometimes lumbar puncture. ^{1}H MRS enables the noninvasive detection of multiple small-molecule brain tissue metabolites in vivo and is therefore in principle a promising means of gathering information relevant to multiple sclerosis diagnosis and subtype classification to support these clinical decision pipelines. Three decades of research, the majority at fields of 3 Tesla and below, applying proton spectroscopy to investigate multiple sclerosis have failed to yield, however, a sensitive and specific single-molecule benchmark for differentiating among controls and the diverse phenotypes of multiple sclerosis. Furthermore, the small size of most proton magnetic resonance data sets demands extra care in the application of flexible multivariate approaches like those offered by machine learning techniques in the service of developing such a classification scheme. To the end of such a classification algorithm, we employed, at 7 Tesla, a previously validated ^{1}H-MRS protocol to measure glutamate, GABA, glutathione, glutamine, N-acetyl aspartate, choline, and myoinositol in the frontal cortex of individuals with relapsing-remitting (N=26), progressive (N=21), and no (N=25) MS in a cross-sectional analysis. Only individuals with progressive MS demonstrated reduced glutamate (12.4±0.6 mM versus control 13.2±1.0 mM, $p = 0.03$) but not glutamine (4.7±0.4 mM versus control 4.8±0.4 mM), reduced GABA (1.3±0.2 mM versus control 1.5±0.3 mM, $p = 0.05$), and possibly reduced glutathione (2.2±0.5 mM versus control 2.5±0.5 mM, $p < 0.1$). These results indicate that frontal cortex metabolism is differentially disturbed in progressive and relapsing-

remitting MS and that ^{1}H MRS may therefore be employed in classification of these disease states. Therefore, with special attention to the dual challenges posed by subtle single-molecule between-group differences and small sample sizes, we show that the multivariate evaluation of these frontal cortex small-molecule metabolites measured by proton magnetic resonance spectroscopy at 7 Tesla alone can yield sensitive and specific distinction between individuals with progressive multiple sclerosis from control (maximum held-out validation sensitivity 79% and specificity 68%), as well as between relapsing and progressive multiple sclerosis phenotypes (maximum held-out validation sensitivity 74% and specificity 84%). Post-hoc assessment of the most accurate models demonstrated the disproportionate and diverse contributions of glutamate and glutamine, metabolites most reliably measured under the high signal to noise and spectral dispersion of static fields higher than 4 T. Our finding establishes proton magnetic resonance spectroscopy, particularly at ultra-high field, as a viable means of characterizing progressive multiple sclerosis disease status and paves the way for continued refinement of this method as an auxiliary or mainstay of multiple sclerosis diagnostics.

4.1 Introduction

Multiple sclerosis (MS) is an autoimmune condition of unknown antigenic target that damages cells in the central nervous system, particularly oligodendrocytes comprising the myelin surrounding neuronal axons [61]. Though MS affects more than 2 million individuals globally [156], we possess an incomplete understanding of its mechanisms and currently no cure. While it has been shown that MS patients exhibit an abnormal inflammatory response that leads to neurodegeneration and associated disability over a lifetime [157], how these reactions' potential triggers, including mutations in genes central to a number of autoimmune conditions [158] and

environmental causes like smoking, Vitamin D deficiency, or infection with the Epstein-Barr virus [159], unfold into a disease state is still unclear.

In addition to its individualized clinical presentation dependent on patient lesion distribution and perhaps lesion type [160], MS follows multiple potential disease courses, generally categorized as relapsing-remitting, secondary progressive, primary progressive, or progressive relapsing, and exhibits sometimes only subtle clinically evident differences from a number of differential diagnoses like neuromyelitis optica (NMO) and Balo's concentric sclerosis [161]. Relapsing-remitting MS (RR-MS), comprising up to 85% of new diagnoses, is marked by the periodic appearance of neurological symptoms often concomitant with periventricular, infratentorial, juxtacortical, or spinal gadolinium contrast-enhancing lesions indicative of active central nervous system inflammation. The majority of individuals with RR-MS will, within a decade or more, transition to secondary progressive MS (SP-MS), characterized by neurological decline in the absence of relapses, while about 10% of new patients will exhibit primary progressive MS (PP-MS) without having demonstrated a relapsing phase. Finally, a small minority of new MS diagnoses are of the progressive-relapsing variant, marked by consistent decline in tissue and function in parallel with punctuated relapses [64]. While the use of different terms to refer to the varied forms of MS may imply that they are distinct variants or at least stages of illness, it has also been suggested that progressive and relapsing MS in fact represent simultaneously acting pathological mechanisms of the same disease [162].

The following introduction will attempt to review current understanding of metabolic abnormalities in relapsing-remitting, secondary progressive, and/or primary progressive multiple sclerosis that have been previously observed using ^{1}H-MRS of tissue in the central nervous system. It will then discuss some current lines of thinking on the pathophysiological differences between

multiple sclerosis phenotypes broadly characterized as relapsing and progressive and discuss the unique niche that in vivo proton spectroscopy may occupy to facilitate greater clarification of these differences.

4.1.1. Univariate small-molecule abnormalities previously examined in ^{1}H-MRS investigations of multiple sclerosis

Proton spectroscopic analysis of multiple sclerosis has examined a variety of individual small molecules in living central nervous system tissue, including N-acetyl aspartate, creatine, choline, myoinositol, glutamate, glutamine, γ-aminobutyric acid (GABA), glutathione, and lactate. For reasons of difficult isolation from a single spectral dataset, some of these and other metabolites are often grouped under more general categories, like total creatine (creatine and phosphocreatine), total N-acetyl aspartate (N-acetyl aspartate or NAA plus N-acetyl aspartylglutamate or NAAG), total choline (choline, phosphocholine, and glycerophosphocholine), inositol (myoinositol and scylloinositol), or Glx (glutamate and glutamine). Since different authors exhibit varying precision in nomenclature, for simplicity in the present review the terms N-acetyl aspartate, creatine, and choline may refer to any subset of biomolecules listed above in the "total" definitions thereof. In addition to small-molecule metabolites comprising the principal peaks of a ^{1}H-MRS spectrum, the less well-defined lipids and macromolecules constituting the broader background signatures of some sequences have also been examined for differences between individuals with and without multiple sclerosis.

By far the majority of ^{1}H-MRS studies of multiple sclerosis examine one or all of the highest-amplitude signals on a standard ^{1}H-MRS localizing sequence, from N-acetyl aspartate, creatine, and choline. A detailed treatment of the potential roles of each class of molecules in

healthy and diseased brain is well beyond the scope of the present review. It is, however, to be noted that beyond exhibiting high-intensity single peaks (so-called singlets) that facilitate their straightforward quantification, each of these classes of metabolite also possesses a biological function that reasonably implicates it in the existing narrative of multiple sclerosis pathology. Perhaps unsurprisingly, then, all three compounds, among others, have previously demonstrated abnormalities relative to control in brain ^{1}H-MRS studies of multiple sclerosis.

N-acetyl aspartate (NAA). N-acetyl aspartate (NAA) is a small molecule synthesized predominantly in mature neurons from acetate and acetyl-coenzyme A. In addition to displaying concentration abnormalities in a number of neurological disorders and injuries, it may serve in part as a storage and transport reservoir for acetate used in myelin lipid anabolism. N-acetyl aspartylglutamate (NAAG) is also predominantly localized to the neurons, though of a smaller range than N-acetyl aspartate, and may modulate the release of neurotransmitters in a variety of pathways [163]. The acetyl moieties of both molecules exhibit high-amplitude singlets at 2.01 (N-acetyl aspartate) or 2.04 (N-acetyl aspartylglutamate) ppm; both molecules also exhibit additional multiplets, especially from aspartate in the 2.5-2.7 and 4.4-4.6 ppm range as well as further signals from the amine (N-acetyl aspartate) and glutamate (N-acetyl aspartylglutamate) moieties [13].

Creatine-referenced N-acetyl aspartate has shown reductions relative to control in mixed or unspecified multiple sclerosis lesions [164-177], white matter [82], normal-appearing white matter [164, 166, 167, 172, 176, 178-187], and mixed tissue [188]; in relapsing-remitting multiple sclerosis lesions [26, 189-196], white matter [79, 82, 195, 197-203], normal-appearing white matter [189, 191-193, 204-209], grey matter [195, 209], mixed tissue [195, 198, 203, 210-214], and spine [215]; and in progressive multiple sclerosis lesions [81, 191, 193, 216, 217], white matter

[82, 83, 200, 202], normal-appearing white matter [81, 186, 187, 191, 193, 205, 208, 217-219], grey matter [220], and mixed tissue [210, 212, 221-226]. In addition, N-acetyl aspartate quantified as institutional units or relative to non-creatine references like water or phantom acquisitions has been shown to decrease in mixed or unspecified multiple sclerosis lesions [164, 171, 227-233], white matter [234, 235], normal-appearing white matter [85, 164, 228, 231, 236-241], grey matter [108, 231, 237, 240, 241], mixed tissue [242, 243], spine [244-247], and whole-brain measures [248, 249]; in relapsing-remitting lesions [191, 194, 233, 250-252], normal-appearing white matter [84, 191, 206, 250, 252-255], grey matter [209, 250, 253, 254, 256], mixed tissue [257, 258], and whole-brain measures [259-262]; and in progressive lesions [191, 217, 233, 263], white matter [83, 202], normal-appearing white matter [84, 191, 217, 219, 255, 263-265], grey matter [108, 255, 265-267], mixed tissue [146, 225, 264, 268], spine [269], and whole-brain measures [260].

Creatine (Cr). Creatine (Cr) and phosphocreatine (PCr) support the equilibrium of phosphorylated adenosine species useful for cellular energy metabolism by way of kinase enzymes that shuttle phosphates among these molecules [163]. Both molecules exhibit overlapping singlets at 3.0 ppm and 3.9 ppm from methyl and methylene, respectively, in addition to amine signals [13]. The effect of multiple sclerosis on creatine concentrations in the central nervous system is still unclear, as creatine has been suggested to increase in mixed or unspecified multiple sclerosis lesions [229] and normal-appearing white matter [178]; in relapsing-remitting multiple sclerosis lesions [270], normal-appearing white matter [191, 208, 270], and mixed tissue [257]; and in progressive multiple sclerosis lesions [191], white matter [202], normal-appearing white matter [191, 208], and mixed tissue [221, 268]. It has also demonstrated decreases, however, in unspecified and mixed multiple sclerosis lesions [231], normal-appearing white matter [85], and grey matter [240];

in relapsing-remitting lesions [251]; and in progressive grey matter [267] and mixed tissue [225].

Choline (Cho). Choline-containing compounds, the majority of which are attached to the phospholipid membrane (much of choline or Cho not visible to ^{1}H MRS) but also found as small molecules in aqueous solution (phosphocholine or PCho and glycerophosphocholine or GPC), are thought to be taken into brain tissue through the blood-brain barrier as choline and represent the precursors and byproducts of phospholipid membrane metabolism [163]. Choline and phosphocholine exhibit high-intensity methyl singlets at 3.2 ppm with additional methylene multiplets at 4.1-4.3 ppm and 3.5-3.6 ppm, while glycerophosphocholine demonstrates a range of complex resonances from 3.2 to 4.3 ppm [13]. Creatine-referenced choline has demonstrated increases in mixed or unspecified multiple sclerosis group lesions [165-167, 176, 182, 271] and normal-appearing white matter [176, 182]; in relapsing-remitting lesions [190, 272, 273], normal-appearing white matter [274], and spine [275]; and in progressive lesions [217] and spine [215]. Decreases, however, have also been shown in mixed multiple sclerosis lesions [171] and in relapsing-remitting lesions [276], normal-appearing white matter [205], grey matter [277], and mixed tissue [277, 278]. Increases in choline quantified otherwise have been shown in mixed multiple sclerosis lesions [169, 227, 229] and normal-appearing white matter [229, 238]; in relapsing-remitting lesions [270, 279], white matter [79], normal-appearing white matter [270], and grey matter [256]; and progressive mixed tissue [221, 268], but decreases have also been demonstrated in mixed multiple sclerosis lesions [228, 231], normal-appearing white matter [85], and grey matter [231]; relapsing-remitting lesions [251] and grey matter [254]; and progressive mixed tissue [264].

Inositols (Ins). Inositols are cyclic organic molecules comprising nine different isomers, of which myoinositol and scylloinositol are the most abundant in human tissue. Myoinositol (mIns) can be found intracellularly within both glial cells and some neuronal types, where it serves as an osmolyte and metabolic precursor to a class of signaling molecules [21]. Inositols, particularly myoinositol, have demonstrated central nervous system abnormalities in multiple sclerosis. Creatine-referenced inositol or myoinositol has been shown to increase in mixed or unspecified multiple sclerosis lesions [166, 170, 171, 271, 280]; in relapsing-remitting lesions [190, 194, 272, 273, 281], normal-appearing white matter [206], and mixed tissue [221]; and in progressive mixed tissue [221] and spine [215], while inositols otherwise quantified have demonstrated increases in multiple sclerosis lesions [171, 229], normal-appearing white matter [229, 236, 238, 239, 245], and grey matter [108, 236, 239]; relapsing-remitting multiple sclerosis lesions [194], normal-appearing white matter [206, 208, 252, 254], and mixed tissue [258]; and progressive lesions [269], normal-appearing white matter [208, 265], grey matter [108], and mixed tissue [221].

Lactate (Lac). Lactate is a byproduct of pyruvate reduction in anaerobic glycolysis that is thought to serve as an alternative cellular energy source during high levels of neural activity. While transient increases of lactate have been observed in healthy brain, its prolonged presence in neural tissue is typically considered a mark of pathology [163]. Accordingly, some evidence exists of enhanced lactate signal in mixed or unspecified multiple sclerosis lesions [166, 173, 282] and relapsing-remitting lesions [273].

Glutamate (Glu) and glutamine (Gln). A large body of data suggests that α-amino acid glutamate, the primary excitatory neurotransmitter in the brain and a constituent of the glutathione (GSH)

tripeptide, also plays a complex and multifaceted role in multiple sclerosis pathology. Biochemical analyses of normal-appearing grey matter have demonstrated reductions in mRNA expression levels for enzymes associated with glutamate cycling, in particular amino acid transport proteins, in progressive multiple sclerosis relative to control [283], a pattern mirrored by the loss of astrocytic excitatory amino acid transporters relative to control in demyelinated progressive multiple sclerosis hippocampi [284] as well as in relapsing-remitting and progressive multiple sclerosis cortical lesions [285]. By contrast, expression of excitatory amino acid transporter mRNA and protein [286] as well as cysteine-glutamate antiporter system xc- mRNA [287] have been reported to increase in optic nerve white matter of multiple sclerosis patients relative to control; the latter has also been shown to be upregulated relative to control in multiple sclerosis normal-appearing white matter [288]. Excess extracellular glutamate has been reported to cause calcium-mediated apoptosis in an in vitro model of MS, and a lack of oligodendrocytic glutamate transporters has been speculated to be a cause for excitotoxicity [289]. Initial evidence for an excess of glutamate in acute MS lesions has been presented previously [229]. Additionally, at least one recent study has tied alterations in genes associated with glutamate metabolism to greater longitudinal declines in brain volume and N-acetyl aspartate in MS [290].

Synthesized in situ from glucose, glutamate is associated across both neurons and glia with the metabolism of other compounds also measurable by ^{1}H MRS, including glutamine, glutathione, and GABA. Briefly, glutamate synthesized in excitatory neurons is released by synaptic vesicles into the pericellular space, where it binds to depolarizing or metabotropic neurotransmitter receptors of postsynaptic neurons and/or traverses the excitatory amino acid transport proteins of nearby glial cell membranes to be converted to Krebs cycle intermediate α-ketoglutarate or recycled to glutamine. This glutamine is, in turn, released by glial cells for uptake and reconversion

to glutamate by nearby neurons. In inhibitory neurons, glutamate is converted to GABA by glutamate decarboxylase (GAD) and similarly released from synaptic vesicles into the pericellular space for binding to a different suite of hyperpolarizing or metabotropic receptors [291].

Similarly to glutamate, excess pericellular GABA is taken up by nearby glial cells for recycling to succinic semialdehyde, α-ketoglutarate, and then glutamate for participation in the aforementioned glutamate-glutamine cycle [291]. Notably, in addition to vesicular release by neurons, intracellular glutamate can also be transported out of neurons and glial cells by membrane cystine-glutamate antiporter system xc-, the main route of entry for the oxidized precursor to the intracellular cysteine necessary for GSH production [292]. In addition, GSH synthesis is triggered by changes in the extracellular concentration of glutamate [293]. Glutamate is thus both a product of and precursor to endogenous glutamine in a metabolic cycle that spans multiple cell types and implicates both GSH and GABA. Therefore, to fully understand the histological changes that accompany MS, it is important that changes to the concentrations of this particular molecule be isolated from those of glutamine and investigated in living human patients.

Isolating glutamate from its metabolic precursor and spectral neighbor glutamine (Gln) [163] is difficult at magnetic field strengths of 3 T and below, so ^{1}H-MRS experiments involving this metabolite in multiple sclerosis have been sparse. Glutamate concentration not referenced to creatine has shown decreases in multiple sclerosis mixed tissue [242] and relapsing-remitting mixed tissue [294] but also increases in multiple sclerosis lesions [229] and normal-appearing white matter [229, 237].

γ-aminobutyric acid (GABA). γ-amino-butyric acid (GABA) is a γ-amino acid that serves as an inhibitory neurotransmitter in mature central nervous circuits. The immediate role of GABA in MS

is unknown, but an inhibitory, immuno-modulatory effect has been suggested based on the concurrent observations of increased GABAergic activity and reduced immune activity in a mouse model of brain inflammation [115, 295].

GABA is naturally present at low concentrations in the brain compared with most other ^{1}H-MRS-visible molecules, and the signal amplitude of its peaks is further reduced by *J*-coupling interactions among its protons. Isolating its signature from those of nearby metabolites choline and creatine is therefore difficult in one-dimensional spectroscopy without additional spectral editing methods. While research on the molecule is therefore sparse, edited GABA concentration has been shown to decrease in relapsing-remitting [296] and progressive [146] mixed tissue. Limited research in humans has suggested a possible dichotomy between disease types, with GABA levels equivalent to control in the sensorimotor cortices of RR-MS patients [297] but lower than control in the sensorimotor cortices and hippocampi of SP-MS patients [146]. These suggestions of the potential role of GABA in MS pathology have been corroborated by biochemical studies showing decreases in the mRNA expression levels of proteins involved in both pre- and postsynaptic GABAergic signaling, including GABA receptors and GAD67, involved in GABA synthesis, in the white matter of MS patients relative to control [298]. As both an inhibitory neurotransmitter and signal molecule involved in the suppression of antigen-presenting cell (APC) activity, GABA has additionally exhibited treatment efficacy in animal models of some inflammatory diseases and therefore been proposed as a viable therapeutic for multiple sclerosis [299].

Glutathione (GSH). Glutathione, or the tripeptide GSH (glutamate, cysteine, and glycine), is endogenously synthesized by a number of cell types in the human body, including neurons and especially glial cells in the central nervous system [114]. Known to be an antioxidant for its

enzymatic and free oxidation to glutathione disulfide or GSSG, glutathione also exhibits a number of other biological functions, including roles in the storage and possibly cycling of its constituent amino acids, the synthesis of deoxyribonucleic acid triphosphates, and the enzymatic reduction of protein disulfide bonds [114]. Previous spectroscopy work has demonstrated lower concentrations of glutathione in multiple cortical regions of progressive MS patients relative to age- and sex-matched controls [300]. Given, however, that the proton spectroscopic resonances of glutathione overlap with those of small molecules and macromolecules of significantly higher concentration [301], its accurate measurement by traditional localization techniques is challenging, as indicated by the relative dearth of in vivo MRS research into this molecule's role in multiple sclerosis.

Limited work using ^{1}H-MRS has been performed to assess the effects of multiple sclerosis on endogenous antioxidant glutathione in the brain. Like GABA, glutathione possesses a low-amplitude spectral signature that overlaps heavily with metabolites of much higher brain concentrations, therefore requiring spectral editing for accurate quantification by one-dimensional ^{1}H-MRS. Previous research employing this editing has suggested that multiple sclerosis is associated with glutathione decreases in grey but not white matter voxels measured superior to the ventricles [241]; some evidence also exists of reduced glutathione concentration in secondary progressive mixed-tissue voxels in the frontal [300, 302] and parietal [300] cortex.

4.1.2. Heterogeneity of multiple sclerosis phenotypes: Review of current knowledge

It has been proposed that the pathology of multiple sclerosis be described in terms of two parallel but potentially independent metrics, disease activity and disease progression. Activity, more common in acute and relapsing forms of the disease, can be reflected in either acute relapses of clinical symptoms and/or visible as gadolinium contrast enhancements on T_1-weighted magnetic

resonance imaging scans. Progression is by definition restricted to disease exacerbation independent of relapses; as such, it describes disease-related changes that are more apparent in the primary or secondary progressive phenotype or phase. Along these lines, the term "worsening" has been recommended as a mechanism-agnostic clinical descriptor where "progression," now advised for use with greater precision to denote worsening independent of activity, has been in the past employed. It has been hypothesized that the two metrics activity and progression may themselves reflect, to an uncertain degree of independence, potentially interrelated mechanisms in inflammation and neurodegeneration, respectively [303].

Regardless of their direct function to any independently disparate mechanisms involving activity and/or progression, relapsing-remitting and progressive multiple sclerosis have exhibited different clinical and pathological manifestations. In contrast to the periodic appearance of new focal inflammatory lesions in relapsing-remitting or acute multiple sclerosis, progressive multiple sclerosis is marked by slow expansion of preexisting lesions, axonal degeneration, cortical lesions, and general microglial activation in and near existing lesions [304]. Particularly with regard to the conceptualization of progression as a later stage of an initially relapse-onset (initially relapsing-remitting and ultimately secondary progressive) disease course, hypotheses surrounding the mechanistic differences between the relapsing and progressive manifestations of multiple sclerosis have included, but are not limited to, normal aging, as well as metabolic disruptions secondary to tissue damage including oxidative stress, energy dysfunction or "virtual hypoxia," loss of glial trophic support, and immune activation. Research into the links between each of these processes and the onset of or transition to progressive multiple sclerosis is discussed in turn below.

Advanced age appears to contribute strongly to the progressive manifestation of multiple sclerosis pathology. Primary progressive multiple sclerosis appears to manifest on average ten

years later in life than relapsing-remitting multiple sclerosis [37, 38], around the time that relapse-onset disease also transitions to the progressive stage [305, 306]. It has been previously observed that regardless of the initial disease presentation, transition to progression clusters around similar ages near the end of the fourth decade of life [307]. It has also been shown that older age at disease onset associates with higher probability of progressive manifestation [38] and that a patient's current age can be an even stronger predictor than onset age for severity of disability, with faster disability progression rates among older patients even when controlling for onset age [308].

In rodent models, age relates inversely with the speed of remyelination [309], with evidence of stronger decline in males than females [310], and directly with vulnerability of demyelinated axons to degeneration [31, 311]. The antigen-presenting cells of older mice have also demonstrated higher constitutive expression of major histocompatibility complex II and evidence of enhanced antigen presentation, despite similar ability of lymphocytes from both young and old individuals to induce disease in others [312]. In humans, age at scan has also been shown to decrease the probability, number, or frequency of MR-visible enhancing lesions, even within the relapsing-remitting phenotype alone [313, 314].

The positive relationship between disease progression and age may also be associated with age-related changes in hormonal modulation. One study, for instance, showed that women with multiple sclerosis exhibited an increase in disease progression despite a highly significant decrease in annual relapse rate following menopause [315]. It is well-documented that primary progressive multiple sclerosis exhibits a female-male ratio closer to 1 than the 2:1 generally reported for the relapsing-remitting phenotype [37], suggesting a role for sex hormones in their respective underlying pathophysiologies.

Other work has suggested that, at least in relapse-onset multiple sclerosis, continuing

progression may be triggered when brain damage has exceeded a certain threshold. Not only higher age at relapse onset but also the frequency of early relapses themselves have exhibited a positive relationship with the probability and rapidity of transition from relapsing-remitting to secondary progressive multiple sclerosis [316]. High frequency of early relapses was also associated with faster functional declines once the progressive phase had been reached [316, 317]. The number of superimposed or continued relapses once the progressive phase has started has not shown such a positive relationship with progression onset or severity [318]. Rates of symptom worsening in relapse-onset populations differ by certain clinical and demographic variables only up to a certain threshold of disability, beyond which they are not predictive of symptomatic decline, while primary progressive patients exhibited no association between these variables and rates of decline [319]. Similarly, symptomatic decline up to an extended disability status score (EDSS) of 3 did not predict rates of decline to higher scores, which were generally faster [320].

The threshold beyond which relapse transitions to progression has also been hypothesized to reflect breakdowns of mitochondrial energy production [321], mitochondrial maintenance of redox potential [322], and/or trophic support from nearby glial cells or other neurons [323]. The molecular endpoint of these influences may be axonal degeneration, considered irreversible in comparison to demyelination, which to can be compensated to a point by mechanisms like remyelination and ion channel redistribution [324]. The energy deficiency or "virtual hypoxia" model states that demyelinated axons experience both increased energy demand and concomitantly decreased energy supply, resulting in neuronal dysfunction and death [321, 325]. Redistribution of Na+ channels due to K+ leaks across demyelinated axons increases energy demand by ATP-powered pumps following depolarization. Increases in intra-axonal sodium concentration due to incomplete resolution of membrane depolarization by Na+-K+ ATPase [326] may cause reversals

of the Na+/Ca2+ transporter [325] as suggested previously in anoxic rat optic nerve preparations [327], leading to pathologically high intracellular calcium concentrations that may contribute to proteolytic enzyme activation [328], neurofilament dephosphorylation previously observed in lesions [329], neurofilament fragmentation [298], microtubule depolymerization, and decreases in organelle content [298] as observed in lesions or nonlesioned cortex of multiple sclerosis [321]. In support of this hypothesis, sodium channel density increases have indeed been shown in demyelinated axons [330], with evidence of colocalization with sodium-calcium exchanger and axonal damage marker amyloid precursor protein [32]. Chronically demyelinated lesions, both active and inactive, have demonstrated reductions in axons positive for Na+-K+ ATPase indicative of energy failure despite possible initial compensation [331].

Increased mitochondrial numbers in response to the greater energy demand of demyelinated axonal segments with increased voltage-gated sodium influx may result in higher concentrations of intracellular reactive oxygen species (ROS), of which mitochondria constitute an important source [332]. Accumulated oxidative damage to mitochondria themselves, their genetic material rendered particularly susceptible by the lack of histones and limited repair mechanisms [326, 333], may also comprise an additional source of excessive ROS [326]. Histopathology data suggest, however, that an important initial source of ROS in lesioned tissue is their release via oxidative burst by activated macrophages and microglia [43]. Increased nitrotyrosine, a metabolic product of ROS damage to proteins, has been found in macrophages and astrocytes in active multiple sclerosis lesions and associated with higher expression of antioxidant enzymes in these cells but not surrounding neurons or oligodendrocytes [334]. Cerebrospinal fluid levels of nitrotyrosine oxidation product nitrate are higher than control during acute relapses but not during remission [335]. Evidence of nitrosative stress has additionally been observed relative

to control in multiple sclerosis normal-appearing white matter [336], and transcripts for enzymes that generate or detoxify ROS have shown abnormal expression in early, “pre-phagocytotic” lesions lacking evidence of overt demyelination [43]. Similarly, antioxidant gene transcription factor Nrf2, whose stability is increased by ROS exposure, demonstrates increases in active multiple sclerosis lesions [337].

Oxidative stress contributing to progressive degeneration may also be exacerbated by the enhanced release of iron from oligodendrocytes under immune attack as well as in some cases by consequence of normal aging [322, 338], and mitochondrial damage may itself also raise ROS levels via disturbances in oxidative phosphorylation [339]. Both lesions and normal-appearing grey matter in some individuals with secondary progressive multiple sclerosis have also demonstrated neuronal mitochondrial DNA deletions as well as diffuse loss of mtDNA-encoded mitochondrial respiratory chain complex IV relative to nucleus-encoded complex II [340]. Neuron-specific decreases in nuclear mitochondrial protein transcripts and lower mtDNA-encoded mitochondrial complex I and III function have been found in nonlesioned progressive multiple sclerosis motor cortex, with reduced organelle content and neurofilament fragmentation preferentially in demyelinated axons [298]. Nuclear and mtDNA-encoded mitochondrial transcripts have also shown reductions in the aforementioned early pre-phagocytotic lesions [43]. Neuronal mitochondrial complex activity deficits with evidence of increased axonal transport disruption marker amyloid precursor protein have been seen in active progressive multiple sclerosis lesions [341]. A portion of chronically demyelinated axons have shown increased mitochondrial mass relative to myelinated ones in patients [341]; evidence of abnormally increased mitochondrial to nuclear DNA copy number ratios in multiple sclerosis grey-matter neurons has similarly been observed [342]. Notably, reductions in mitochondrial gene transcript indicative of

mtDNA damage have been disproportionately observed in neurons relative to glial cells [298]. This state of reduced energy supply due to mitochondrial damage also itself contributes to the failure of axonal ionic homeostasis described above to underlie the “virtual hypoxia” model of multiple sclerosis progression [325].

Chronic disruption of trophic support from glial cells, in particular oligodendrocytes, may additionally contribute to continuing neuronal dysfunction and necrosis [321]. Genetically engineered mice with deficiencies in myelin proteolipid [343] and Cnp1 [344] display signs of central nervous system axonal degeneration in adulthood. Notably, the late timing of axonal degeneration in myelin protein-deficient mice suggests an analogous developmental timescale on the order of years in humans [321, 345]. Similarly, mice exposed to the demyelinating influence of oral cuprizone for several weeks exhibited a reduction and then full recovery in locomotor function followed by a second, delayed functional decline concomitant with reduced callosal axon number, brain atrophy, and increase in axonal amyloid precursor-protein 6 months after cessation of administration [346]. While neither oligodendrocyte precursor cells nor remyelinated axons have been shown to deplete following repeated episodes of focal demyelination in rats [347], sustained chronic demyelination has been shown to reduce local oligodendrocyte precursor cell availability [31, 348], and demyelination persists even after the chronically demyelinating factor is removed [349]. The risk of chronically demyelinated tissue becoming permanently demyelinated is potentially exacerbated by the finding that previously demyelinated edges of slowly expanding lesions are more likely to be demyelinated again than never-demyelinated edges [55]. Chronically demyelinated lesions exhibit chemical environments inhibitive to the differentiation of mature oligodendrocytes; this rather than precursor cell availability is thought to be the limiting factor in age-related failure to remyelinate [31]. Oxidative stress, to which

oligodendrocytes and especially their precursors are particularly vulnerable [332], has itself been demonstrated to impair OPC differentiation and maturation [350]. Even transient inhibition of complex IV activity within the mitochondrial respiratory chain was shown to impair the differentiation of oligodendrocyte progenitor cells in cultures taken from postnatal rats [351]. Additionally, both demyelination and oligodendrocyte degeneration have been observed to follow primary injury to astrocytes by microglia locally activated by lipopolysaccharide injection in a rat model of brain inflammation, further demonstrating the potentially complex dependencies among different cell types in tissue environments, particularly in the subset of multiple sclerosis lesions demonstrating postmortem evidence of astrocytic process loss [352].

A related hypothesis posits that focal white matter inflammation, potentially driven by peripheral autoimmunity, induces neuronal death that activates CNS microglia, which then drives wider cortical neurodegeneration [353]. On a more macroscopic scale, compensatory plasticity may also prove insufficient once the brain reaches a critical threshold of axonal loss by a variety of mechanisms such as those detailed above [321].

In addition to the above investigations into the various physiological triggers that may underlie delayed transition from relapsing to progressive multiple sclerosis pathology, evidence also exists that at least some of the pathological mechanisms potentially driving progression feature in multiple sclerosis pathogenesis from the start, even in relapse-onset phenotypes. Evidence of axonal damage, including amyloid precursor protein [354] positively correlated with numbers of macrophages and CD-8+ T-lymphocytes [355, 356], as well as axonal transection [357], is present in acute lesions [326]. Indeed, transected axons have been observed in individuals with relapsing-remitting multiple sclerosis as soon as two weeks after diagnosis [357], supporting the hypothesis that progression constitutes the symptomatic manifestation of exceeding plasticity and

redundancy thresholds in central nervous networks compensating for damage since early in disease [284]. Relapsing-remitting disease of duration less than three years has been associated with both grey and white matter cortical atrophy relative to control values, even when considering age and sex [358]; patients with clinically isolated syndrome, a pathology that is symptomatically indicative of multiple sclerosis but that does not fulfill all of its diagnostic criteria, who eventually developed multiple sclerosis also exhibited larger ventricular volumes indicative of brain atrophy than those who did not develop the disease [359].

Similarly, MRI analysis of head size-normalized cortical volumes in both relapsing-remitting and primary progressive patients demonstrated decreases in both patient groups relative to control without differences between them; notably, cortical volume decreases were found even in patients with short disease duration and low lesion load and were interpreted to be suggestive of a disease process parallel to but not necessarily dependent on white-matter inflammation [360]. In primary progressive disease, diffusion-tensor magnetic resonance measures of diffuse normal-appearing tissue damage has exhibited no correlation with T_2-weighted lesion volume [361]. Along the same vein, no appreciable difference in either cortical atrophy or creatine-referenced N-acetyl aspartate was seen between primary progressive patients with low and high T_2-weighted lesion volume [226]. Histological analysis of post-mortem brains from acute, relapsing, secondary progressive, and primary progressive patients has supported this finding, demonstrating the simultaneous presence of focal lesioning and diffuse white-matter inflammation and cortical demyelination, as well as the lack of significant correlation between the former and either of the latter [40]. Notably, relapse-onset patients have demonstrated expression abnormalities in proteins involved in leukocyte trafficking across the blood-brain barrier that were absent in individuals with primary progressive disease, suggesting that at least some inflammatory mechanisms may play a

greater role in the pathogenesis of the former than the latter [362]. It bears mention, however, that the weak associations reported throughout the literature between white-matter lesion load and grey-matter atrophy may still reflect a delayed rather than an absent or third-variable causative relationship, as has been argued previously [363] on the basis of findings that longitudinal whole-brain atrophy endpoints tracked more closely with earlier than later lesion formation [364].

Brain atrophy in multiple sclerosis may disparately affect different tissues, with greater accelerations in grey than white matter loss as the disease progresses [365]. Studies of whole-brain atrophy have not uncovered differences among multiple sclerosis subtypes [366-368]; by contrast, cross-sectional or longitudinal grey but not white matter volume reductions have been shown relative to control in both early relapse-onset [369, 370] and primary progressive disease [34]. Either increased or decreased concentrations of proteins associated with grey-matter tissue have been observed in the CSF of multiple sclerosis patients undergoing a first attack relative to not only controls but also patients with more established disease [371]. Accelerated grey but not white matter atrophy has been seen in the progressive stage of relapse-onset disease [365, 372]. In line with this, secondary progressive but not relapsing-remitting patients have shown abnormally low age-adjusted grey- but not white-matter volumes [373]. Relapsing-remitting multiple sclerosis patients analyzed alone have shown correlations between longitudinally measured grey-matter atrophy rate and lesion magnetic transfer ratio, presence of lesion contrast enhancement, and increase in T_2-weighted lesion volume not found in secondary progressive multiple sclerosis [365].

More cortical demyelination and smaller white-matter involvement in cortical lesions have been suggested in primary progressive MS patients than secondary progressive or relapsing-remitting patients, though the differences did not reach statistical significance [374]. Histological analysis has also demonstrated no significant correlation between demyelination of cortex and

white matter [40, 374, 375], leading to the claim that these may represent independent pathologies [375]. CSF neurofilament light chain protein levels, shown to predict risk of cortical atrophy in MS, correlates with cortical but not white-matter lesion number and volume [376]. Cortical lesions themselves have demonstrated minimal infiltration by lymphocytes and myelin-laden macrophages or complement deposition, little astrogliosis, and in some cases rims of astroglial excitatory amino acid transporter overexpression, in contrast to active white-matter lesions [285].

Other pathological manifestations, such as ectopic B-lymphocyte follicles in some secondary progressive cases [49], appear to play a role in more severe and progressive, but not necessarily later [377], disease. Early relapse frequency associated negatively with age at death in progressive patients without ectopic B follicles but not in those with, suggesting the importance of nonlocal mechanisms of disease progression in at least one phenotype [48]. Inflammatory cytokine and chemokine profiles supportive of B-lymphocyte function have been associated with higher cortical lesion loads in early relapsing-remitting multiple sclerosis despite the apparent absence of follicles at this stage [376]. In turn, secondary progressive patients with ectopic B-lymphocyte follicles have been shown to exhibit more microglial activation in normal-appearing grey matter than those without or primary progressive patients [48].

The parallel development of progressive with relapsing pathology, as well as its exacerbation with age or disease duration, need not be mutually exclusive models of disease. Grey-matter atrophy has been demonstrated as early in the multiple sclerosis disease course as the relapsing-remitting stage [358] and even clinically isolated syndrome [369], but patients with clinically isolated syndrome and relapsing-remitting multiple sclerosis have shown less atrophy than the progressive phenotypes [40]. Conversely, histological evidence of acute axonal damage, via local amyloid precursor protein deposition, is greatest in lesions biopsied early in the course

of disease, especially in relapsing-remitting multiple sclerosis; interestingly, no such temporal relationship was shown for patients of the primary progressive phenotype [356]. More pronounced diffuse inflammation, characterized by perivascular monocyte aggregation, T-lymphocyte infiltration, and microglial activation, as well as more diffuse axonal injury, have been observed in the normal-appearing white matter of secondary and primary progressive patients than in relapsing-remitting and acute multiple sclerosis [40]; in cortex, infiltration of T- or B-lymphocytes was reduced in progressive relative to relapsing-remitting multiple sclerosis, while plasma cell infiltrates were increased [42].

Regardless of the degree to which they may represent parallel and/or serial manifestations of independent or overlapping disease states, then, relapsing and progressive multiple sclerosis phenotypes have been associated with a number of symptomatic, anatomical, and histopathological differences that justify their investigation as distinct entities in addition to or even instead of, as has often been employed in the ^{1}H MRS literature in studies containing individuals of either diagnosis (see, for example, Table 1.1 in Chapter 1), as a single "multiple sclerosis" cohort.

4.1.3. Relapsing versus progressive MS: The utility of targeted in vivo ^{1}H MRS research in human participants

The insufficiency of current treatments for progressive relative to relapsing-remitting multiple sclerosis, in addition to the relatively less convincing validity of current animal models for the former compared to the latter, especially motivate the development of experimental techniques like ^{1}H MRS that can be applied to the distinction and further study of these two phenotype classes in human patients.

The first justification for ^{1}H MRS research into progressive multiple sclerosis in particular

is that few disease-modifying therapies have demonstrated efficacy for this phenotype relative to the more common relapsing-remitting condition: Despite more than a dozen approved therapies for relapsing-remitting multiple sclerosis, as of 2020 the FDA has approved only three—sphingosine-1-phosphate (S1P) receptor ligand siponimod, chemotherapy agent mitoxantrone, and monoclonal antibody ocralizumab—specifically for secondary or primary progressive phenotypes, two over the last three years [378] (this does not count cladribine, which has also been approved for "relapsing" multiple sclerosis, including secondary progressive cases that still demonstrate relapse activity [379]). Existing disease-modifying therapies for relapsing-remitting multiple sclerosis, including interferon β1a [380], glatiramer acetate [381], and rituximab [382] have been applied without significant efficacy in phase III trials for primary progressive multiple sclerosis [353]. Indeed, an earlier, more relapsing disease phase has been thought to contribute to the greater treatment-associated delay in progression seen in the European trial for interferon β-1b on progressive disease [383], which recruited younger patients with more recent relapses and greater decrease in extended disability status scale (EDSS) than those in the American trial for interferon β-1b, which provided no evidence for such a delay [384, 385]. In short, disease progression as opposed to acute relapses has proven a more elusive endpoint for pharmacotherapeutic intervention.

For example, despite years of research demonstrating a degree of therapeutic efficacy against acute disease activity by autologous hematopoietic stem cell therapy, meta-analyses thereof have concluded greater benefit for relapsing-remitting than progressive multiple sclerosis [386, 387]; autologous hematopoietic stem cell therapy is therefore not recommended for patients of progressive multiple sclerosis without superimposed clinical relapses [388]. Some studies using autologous mesenchymal stem cell transplantation to treat progressive multiple sclerosis have,

however, demonstrated efficacy [389]. One study in particular demonstrated decreases in median expanded disability status scale (EDSS) score from baseline to six months following the six-month treatment schedule [390].

Such positive results as this one have nonetheless often been rendered inconclusive by study designs lacking control by placebo or gold standard. For example, open-label natalizumab administration to secondary and primary progressive multiple sclerosis patients reduced cerebrospinal fluid biomarkers of inflammation and axonal damage from baseline to week 60, in addition to effecting decreases in EDSS from baseline; lack of placebo control, however, makes these results difficult to interpret [391]. Placebo-controlled phase-3 testing of natalizumab similarly demonstrated some benefit of the drug to upper limb function in secondary progressive patients but failed to meet its primary endpoint of improvements relative to placebo in multi-functional disability progression over two years [392].

The administration of siponimod, approved for relapse-active secondary progressive MS in 2019 [378], in a secondary progressive cohort demonstrated decreases relative to placebo in brain volume reductions as well as significant reductions in T_2-weighted lesion volume expansion at 12 and 24 months [393]. While post-hoc analysis on these data demonstrated that a large proportion of the drug's therapeutic effect on disability progression could be attributed to processes beyond simply reducing relapses [394], differences in the proportion of patients with confirmed disability progression at six months were only marginally significant [393].

Ibudilast administration effected reductions in brain atrophy relative to placebo over 96 weeks, though the relative reduction in disability progression was not significant [394, 395]. Similarly, a placebo-controlled trial of laquinimod showed no therapeutic effect on parenchymal brain volume changes over 48 weeks in primary progressive multiple sclerosis [396]. Lamotrigine

administration to secondary progressive multiple sclerosis patients appeared to result in decreased reduction in timed 25-foot walk function over 24 months but appeared to increase brain volume losses relative to placebo over the study period [397].

In individuals with primary or secondary progressive multiple sclerosis, cladribine reduced the proportion of patients who developed, as well as the mean volumes and numbers, of enhancing T_1-weighted lesions through six months but, like many of the other trials listed here, had no significant effect on disability progression [398].

Sulphasalazine was found to transiently decrease the rate of disability progression over 18 months in a progressive multiple sclerosis subgroup relative to placebo, but this effect was not sustained over the second half of the four-year trial [399]. Similarly, glatiramer acetate was found in chronic progressive multiple sclerosis patients to yield lower two-year progression rates for either unconfirmed progression or progression of 0.5 units relative to placebo, but no effect was seen for the primary study endpoint confirmed disability progression of 1-1.5 units [400].

Some notable exceptions to this pattern of null or inconclusive results for treatment efficacy on progressive multiple sclerosis exist. Ocrelizumab has been shown in primary progressive multiple sclerosis to reduce 24-week disability progression by 24% relative to placebo, decrease T_2-weighted lesion volume by 3.4% (as opposed to a 7.4% increase in placebo), and reduced the rate of brain volume loss by 17.5% [401, 402]. This demonstrated effect contrasts with that shown for rituximab on primary progressive patients, who demonstrated decreased rates of T_2-weighted lesion expansion but no change in time to disability progression or rate of brain volume loss over 122 weeks with treatment, though time to disability progression was delayed with rituximab in subgroups involving only individuals under 51 years or with enhancing lesions [382]. Treatment with alemtuzumab has been shown to precede decreases in annual relapse rate

without marked improvements in disability progression or cerebral atrophy for secondary progressive multiple sclerosis [403].

High doses of biotin appeared to effect clinical improvements in a majority of primary and secondary progressive multiple sclerosis patients in an open-label pilot study [404]. In a randomized, placebo-controlled trial, about one-tenth of patients on biotin, and none of those on placebo, met primary endpoints of disability reversal as defined by EDSS decrease of at least 1 (or at least 0.5 for those with baseline EDSS of at least 6) by 9 months, and confirmed again at 12, months [405]. Another blinded placebo-controlled trial in patients demonstrating chronic MS-related visual loss in at least one eye did not meet its primary endpoint of visual acuity improvement in the affected eye relative to the placebo group [406]. Despite these promising findings, preliminary results have also suggested increased breakthrough acute inflammatory disease activity in primary progressive patients [407].

Beyond this litany of negative or inconclusive clinical trials for novel therapeutics of progressive multiple sclerosis suggesting the need for a paradigm shift, either involving ^{1}H MRS or not, in current drug development pipelines for the disease, the second line of argumentation that supports the potential utility of in vivo magnetic resonance spectroscopy work within the field of progressive multiple sclerosis is the limited generalizability of animal models particularly for this class of disease phenotypes.

Experimental autoimmune encephalomyelitis is a model of brain inflammation that can be induced by the peripheral injection of emulsified central nervous system antigen, particularly myelin oligodendrocyte glycoprotein (MOG), myelin-associated glycoprotein (MAG), myelin basic protein (MBP), and proteolipid protein (PLP) [353], with one or more inflammatory agents, like complete Freund's adjuvant or pertussis toxin [304]; by the adoptive transfer of T-lymphocytes

from animals such injected [408], sometimes with additional myelin-directed antibodies [409]; or by animals inbred with T-cell receptors autoreactive for myelin peptides who exhibit the disease spontaneously [410]. As pathology centered on autoreactive CD4+ or, more rarely, CD8+ T-lymphocytes, this animal model is disproportionately useful for studying the de/remyelinating aspects of human multiple sclerosis [304]. None among the autoantigens used to induce experimental autoimmune encephalomyelitis (EAE) in nonhuman animals has yet been identified as a singular target for multiple sclerosis in humans [162], though evidence has been found of increased myelin basic protein reactivity by serum and cerebrospinal fluid lymphocytes from both acute and progressive multiple sclerosis patients [411]. By contrast, autoantibodies for one of these antigens, myelin oligodendroglial glycoprotein, have been observed in the serum of acute disseminated encephalomyelitis and optic neuritis patients [39, 353]. Increases in MOG have not been shown in serum [412, 413] or CSF of most individuals with adult-onset multiple sclerosis [414]. Furthermore, the phenotypic manifestation of often severe focal lesioning followed by remission with or without continued relapses in affected rodents most resembles the relapsing-remitting aspects of the disease.

Few exceptions exist [304]. Some rat strains with certain major histocompatibility complex (MHC) I and II isotypes and alleles [415] as well as marmosets [416] have manifested EAE as cortical lesioning, shown to predominate in human secondary and primary relative to relapsing-remitting multiple sclerosis [40]. EAE in the non-obese diabetic mouse displays relapses followed by focal contrast enhancement and immune cell infiltration in a “chronic progressive” stage [417]. Additionally, meningeal inflammation and ectopic lymphoid follicle-like formations without subpial cortical demyelination have been shown in some EAE mouse strains [418].

Other animal models of multiple-sclerosis-like pathology include exposure to

demyelinating viral infections like Theiler's virus and murine coronavirus or toxins like cuprizone, lysolethicin, and ethidium bromide [304]. Unlike EAE, murine coronavirus models exhibit widespread microglial activation [419], also seen in progressive multiple sclerosis [40, 48]. The induction of these models via exogenous virus means, however, that pathology may be exacerbated by therapies shown beneficial in multiple sclerosis, which limits their utility for novel target identification in human disease [304]. Animals exposed to cuprizone may exhibit progressive neurodegeneration after an initial demyelinating relapse and remission [346], but the absence of a diffuse inflammatory component may limit the generalizability of this model to progressive multiple sclerosis.

Taken together, these data from clinical and preclinical work demonstrate that further targeted in vivo magnetic resonance spectroscopy research into progressive as distinct from relapsing-remitting multiple sclerosis, particularly with a mind to investigations that may ultimately support the development of disease-modifying therapies efficacious for the former, is warranted. In particular, noninvasive investigations of in vivo human tissue metabolism enabled by ^{1}H MRS may exhibit special utility for informing drug development pipelines in progressive MS given the relative inadequacy of animal models for this class of multiple sclerosis phenotypes.

4.1.4. Improving upon the failure of single ^{1}H-MRS-measurable metabolic abnormalities to support multiple sclerosis diagnosis

Since its first application in 1946, ^{1}H MRS has offered a safe and flexible means of noninvasively estimating the concentrations of various small-molecule metabolites in living tissue, including the brain. Though over 190 original research and case reports using this molecule to examine the central nervous system metabolic signatures of multiple sclerosis have been published since 1990,

the field continues to lack knowledge of a single metabolite alteration that can enable the identification of multiple sclerosis with sufficient sensitivity and specificity for appropriate clinical use.

In principle, ^{1}H-MRS data should be useful for differentiation among distinct multiple sclerosis phenotypes, especially given that progressive subtypes may predominantly exhibit cortical as opposed to active white-matter lesioning [40], the former largely invisible to conventional clinical imaging [374, 420, 421]. While some evidence exists that relapsing and progressive multiple sclerosis may express differential metabolic signatures in white-matter N-acetyl aspartate [81-85] and perhaps creatine [202] as well as grey-matter N-acetyl aspartate [220, 255] and inositols [108], direct phenotypic comparisons by proton spectroscopy remain sparse [24], and, as mentioned, univariate abnormalities in either group appear subtle and inconsistent.

In addition, while a number of studies, as outlined above, have used ^{1}H MRS to examine the in vivo cortical metabolic signatures of multiple sclerosis, none has yet examined three key metabolites glutathione, GABA, and glutamate in the same investigation.

The quantification of neurochemicals with conventional ^{1}H MRS is difficult if concentrations are small and resonances overlap with signals from other substances. While glutathione and GABA are both biomolecules that have been implicated in MS pathology as outlined previously, their quantification by ^{1}H MRS is complicated by both of these factors. In the cortex, both exist in the low millimolar range, and their resonances are hidden under signals on the order of up to approximately twenty times more intense from neighboring metabolites like creatine. The unobstructed measurement and quantification of both GSH and GABA are therefore particularly challenging. Spectral editing techniques can exploit the specificity of intra-molecular nuclear couplings to extract a desired signal from the rest of the spectrum [19]; the benefits of this

kind of spectral editing for quantification of GSH were first presented by Terpstra and colleagues in healthy individuals [422] and subsequently by others in MS patients [62, 241]. Spectral editing has also been similarly applied in healthy participants [423] and in MS patients [296, 297] to quantify GABA.

Similarly, resolving the proton spectroscopic resonance for glutamate from that for glutamine can be difficult at field strengths lower than 7 Tesla. As a result, much previous work examining the effects of MS disease state on brain glutamate concentrations has not isolated the molecule, instead conflating it with glutamine under the term glutamate-glutamine (Glx). Within this paradigm, reductions in Glx have been found in the cortical grey matter of both RR-MS patients [254, 258] and PP-MS patients [265] as well as in the predominantly grey-matter parietal and cingulate cortical voxels of RR-MS patients [294] and in the cervical spinal cords of PP-MS patients [269], while elevations in Glx [229, 236] and glutamate/NAA ratio [237] have been reported in the normal-appearing white matter of mixed MS patient cohorts.

To this end, the present chapter attempts to assess the use of proton MR spectroscopy as a means to distinguish among individuals with progressive, relapsing-remitting, and no multiple sclerosis on the basis of proton MR-visible prefrontal cortex metabolic signature acquired at 7 Tesla. This will be attempted from two novel approaches: First, we assess single-variable cross-sectional differences using a constellation of prefrontal cortex metabolite signatures never previously measured together in a single study of multiple sclerosis: the rarely considered glutamate as isolated from glutamine, GABA, and glutathione, as well as the more commonly measured total N-acetyl aspartate, myoinositol, total creatine, and total choline. Second, by applying either multivariate statistical techniques (e.g., discriminant analysis) or supervised machine-learning approaches to these data, we attempt to simultaneously employ the full suite of

metabolic information in hand to classify multiple sclerosis phenotype on the basis of these prefrontal cortex metabolite concentrations alone.

4.2 Single-variable cross-sectional analysis of prefrontal cortex metabolic abnormality in relapsing-remitting and progressive multiple sclerosis

4.2.1. Motivation

To date, the relevance of GSH, GABA, and glutamate to multiple sclerosis pathology has not been satisfactorily explored in the same study; an extant need therefore exists to understand disease-related alterations to these three molecules in concert with each other and the rest of their biochemical environments. To this end, the present study attempts to fill some gaps in our knowledge of the relationship between MS and glutathione, GABA, and glutamate, particularly in their potentially disparate presentations in the relapsing-remitting and progressive disease course. Here we apply a ^{1}H-MRS protocol of previously validated quality and reproducibility [106] to compare the endogenous concentrations of glutathione, GABA, and glutamate, in addition to total NAA (N-acetyl aspartate plus N-acetyl aspartylglutamate), total creatine (creatine plus phosphocreatine), total choline (choline plus phosphocholine), and the inositols (myoinositol and scylloinositol) in a single mixed-tissue frontal cortex voxel of forty-seven patients of relapsing-remitting and progressive MS with those of age- and sex-matched non-MS controls. In addition to exploiting the higher signal to noise ratio and increased spectral dispersion enabled by scanning at 7 Tesla, our methodology included *J*-difference editing to separate glutathione and GABA resonances from surrounding metabolite peaks as well as a low-echo-time macromolecule-suppressed STEAM sequence to acquire glutamate peaks distinct from those of the structurally similar glutamine. We chose to study a prefrontal cortex (PFC) voxel because it is a large accessible

Table 4.1. Scan participant demographics and clinical characteristics

	Controls (N = 25)	Relapsing-remitting multiple sclerosis (N = 26)	Progressive multiple sclerosis (N = 21)
Sex	16 female, 9 male	18 female, 8 male	12 female, 9 male
Age[a] (years)	43 ± 15 (21 – 69)	44 ± 13 (26 – 68)	55 ± 8 (43 – 68)
Years with multiple sclerosis since symptom onset[b]		13 ± 12	23 ± 14
Years with multiple sclerosis since diagnosis[b]		9 ± 7	16 ± 13
Disease-modifying therapy at time of scan		10 dimethyl fumarate 5 natalizumab 2 glatiramer acetate 2 rituximab 1 interferon beta 1 steroids 5 none reported	7 dimethyl fumarate 0 natalizumab 4 glatiramer acetate 1 rituximab 1 interferon beta 0 steroids 8 none reported
Voxel brain tissue partial volume[c]	0.97 ± 0.05	0.98 ± 0.06	0.93 ± 0.08
Voxel brain tissue grey-matter fraction	0.54 ± 0.06	0.50 ± 0.1	0.51 ± 0.09

[a] Mean ± standard deviation (range)
[b] Mean ± standard deviation
[c] Significant age coefficient for general linear model in controls; statistics corrected for age

area of cortical tissue that would presumably reflect any global disease-related changes to brain metabolism; in addition, MS research using ^{1}H MRS on this region of the brain is limited, due in part to the methodological challenges of acquiring high-quality spectra in this region of typically high field inhomogeneity.

4.2.2. Methods

Participants. Adult volunteers with relapsing-remitting (eighteen female; mean ± standard deviation 44 ± 13 years old), progressive (six primary, fifteen secondary; twelve female; 55 ± 8 years), and no (sixteen female; 43 ± 15 years) multiple sclerosis were studied in a single one-hour

magnetic resonance scan (Table 4.1). Eligible participants were between the ages of 18 and 70 and recruited through the Yale Center for Clinical Investigation (YCCI) and the Yale-New Haven Health Interventional Immunology Center. All non-control participants had been previously diagnosed with multiple sclerosis by a physician. All participants provided written informed consent prior to scanning according to the Declaration of Helsinki, and experimentation was conducted in accordance with protocol #1107008743 approved by the Yale School of Medicine Human Investigation Committee. Power analysis estimated a group size of fifteen as sufficient for pairwise detection at $\alpha = 0.05$ and 80% power of previously published meta-analytic effect size of -0.92 (Hedges' *g*) for N-acetyl aspartate in normal-appearing grey matter for moderately severe multiple sclerosis [424].

Experimental setup. Spectroscopy data were obtained on a 7-Tesla head-only magnetic resonance system (Agilent, Santa Clara, CA, USA) at the Yale School of Medicine Magnetic Resonance Research Center (MRRC) using a previously described acquisition protocol [106] for improved spectral dispersion and detection sensitivity. *J*-difference editing (MEGA) of semi-LASER (echo time T_E 72 ms; repetition time T_R 3 s) sequences for acquisition of glutathione or GABA and low-echo-time macromolecule-suppressed STEAM (T_E 10 ms, mixing time T_M 50 ms, T_R 3 s) for acquisition of glutamate, glutamine, total N-acetyl aspartate (N-acetyl aspartate and N-acetyl aspartylglutamate), total choline (choline, phosphocholine, and glycerophosphocholine), and myoinositol were employed in a single 27-cc cubic voxel at the longitudinal fissure of the medial prefrontal cortex (Figure 4.1). Quantification was achieved by linear combination modeling of density-matrix simulated basis spectra, and the lower bounds of standard deviations on spectral quantification error were estimated for each metabolite via Cramér-Rao Lower Bounds. Metabolite

concentrations were referenced to 10 mM total creatine (creatine and phosphocreatine) quantified from either STEAM or the *J*-difference edit-off condition of the appropriate semi-LASER sequence. Voxels were segmented into grey matter, white matter, and cerebrospinal fluid for investigation of potential confound of metabolite values by voxel tissue composition.

Spectral acquisition. An eight-channel phased-array radiofrequency coil was used for spin handling and signal reception [425]. Voxel placement was guided by T_1-weighted imaging. B_1 phase shimming was achieved through in-house software (IMAGO). B_0 shimming was performed with customized software (B0DETOX) [426] and comprised zero- through third-order spherical harmonics shapes.

Glutathione (2.95-ppm cysteine $^{7'}CH_2$ resonance; editing on the 4.56-ppm cysteine ^{7}CH resonance) and GABA (3.01-ppm $^{4}CH_2$ resonance; editing on the 1.89-ppm $^{3}CH_2$ resonance) were measured with single-voxel *J*-difference editing based on a MEGA semi-localized by adiabatic selective refocusing (sLASER) [427] sequence as previously applied in vivo [19, 422]. Water suppression was achieved using the CHEmical Shift Selective (CHESS) technique [428], and potential macromolecule signals at 3.0 ppm were nulled by an inversion-recovery preparation for measurement of GABA [429]. In addition, double-banded Gaussian radiofrequency pulses were applied for simultaneous spectral editing and improved water suppression as employed previously [106].

Glutamate and several other metabolites, including total creatine (creatine and phosphocreatine), total choline (choline, phosphocholine, and glycerophosphocholine), total N-acetyl aspartate (N-acetyl aspartate and N-acetyl aspartylglutamate), glutamine, and myoinositol were measured using short echo-time stimulated echo acquisition mode (STEAM) [430]. Water

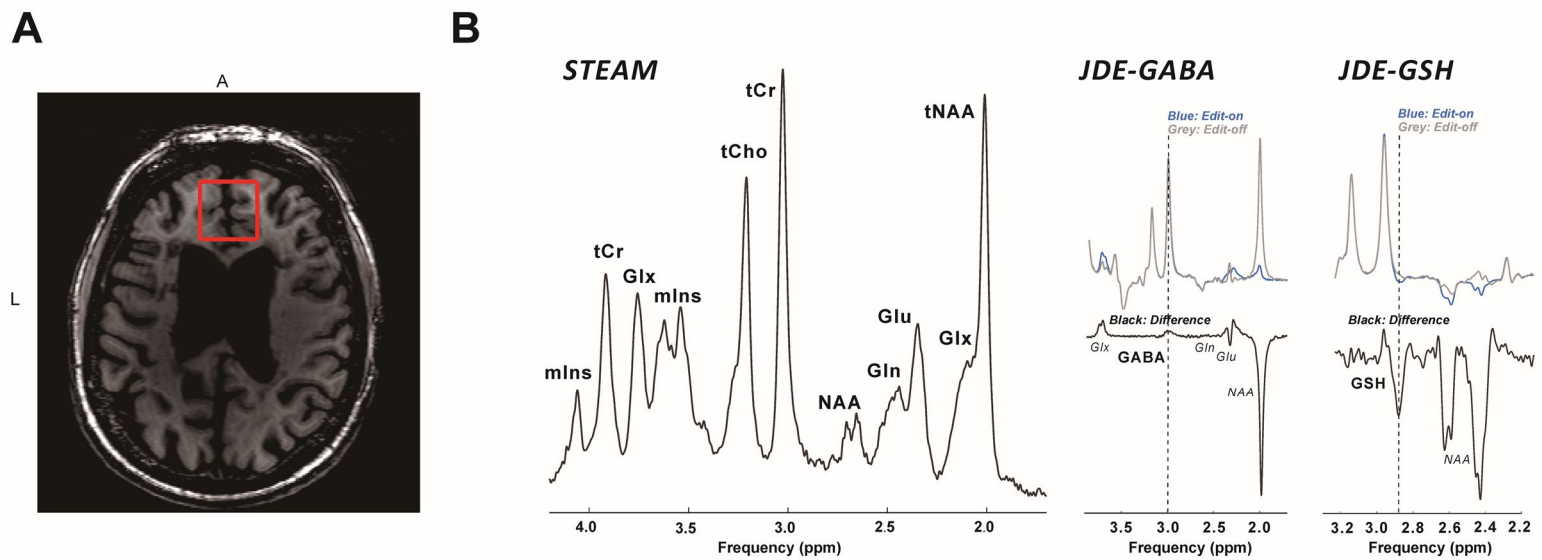

Figure 4.1. Experiment pipeline for in vivo biochemical profiling of multiple sclerosis pathology in the frontal cortex. A) T_1-weighted imaging was used to place a 3-cm isotropic cubic spectroscopy voxel in the prefrontal cortex. Depicted is the transverse slice through the center of the spectroscopy voxel in a 62-year-old male individual with progressive multiple sclerosis. Third-order spherical harmonics B_0 shimming maximized local static field homogeneity for optimal spectral quality. B) Single-voxel proton spectroscopy acquisitions comprised three experiments optimized for the measurement of glutamate (STEAM), γ-amino butyric acid (JDE-GABA), and glutathione (JDE-GSH). JDE: *J*-difference editing, Glu: glutamate, Gln: glutamine, Glx: glutamate + glutamine, mIns: myoinositol, tNAA: total N-acetyl aspartate, tCr: total creatine, tCho: total choline, ppm: parts per million. Displayed as appears in Swanberg, Prinsen et al., *NMR Biomed* 2021; 34(11): e4590.

suppression was similarly based on CHESS, with two additional pulses applied during mixing time, and complementary outer-volume suppression was used to improve localization specificity [431]. Macromolecule signals from lipids and proteins, potentially altered by multiple sclerosis disease activity [432], are known to cause a nonlinear baseline, thereby complicating metabolite quantification [429, 433]. The STEAM acquisition was therefore preceded by an inversion-recovery preparation to minimize macromolecule signals (inversion time T_I 320 ms). Water-unsuppressed signals from each experiment were acquired for later use in eddy current correction.

Spectra were acquired as series of 4096 complex points in two blocks of 32 traces (STEAM) or two to six blocks of 64 traces (sLASER with JDE for GSH or GABA) each preceded by two dummy scans.

Spectral processing and quantification. Spectral datasets were stripped of group identifiers and recoded to blind the investigators to disease conditions during processing and quantification. Processing was achieved in INSPECTOR [106, 434]. Eddy current phase correction [118] was applied, followed by frequency and phase correction of individual spectral traces before signals from individual receiver channels were combined in a sensitivity-weighted fashion and repetitions were summed. These corrections were applied in an editing condition-specific fashion for *J*-difference-edited acquisitions, following which the spectra of each condition were averaged separately as edit-off and edit-on means, which were then mutually aligned before they were subtracted from each other to derive the edited glutathione and GABA signals (Figure 4.1B).

Metabolite signal intensities were estimated by linear combination model fitting of basis spectra to each aligned, averaged, and preprocessed complex vector of spectral data in LCModel [20]. This fit algorithm was chosen according to an assessment of several linear combination model

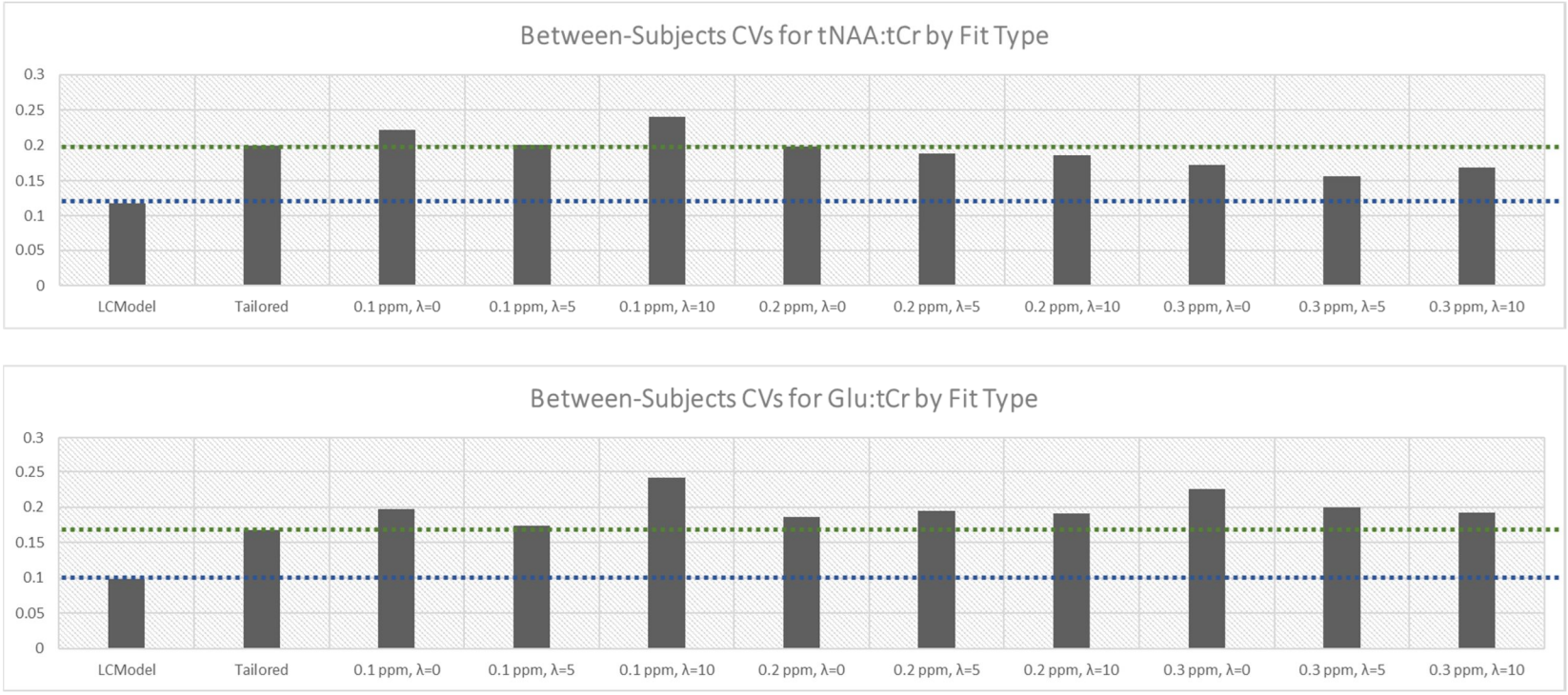

Figure 4.2. Linear combination modeling approaches differing predominantly in baseline handling were assessed against control-group between-subjects coefficients of variation (CVs) to determine the final spectral quantification method employed in this analysis. Linear combination modeling approaches with regularized cubic spline baseline handling were either defined manually using knot spacing in frequency domain unit parts per million (ppm) and spline baseline regularization coefficient weight λ implemented for INSPECTOR as developed and described in Chapter 2 or determined automatically for the data by fits in LCModel. "Tailored" baselines shown represent results drawn from one each of the other non-LCModel manual baseline selections on a case-by-case basis following subjective visual inspection of apparent fit integrity. Y-axis shows between-subjects coefficients of variation (CVs) for control group participants only. Glu: glutamate; tNAA: total N-acetyl aspartate; tCr: total creatine; ppm: parts per million; λ: spline baseline regularization coefficient weight.

fitting approaches and baseline handling procedures that minimized between-subjects coefficients of variation in key metabolites of the control group (Figure 4.2), performed as a result of Chapter 2 analyses demonstrating the interactions between spectral quality and baseline modeling on metabolite quantification accuracy. Fits were further defined within LCModel at either 1024, 2048, or 4096 complex points according to between-subject metabolite coefficients of variation in the control group. Absolute quantification was achieved relative to 10 mM total creatine according to Chapter 3 analysis demonstrating disease influences on water T_2 and consequent effects on metabolite concentration referencing by voxel water. For the glutathione *J*-difference editing experiment, differences in metabolite signal intensity and thus estimated concentration expected as a result of different T_2 relaxation in total creatine relative to glutathione could have been corrected with a constant according to sequence-specific data previously published [116]. In order to maintain consistency with uncorrected concentrations of edited GABA, for which a sequence-specific correction value was not available, this constant factor was not employed.

Basis spectra were simulated in SpinWizard [435] by employing the density matrix formalism based on previously published chemical shift and *J*-coupling values [436, 437]; this approach was similarly applied to both *J*-difference edited and STEAM acquisitions [438]. Basis sets for both sequences included simulated spectra of ascorbate, aspartate, choline, creatine, GABA, glycerophosphocholine, glutathione, glutamate, glutamine, glycine, myoinositol, N-acetyl aspartate, N-acetyl aspartylglutamate, phosphocholine, phosphocreatine, phosphorylethanolamine, scylloinositol, and taurine. The basis set for low-echo-time STEAM also included simulated spectra for glucose. Metabolite basis functions for glutathione and N-acetyl aspartate difference spectra were used for the linear combination modeling of *J*-difference edited glutathione signals, while those for GABA, N-acetyl aspartate, glutamate, and glutamine were used for the *J*-

difference-edited GABA spectra (Figure 4.3). Quantification precision was estimated for each fit basis spectrum using Cramér-Rao lower bounds [439]. Every *J*-difference editing experiment was accompanied by an explicit efficiency measurement of the editing radiofrequency pulses subsequently used to correct the obtained glutathione and GABA signals.

Image segmentation. Image segmentation was achieved as described in Section 2 of Chapter 3. Namely, T_1-weighted images were skull-stripped using the Brain Extraction Tool in FSL [153]. BrainSuite (v16a1, http://brainsuite.org/) was then employed for bias field correction and partial volume segmentation into grey matter, white matter, and cerebrospinal fluid. After a composite mask was created for each of the three tissue types, extraction of partial volume statistics in the spectroscopy voxel was achieved in custom MATLAB (v2013b, The Mathworks, Natick, MA) package IMAGO.

Validation of total creatine as a quantification reference. Water-referenced creatine concentrations were calculated for each participant using a Lorentzian basis fit to water-unsuppressed STEAM spectra and refined using either a uniform or individualized creatine-water T_2 differential for all subjects as well as segmentation-derived GM, WM, and CSF partial volumes for voxel water molarity estimates.

Conversion factors for correcting for T_2 differences between water and tCr signal were calculated as follows. First, monoexponential models were fit by least-squares minimization on the residual to the magnitude water peak measured using the STEAM sequence at twelve echo time delays from 10 ms to 250 ms; for 25 healthy adult control participants, this procedure yielded an average STEAM water T_2 value of 44 ± 4 ms, as reported previously [440].

A similar method was applied to magnitude water peaks from the JDE-GSH sLASER

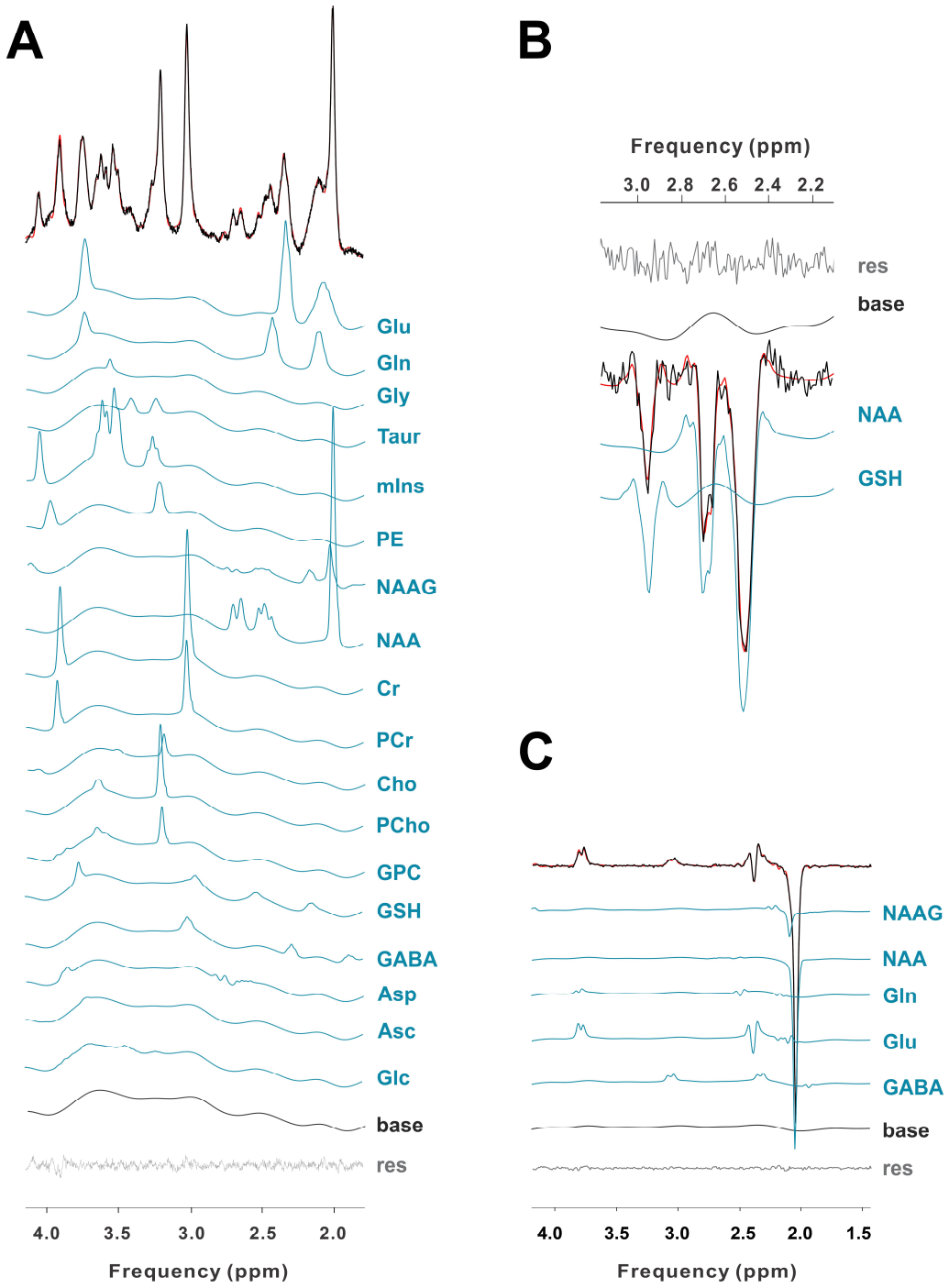

Figure 4.3. Spectral quality enabled quantification of seven different metabolites from three ^{1}H MRS acquisition sequences. Seven metabolites were quantified by linear combination model fitting (red) of simulated metabolite basis sets (blue) to spectra (black) from three different acquisition experiments. A) Macromolecule-suppressed low-echo-time STEAM acquisition sequence. B) Glutathione (GSH) was quantified via its 2.95-ppm $^{7}CH_2$ resonance using difference spectra acquired by a MEGA-sLASER experiment with *J*-difference editing at 4.56 ppm. (C) GABA was quantified from the 3.01-ppm $^{4}CH_2$ multiplet using difference spectra from a MEGA-sLASER experiment with *J*-difference editing at the 1.89-ppm resonance preceded by an inversion pulse for macromolecule nulling. ppm: parts per million, base: fit baseline, res: fit residual, Glu: glutamate, Gln: glutamine, Gly: glycine, Taur: taurine, PE: phosphorylethanolamine, NAAG: N-acetyl aspartylglutamate, NAA: N-acetyl aspartate, Cr: creatine, PCr: phosphocreatine, Cho: choline, PCho: phosphocholine, GPC: glycerophosphocholine, Asp: aspartate, Asc: ascorbate, Glc: glucose, mIns: myoinositol. Displayed as appears in Swanberg, Prinsen et al., *NMR Biomed* 2021; 34(11): e4590.

sequence at eight echo time delays from 72 ms to 322 ms to yield a sLASER water T_2 value of 90.3 ± 21.7 ms across ten scans of a separate group of nine healthy participants. Finally, total creatine T_2 using the sLASER sequence was calculated by least-squares monoexponential curve fitting to complex signal magnitudes estimated by linear combination model fitting of simulated basis spectra to creatine signal across the same eight delays as the water, yielding T_2 values of 153.0 ± 19.9 ms across the same ten scans of nine healthy participants [116]. All T_2 measurement arrays were shuffled so as to interleave alternate measurements of longer and shorter echo times with each repetition to prevent systematic temporal influences of the scan procedure on apparent T_2.

As previously asserted [441], T_2 can be conceptualized as the inverse of a relaxivity value comprising influences both intrinsic and extrinsic to the nucleus at hand. Apparent T_2 values as measured by STEAM and sLASER, the latter based on the Carr-Purcell-type LASER sequence [442], are thus not expected to be equivalent due to differential influence by factors extrinsic to inherent metabolite T_2, such as diffusion and exchange [441], as follows for the example calculation of total creatine T_2 as measured by each method:

$$T_{2\_tCr\_STEAM}^{-1} = T_{2\_int\_tCr}^{-1} + T_{2\_ext\_STEAM}^{-1} \rightarrow T_{2\_tCr\_STEAM}^{-1} - T_{2\_ext\_STEAM}^{-1} = T_{2\_int\_tCr}^{-1}$$

$$T_{2\_tCr\_sLASER}^{-1} = T_{2\_int\_tCr}^{-1} + T_{2\_ext\_sLASER}^{-1} \rightarrow T_{2\_tCr\_sLASER}^{-1} - T_{2\_ext\_sLASER}^{-1} = T_{2\_int\_tCr}^{-1}$$

$$\therefore$$

$$T_{2\_tCr\_STEAM}^{-1} - T_{2\_ext\_STEAM}^{-1} = T_{2\_tCr\_sLASER}^{-1} - T_{2\_ext\_sLASER}^{-1} \rightarrow$$

$$T_{2\_tCr\_STEAM}^{-1} - T_{2\_tCr\_sLASER}^{-1} = T_{2\_ext\_STEAM}^{-1} - T_{2\_ext\_sLASER}^{-1} \quad (11)$$

where $T_{2\_int\_tCr}$ is the intrinsic T_2 of total creatine, $T_{2\_tCr\_STEAM}$ is the T_2 of total creatine using

STEAM being estimated, $T_{2\_tCr\_sLASER}$ is mean total creatine T_2 as measured by sLASER, and $T_{2\_ext\_STEAM}$ and $T_{2\_ext\_sLASER}$ are the extrinsic influences on T_2 measurement specific to each pulse sequence.

These influences can be similarly calculated for water and set equal across the two metabolites, as follows:

$$T_{2\_tCr\_STEAM}^{-1} - T_{2\_tCr\_sLASER}^{-1} = T_{2\_H2O\_STEAM}^{-1} - T_{2\_H2O\_sLASER}^{-1} \rightarrow$$

$$T_{2\_tCr\_STEAM} = (T_{2\_H2O\_STEAM}^{-1} - T_{2\_H2O\_sLASER}^{-1} + T_{2\_tCr\_sLASER}^{-1})^{-1} \quad (12)$$

where $T_{2\_tCr\_STEAM}$ is the T_2 of total creatine using STEAM being estimated, $T_{2\_H2O\_STEAM}$ is the aforementioned mean water T_2 as measured by STEAM, $T_{2\_H2O\_sLASER}$ is mean water T_2 as measured by sLASER, and $T_{2\_tCr\_sLASER}$ is mean total creatine T_2 as measured by sLASER, respectively.

Substituting the above-reported previously published empirical measurements for $T_{2\_H2O\_STEAM}$, $T_{2\_H2O\_sLASER}$, and $T_{2\_tCr\_sLASER}$ yielded an expected tCr T_2 of 55 ms as measured by our STEAM sequence at 7 Tesla. As expected, this is much shorter than previously reported T_2 of ~140 ms for composite total creatine measured by STEAM in occipital cortex at 4 T [443] and more similar to the ~72-ms creatine T_2 relaxation values published for STEAM at 9.4 T, also for the occipital lobe [444, 445].

Using our measured T_2 for water and our calculated result for total creatine, we then estimated STEAM signal ratios for water versus tCr as follows:

$$S_{H20} : S_{tCr} = \frac{e^{\frac{-T_E}{T_{2\_H2O\_STEAM}}}}{e^{\frac{-T_E}{T_{2\_tCr\_STEAM}}}} \quad (13)$$

where $S_{H2O} : S_{tCr}$ is the T_2 correction factor under investigation, T_E is 10 ms for the STEAM sequence applied in the experiment, $T_{2\_H2O\_STEAM}$ is the aforementioned mean water T_2 as measured by STEAM, and $T_{2\_tCr\_STEAM}$ is the T_2 of total creatine using STEAM estimated as detailed in Equation 12. Using the average control water T_2 reported above, the signal ratio was calculated to be 0.96. In addition, signal ratios were also calculated individually for all 72 study participants based on their measured water T_2 values with an assumed constant tCr T_2 of 55 ms estimated as described above. The [tCr] outputs based on each of these are reported below as uniform T_2-corrected and individual T_2-corrected, respectively.

Absolute concentrations of total creatine were calculated by multiplying the T_2 correction factor in Equation 13 by the ratio of tCr signal to H_2O as measured by linear combination model fitting of the appropriate basis spectra to complex signals in STEAM as described above, as follows:

$$(tCr : H_2O)_{T2\text{-corrected}} = (S_{H2O} : S_{tCr})\ tCr : H_2O \quad (14)$$

where $(tCr : H_2O)_{T2\text{-corrected}}$ is the T_2-corrected relative concentration of tCr being estimated, tCr : H_2O is the ratio of complex signal magnitudes experimentally measured in STEAM, and $S_{H2O} : S_{tCr}$ is the relative T_2 correction factor calculated as in Equation 13. Note that in this equation both total creatine and H_2O signals are already normalized for relative proton number.

Absolute concentrations of tCr were calculated using these T_2-corrected relative tCr : H_2O values and expected absolute concentrations of water in the voxel as estimated by segmentation

analysis, as follows. First, concentrations of voxel water were assessed according to the following equation:

$$[H_2O] = 43300PV_{GM} + 35880PV_{WM} + 55556PV_{CSF} \quad (15)$$

where $[H_2O]$ is the estimated concentration of water in the voxel and PV_{CSF}, PV_{WM}, and PV_{GM} are normalized to a sum of one and represent the partial volumes of cerebrospinal fluid, white matter, and grey matter, respectively, within the segmented voxel [446].

Note that these widely employed assumptions of tissue water molarity, key to the correct estimation of absolute metabolite concentrations using water as an internal reference, are derived from occipital cortex measurements in healthy control adults [447] and are likely not to hold in all regions and experimental cohorts, especially those exhibiting pathology expected to affect tissue composition and/or structure.

Finally, the absolute concentration of tCr given the estimated concentration of water was calculated as follows:

$$[tCr] = (tCr : H_2O)_{T2\text{-corrected}}[H_2O](PV_{TS})^{-1} \quad (16)$$

where [tCr] is the absolute concentration of total creatine in the voxel, $(tCr : H2O)_{T2\text{-corrected}}$ is the T_2-corrected tCr concentration relative to water as measured by STEAM, $[H_2O]$ is the expected concentration of water as calculated in Equation 15, and PV_{TS} is voxel partial volume of tissue or $(1\text{-}PV_{CSF})$, thus correcting for the fact that tCr concentrations are not expected to be averaged over volumes of free CSF while H_2O concentrations are expected to derive from this voxel

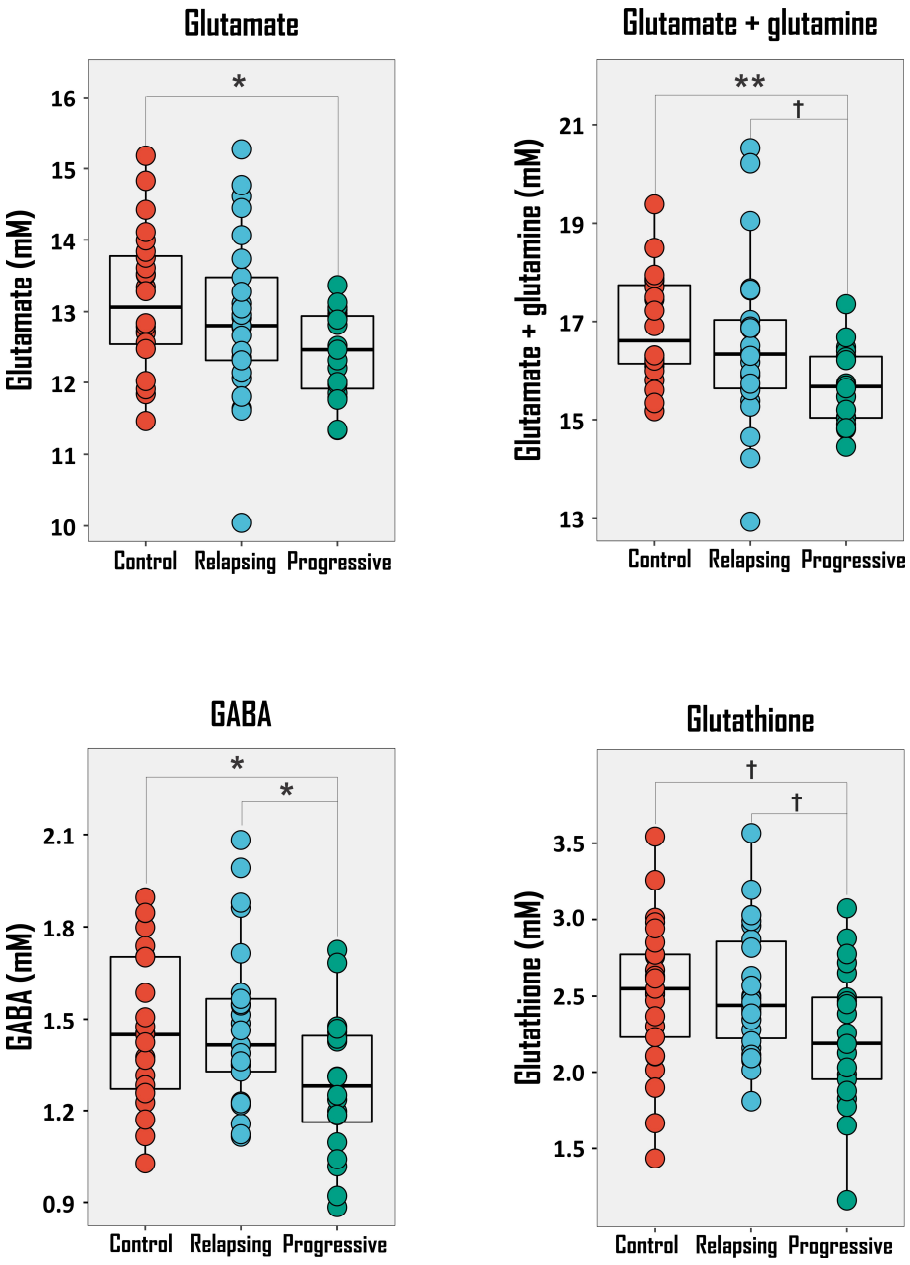

Figure 4.4. Progressive but not relapsing-remitting multiple sclerosis patients showed reductions in key frontal cortex metabolites as measured by in vivo magnetic resonance spectroscopy. Progressive multiple sclerosis patients exhibited reductions in glutamate (12.4±0.6 mM versus control 13.2±1.0 mM; $F_{2,65} = 3.4$, $p = 0.04$; mean difference 95% confidence interval CI -0.1 to -1.5 mM, $p = 0.03$). This abnormality was reflected in a significant disease effect on glutamate + glutamine ($F_{2,65} = 4.8$, $p = 0.01$; progressive 15.7±0.8 mM versus control 16.9±1.1 mM; mean difference 95% CI -0.3 to -2.1 mM, $p = 0.009$; versus relapsing-remitting 16.5±1.7 mM; mean difference 95% CI +0.1 to -1.8 mM, $p = 0.09$) despite no change in glutamine (4.7±0.4 mM versus control 4.8±0.4 mM). Progressive multiple sclerosis patients also exhibited low GABA ($F_{2,65} = 3.9$, $p = 0.03$; 1.3±0.2 mM versus control 1.5±0.3 mM; mean difference 95% CI +0.001 to -0.4 mM, $p = 0.05$; versus relapsing-remitting 1.5±0.3 mM; mean difference 95% CI -0.01 to -0.4 mM, $p = 0.04$) and a trend to reduced glutathione ($F_{2,69} = 3.0$, $p = 0.056$; 2.2±0.5 mM versus control 2.5±0.5 mM; mean difference 95% CI +0.04 to -0.6 mM, $p = 0.099$; versus relapsing-remitting 2.5±0.4 mM; mean difference 95% CI +0.02 to -0.6 mM, $p = 0.07$). Tukey's Honest Significant Difference test post-hoc to analysis of variance * $p \leq 0.05$, ** $p < 0.01$, † $p < 0.1$. Displayed as appears in Swanberg, Prinsen et al., *NMR Biomed* 2021; 34(11): e4590.

Table 4.2. Frontal cortex metabolite concentrations by multiple sclerosis group (mM)

Metabolite	No multiple sclerosis (N=24)	All multiple sclerosis (N = 44)	Relapsing-remitting multiple sclerosis (N=25)	Progressive multiple sclerosis (N=19)
Glutamate[a]	13.17±0.95	12.70±0.99[f]	12.92±1.15	***12.40±0.62***[d]
Glutamine	4.84±0.42	4.75±0.51	4.77±0.62	4.71±0.35
Glutamate + glutamine	16.89±1.09	***16.17±1.42***[d]	16.53±1.69	***15.69±0.77***[d,g]
GABA[b]	1.47±0.25	1.39±0.26	1.48±0.26	***1.29±0.23***[h,e]
Glutathione[c]	2.51±0.48	2.40±0.46	2.53±0.42	2.23±0.46[f,g]
Total N-acetyl aspartate[a]	14.25±1.06	14.15±1.00	14.33±1.13	13.90±0.75
Total choline[a]	1.57±0.24	1.57±0.19	1.57±0.17	1.58±0.22
Myoinositol[a]	6.20±0.78	6.08±1.05	6.22±1.04	5.90±1.07

[a] Significant age coefficient for general linear model in controls; statistics corrected for age
[b] Control N = 23; multiple sclerosis N = 45; relapsing-remitting N = 25; progressive N = 20
[c] Control N = 25; multiple sclerosis N = 47; relapsing-remitting N = 26; progressive N = 21
[d] Omnibus and post-hoc difference from control both $p < 0.05$
[e] Omnibus and post-hoc difference from relapsing-remitting both $p < 0.05$
[f] Omnibus and post-hoc difference from control both $p < 0.1$
[g] Omnibus and post-hoc difference from relapsing-remitting both $p < 0.1$
[h] Omnibus and post-hoc difference from control both $p \leq 0.05$

compartment as well.

Statistical analysis. Statistics were calculated in R (v. 3.4.4; R Foundation for Statistical Computing, Vienna, Austria) with $\alpha = 0.05$. Age and tissue grey-white matter composition were analyzed for effect on metabolite concentrations in control voxels and corrected for cross-sectional comparisons using general linear model coefficients in the case of significance [448]. One-way ANOVA with main effect disease group (relapsing-remitting, progressive, or control) with Tukey's Honest Significant Difference test examined disease effects and post-hoc mean differences, respectively; ANOVA residuals were confirmed not significantly non-normal by Shapiro-Wilk test for all groupwise comparisons of single metabolites. Spearman correlations of metabolite concentrations against years since diagnosis, controlling for age under the same circumstance of significant age effect in control linear models, were independently performed on non-control participant data.

Table 4.3. Group statistics on total creatine concentrations referenced using internal voxel water

		Age correction?	No multiple sclerosis (N = 24)	Relapsing-remitting multiple sclerosis (N = 25)	Progressive multiple sclerosis (N = 19)	Omnibus test statistic[b]	Omnibus test statistic *p*-value
tCr (a.u.)		No	6.42±1.69	6.55±2.08	5.74±1.31	$F_{2,65}$=1.26	0.29
		Yes[a]	9.64±1.25	9.90±2.28	9.85±1.24	$F_{2,65}$=0.162	0.85
H_2O (10^4 a.u.)		No	6.19±1.37	6.28±1.53	5.72±1.30	$F_{2,65}$=0.933	0.40
		Yes	8.84±1.01	9.03±1.73	9.11±1.21	$F_{2,65}$=0.22	0.80
[tCr] (mM)	**Estimated using uniform water T_2**	No	9.48±1.23	9.28±1.30	10.25±1.84	$\chi^2(2) = 3.86$	0.15
		Yes	8.65±1.19	8.42±1.28	9.20±1.76	$\chi^2(2) = 2.22$	0.33
	Estimated using individual water T_2	No	9.46±1.29	9.28±1.36	10.40±1.99	$\chi^2(2) = 4.43$	0.11
		Yes	8.51±1.25	8.30±1.32	9.19±1.89	$\chi^2(2) = 2.64$	0.27

[a]Values corrected on metabolite vs. age regression beta for control subjects as described in Methods
[b]Kruskal-Wallis test statistic reported in case of ANOVA residuals identified as non-normal by Shapiro-Wilk test

4.2.3. Results

Spectral quality. Average singlet full width at half maximum was <15 Hz for STEAM with comparable results for both *J*-difference editing acquisitions. At least one of three sequences was acquired in each of 72 participants, and all three sequences were acquired in 66/72 participants. Glutathione was quantified in all 72 participants, while GABA and glutamate were quantified in 68/72 participants. Average Cramér-Rao Lower Bounds on all metabolite concentration estimates were < 20% over quantified cases.

N-acetyl aspartate, total choline, and myoinositol exhibited significant linear relationships with age in control subjects. General linear modeling demonstrated statistically significant relationships between age and N-acetyl aspartate (-0.04 ± S.E.M. 0.02 mM/year; $p = 0.02$), total choline (+0.01 ± 0.003 mM/year; $p = 0.02$), and myoinositol (+0.04 ± 0.01 mM/year; $p = 0.0005$)

among control participants (age range 21-69). Additionally, glutamate (-0.03 ± 0.01 mM/year; p = 0.07) and glutathione (-0.01 ± 0.006 mM/year; p = 0.09) concentrations exhibited marginally significant linear relationships with age in control subjects; glutamate concentration values were conservatively age-corrected in all subsequent analyses.

Frontal cortex glutamate but not glutamine decreased in progressive but not relapsing-remitting multiple sclerosis. Analysis of variance demonstrated a significant effect of disease on glutamate concentration ($F_{2,65}$ = 3.4, p = 0.04) and on glutamate + glutamine concentration ($F_{2,65}$ = 4.8, p = 0.01) but not on glutamine concentration. Progressive multiple sclerosis patients exhibited low glutamate (12.4±0.6 mM versus control 13.2±1.0 mM; mean difference 95% confidence interval CI -0.1 to -1.5 mM, p = 0.03) but not glutamine (4.7±0.4 mM versus control 4.8±0.4 mM), while relapsing-remitting patients demonstrated no abnormality in either (glutamate 12.9±1.2 mM; glutamine 4.8±0.6 mM). The result for glutamate but not glutamine was reflected in reductions in progressive patients of glutamate + glutamine (15.7±0.8 mM versus control 16.9±1.1 mM; mean difference 95% CI -0.3 to -2.1 mM, p = 0.009; versus relapsing-remitting 16.5±1.7 mM; mean difference 95% CI +0.1 to -1.8 mM, p = 0.09) (Figure 4.4).

Frontal cortex GABA decreased in progressive but not relapsing-remitting multiple sclerosis. A significant effect of disease was found on GABA concentration ($F_{2,65}$ = 3.9, p = 0.03). Progressive multiple sclerosis patients exhibited low GABA (1.3±0.2 mM versus control 1.5±0.3 mM; mean difference 95% CI +0.001 to -0.4 mM, p = 0.05; versus relapsing-remitting 1.5±0.3 mM; mean difference 95% CI -0.01 to -0.4 mM, p = 0.04), while relapsing-remitting patients did not (Figure 4.4).

Frontal cortex glutathione exhibited a trend to decrease in progressive but not relapsing-remitting multiple sclerosis. A trend to disease effect was demonstrated for glutathione ($F_{2,69}$ = 3.0, p = 0.056). Progressive multiple sclerosis patients exhibited a trend to low glutathione (2.2±0.5 mM versus control 2.5±0.5 mM; mean difference 95% CI +0.04 to -0.6 mM, p = 0.099; versus relapsing-remitting 2.5±0.4 mM; mean difference 95% CI +0.02 to -0.6 mM, p = 0.07), while relapsing-remitting patients did not (Figure 4.4). This disease effect disappeared when glutathione concentrations were adjusted for a marginally significant age effect (progressive 2.9±0.5 mM; relapsing-remitting 3.0±0.4 mM; control 3.0±0.5 mM).

Frontal cortex neurotransmitter concentrations exhibited significant negative correlations with years since diagnosis in all multiple sclerosis patients. Multiple sclerosis patients taken together demonstrated negative correlations between years since diagnosis and frontal cortex concentrations of glutamate (ρ = -0.4, p = 0.02) and GABA (ρ = 0.4, p = 0.02). This result was reflected in a similar correlation between years since diagnosis and glutamate + glutamine (ρ = -0.6, p = 0.0009) despite no significant relationship with glutamine alone. Relapsing-remitting but not progressive patients exhibited a negative correlation between years since diagnosis and frontal cortex GABA (ρ = -0.5, p = 0.03) (Table 4.2).

No effect of multiple sclerosis was observed on water-referenced total creatine concentration. We observed no significant disease effect on either uniform T_2-corrected and individual T_2-corrected total creatine (Table 4.3).

Table 4.4. Metabolite correlations with years since multiple sclerosis diagnosis

Metabolite	All multiple sclerosis (N=31)		Relapsing-remitting (N=18)		Progressive (N=13)	
	ϱ	*p*	ϱ	*p*	ϱ	*p*
Glutamate[a]	***-0.4****	***0.02***	-0.3	0.3	-0.3	0.4
Glutamine	0.01	0.96	0.1	0.8	-0.2	0.5
Glx	***-0.6*****	***0.0009***	-0.4	0.09	-0.5	0.06
GABA	***-0.4****	***0.02***	***-0.5****	***0.03***	0.2	0.5

[a] Significant age coefficient for general linear model in controls; age-controlled partial correlations reported

4.2.4. Discussion

The present work employed proton magnetic resonance spectroscopy at 7 Tesla to assess frontal cortex concentrations of metabolites glutamate, GABA, and glutathione in adults with progressive, relapsing-remitting, and no multiple sclerosis. We have for the first time employed short-echo-time STEAM and *J*-difference editing in the same scan session at 7 T to enable the concomitant but independent in vivo investigation of cortical GABA, glutathione, and glutamate as separate from glutamine, with tailored validated MRS methods [106] all without significant contamination from macromolecule resonances, in multiple sclerosis patients. These techniques additionally enabled the in vivo query of glutamine, N-acetyl aspartate, choline, and myoinositol from the same data sets.

While the progressive multiple sclerosis group exhibited abnormalities in glutamate as separate from glutamine, GABA, and possibly glutathione concentration, we observed no evidence of similar metabolic abnormalities in the relapsing-remitting phenotype.

Our method enabled in vivo observation of decreased frontal cortical glutamate but not glutamine in progressive multiple sclerosis patients. Preclinical and human histology investigations of relapsing-remitting and progressive multiple sclerosis have suggested disrupted transport and cycling of neurotransmitter glutamate as well as excitotoxic cell death in a variety of tissue types [283, 285, 449]. Notably, claims of glutamate's isolation from glutamine by conventional proton magnetic resonance spectroscopy sequences at field strengths lower than

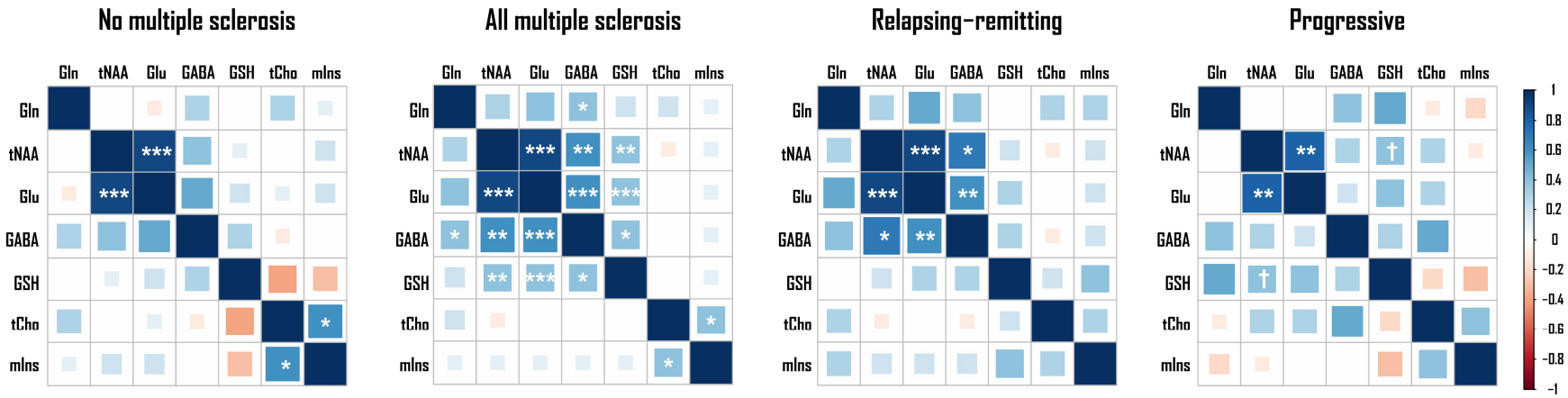

Figure 4.5. Bivariate metabolite correlations within each experimental group support independence of glutamate and glutamine measurements. Spearman correlations between age-uncorrected metabolite concentration values were calculated within each experimental group for all participants with complete data sets across all metabolites (N = 66). Significance values were corrected within each experimental group using adjustment for false discovery rate (FDR). All statistics and visualizations were computed in R (v. 3.4.4; R Foundation for Statistical Computing, Vienna, Austria). Glu: glutamate, Gln: glutamine, tNAA: total N-acetyl aspartate, GSH: glutathione, tCho: total choline, mIns: myoinositol. Spearman correlation corrected † $p < 0.1$, * $p < 0.05$, ** $p < 0.01$, *** $p < 0.001$. Displayed as appears in Swanberg, Prinsen et al., *NMR Biomed* 2021; 34(11): e4590.

4 Tesla are controversial at best given their minimal spectral separation in even simulated ideal datasets at this field strength [450]. Our glutamate-specific data derived from investigation at 7 Tesla therefore inform previously reported cross-sectional [265] and longitudinal [451] decreases in progressive multiple sclerosis cortical glutamate + glutamine assessed at lower field strengths. Importantly, the present work also elaborates on these observations in progressive patients with null findings in a relapsing-remitting group, studied in parallel, that had yet not transitioned to a progressive phenotype. In contrast to previous work, conducted at lower field strength and thus insufficient spectral dispersion to reliably quantify the two molecules in isolation, we report no disease effects on glutamine alone [451]. High field strength and sufficient spectral quality enabled unequivocal spectral separation of glutamate from glutamine (Figure 4.3), and significant correlations between the two were not seen in any group (Figure 4.5), supporting the independence of their concentration values in the present analysis. Finally, we reported a significant negative correlation between time since diagnosis in glutamate but not glutamine in all multiple sclerosis patients together (Table 4.4). Taken together, these findings underline a significant loss of frontal cortex glutamate as separate from glutamine in progressive but not relapsing-remitting multiple sclerosis, supporting with greater precision a previously tentative interpretation of glutamate + glutamine findings as indicative of neuronal cell death given the higher concentration of glutamate but not glutamine in neurons than glial cells [265]. These results in a normal-appearing cortical mixed-tissue grey- and white-matter voxel contrast with MR-visible increases in glutamate previously observed in normal-appearing white matter of multiple sclerosis patients and, when associated with the subsequent decline of N-acetyl aspartate in the latter [237], interpreted as suggestive of in vivo evidence of excitotoxic conditions in those tissues.

We also observed decreased concentrations of GABA in progressive but not relapsing-

remitting multiple sclerosis patients. GABA (γ-amino-butyric acid) is an inhibitory neurotransmitter that has reportedly mitigated immune activity in experimental autoimmune encephalomyelitis [115, 295], suggesting that these results may be consistent with reduced inhibition of autoimmune inflammation, among other possible but not mutually exclusive interpretations including the loss of GABAergic neurons. Limited human research has reported reduced GABA in the sensorimotor cortices and hippocampi of secondary progressive [146] but not relapsing-remitting [297] multiple sclerosis patients. GABA additionally exhibited negative correlations with time since diagnosis in both relapsing and progressive multiple sclerosis patients taken together and relapsing-remitting patients taken separately. Notably, frontal cortex GABA did not exhibit a significant age effect in control patients, further underscoring the nature of this correlation as mediated by disease duration and not a confounding influence of age. To our knowledge, this is the first such published suggestion of a temporally mediated multiple sclerosis effect on bulk GABA concentration in even normal-appearing tissue.

It bears emphasis that despite this suggestion, the data reported here do not constitute direct support for the conclusion that multiple sclerosis is associated with time-dependent reductions in tissue neurotransmitter concentrations that reach statistical significance only with relatively increased disease duration, here more likely seen in the secondary progressive than the relapsing-remitting multiple sclerosis cohort. In addition to the important caveat that these correlations are cross-sectional and not longitudinal, we did not observe a significant negative correlation between disease duration and prefrontal cortex glutamate concentration in either relapsing-remitting multiple sclerosis or progressive multiple sclerosis taken alone. While we did observe such a negative relationship for GABA in the relapsing-remitting group only, this finding was not recapitulated in either the progressive cohort or multiple sclerosis patients in general. Taken

together and considered in light of the small group sizes assessed here, these correlation findings suggest the utility of further longitudinal, not merely cross-sectional, analysis of multiple sclerosis progression targeting measurements of GABA and glutamate.

Glutathione is an antioxidant synthesized by neurons but particularly by glia [114]. Evidence of disrupted glutathione metabolism has been previously observed in the cerebrospinal fluid of multiple sclerosis patients [452] and in experimental autoimmune encephalomyelitis [295]. Disturbances in glutathione activity may impair the brain's defenses against oxidative stress, thereby implicating cell death as a possible basis for functional decline in multiple sclerosis [453]; our tentative observation of abnormally low glutathione in progressive multiple sclerosis cortex is therefore potentially consistent with reduced protection against local oxidative stress in this region. Limited ^{1}H-MRS work has likewise also demonstrated reduced cortical glutathione in progressive multiple sclerosis [300, 302, 454]. Our own data suggested a possible disease effect in progressive but not relapsing-remitting multiple sclerosis on frontal cortex glutathione, though it should be emphasized that this finding a) was only of marginal statistical significance and b) disappeared when concentration values were corrected for age according to a marginally significant linear relationship seen in controls. The aforementioned demonstrations of significant progressive multiple sclerosis-specific decreases in glutathione, as well as the fact that Cramér-Rao Lower Bounds, which theoretically track with variance in quantification error, were among the highest for this metabolite in our experiment, suggest that this weak result may indicate a shortcoming in our methodological sensitivity as opposed to a true negative. Notably, previous cross-sectional ^{1}H-MRS work on glutathione in multiple sclerosis has exhibited a high degree of pairwise age- and sex-matching relative to the present analysis, which likely resulted in higher sensitivity to possible biological effects [24]. Our own insinuated but tenuous result underscores the need for further in

vivo magnetic resonance spectroscopy research on the role of this still-understudied endogenous antioxidant in multiple sclerosis.

We did not observe in the normal-appearing mixed prefrontal cortex tissue of either multiple sclerosis group increased total choline or increased inositols, which have been more often associated with the ^{1}H-MRS-visible cortical metabolic signatures of relapsing-remitting or progressive multiple sclerosis in either white-matter lesions or normal-appearing white matter [24]. Previous ^{1}H-MRS research into mixed or grey-matter cortical tissue of either relapsing-remitting or progressive multiple sclerosis has reported inconsistent observations of either significant decreases [231, 264, 277, 278, 455] or increases [221, 257, 268] in total choline against a sizeable background of published null findings ([108, 203, 252], among others) [24]; it should also be mentioned that the "mixed" voxel in [257] was predominantly (~70%) white matter, and the observation in [268] involved a single multiple sclerosis patient versus a control distribution. Similarly, for grey-matter or mixed cortical voxels, only a few observations of abnormal multiple sclerosis-mediated increases in myoinositol [221, 239] compare against several non-significant findings [108, 203, 252, 253, 265], some of which studies themselves also reported in parallel myoinositol increases in white matter [203, 252, 265] or select grey-matter nuclei [108]. Our replication of these null results for total choline and myoinositol in cortical tissue also containing a large proportion of grey matter underlines the importance of consistently distinguishing among voxels of differing composition in ^{1}H-MRS investigations of multiple sclerosis.

In parallel with disease-associated findings in neurotransmitters and glutathione and replication of previously reported conflicting or null results for total choline and myoinositol, this study did not replicate previously reviewed reports of decreased N-acetyl aspartate in normal-appearing mixed cortical tissue in either relapsing-remitting or progressive multiple sclerosis [24].

Two factors are of note here. First, it bears mention that a significant apparent disease effect on N-acetyl aspartate, with trend to decrease in the progressive multiple sclerosis group, was observed until concentration values were corrected for age. A meta-analysis of the existing literature on multiple sclerosis has demonstrated a systematic reliance on control groups that are significantly younger than relapsing-remitting and especially progressive multiple sclerosis groups, with inconsistent and heterogeneous approaches to control for this confound [24]. Because the present investigation is no exception, we controlled for age by subtracting its influence from metabolite concentration values according to a significant linear model based on the younger controls, based on [448]. This may serve to mask a difference between age-corrected concentration values in the control and older progressive multiple sclerosis groups if annual reductions in N-acetyl aspartate due to baseline healthy aging are not in reality linear, i.e., drop below the modeled slope as one becomes older. Second, a reduction in N-acetyl aspartate is the most replicated metabolic abnormality for multiple sclerosis in the existing ^{1}H-MRS literature. Even this phenomenon, however, is not reported by a large proportion of published studies with findings involving other metabolites [24]. While the heterogeneity of the disease itself, selection of sub-populations under study, and expected statistical stochasticity may of course contribute to this variability across investigations, the existing ^{1}H-MRS literature also demonstrates a wide variety of acquisition, processing, and quantification techniques, all of which steps affect the patterns of metabolite concentrations ultimately reported. Until widespread, evidence-based methodological standardization as endorsed by recent consensus efforts [91, 137] is achieved, this degree of heterogeneity in ^{1}H-MRS findings across the literature, even once critical confounds like voxel composition and age control are considered as outlined above, may well continue to be the norm.

As has been shown previously in voxels with high simulated hypointense white-matter

lesion load [456], T_1-hypointense lesions in multiple sclerosis patients may be misclassified as cerebrospinal fluid, leading to underestimation of tissue partial volume by image segmentation and therefore overestimation of tissue-bound metabolite concentrations when they are referenced to water. In addition, multiple sclerosis-related changes in water T_2 have been previously reported [24, 440], including for this cohort as reproduced in Chapter 2. Finally, the question remains open about the generalizability of assumed tissue-specific water molarities from control to disease group individuals. In the present analysis, we therefore avoided these confounds to water-referenced concentration values by referencing our data to total creatine exclusively.

Some previous research has, however, inconsistently suggested that creatine concentration itself may potentially change with multiple sclerosis disease state [24, 424]. In our study, in addition to not observing monopolar disease-associated reductions in all metabolites expected not to increase in multiple sclerosis (i.e., including N-acetyl aspartate) as would be expected from findings significantly driven by abnormalities in reference signal creatine, we also observed no disease effects on the total creatine signal itself regardless of whether age correction was employed. Additionally, we observed no disease effects on water-referenced total creatine regardless of whether we used a constant water T_2 or the voxel water T_2 measured for each individual participant, also independent of whether age correction was employed. Methodological details and group statistics for these analyses can be found in the Supplementary Data. It bears repeating that using water as a quantification reference for individuals with multiple sclerosis is vulnerable to several confounds as described above.

4.2.5. Limitations and Conclusions

The findings presented here establish the importance of glutamate metabolism, additionally

implicating it together for the first time with both neurotransmitter GABA and antioxidant glutathione in the same experiment, in the distinction between progressive and relapsing-remitting multiple sclerosis. Using optimized proton magnetic resonance spectroscopy techniques along with ultra-high 7-Tesla field for increased spectral dispersion and sensitivity in the human prefrontal cortex, we report in vivo evidence for multiple sclerosis phenotype-specific abnormalities in glutamate, GABA, and glutathione metabolism. Further targeted research into the mechanistic undercurrents of these in vivo observations will enable us to move closer to the long-term goal of developing more effective disease-modifying therapies, especially for progressive multiple sclerosis.

Notably, however, and counter to the overall goal of this dissertation chapter to work toward a sensitive and specific diagnostic biomarker for progressive relative to relapsing-remitting multiple sclerosis, none of the significant between-group disease effects observed in this experiment served as a strong predictor of multiple sclerosis disease state. For this reason a supervised learning pipeline, detailed below in Section 3, was developed in order to attempt groupwise classification using potentially more subtle patterns of metabolic abnormality discernable by multivariate rather than single-variable statistical approaches.

4.3 Binary classification of multiple sclerosis status and phenotype by supervised machine learning on multivariate metabolic signatures from prefrontal cortex

4.3.1. Motivation

Multiple sclerosis is an inflammatory neurodegenerative condition that damages both white and grey matter in the central nervous system. Heterogeneity in the clinical presentation of multiple sclerosis can complicate its diagnosis, typically achieved by a combination of symptomatic report,

neurological assessment, magnetic resonance imaging, and occasionally lumbar puncture [39]. While recent revisions to the McDonald diagnostic criteria [30] as applied to magnetic resonance imaging, particularly T_1-weighted sequences that can demonstrate local abnormalities in blood-brain barrier permeability to injectable gadolinium contrast indicative of inflammatory lesion activity and T_2-weighted FLAIR that can indicate lesions of some age, have improved diagnostic accuracy for new multiple sclerosis cases, specificity remains low [68].

As mentioned previously in this chapter, compounding both the difficulty and importance of accurate multiple sclerosis diagnosis is the existence of diverse disease courses with disparate responsivity to currently available disease-modifying therapies. The majority of individuals with multiple sclerosis exhibit the relapsing-remitting phenotype, marked largely by intermittent immunological flares called relapses, for which the arsenal of modern pharmacotherapies, including monoclonal antibodies, inhibitors of immune cell proliferation or migration, and other immunosuppressive drugs, has demonstrated relative efficacy. Up to a third or more of these individuals, however, will transition to the secondary progressive phenotype, marked rather by steady neurodegeneration exhibited by cortical atrophy and functional decline largely resistant to currently available treatments [39]. About 15% of patients manifest a progressive phenotype from the outset with minimal overt relapse, called primary progressive multiple sclerosis. Uncertainty surrounds not only initial identification but also phenotypic classification of multiple sclerosis, especially during the transition from relapsing to progressive manifestation, for which a mean duration of diagnostic uncertainty as high as three years has previously been calculated [67].

Despite continued shortcomings of current imaging-supported diagnostic pipelines in identifying multiple sclerosis, magnetic resonance techniques in general are attractive as potential diagnostic tools. Magnetic resonance is noninvasive and safe, facilitating its repeated use for not

only initial identification of disease state but also for continued monitoring of treatment and transition between phenotypes. In part for these reasons, “advanced” magnetic resonance techniques, including magnetic transfer imaging [69, 70], diffusion tensor imaging [71], and proton magnetic resonance spectroscopy [24] have been explored for their potential use in multiple sclerosis prognosis, disease progression, or diagnosis [72].

Among these, proton magnetic resonance spectroscopy is unique in its ability to simultaneously query concentrations of several small-molecule metabolites in one or more regions of interest. This is particularly advantageous for diagnosing a disease like multiple sclerosis, associated to some degree of reproducibility with abnormalities in multiple spectroscopy-visible metabolites, including N-acetyl aspartate, choline, myoinositol, glutamate, glutathione, GABA, and potentially common spectroscopy quantification reference creatine [24]. As previously mentioned, it is also potentially advantageous for differentiation among different multiple sclerosis phenotypes. This is particularly true for progressive subtypes for which cortical as opposed to active white-matter lesioning may constitute the predominant manifestation [457]; as the former is, as previously mentioned, largely invisible to conventional clinical imaging [420, 421, 458], other techniques like ^{1}H MRS may have something to offer in this niche. As previously described, different metabolic abnormalities associated with progressive relative to relapsing-remitting multiple sclerosis have been previously observed in white-matter N-acetyl aspartate [81, 84, 459-461] and perhaps creatine [462] as well as grey-matter N-acetyl aspartate [255, 463] and inositols [464]. Direct comparisons between the two by proton spectroscopy remain, however, sparse [24].

Given previously published findings of 80 ± 13% (average ± standard deviation over comparisons reported) sensitivity and 63 ± 13% specificity for MS diagnostics combining imaging and CSF analysis [465], the 80% thresholds previously recommended for each in novel

Alzheimer's disease diagnostic biomarkers [466] might be reasonably applied to the improvement of multiple sclerosis diagnosis as well. One major shortcoming of proton magnetic resonance spectroscopy as currently employed is the typically low sensitivity and specificity of any single metabolite to disease effects, and currently published investigations demonstrate multiple sclerosis to be no exception. N-acetyl aspartate, the metabolite demonstrating the most extensively reported abnormality in multiple sclerosis central nervous tissue, is neither reliably reproduced nor specific to this disease [24]. Similarly, a promising finding of diffusely localized cortical and subcortical choline concentration as a 100% sensitive and 90% specific biomarker for relapsing-remitting multiple sclerosis in a cohort of 20 individuals [257] has yet to be replicated among a larger sample.

Despite the failure of nearly thirty years of proton magnetic resonance spectroscopy research to identify a single-molecule diagnostic biomarker for multiple sclerosis, it is plausible that the rich multivariate datasets provided by this method enable the accurate classification of individuals by multiple sclerosis state and/or phenotype when assessed using measures that more fully address their inherent complexity. Recursive methods for classifying data via simultaneous consideration of multiple variables are growing in feasibility and therefore popularity for uncovering patterns that may be too subtle and/or complex for traditional hypothesis testing, typically of one dependent variable at a time. Two of the most widely employed methods for classifying small data sets from multiple sclerosis patients have been support vector machines, used on a variety of data types to separate patients from control [467-476], each other [469, 477, 478], future non-converters with clinically isolated syndrome [92], and individuals with other neurological disorders [479]; as well as random forest algorithms, used to separate patients from control [468, 472, 475, 476, 480-483] and individuals with neuromyelitis optica [480]. Additional techniques used to classify multiple sclerosis state or subtype have included neural networks [468,

475, 476, 484-488], k-nearest neighbors [467, 470, 475, 477, 486], decision trees [467, 468, 476, 489], logistic regression [467, 477], Naïve Bayes [475], and least squares [477] or maximum likelihood estimation [490]. A range of classifiers has additionally been employed to characterize or predict disease conversion [491], symptom severity [242, 492-499], or treatment effect [500-503], and especially to automatically segment MR-visible multiple sclerosis lesions [504].

With a nested optimization pipeline designed with care to the considerations inherent in potentially overfitting flexible classifiers to small data sets, here we apply a number of supervised learning algorithms, including support vector machines, random forests, k-nearest neighbors, quadratic discriminant analysis, gradient-boosted decision trees, extremely randomized trees, and logistic regression to explore the feasibility of diagnosing multiple sclerosis from proton magnetic resonance spectroscopy measurements of prefrontal cortex metabolite concentrations alone. Due to the low degrees of freedom offered by a small number of cases, we split our diagnostic pipeline into two independent problems: First, deciding whether an individual has multiple sclerosis; second, deciding whether individuals with multiple sclerosis exhibit a relapsing-remitting or progressive phenotype. Binary classifications between controls and each phenotype separately were further developed to inform the interpretation of potential differences in model accuracies.

4.3.2. Methods

Participants and acquisition. As detailed in Section 2 of this chapter, metabolite spectra were obtained from a single 27-cm^3 cubic voxel in the medial prefrontal cortex using a 7-Tesla head-only scanner (Varian Medical Systems, Inc., Palo Alto, CA, USA) with actively shielded gradients and zero- through third-order shims. Spin handling and signal reception were achieved via a custom-built eight-channel transceiving radiofrequency head coil as previously described in detail

for a similar protocol [106]. Briefly, short echo time STEAM (T_E 10 ms, T_M 50 ms, T_R 3 s) and semi-LASER (T_E 72 ms, T_R 3 s) with *J*-difference editing for GSH (on 4.56 ppm to isolate the 2.95-ppm $^{7'}CH_2$) and GABA (on 1.89 ppm to isolate the 3.01-ppm $^{4}CH2$) sequences were custom written for VnmrJ software. Water suppression by CHESS in all sequences, outer-volume suppression by cuboid saturation bands in STEAM, and inversion recovery for macromolecule suppression in STEAM and JDE-GABA sLASER were additionally employed. B_0 shim coefficients through third order were calculated on gradient-echo images (T_E 3.8, 4.0, 4.3, 5.3, 6.8 ms) in B0DETOX [426], and B_1 phase shimming was achieved by in-house software IMAGO, written in MATLAB (v. 2013b, MathWorks, Natick, MA, USA).

STEAM and at least one *J*-difference acquisition were completed for 68 of 72 participants, leaving groups for progressive multiple sclerosis (N = 19; 11 women, 8 men; 55 ± S.D. 8.3 y.o.), relapsing-remitting multiple sclerosis (N = 25; 17 women, 8 men; 45 ± 13 y.o.) and no multiple sclerosis (N = 24; 15 women, 9 men; 43 ± 15 y.o.). All participants provided informed consent to study enrollment prior to scanning, and in vivo scanning and subsequent data analysis were conducted in accordance with Yale School of Medicine Human Investigation Committee protocol #1107008743 and Columbia University Institutional Review Board protocol AAAQ9641.

Spectral processing and quantification. Also as reviewed in detail in Section 2, spectral processing was performed in ^{1}H MRS analysis freeware INSPECTOR [505] as described in detail previously [116]. Briefly, signals from individual receive channels were corrected for eddy currents using water-unsuppressed references [118], phase- and frequency-aligned, and averaged with weighting by receive channel sensitivities [119]. Summed metabolite spectra were zero-order phased but not truncated, zero-filled, or line-broadened before direct quantification or alignment

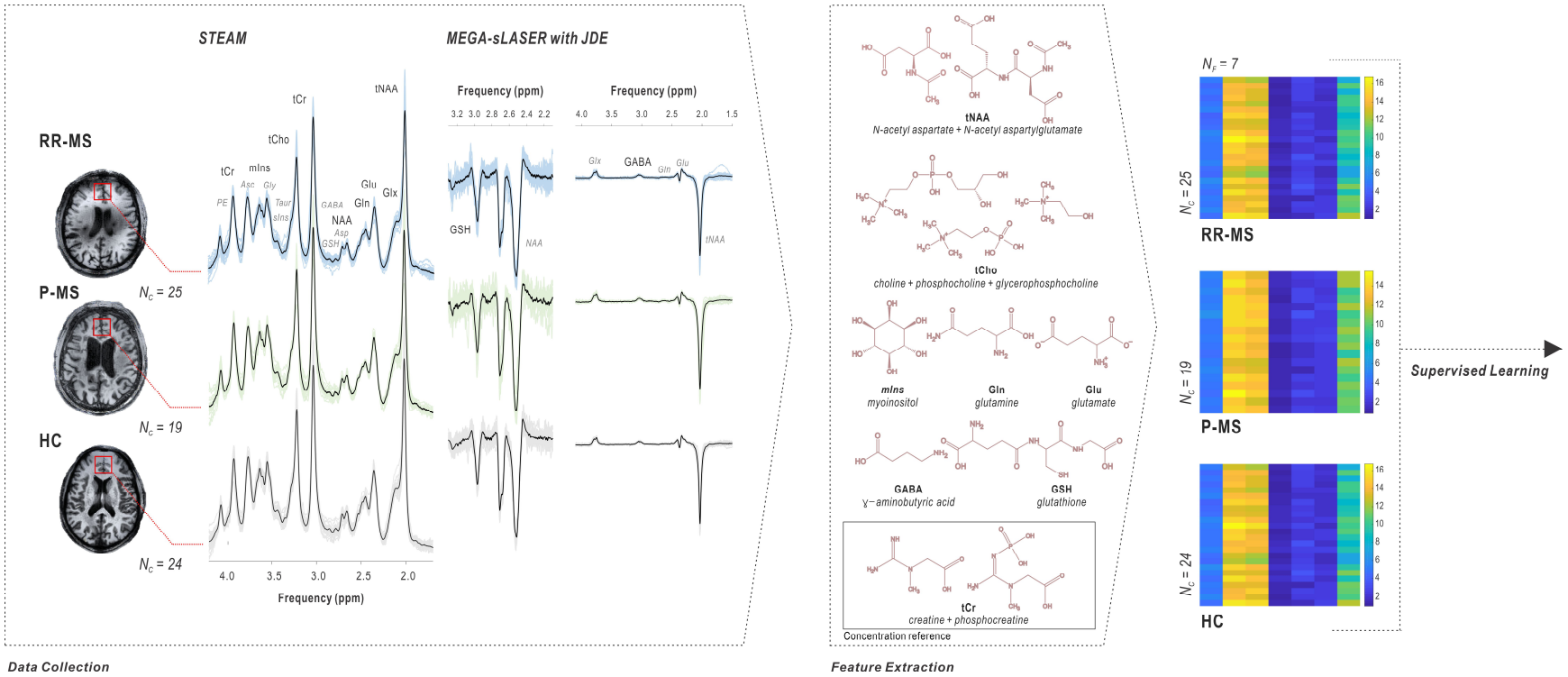

Figure 4.6. Frontal cortex metabolite profiling by proton magnetic resonance spectroscopy in individuals with relapsing-remitting, progressive, and no multiple sclerosis. Seven metabolites were measured in a single 27-cc cubic voxel in the prefrontal cortex of individuals with relapsing-remitting (N = 25), progressive (N = 19), or no (N = 24) multiple sclerosis. Individual spectra shown in color; group averaged spectra shown in black. Signals from five compounds, including total N-acetyl aspartate (tNAA: N-acetyl aspartate plus N-acetyl aspartylglutamate), total choline (tCho: choline, phosphocholine, and glycerophosphocholine), myoinositol (mIns), glutamate (Glu), and glutamine (Gln), were obtained via macromolecule-suppressed Stimulated Echo Acquisition Mode (STEAM: echo time T_E 10 ms, repetition time T_R 3 s, mixing time T_M 50 ms, inversion time T_I 300 ms); glutathione (GSH) and GABA were estimated by *J*-difference editing (JDE) on a semi-localized by adiabatic selective refocusing sequence (MEGA-sLASER: T_E 72 ms, T_R 3 s). Total creatine (tCr) served as a concentration reference for these seven metabolite features, which were calculated in millimolar (mM) assuming 10 mM tCr; additional metabolites listed in italics, including aspartate (Asp), ascorbate (Asc), phosphorylethanolamine (PE), glycine (Gly), taurine (Taur), scylloinositol (sIns), GSH and GABA from STEAM, and glutamate, glutamine, and/or NAA in *J*-difference-edited spectra, were employed in spectral data quantification for one or more experiments but not included in the machine-learning feature set. RR-MS: relapsing-remitting multiple sclerosis; P-MS: progressive multiple sclerosis; HC: healthy control; ppm: parts per million; N_C: number of cases; N_F: number of features.

between summed editing conditions for difference spectrum calculation, as applicable. Spectral quantification proceeded as described in Section 2, yielding concentration estimates of glutamate, glutamine, GABA, glutathione, total choline, total N-acetyl aspartate, and myoinositol referenced to 10 mM total creatine. Total N-acetyl aspartate, total choline, myoinositol, and glutamate concentrations were corrected using significant linear regression betas on subject age, calculated from the control cohort as detailed in Section 2. These seven metabolite concentrations were used as input features for each classification pipeline (Figure 4.6).

All participants in this analysis had full STEAM and GSH data sets; two subjects (one control and one progressive MS patient) were missing GABA concentrations that were imputed as the average of their respective classes prior to analysis.

Binary classification of multiple sclerosis condition and phenotype. Classification pipelines were developed in Python 3.5 and constituted four types of binary classifications. The first established among all available participants the absence or presence of multiple sclerosis. The second decided among all participants with multiple sclerosis whether they exhibited the relapsing or progressive phenotype. Two additional comparisons between control and each multiple sclerosis subtype were also performed to enhance the interpretability of relative model accuracies. Support vector machines (SVM), k-nearest neighbors (KNN), and quadratic discriminant analysis (QDA) were selected for detailed report among all approaches employed for testing based on held-out validation accuracies in the relapsing versus progressive question. Additional classification algorithms tested but not reported included random forests, gradient-boosted decision trees, extremely randomized trees, and logistic regression. All techniques were implemented in Sci-Kit Learn [94].

Data were split into training and validation sets by removing one data set at a time for use

as a held-out validation set, yielding a total of N_1 x 2 runs for data with smaller group size N_1. Model training was performed on only members of each training set. Leave-one-out cross validation (LOOCV) statistics were also calculated for each training set for aggregate use in feature selection and optimization of training hyperparameters. This bootstrapping strategy, in which LOOCV accuracies were aggregated across multiple training sets, each itself missing one held-out validation set, struck a balance between the low statistical confidence offered by the small validation set Ns of a single-loop approach and the computational intensity of separately optimizing features and hyperparameters against individual training sets for each held-out validation case (i.e., a true test case) in a fully nested approach, and the small range of parameters optimized did not render hyperparameter overfitting a concern for this particular application.

Undersampling proceeded similarly for cross-validation as for held-out validation in that each of the training cases was removed once for use as a cross-validation set for that training run, with a total of N_2 x 2 cross-validations for data with the smaller training group size N_2 to ensure class balancing in the population of cross-validation sets used for each training run. Class sizes were then balanced after removal of the aforementioned held-out validation and cross-validation sets using the Synthetic Minority Over-Sampling Technique (SMOTE) such that data points were interpolated in the smaller class along line segments joining each case to a predefined number of its nearest neighbors until the class equaled the size of the larger [78].

Each training set was scaled using a matrix calculated over that training set only, after which the same scaling was transferred to the held-out validation case. This enabled each separate model to minimize bias to held-out validation cases while also allowing for the calculation of population validation set statistics via the inclusion of all participants in both training and held-out validation sets. Dimensionality reduction on the already small feature set of seven metabolites was

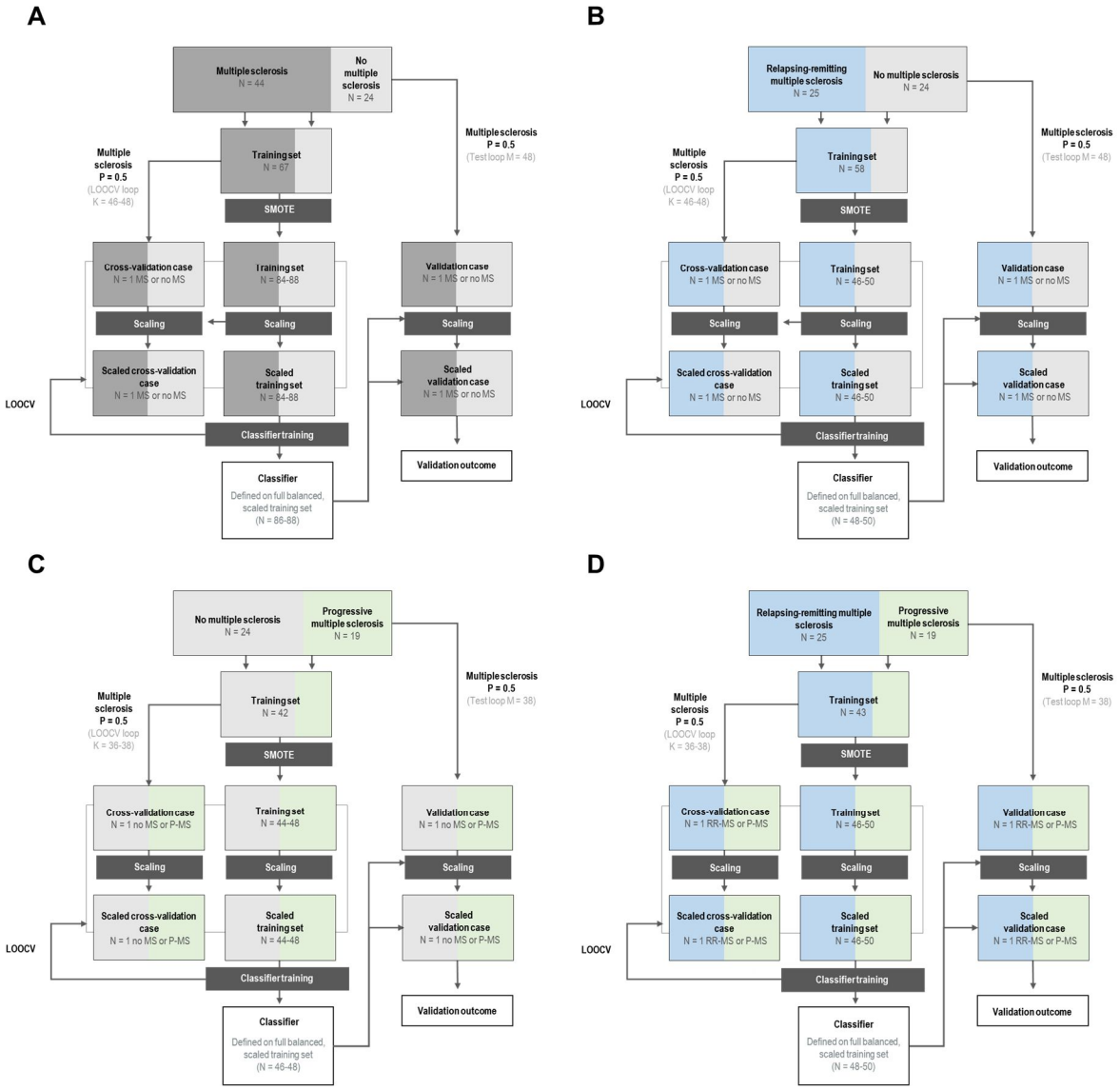

Figure 4.7. Training, optimization, and validation pipeline for multivariate classifiers of multiple sclerosis state and type by frontal cortex metabolite profiles. Classification pipelines constituted two binary decisions: The first (A) established the presence of multiple sclerosis, while the second (D) characterized the phenotype. Models distinguishing from control relapsing-remitting multiple sclerosis (B) and progressive multiple sclerosis (C) were also implemented for context in interpreting performance differences between (A) and (D). One data set at a time was held out for use as the validation set, yielding a total of N_1 x 2 runs for data with smaller group size N_1. Undersampling proceeded similarly for an inner cross-validation loop used for hyperparameter optimization and feature selection, in that each of the training cases was removed once for use as a cross-validation set for that training run, with a total of N_2 x 2 cross-validations for data with the smaller training group size N_2 to ensure class balancing in the population of cross-validation sets used for each training run. Class sizes were then balanced using the Synthetic Minority Over-Sampling Technique (SMOTE). Each training set was scaled using a matrix calculated over that training set only, after which the same scaling was transferred to the held-out validation case. Dimensionality reduction was not performed in order to avoid degrading model interpretability. Classification algorithms tested included support vector machines, k-nearest neighbors, quadratic discriminant analysis, random forests, gradient-boosted decision trees, extremely randomized trees, and logistic regression; only the first three were selected for reporting based on performance separating progressive and relapsing-remitting multiple sclerosis. LOOCV: Leave-one-out cross validation.

not performed to avoid reduction in model interpretability. Optimized hyperparameters and model performance were averaged across all runs for each algorithm (Figure 4.7; Table 4.5).

Metabolite feature selection. Feature selection was performed on hyperparameter-optimized models and consisted of recursive feature elimination according to permutation importance. Permutation importance is proportional to the reduction in model accuracy when the association between feature values and classifications is broken by randomization [506]. Starting from hyperparameter-optimized models retaining all seven metabolites (glutamate, glutamine, GABA, glutathione, total choline, total N-acetyl aspartate, and myoinositol), the feature with the lowest permutation importance was removed and cross-validation accuracies recalculated over the whole data set. Feature elimination was continued as long as the resultant model exhibited superior performance (higher average cross-validation accuracy or comparable cross-validation accuracy with higher area under the receiver operating characteristic or AUROC) relative to the original.

Classification performance assessment. Cross-validation accuracies were averaged over all runs for each classification pipeline. Additionally, receiver operating characteristics were approximated for each algorithm by plotting sensitivities and specificities for each of N(N-1) cross-validation runs. Sensitivity (true positive classifications over all real positives) and specificity (true negative classifications over all real negatives) were calculated over all test classifications. Model error was additionally reported as precision, recall, and the composite thereof F1, or 2(precision x recall)/(precision + recall), where precision is the proportion of negative classifications that were true and recall is the proportion of positive classifications that were true. In each challenge versus control, multiple sclerosis was defined as the positive classification; in the relapsing versus

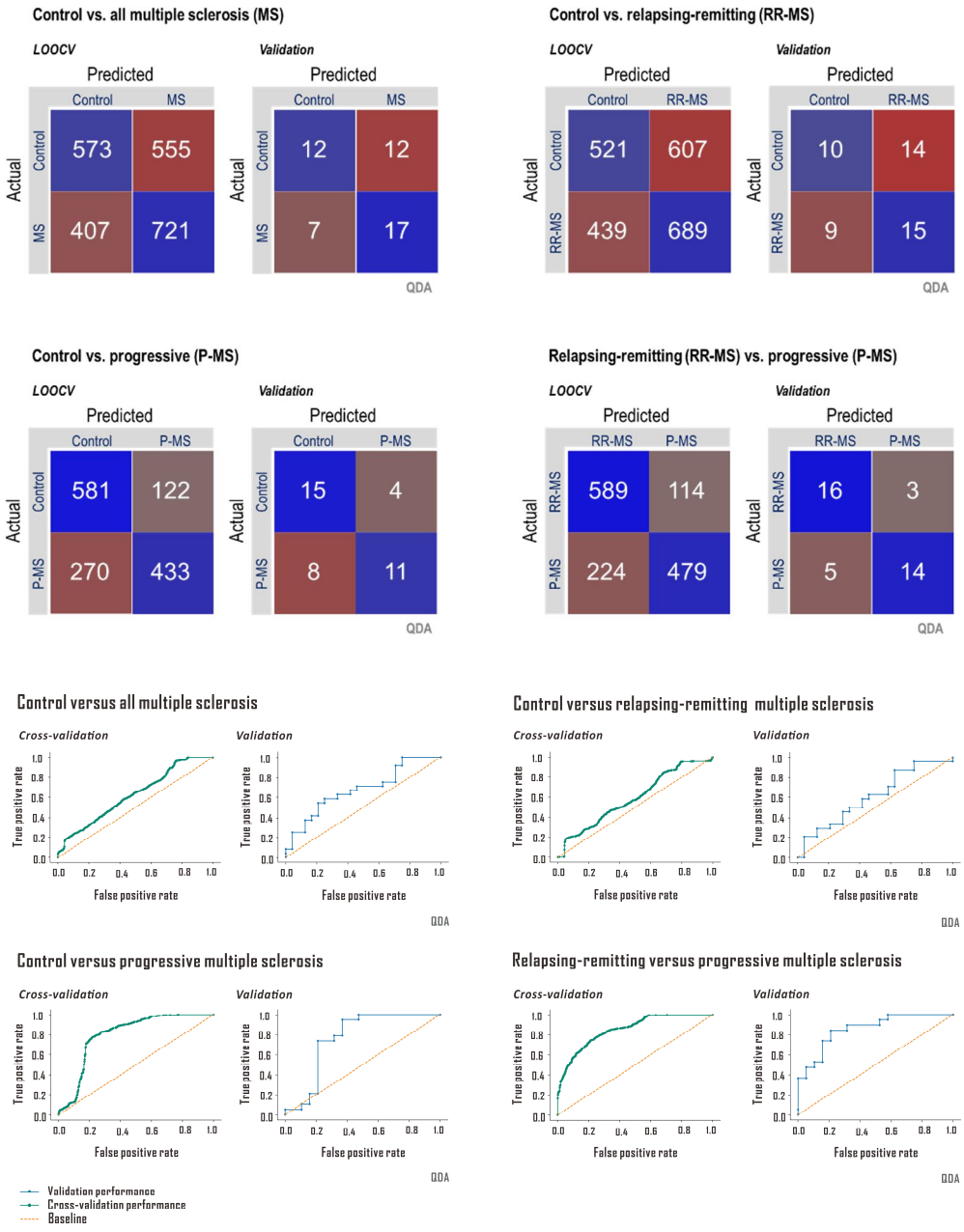

Figure 4.8. Confusion matrices (top) and receiver-operating characteristic curves (bottom) for top-performing pipeline in each binary classification. Quadratic discriminant analysis (QDA) proved to be the top-performing classification algorithm by area under the receiver operating characteristic (ROC) for all four questions, with higher validation sensitivity and specificity for classification of progressive patients than relapsing-remitting or all multiple sclerosis patients taken together, despite a smaller group size (progressive N=19 versus relapsing-remitting N=25 or control N=24). While it is visually clear that metabolite-based classifications between controls and multiple sclerosis patients, or between controls and relapsing-remitting multiple sclerosis patients, exhibited performance marginally better than chance, ROC curves exhibited substantially increased convexity for questions involving the classification of progressive multiple sclerosis patients specifically, also reflected in higher sensitivity and specificities as shown in the confusion matrices. Multiple sclerosis groups defined as positives in all plots; for the relapsing-remitting versus progressive question a positive is defined as relapsing-remitting multiple sclerosis.

progressive question, progressive multiple sclerosis was defined as positive for the calculation of the aforementioned statistics.

Group statistics. All group statistics are reported as means ± standard deviations unless otherwise noted. Model accuracies were compared across classification questions using a student's t-test [507] scripted in MATLAB (v. 2018a, MathWorks, Natick, MA, USA) with two-tailed significance testing and α at 0.05.

4.3.3. Results

Classifiers separating progressive from relapsing multiple sclerosis exhibited increased performance relative to those separating multiple sclerosis from control. Average held-out validation accuracies were higher for separations of relapsing versus progressive (QDA 79%, KNN 74%, and SVM 68%) than for multiple sclerosis versus control (QDA 60%, KNN 63%, SVM 58%). Accuracy averaged across all three classifiers was significantly higher for models separating progressive from relapsing multiple sclerosis than for all multiple sclerosis from control (73.7±5.5% versus 60.3±2.5%, $t(2) = 3.82$, two-tailed $p < 0.05$).

The same trend was also seen in higher held-out validation accuracies for progressive versus control classifications (QDA 68%, KNN 74%, and SVM 74%) than for relapsing-remitting versus the same control (QDA 52%, KNN 58%, and SVM 52%), yielding a mean difference that also exceeded the threshold for statistical significance despite a small sample size of 3 classifiers (72.0±3.5% versus 54.0±3.5%, $t(2) = 6.30$, two-tailed $p < 0.01$) (Figure 4.8; Table 4.6).

Quadratic discriminant analysis and k-nearest neighbors but not support vector machines

yielded ≥80% sensitivity or specificity for at least one classification question. Quadratic discriminant analysis yielded the highest classification accuracies for identification of progressive multiple sclerosis as distinct from relapsing-remitting (held-out validation accuracy 79%; sensitivity 84%, specificity 74%; AUROC 0.86) as well as from control (held-out validation accuracy 68%; sensitivity 58%, specificity 79%; AUROC 0.83). K-nearest neighbors exhibited slightly lower performance than QDA for its top-performing applications, distinguishing progressive from relapsing multiple sclerosis (held-out validation accuracy 74%; sensitivity 68%, specificity 78%; AUROC 0.78) and from control (held-out validation accuracy 74%; sensitivity 95%, specificity 53%; AUROC 0.72). By contrast, support vector machines failed to reach either 80% sensitivity or specificity for any question, though overall accuracy for the classification of progressive multiple sclerosis relative to relapsing-remitting (held-out validation accuracy 68%; sensitivity 68%, specificity 68%; AUROC 0.68) and control (held-out validation accuracy 74%; sensitivity 79%, specificity 68%; AUROC 0.77) still exceeded those of the other two classifications (Table 4.6).

Metabolite feature importance differed more by classification question than by algorithm. Total choline ranked among the most important three features for all progressive versus relapsing models but none of the control versus multiple sclerosis models. Total choline was also the most important feature for distinguishing progressive from control in QDA, while it did not feature among the top three for any model distinguishing relapsing from control. Similarly, glutamine and glutathione ranked among the three most important features for two of the three progressive versus relapsing models but only one (glutamine) or none (glutathione) of those distinguishing multiple sclerosis from control. Additionally, GABA ranked among the three most important features for two of three

models distinguishing progressive MS from control but none distinguishing relapsing-remitting MS from control.

Inversely, two metabolites (myoinositol and glutamate) ranked among the three most important retained features for all three control versus multiple sclerosis models but only one (myoinositol) or none (glutamate) of the progressive versus relapsing models. Both myoinositol and glutamate were each also ranked among the top three features for at least five of six (myoinositol) or all six (glutamate) models distinguishing each multiple sclerosis subtype from control (Table 4.7).

4.3.4. Discussion

We have presented evidence that individuals with progressive multiple sclerosis can be accurately distinguished from those with relapsing-remitting and no multiple sclerosis on the sole basis of frontal-cortex metabolite concentrations, including glutamate, glutamine, glutathione, GABA, N-acetyl aspartate, choline, and myoinositol, measured by proton magnetic resonance spectroscopy at 7 Tesla. By contrast, as shown in Section 2 of this chapter, the same data did not support accurate separation from control of relapsing-remitting multiple sclerosis or of both multiple sclerosis subtypes pooled as a single classification. This finding underlines the potential of proton magnetic resonance spectroscopy as an auxiliary diagnostic tool for progressive multiple sclerosis. Additionally, it highlights the as-yet untapped potential of multivariate approaches to investigating the in vivo ^{1}H-MRS-visible metabolic signatures of multiple sclerosis and its various phenotypes, especially under experimental conditions that enable the separation of visually overlapping but physiologically distinct spectral signals like glutamate and glutamine.

Proton magnetic resonance spectroscopy is an experimental technique of low sensitivity

that has historically led to findings of metabolic abnormality in multiple sclerosis that are subtle and inconsistent at best [24]. Notably, application of data derived from this method alone led to satisfactory differentiation between progressive multiple sclerosis and control, and between progressive and relapsing-remitting multiple sclerosis, in a cohort that exhibited unequivocally significant univariate differences between the former two groups for only two metabolites (GABA and glutamate), and between the latter for only one (GABA) [508]. Our classification pipelines distinguished patients from control with a clarity exceeding the subtle pattern of results yielded by univariate statistical techniques, demonstrating the potential of multivariate approaches to multiple-sclerosis-related abnormalities in small molecule concentrations measurable by proton magnetic resonance spectroscopy. The additional diagnostic utility of simultaneously considering multiple metabolic signals is perhaps especially true when assessing data from tissue voxels that appear grossly normal on T_1-weighted MR scans without contrast, and which would not be expected to demonstrate the more substantial abnormalities, including but not limited to decreased N-acetyl aspartate, increased choline, and differences in macromolecule and lipid contribution to the spectral baseline, previously reported for tissue that is already visibly lesioned [24].

Composite imaging and CSF-based multiple sclerosis diagnostic strategies have reported low average sensitivities and specificities across the literature [465]. At least one investigation using the 2001 McDonald criteria [509] including MR imaging of a cohort with suspected multiple sclerosis has reported higher than 80% diagnostic sensitivity and specificity upon follow-up after several years [510], but the majority of imaging-based diagnostics tested have not exceeded these thresholds [511]. Our finding, in our top-performing hyperparameter-optimized classification scheme, of 84% sensitivity and 74% specificity of differentiating progressive from relapsing-remitting multiple sclerosis on the basis of select metabolite concentrations in normal-appearing

prefrontal cortex alone, also does not exceed but approaches this standard. Importantly, it does so despite very small training samples ($N \leq 25$ per group without synthetic oversampling) using minimally transformed, biologically interpretable features in a pipeline controlled for overfitting.

That reported accuracy decreases with sample size, suggestive of the dangerous potential for overfitting in models produced by iterative learning methods, has been previously shown in a literature review of machine-learning application to multiple neurological disorders [512]. The same review reported that only one-fifth of the literature examined employed held-out validation sets on which classification parameters were not optimized. The present study does not feature among them, as we did optimize a limited range of model hyperparameters and perform feature selection based on cross-validation accuracies pooled over the entire dataset, though all training was conducted on cases kept entirely separate from the held-out validations. Overfitting, however, was not a concern, given the low number of hyperparameters optimized (only one for the consistently top-performing model QDA) and features (de)selected.

Classification accuracies for distinguishing either relapsing-remitting or general multiple sclerosis from control on the basis of the metabolites measured in this study were only a few percentage points above chance (50%), while at least one classifier of progressive versus relapsing-remitting multiple sclerosis nearly achieved the 80% threshold of sensitivity and specificity previously recommended for a diagnostic biomarker [466]. In addition to demonstrating that the pipeline employed here does not inevitably lead to overfitting for data sets that lack clear signals, this pattern of results underscores a phenotype-specific heterogeneity in multiple sclerosis as viewed through the lens of the metabolites measured here. This suggestion dovetails with previous reports of discrepant single-metabolite normal-appearing brain tissue abnormalities in relapsing-remitting and progressive multiple sclerosis patients [221, 222, 225] to further emphasize the

Table 4.5. Model hyperparameters optimized against average training cross-validation accuracy

Model hyperparameters optimized			
Model	**Scaling transformation[a]**	**Model-specific hyperparameters**	
QDA	min-max (0 to 1) unit normalization standardization quantile transformation maximum value normalization quadratic features	N/A	
KNN		neighbors	2-15
		p	1, 2
SVM		γ	0.01, 0.025, 0.05, 0.075, 0.91, 0.1, 0.11, 0.125, 0.15, 0.2, 0.25, 0.5, 1
		c	0.1, 0.2, 0.3, 0.4, 0.5:0.05:1.5, 2, 3, 4, 5, 10
		kernel	Poly (2-6), RBF, linear

Final hyperparameters by question and model type			
Model	**Question**	**Scaling transformation**	**Model-specific hyperparameters**
QDA	Control vs. MS	unit normalization	N/A
	Control vs. RR-MS	unit normalization	N/A
	Control vs. P-MS	quantile transformation	N/A
	RR vs. P-MS	quantile transformation	N/A
KNN	Control vs. MS	unit normalization	5 neighbors; p=2
	Control vs. RR-MS	unit normalization	7 neighbors; p=2
	Control vs. P-MS	standardization	7 neighbors; p=2
	RR vs. P-MS	min-max (0 to 1)	5 neighbors; p=2
SVM	Control vs. MS	unit normalization	$\gamma=(\sigma_x^2 N_f)^{-1}$; c=1; RBF kernel
	Control vs. RR-MS	unit normalization	$\gamma=(\sigma_x^2 N_f)^{-1}$; c=1; RBF kernel
	Control vs. P-MS	min-max (0 to 1)	γ=1.1; c=0.7; RBF kernel
	RR vs. P-MS	quantile transformation	$\gamma=(\sigma_x^2 N_f)^{-1}$; c=1; RBF kernel

σ_x^2: feature variance; N_f: number of features; RBF: radial basis function

[a] Scaling optimized over default model-specific hyperparameters

necessity for targeted study of multiple sclerosis progression as opposed to, or in parallel with, relapse, rather than multiple sclerosis as a reified monolith. The same argument may in principle be extended to our own conflation of secondary and primary progression into a single category of progressive multiple sclerosis, which is an admitted limitation of the present study borne of limited sample size.

Our results also suggest consistently divergent contributions by certain metabolites to the separation of relapsing-remitting or progressive multiple sclerosis subtypes from control versus from each other. It was demonstrated in particular that myoinositol and glutamate were consistently ranked among the most important metabolites for distinguishing from control

Table 4.6. Binary classifier performance by feature-selected algorithm and participant groups

Model	Control versus all multiple sclerosis					Control versus relapsing					Control versus progressive					Relapsing versus progressive				
	Acc.	Sn/Sp	R/P	F_1	AUC	Acc.	Sn/Sp	R/P	F_1	AUC	Acc.	Sn/Sp	R/P	F_1	AUC	Acc.	Sn/Sp	R/P	F_1	AUC
QDA																				
CV	57±5	64/51	64/57	60	0.62	54±5	61/46	61/53	57	0.59	***72±4***	***62/83***	***62/78***	***69***	***0.80***	***76±4***	***84/68***	***84/72***	***78***	***0.85***
Validation	60	71/50	71/59	64	0.68	52	63/42	52/63	57	0.61	***68***	***58/79***	***58/73***	***65***	***0.83***	***79***	***84/74***	***84/76***	***80***	***0.86***
KNN																				
CV	58±6	59/57	59/58	58	0.58	57±3	55/60	55/58	56	0.61	72±3	89/54	89/66	76	0.72	***72±4***	***63/81***	***63/77***	***69***	***0.77***
Validation	63	67/58	67/62	64	0.60	58	54/63	54/59	56	0.60	74	95/53	95/67	78	0.72	***74***	***68/78***	***68/76***	***72***	***0.78***
SVM[a]																				
CV	58±4	57/58	57/58	57	0.36	54±2	49/58	49/54	51	0.49	***71±4***	***76/66***	***76/69***	***72***	***0.74***	68±3	68/69	68/68	68	0.70
Validation	58	58/58	58/58	58	0.41	52	46/58	46/52	49	0.52	***74***	***79/68***	***79/71***	***75***	***0.77***	68	68/68	68/68	68	0.68

[a] No features eliminated for relapsing versus progressive

CV: cross-validation; Sn: sensitivity; Sp: specificity; Acc.: accuracy; AUC: area under receiver operating characteristic (ROC) or AUROC. All statistics reported as means±standard deviations

relapsing-remitting and progressive multiple sclerosis both separately and as a single category of disease. By contrast, total choline, glutathione, and glutamine ranked among the top three features for at least two of the three classifiers separating progressive from relapsing-remitting multiple sclerosis, but never (total choline or glutathione) or only once (glutamine) in any of the three models separating any multiple sclerosis patient from control. It is crucial not to over-interpret feature importances within any single model, especially those deriving from models with low baseline accuracies against which this parameter is calculated. These patterns were consistently observed, however, across multiple model questions and types, including those with accuracies exceeding 70%.

The validity of reporting separate concentrations of glutamate and glutamine derived from ^{1}H MRS experiments at field strengths lower than 7 Tesla is controversial, given previously demonstrated spectral overlap at these fields even under the clean spectral conditions offered by simulations [513]. Our results suggest that at least when considered in concert with other compounds measurable by ^{1}H MRS, these two metabolites may weight differently in characterizing the commonalities versus the differences between the in vivo cortical metabolic signatures of relapsing-remitting and progressive multiple sclerosis. These findings therefore re-emphasize the crucial need for spectroscopy research on the role of glutamate in multiple sclerosis pathophysiology to be conducted under conditions that enable its unequivocal separation from glutamine, especially considering a literature that continues to demonstrate an absence of such investigations [24].

On the sole basis of in vivo proton magnetic resonance spectroscopic metabolite concentrations derived from normal-appearing frontal cortex voxels at 7 Tesla, progressive multiple sclerosis can be distinguished from relapsing-remitting multiple sclerosis or control with

Table 4.7. Effect of metabolite selection on binary classifier leave-one-out cross-validation (LOOCV) performance

Model	Control versus all multiple sclerosis		Control versus relapsing		Control versus progressive		Relapsing versus progressive	
	Δ Value	Metabolites (PI mean ± S.D.)	Δ Value	Metabolites (PI mean ± S.D.)	Δ Value	Metabolites (PI mean ± S.D.)	Δ Value	Metabolites (PI mean ± S.D.)
QDA								
Sn/Sp	+6/+8	mIns (0.13±0.08) GABA (0.10±0.06) Glu (0.09±0.08) tCho (0.04±0.06)	+7/-9	mIns (0.17±0.04) Glu (0.15±0.03) tNAA (0.15±0.03) GABA (0.13±0.03)	+15/+10	tCho (0.21±0.06) Glu (0.20±0.06) GABA (0.18±0.07) tNAA (0.16±0.07) Gln (0.15±0.05)	+7/+12	tCho (0.24±0.03) Gln (0.23±0.04) GABA (0.22±0.03) GSH (0.13±0.03) tNAA (0.08±0.03)
Acc.	+7%		-1%[a]		+13%		+9%	
AUC	+0.09		+0.06		+0.16		+0.14	
KNN								
Sn/Sp	+4/+16	mIns (0.29±0.05) Glu (0.22±0.04) Gln (0.16±0.05)	-12/+18	mIns (0.18±0.03) Glu (0.08±0.03) tNAA (0.06±0.03) GSH (0.01±0.03) GABA (0.01±0.02)	+3/+2	Glu (0.12±0.06) mIns (0.10±0.06) Gln (0.08±0.06)	+2/+2	mIns (0.12±0.05) tCho (0.09±0.04) GSH (0.06±0.03) tNAA (0.06±0.03) GABA (0.05+0.04) Glu (0.03±0.03)
Acc.	+10%		+3%		+2%		+2%	
AUC	+0.09		+0.12		-0.01		+0.02	
SVM								
Sn/Sp	+7/0	Glu (0.02±0.02) mIns (0.02±0.03) GABA (0.007±0.007) GSH (0.006±0.006) tCho (<0)	+14/-3	Glu (0.05±0.02) mIns (0.05±0.03) Gln (0.005±0.007)	+1/0	Glu (0.09±0.06) mIns (0.07±0.06) GABA (0.05±0.05) tCho (0.04±0.05) Gln (0.03±0.06)	--	tCho (0.10±0.03) GSH (0.10±0.02) Gln (0.10±0.03) mIns (0.06±0.03) GABA (0.05±0.02) Glu (0.04±0.02) tNAA (0.03±0.02)
Acc.	+4%		+5%		+0.5%			
AUC	-0.05		-0.005		+0.03			

[a]Feature elimination performed in this algorithm despite no substantial improvement in CV accuracy due to appreciable increase in AUROC.
Grey indicates no feature selection implemented due to resultant reductions in model cross-validation accuracy. PI: permutation importance; S.D.: standard deviation; Sn: sensitivity; Sp: specificity; Acc.: accuracy; AUC: area under receiver operating characteristic (ROC) or AUROC; mIns: myoinositol; Glu: glutamate; tCho: total choline; Gln: glutamine; tNAA: total N-acetyl aspartate; GSH: glutathione

near to or greater than 80% sensitivity and specificity. Relapsing-remitting multiple sclerosis, or both multiple sclerosis subtypes pooled as a single classification, cannot be accurately distinguished from control using the same approach. These results demonstrate the potential of multivariate statistical classifiers as applied to proton magnetic resonance spectroscopy as an auxiliary diagnostic tool for progressive multiple sclerosis as well as of multivariate approaches to researching in vivo metabolic signatures of diverse multiple sclerosis phenotypes, especially under ultra-high-field conditions enabling the separation of key spectral signals like glutamate and glutamine.

On the basis of in vivo proton magnetic resonance spectroscopic metabolite concentrations derived from normal-appearing frontal cortex voxels at 7 Tesla, progressive multiple sclerosis can be distinguished from relapsing-remitting multiple sclerosis and control with near to or greater than 80% sensitivity and specificity, though these 80% thresholds previously proposed as a standard for novel diagnostic biomarkers were not consistently achieved. Additionally, relapsing-remitting multiple sclerosis, or both multiple sclerosis subtypes pooled as a single classification, cannot be accurately distinguished from control using the same approach. These results demonstrate the potential of proton magnetic resonance spectroscopy as an auxiliary diagnostic tool for progressive multiple sclerosis as well as of multivariate approaches to researching in vivo metabolic signatures of diverse multiple sclerosis phenotypes, especially under high-field (e.g., 4 T or above) conditions enabling the separation of key spectral signals like glutamate and glutamine.

4.4 General summary and conclusions

This chapter aimed to address the following questions: Can ^{1}H MR spectra quantified using an analytic pipeline that considers the results of Chapters 2 and 3 indicate disease-related

concentration abnormalities in frontal cortex glutathione, GABA, glutamate, or other ^{1}H MRS-visible small-molecule metabolites? Furthermore, can these metabolic differences alone be used to distinguish progressive and relapsing-remitting multiple sclerosis from each other and from control?

Taken together, our findings suggest that employing an evidence-based spectral processing and quantification pipeline with particular attention to spectral baseline modeling and potential relaxation-based confounds on internal concentration referencing according to the results of Chapters 2 and 3, it was shown that progressive but not relapsing-remitting multiple sclerosis is associated with disease-related decreases in frontal cortex glutamate, GABA, and possibly glutathione as measured by ^{1}H MRS. While even significant between-group differences in single metabolites were not sufficient to distinguish accurately among disease groups, using multivariate discriminant analysis or supervised learning, progressive multiple sclerosis can be differentiated from control or relapsing-remitting multiple sclerosis with nearly 80% sensitivity and specificity solely on the basis of ^{1}H-MRS-visible frontal cortex metabolites.

Chapter 5: Generalization.

Application of optimized spectral quantification and statistical analysis techniques from ^{1}H-MRS investigation of multiple sclerosis to post-traumatic stress disorder and comorbid major depression

Post-traumatic stress disorder (PTSD) is a condition wherein the experience of a traumatic event induces emotional dysregulation that chronically disrupts daily function. With estimated lifetime prevalence as high as 1 in 12, PTSD is a complex and multifactorial illness. Correspondingly, the effect sizes of disease-related alterations in individual tissue metabolites as measured by ^{1}H MRS, including NAA, choline, inositols, glutamate, GABA, and glutathione, tend to be small and varied, and still lacking is a comprehensive model demonstrating the relationships among sundry single-compound findings.

^{1}H MRS is the ideal tool for embarking on such a study as it can directly assess multiple biomolecules in the tissue of living subjects, enabling concomitant association of several in situ metabolic endpoints with the clinical presentation of disease. This work employs the spectral quantification, absolute quantification, and statistical analysis pipelines validated in Chapters 2 through 4 to perform a cross-sectional analysis of cortical biochemistry, including glutamate, GABA, and glutathione, in addition to five other metabolites previously implicated in neurological disease (choline, creatine, myoinositol, N-acetyl aspartate, and glutamine), in forty-one individuals with and without PTSD and/or common psychiatric comorbidity major depressive disorder (MDD). We hypothesize that the condition of either PTSD and/or MDD alters concentrations of these metabolites in a pattern that can be exploited to enable the cost-efficient and accurate diagnosis of this disease. As such, we use a battery of machine-learning classifiers to develop a transparent and interpretable model that uses ^{1}H-MRS-measured cortical metabolite concentrations to differentiate between individuals with and without at least one of these psychiatric diagnoses. Quadratic discriminant analysis (QDA), k-nearest neighbors (KNN), and support vector machines (SVM)

have been selected based on their superior performance in Chapter 4.

Here we find altered glutamine : neurotransmitter (namely, glutamate and GABA) ratios in post-traumatic stress disorder that became a significant effect of major depressive disorder on glutamine concentration and neurotransmitter ratios when this comorbidity is considered. Additionally, a trend to decreased glutathione was observed in post-traumatic stress disorder that became a significant effect of diagnosis with any disorder (either post-traumatic stress disorder and/or major depressive disorder) when comorbid major depression was considered. Similarly, supervised binary classifiers (quadratic discriminant analysis, k-nearest neighbors, and support vector machines) were able to be generalized from the multiple sclerosis and control cohorts presented in Chapter 4 to this similar but distinct ^{1}H MRS data set for comparably accurate (maximum 83% sensitivity and specificity) binary classification of post-traumatic stress and/or major depressive disorder and control.

5.1 Introduction: Systematic review and meta-analysis of existing literature on ^{1}H MRS in PTSD

5.1.1. Motivation

Post-traumatic stress disorder (PTSD) is a condition wherein one or more exposures to a strong stressor is followed by chronic and debilitating disruption to sensory, emotional, and cognitive function. PTSD entered the Diagnostic and Statistical Manual (DSM) of the American Psychiatric Association in its third edition, first published in 1980 [514]. Since then, the definitions surrounding qualifying traumas and symptomatic manifestation have changed, most notably between the DSM-IV and DSM-V, resulting in diagnostic discrepancies in as many as 30% of patients in at least one analysis [515, 516]. PTSD as currently defined in the DSM-V takes on four

clusters of symptoms that must persist for at least one month following either direct or extensive indirect exposure to a traumatic event, including “actual death, serious injury, or sexual violence”: intrusive memories, dreams, sensory flashbacks, or triggered associations to psychological distress or physiological reactivity; avoidance of internal or external reminders of the trauma; negatively altered cognition and mood; and significantly altered arousal and reactivity [517].

Both sex and age appear to be important mediators of PTSD development following trauma exposure and are therefore salient considerations for the design of experiments that investigate possible mechanisms thereof. Lifetime prevalence of PTSD has been estimated as much as twice as high in women as in men [518, 519]. Hypotheses regarding the reasons behind this disparity have included greater lifetime exposure to trauma in the former than the latter, though reported not to be the case in at least one meta-analysis [520]; greater exposure to trauma types, like sexual violence, disproportionately likely to precede PSTD development [521-523]; and differential rates of conversion from trauma exposure to PSTD even once trauma frequency and type are controlled, previously demonstrated in at least one mixed-sex cohort exposed to multiple incidents of non-combat assaultive violence [516, 524].

A 2017 survey of individuals in 24 countries yielded reports of traumatic stressors in 70.4% of respondents, with conditional risks of PTSD development ranging from 0.1% to 19.0%, depending on trauma type, among those exposed [523]. Because traumatic stress and PTSD thus do not exhibit a one-to-one relationship, a persistent question in especially post-trauma case-control analyses of PTSD is the degree to which differences observed between patients and study control are due to factors that may predispose trauma-exposed individuals to developing diagnosable PTSD relative to downstream effects of either the trauma itself or the ensuing illness. Studies involving both trauma-exposed individuals with PTSD and their genetically identical

trauma-unmatched twins have been useful in unraveling the distinctions among such putative causative mechanisms [525]. For example, reductions in hippocampal volume observed in PTSD patients has similarly been observed in their trauma-unmatched twins relative to control, supporting the conclusion that reduced hippocampal volume may act as a predisposing factor for PTSD development following trauma exposure [526], an interpretation that has been since reiterated in a more recent meta-analysis [527]. On the other hand, reduced retention of extinction learning as measured by skin conductance alterations in a fear conditioning task for PTSD patients relative to non-PTSD trauma-exposed controls has been observed in PTSD patients but not their trauma-naïve twins, supporting the conclusion that this observed abnormality may be more difficult to link with genetic predisposition to PTSD development [528].

In considering such questions of causation in PTSD it is important to remember that predispositions to and effects of trauma and/or PTSD are not necessarily mutually exclusive phenomena [525]. Indeed, despite the aforementioned literature suggestive of reduced hippocampal volumes as risk factor for PTSD development [526, 527], it has also been shown meta-analytically that even trauma-exposed individuals who did not develop PTSD also demonstrate reduced hippocampal volumes relative to trauma-unmatched controls, suggesting an additional role for trauma itself in hippocampal volume reductions observed in PTSD [529]. Especially in the proton magnetic resonance spectroscopy literature, where studies are often small and designs correspondingly simple, in the absence of identical twin cohorts some attempt has been made to tease out the effects of trauma itself from those of either predisposition to or effect of PTSD by distinguishing between trauma-unmatched and trauma-exposed or, especially in the case of PTSD following combat trauma, military veteran controls.

Regardless of whether attributable as cause and/or effect of illness, a broad range of

difference from the physiological to the molecular levels of detail have been observed in PTSD patients relative to various control groups (Figure 5.2). The description that follows is intended only as a brief summary of PTSD's biological context, and the reader is referred elsewhere for comprehensive reviews of PTSD [516] and its genetic associations [522], transcriptionally visible sex differences [530], interaction with brain development [531], pharmacologically manipulable manifestations [532], functional correlates in the brain [533], and biological studies in both human and animal models [525].

Twin studies have supported PTSD heritability estimates ranging from 23% to 71% depending on the cohort under study, with suggestions that women exhibit higher heritability than men, as well as on trauma type, with interpersonal trauma exhibiting higher heritability for PTSD development than accidents or natural disasters [522]. A number of disease-associated loci have been identified across both intergenic and potentially protein-coding regions of the genome, supporting the idea that predisposition to the condition has polygenic origins [522]. Patterns of gene expression in plasma mononuclear cell samples taken both at time of stress exposure and at four months follow-up have correspondingly been shown to differ between trauma-exposed individuals who did and did not eventually develop PTSD [534], an observation replicated by a more recent, larger study of peripheral blood cell gene transcription patterns acute to stress exposure in those who later did versus did not develop PTSD symptoms [535]. Disparities in methylation on certain genes have additionally been observed between PTSD patients and trauma-exposed controls [536, 537].

Phenotypically, individuals with PTSD demonstrate differential reactivity to sensory stimuli both unrelated and related to traumatic experience [525]. For example, heart rate, skin conductance, and ocular electromyographic responses to sudden loud tones have shown

enhancements in PTSD patients relative to their non-trauma-exposed twins, whose attenuated reactions were similar to those of trauma-exposed individuals without PTSD and their non-trauma-exposed twins [538]. Similarly, enhanced reactivity to trauma-related audiovisual cues or imagery scripts, including but not limited to heart rate, skin conductance, diastolic blood pressure, and self-reported subjective distress, have been observed in combat veterans with PTSD relative to those without [539]. Disparities between individuals with PTSD and trauma-exposed or unexposed controls at various stages of cortical event-related potentials to a variety of stimuli have also been interpreted as supporting a narrative of dysregulated automatic rapid processing and abnormal cognition. This includes reduced orientation to emotional stimuli, enhanced attention to threatening or ambiguous stimuli, and reduced attention to non-affective target stimuli followed by indications of reduced update to working memory [540].

PTSD-associated abnormalities in arousal state have also manifest in a number of disparities in endocrine function, including smaller pituitary gland volume [541]; reductions in plasma cortisol, prolactin, and thyroid-stimulating hormone [542]; lower baseline plasma [543] and CSF [544] neuropeptide Y (NPY), thought to serve as a sympathetic nervous system modulator and endogenous anxiolytic; reduced plasma NPY response to α2-adrenergic receptor antagonist yohimbine, with baseline plasma NPY negatively correlated in PTSD with reported panic symptoms [543]; and lower baseline plasma adrenocorticotropin-releasing hormone (ACTH) but increased ACTH following exposure to cognitive stress [545] and reduced ACTH release following dexamethasone injection [546], in PTSD patients than in either healthy civilian or veteran controls [532]. Possibly in line with heightened ACTH responsivity, increased plasma concentrations of arginine vasopressin (AVP), a hormone that may potentiate ACTH release, have been observed in male PTSD patients relative to both trauma-unmatched and trauma-exposed

controls; in addition, among individuals with PTSD but not major depressive disorder, plasma AVP correlated negatively with avoidance symptoms as measured by the Clinician-administered PTSD Scale (CAPS) [547]. Moreover, a subset of PTSD patients has been observed to exhibit heighted ACTH release in response to low-dose naloxone, an endocannabinoid receptor antagonist that is thought to reduce endogenous opioidergic inhibition of the hypothalamic CRH signaling that facilitates ACTH secretion [548].

PTSD symptom severity has been negatively correlated with serum cortisol [542]; higher plasma corticotropin-releasing hormone has been seen in PTSD than in either trauma-unmatched or veteran controls [549] and has been shown to decrease in PTSD upon exposure to trauma-related relative to neutral stimuli [550]. Plasma cortisol has shown reductions or no difference in PTSD versus control, while higher concentrations have been demonstrated in the CSF of PTSD patients relative to trauma-naïve controls [551]. Lymphocytes taken from PTSD patients demonstrate a higher number of glucocorticoid receptors across the day than those in trauma-unmatched controls, with receptor density in the morning positively correlated with PTSD and anxiety symptoms [525, 552]. Plasma GABA has shown decreases in PSTD patients relative to trauma-exposed or trauma-unmatched controls [532], with at least one study demonstrating a negative correlation between plasma GABA and both depression and anxiety symptoms [553]. In line with these GABA findings, allopregnanolone and pregnanolone, agonists of GABA activity at $GABA_A$ receptors, have also demonstrated reductions in CSF of women with PTSD relative to trauma-unmatched controls [554]. Similarly, plasma concentrations of metabolic androgen precursor and $GABA_A$ antagonist dehydroepiandrosterone (DHEA) of both women and men with PTSD have been reported higher than those of either trauma-naïve or trauma-exposed controls [525]. Relative to trauma-naïve controls, CSF and plasma in PTSD have also shown decreased orexin-A, a neuropeptide produced

in the hypothalamus that is involved in the production of hormone norepinephrine; in addition, CSF orexin-A demonstrated a negative correlation with CAPS score [532, 555].

This evidence of PTSD-associated abnormalities in autonomic and cortical reactivity to a variety of inputs is accompanied by observations of anatomical and metabolic differences in key brain regions in the disease, including those targeted by magnetic resonance spectroscopy experiments: frontal cortex and anterior cingulate cortex, basal ganglia, occipital cortex, parietal cortex, insula, temporal cortex, hippocampus, and amygdala.

Meta-analysis of anatomical MR studies has demonstrated reductions in grey-matter volume of medial prefrontal cortex (mPFC), anterior cingulate cortex (ACC), striatum, insula, left hippocampus, and amygdala relative to trauma-exposed controls in individuals with PTSD, particularly in those who developed the condition following a single traumatic event; for those with prolonged trauma exposure, grey-matter reductions were seen in striatum, middle temporal gyrus, insula, and amygdala [556]. A more recent meta-analysis confirmed findings of decreased hippocampal volume in PTSD relative to trauma-exposed controls [557]. Hippocampal volume losses have been observed across multiple symptomatic presentations of PTSD, including with and without dissociative symptoms [533]. At least some of these differences are thought to be acquired, as evidenced by observations of right hippocampus, anterior cingulate cortex, and bilateral insula grey-matter density reductions in combat-exposed PTSD patients relative to both their own combat-unexposed twins and non-PTSD combat-exposed controls with their combat-unexposed twins [558]. As previously mentioned, however, other evidence points to reduced hippocampal volume additionally serving as a predisposing trait for PTSD development in trauma-exposed individuals [527]. Both smaller size of pre-trauma right anterior cingulate cortex and larger magnitude (more negative difference) of pre-to-post-trauma reductions in left orbitofrontal cortex

(OFC) grey matter volumes have also been associated with exacerbated PTSD-like symptoms as indicated by higher CAPS scores, suggesting disparate roles of these different regional brain tissue volumes as either predisposing factors (pre-trauma ACC) or indicative of disease progression (post vs. pre-trauma OFC) [559]. Like the hippocampus, PTSD has been inconsistently linked to alterations in amygdalar volume, with both decreases [560] and increases [561] previously observed in combat-exposed veterans with PTSD relative to those without, with the latter study also observing an additional effect of combat exposure severity associated with volume reductions only in patients also exposed to early-life trauma. Disparate polarities of PTSD-associated effect on both volume and shape have also been observed in distinct amygdalar nuclei [562].

In addition to regional alterations in grey matter, white-matter integrity as measured by diffusion tensor imaging, including in the corpus callosum, anterior cingulum, hippocampus, and/or tracts connecting prefrontal regions with the amygdala, has also demonstrated abnormalities relative to trauma-unmatched control or trauma-exposed control in individuals with PTSD [563]. The cingulum bundle, which connects the dorso- and ventromedial prefrontal cortex, has demonstrated reduced structural connectivity in individuals with PTSD relative to trauma-exposed controls; similarly, the uncinate fasciculus, which connects the ventromedial prefrontal cortex with the amygdala, has demonstrated MR-visible suggestions of structural integrity reduction in PTSD relative to trauma-unmatched or trauma-exposed controls [533]. Notably, at least one study demonstrates that while several regional differences to white-matter integrity in trauma-exposed individuals relative to trauma-unmatched controls were not recapitulated in similar differences between trauma-exposed individuals with relative to without PTSD, they have been shown to correlate significantly with PTSD symptom severity as measured by CAPS [564].

Beyond gross anatomical differences suggested by magnetic resonance imaging, nuclear

imaging has additionally indicated PTSD- or trauma-related reductions in regional densities of certain neurotransmitter receptors. Positron emission tomography (PET) has demonstrated reduced 5HT transporter binding in bilateral amygdala in PTSD relative to trauma-unmatched controls [565] as well as reduced $5HT_{1B}$ receptor ($5HT_{1B}R$) binding in amygdala, caudate, and anterior cingulate cortex relative to trauma-unmatched but not trauma-exposed controls [566]. Reduced PET radioligand binding to benzodiazepine $GABA_A$ receptor across multiple regions of cortex as well as bilateral hippocampus and thalamus has been seen, however, in veterans with PTSD relative to veteran controls deployed to the same regions, consistent with the idea that PTSD-related differences in $GABA_A$ receptor availability may evince a mechanism auxiliary to any effects of traumatic stress itself [567]. Correspondingly, three polymorphisms in the $GABA_A$ receptor subunit α_2 have preliminarily been shown to significantly interact with exposure to childhood trauma to affect risk of ultimate PTSD development [568]. Along the same vein, PET analysis has demonstrated dorsolateral and orbitofrontal cortical $mGluR_5$ availability to be higher in individuals with PTSD than trauma-naïve control, as well as positively correlated with PTSD checklist (PCL) avoidance subscale scores [569]. Similarly, reduced μ-opioid receptor binding has also been observed across the anterior cingulate cortex of male PTSD patients relative to male trauma-exposed and trauma-naïve controls [570]. By contrast, cannabinoid receptor 1R (CB_1R) density was also higher across the brain in PTSD patients relative to either trauma-unmatched or -exposed controls and together with peripherally measured concentrations of anandamide and cortisol served to classify with 85% accuracy PTSD patients relative to either control group [571].

Metabolic rates of glucose in the orbitofrontal and prefrontal cortex were also reported to change differently in response to α_2-adrenergic receptor antagonist yohimbine, which tended to effect larger increases in trauma-unmatched controls than in PTSD patients, for whom tendencies

to decreases in metabolic rate were observed [572]. Based, however, on the selective induction of panic attacks in PTSD patients exposed to agonists of either noradrenergic or serotonergic receptors but not both, it has been hypothesized that the symptoms of different subsets of PTSD patients may exhibit abnormality in different neurotransmitter systems [573]. Injection of hydrocortisone was shown to restore lateral asymmetry in resting glucose consumption of the dorsal amygdala as well as improve subsequent working memory task performance in veterans with PTSD, while the same injection disrupted both dorsal amygdala metabolic lateral asymmetry and working memory task performance in veterans without it [574].

Functional brain imaging studies have also demonstrated a profusion of disparities between individuals with PTSD and either trauma-exposed or naïve controls, including in brain regions assessed by ^{1}H MRS. A number of functional MRI (fMRI) and/or PET studies have reported results consistent with decreased prefrontal cortex activation and abnormal amygdala activation in response to both trauma-associated and non-associated stimuli relative to either trauma-exposed or -unmatched controls [516, 575], with different activation patterns seen in PTSD patients who demonstrated emotional detachment symptoms relative to those experiencing flashbacks and hyperarousal [516, 576]. Ventromedial prefrontal cortex blood-oxygen-level-dependent (BOLD) fMRI signal changes were attenuated during fear extinction in PTSD patients relative to trauma-unmatched controls and associated with greater failure in the former to extinguish conditioned fear [577]. Similarly, medial prefrontal cortex (including anterior cingulate cortex) activity as measured by BOLD fMRI in response to fearful faces was shown to be lower in PTSD patients than in trauma-unmatched controls, with task-based BOLD signal in a subset of this region negatively correlated with total CAPS score [578]. Task-based BOLD signal contrast in response to fearful versus neutral faces in the rostral anterior cingulate region of the

ventromedial PFC has been shown to increase, with correlated reductions in CAPS scores, following cognitive behavioral therapy in PTSD patients [579]. Similarly, rostral anterior cingulate cortex BOLD contrasts for combat-related versus generally negative emotional interference tasks were reduced in veterans with PTSD relative to veteran controls [580]. Medial frontal gyrus blood flow as measured by PET during traumatic recollection has been shown to correlate negatively with both CAPS symptom severity and concomitant amygdalar blood flow in PTSD [581]. Such differential patterns of activation in response to trauma-related versus other negative emotional stimuli have been previously extended to the sensorimotor cortex as well as the periaqueductal grey, a midbrain region associated with automatized threat responses [532], and thereby associated with motor preparation following threatening stimuli [582]. Interestingly, despite these opposite polarities in dorsomedial versus ventromedial PFC activity in PTSD patients versus control, both regions have demonstrated reduced grey-matter volumes in PTSD patients relative to trauma-exposed or trauma-unmatched controls, respectively [533].

In contrast to ventromedial prefrontal regions, the dorsomedial prefrontal cortex, associated with comparing learned threat-related expectations to current threat-related information, has been linked with greater task-based activity relative to control in individuals with PTSD [533]. In particular, the dorsal anterior cingulate cortex (dACC) has generally demonstrated hyperactivity in PTSD relative to control as studied by fMRI and PET in response to a number of fear-conditioning, emotional interference, and other cognitive tasks [525]. Due to observation of similarly increased dACC activation in trauma-naïve co-twins of PTSD patients, abnormal activity in this area has also been postulated to serve as a risk factor for disease development as opposed to only or additionally a sequelae of either trauma exposure or PTSD [525].

The amygdala has demonstrated increased BOLD fMRI contrast in response to trauma-

related and -unrelated stimuli as well as increased PET-measured cerebral blood flow during conditioned fear acquisition in individuals with PTSD relative to trauma-unmatched or trauma-exposed controls [525, 583]. As mentioned, overactivity in the amygdala has been associated in PTSD with hypoactivity in the ventromedial PFC; together, these have been interpreted as reduced prefrontal inhibition of fear-conditioning responses that could disrupt subsequent learning processes [533]. However, also as noted, in some individuals, a dissociative subtype of PTSD has been observed wherein amygdalar hypoactivity and ventromedial prefrontal hyperactivity are paired with symptoms of emotional detachment [533, 584]. In addition, meta-analysis has suggested ventral anterior amygdala hyperactivity in concert with dorsal posterior amygdala hypoactivity during fear conditioning in PTSD relative to individuals with other anxiety disorders [575], underlining the potential importance of high spatial resolution in discussions of regional abnormality. Similarly, imaging studies of hippocampal function in PTSD have also demonstrated mixed results [525] depending on details of the task and analytical framework at hand [585].

Comorbidities, including to mood disorders and/or substance use, are an important consideration for studies of PTSD; as a common example, the prevalence of major depressive disorder in individuals with PTSD has been reported as high as 50% [586]. At least some studies reporting the aforementioned PTSD-associated abnormalities have explicitly controlled for these factors: While comorbidities like alcohol abuse [587] and borderline personality disorder [588] have, like PTSD, themselves been associated with reduced hippocampal volume [589], at least one report concludes that reductions in hippocampal volume in PTSD patients relative to trauma-unmatched control, for example, are not accounted for by depression or substance use [525]; another suggested greater PTSD-associated volume reductions in alcoholic than in non-alcoholic cohorts [590]. On the other hand, reductions in anterior cingulate cortex 5HT binding in PTSD

patients relative to trauma-unmatched controls have been shown to be driven by comorbidity with major depressive disorder [566]. Similarly, it has been noted that while increased plasma cortisol has generally not been observed generally in PTSD, this may not apply to individuals with comorbid major depressive disorder [525].

Despite the unequivocal involvement of a number of biological systems in either predisposition or unfolding of PTSD, still no definitive biomarker, MR-visible or otherwise, exists for diagnosis, prognosis, or treatment monitoring. Incomplete biological understanding of PTSD pathogenesis and symptomology is also evinced by the limited pharmacological treatment options available. Despite a number of non-pharmacological therapies for PTSD, only two medications, sertraline and paroxetine, both SSRIs, have been FDA-approved for the condition [532]. A recent systematic review and meta-analysis of clinical trials suggested some treatment efficacy in not only these two therapeutics but also a number of others, including antidepressants venlafaxine and fluoxetine, atypical antipsychotics risperidone and quetiapine, and anticonvulsant topiramate [591], though low rates of selective serotonin reuptake inhibitor (SSRI) treatment response and subsequent disease remission have justified interest in potential therapeutics targeting the glutamatergic rather than monoamine systems: for example, anticonvulsant lamotrigine, glutamate modulator riluzole, NMDAR antagonist ketamine, and NMDA agonist D-cycloserine [592].

In addition to the as-yet incomplete armamentarium of pharmacologic interventions for the condition, further motivating the utility of ^{1}H MRS as a tool for examining the in vivo neurobiology of PTSD is, similarly to progressive multiple sclerosis as discussed in Chapter 4, the continued limitation of rodent models for the disease. Commonly employed paradigms for PTSD induction in rodents that exhibit both some face validity (in surface appearance) and construct validity (in underlying sequelae) for modeling the human condition include footshock plus

additional stress, predator exposure, and single prolonged stress (SPS) [525]. Systematic analysis of these and other PTSD rodent models against DSM-V criteria for PTSD has found inconsistent support for their correspondence, especially in female rodents despite the greater published prevalence of PTSD in women than men [518, 519], and concluded that no one model currently captures the complexity of PTSD in humans [593]. Notably, while as mentioned a minority of trauma-exposed individuals actually develop PTSD, in rodent exposure paradigms like SPS, measured endpoints like reduced fear extinction retention can be observed in enough test subjects to drive, without subsampling, a significant exposure-based cross-sectional statistic [594], raising questions of construct validity. In addition, in humans PTSD has implicated possibly differential roles of prefrontal subregions like the ventromedial prefrontal cortex and dorsal anterior cingulate cortex, brain regions that do not appear in rodents, for which the closest functional homologues with regard to fear conditioning are arguably the infralimbic and prelimbic cortices [525].

Toward the end of characterizing the present state and potential future of ^{1}H-MRS-based contributions to understanding the metabolic manifestations and possibly underlying pathophysiology of PTSD, the present literature review serves as an update and extension to two previously published surveys of the ^{1}H-MRS literature on PTSD, including a 2010 meta-analysis of NAA, choline, creatine, and/or inositol findings in hippocampus and anterior cingulate cortex [104] as well as a 2019 systematic review without meta-analysis of 24 research reports published between 1998 and 2017 [105]. The present report includes a systematic review of all published metabolite cross-sectional findings relative to control and correlations in PTSD as reported by located records, as well as meta-analyses involving more recently published studies in all regions and metabolites involving at least five reported comparisons with control.

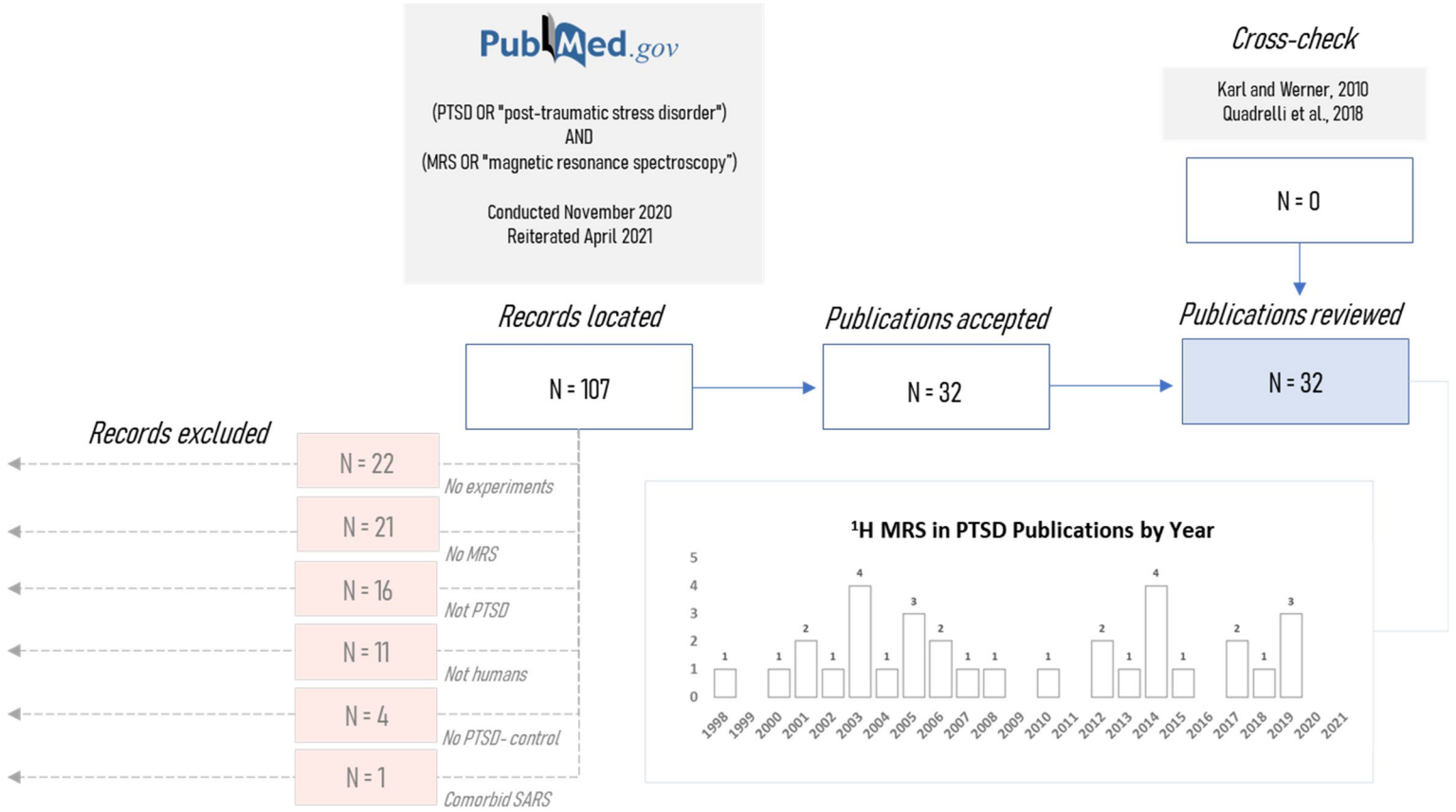

Figure 5.1. Records processing pipeline for systematic review of published proton magnetic resonance spectroscopy (^{1}H MRS) investigations of post-traumatic stress disorder (PTSD). Initial records (N=107) were located via designated search terms on PubMed based on [105], following which abstracts were screened for exclusion on the basis of not being a human ^{1}H MRS case study of PTSD or case-control analysis with at least one healthy non-PTSD control. Remaining studies (N=32) were cross-checked against an older systematic review [105] and meta-analysis [104] to confirm inclusion of all relevant studies in the present investigation. SARS: Severe Acute Respiratory Syndrome.

5.1.2. Methods

Literature review was conducted according to search terms described previously [105], including all combinations of "post traumatic stress disorder" or "PTSD" with "magnetic resonance spectroscopy" or "MRS." This search yielded thirty-two unique publications that applied magnetic resonance spectroscopy to at least one individual reported to have post-traumatic stress disorder; this set was cross-checked with the previously mentioned 2019 systematic literature review [105] and 2010 meta-analysis [104] to ensure that it encompassed all studies included in these two latter reports. Studies were excluded if they did not report experiments (N = 22), did not use ^{1}H MR spectroscopy (N = 21) or examine PTSD patients (N = 16), humans (N = 11), include a matched non-PTSD control group (N = 4), or involve non-psychiatric comorbidity (N=1) (Figure 5.1). One exception to these exclusion criteria was a case study included for examination of methodological variables [595].

For completeness all reported significant and null findings in cross-sectional metabolite comparisons are described in the text; for simplicity only significant correlations are reported in the text. For simplicity and because precise linguistic distinctions are often not made in the existing literature, the designations N-acetyl aspartate (NAA), creatine (Cr), and choline (Cho) are used to describe their respective common metabolite summations N-acetyl aspartate + N-acetyl aspartylglutamate (total N-acetyl aspartate or tNAA), creatine + phosphocreatine (total creatine or tCr), and choline + phosphocholine + glycerophosphocholine (total choline or tCho), respectively.

Random-effects meta-analysis [596] on the influence of PTSD on regional metabolite concentration was conducted for all metabolites and brain regions exhibiting at least five published cross-sectional analyses against either trauma-exposed or trauma-unmatched groups, with or

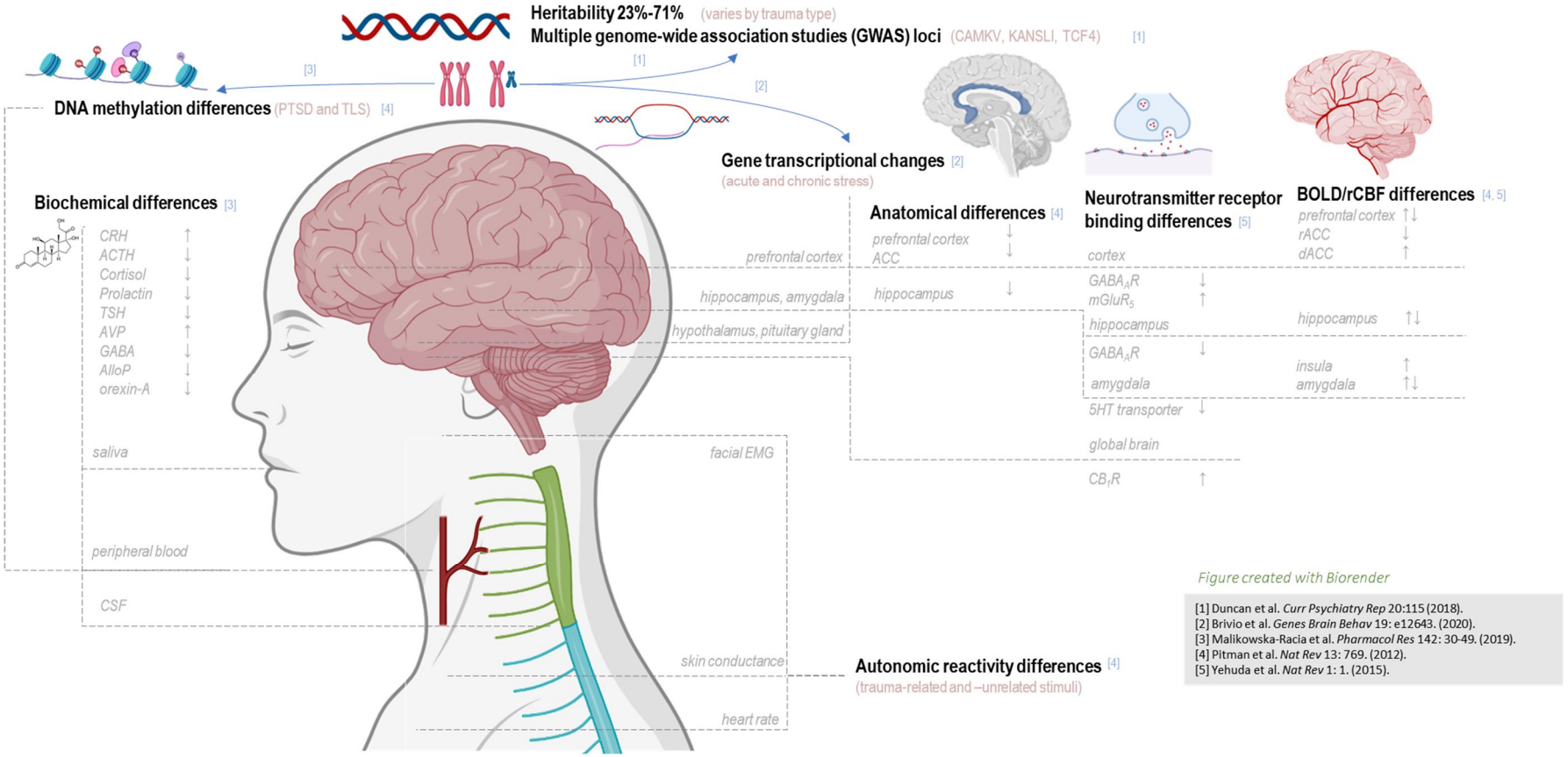

Figure 5.2. Post-traumatic stress disorder (PTSD) has been associated with observed disparities from various controls over multiple biological levels of detail. Post-traumatic stress disorder (PTSD) has been associated with allelic variations at multiple genetic loci; DNA methylation patterns and gene transcription patterns have also been reported to differ with PTSD status and/or stress exposure. Disparate levels of multiple hormones and other biochemicals have been observed in saliva, blood, or cerebrospinal fluid (CSF), and differences in autonomic reactivity to either trauma-related or -unrelated stimuli have been suggested via measures of electromyography (EMG), skin conductance, and heart rate. Brain regions additionally examined by proton magnetic resonance spectroscopy (^{1}H-MRS), such as the prefrontal cortex, hippocampus, and amygdala, have demonstrated abnormalities in volume, neurotransmitter receptor binding, and patterns of BOLD contrast in PTSD. In assessing these reported differences, as in ^{1}H-MRS findings, it should be noted that depending on study design, biological differences observed between PTSD patients and control may elucidate predisposition to develop PTSD, effect of trauma exposure or PTSD pathology, or all of the above. CRH: corticotrophin-releasing hormone; ACTH: adrenocorticotropic hormone; TSH: thyroid-stimulating hormone; AVP: arginine vasopressin; AlloP: allopregnanolone; CSF: cerebrospinal fluid; ACC: anterior cingulate cortex; 5HT: 5-hydroxytryptamine (serotonin); mGluR$_5$: metabotropic glutamate receptor 5; CB$_1$R: cannabinoid-1 receptor; GABA$_A$R: GABA receptor A; rACC: rostral anterior cingulate cortex; dACC: dorsal anterior cingulate cortex.

without comorbidities. When PTSD groups were compared with both trauma-unmatched and trauma-exposed or veteran controls in the same study, only comparisons with trauma-exposed or veteran controls were included for meta-analysis. When PTSD groups with and without additional comorbidities (e.g., alcohol use disorder, bipolar disorder) were compared against distinct matched controls, both comparisons were included in meta-analysis. All statistics were conducted in R version 4 (R Foundation for Statistical Computing, Vienna, Austria).

5.1.3. Results

Methodological Overview. N=33 PTSD vs. control comparisons from N=28 studies were assessed for average age of the PTSD group as well as age-matching between PTSD and control. Four studies [597-599] did not provide patient group age means or was a case study with no control [595], and were excluded from age analysis. PTSD group average ages most frequently represented the 30-40 year range and demonstrated a marginal trend to increase relative to control (random-effects model standardized mean difference 0.11 ± 0.062, p =0.09) (Figure 5.3A). While N=10 studies not including the case study on a single male patient [595] included all-male PTSD cohorts, N=3 studies included all-female PTSD cohorts, with a median 2% decrease in control versus PTSD percent women among those N=13 studies that did not exhibit sex-matched groups (Figure 5.3B). N=4 of 32 studies acquired data at 4 Tesla field strength, while none had been conducted at 7 Tesla or above (Figure 5.3C). N-acetyl aspartate (N=67), choline (N=37), creatine (N=25), and myoinositol (N=17) comprised the majority of metabolite concentrations reported, particularly in non-cortical voxels, with a minority of comparisons involving glutamate and/or glutamine (N=13), GABA (N=7), glutathione (N=2), or other resonances including fucoses and lipids (N=1) (Figure 5.3D).

Regional cross-sectional metabolite findings (Figure 5.4) and correlations (Figure 5.5) were observed as follows.

Frontal Cortex (non-ACC). In humans the frontal cortex comprises the six cortical layers of the brain's frontal lobe and is thought to be involved in a large number of executive processes integrating and mediating activity in other brain regions. Regions of the prefrontal cortex (PFC) in particular have been implicated in PTSD vulnerability and/or pathogenesis for their connections with the hippocampus and amygdala that together regulate fear learning and memory [533]. PTSD has been previously associated with alterations in grey-matter volumes in medial prefrontal cortex [556] and pre- to post-trauma changes in orbitofrontal cortex [559] as well as losses of white-matter integrity in frontal cortex regions including the cingulum bundle and uncinate fasciculus [533, 563]. Alterations have been seen in frontal cortex metabotropic glutamate receptor density [569] as well as either heightened (dorsomedial prefrontal) [533] or diminished (ventromedial prefrontal) [577] activity responses to traumatic and neutral stimuli, and it has been hypothesized that glutamatergic excitotoxicity in this region may play a role in PTSD pathogenesis [600].

In frontal and periventricular white matter, NAA/Cr has exhibited no abnormality [601] (versus trauma-unmatched control, HC); similarly, in left dorsolateral PFC, NAA/Cr has also exhibited no abnormality [600] (versus trauma-exposed control, TEC).

In frontal and periventricular white matter, Cho/Cr has exhibited no abnormality [601] (HC). In left dorsolateral prefrontal cortex (PFC) Glu/Gln has also demonstrated no abnormality [600] (TEC).

By contrast, in left dorsolateral PFC GABA/Cr has exhibited increases [600] (TEC); GSH/Cr has also exhibited increases [600] (TEC). Left dorsolateral prefrontal cortex GSH/Cr

correlated positively with PTSD duration [600].

Anterior Cingulate Cortex. The anterior cingulate cortex overlaps with portions of both ventromedial and dorsomedial prefrontal cortex, both of which have demonstrated structural and functional abnormality in PTSD [533]. In addition to grey-matter volume reductions [556] interpreted as either acquired difference [558] or predisposing factor [559], the ACC in PTSD patients has also demonstrated reduced μ-opioid receptor binding [570] and increased task-based fMRI or PET contrast in fear-conditioning, emotional interference, and other cognitive paradigms [525], though some observations of decreased BOLD fMRI-measured activity within the general context of the medial PFC during visual presentation of fearful faces have been made [578]. It is thought that with roles in fear conditioning and extinction, the dACC in particular could contribute to PTSD vulnerability and/or pathogenesis [602], with local functional abnormalities possibly contributing to disruptions in the salience network leading to hypervigilance [603].

In the anterior cingulate cortex of individuals with PTSD relative to control, NAA/Cr has exhibited decreases [597, 599, 604] (HC) [605] (TEC+HC) or no abnormality [606] (HC) [600, 607, 608] (TEC). NAA referenced otherwise has demonstrated increases [609] (TEC), decreases [610] (HC) [611] [612] (TEC), unilateral decreases (right only) [605] (TEC+HC), trend to decrease [613] (HC), or no abnormality [602] (HC), (TEC). Individuals with both PTSD and alcohol use disorder (AUD) demonstrated no NAA changes in this region relative to PTSD control [613]. Anterior cingulate cortex NAA correlated negatively with CAPS symptom re-experience scores in PTSD [610] and CAPS arousal scores in PTSD [611, 613]. Anterior cingulate cortex NAA has also demonstrated a negative correlation with time since trauma as well as a trend to negative correlation with CAPS total score in PTSD [609].

Anterior cingulate cortex creatine has exhibited no abnormality [602, 610, 613] (HC) [602, 609, 611, 612] (TEC). Individuals with PTSD and AUD demonstrated no creatine changes in this region relative to PTSD control [613]. Anterior cingulate cortex creatine correlated negatively with CAPS arousal scores in PTSD [611, 613]. It has also demonstrated a significant negative regression coefficient with auditory verbal learning test (AVLT) immediate recall scores, as well as a trend to negative regression coefficient with auditory verbal learning test delayed recognition scores, in trauma-exposed controls but not PTSD patients [612].

Anterior cingulate cortex Cho/Cr has demonstrated increases [597] (HC) [607] (TEC) or no abnormality [599, 604, 607] (HC) [608] (TEC). Choline has exhibited no abnormality [602, 610] (HC) [602, 609, 611, 613] (TEC). Individuals with both PTSD and AUD demonstrated choline reductions in anterior cingulate cortex relative to PTSD control [613].

Anterior cingulate cortex mIns/Cr has demonstrated increases [607] (TEC) or no abnormality [607] (HC) [608] (TEC). Myoinositol has demonstrated increases [609] (TEC) or no abnormality [602, 610] (HC) [602, 611-613] (TEC). Individuals with both PTSD and AUD demonstrated myoinositol reductions in anterior cingulate cortex relative to PTSD control [613]. Anterior cingulate cortex myoinositol correlated negatively with CAPS total scores, CAPS arousal scores, and CAPS intrusion scores in PTSD [611] and reported again with CAPS intrusion scores in PTSD [613].

Anterior cingulate cortex Glx/Cr has exhibited decreases [608] (TEC), while Glx has exhibited no significant abnormality [609] (TEC). Similarly, glutamate has exhibited no significant abnormality [602] (HC) [602, 611-613] (TEC). Individuals with both PTSD and AUD demonstrated glutamate reductions in anterior cingulate cortex relative to PTSD control [613]. Anterior cingulate cortex glutamate correlated negatively with CAPS arousal scores in PTSD [611, 613]. It was additionally found to correlate negatively with CAPS total scores [613]. Finally,

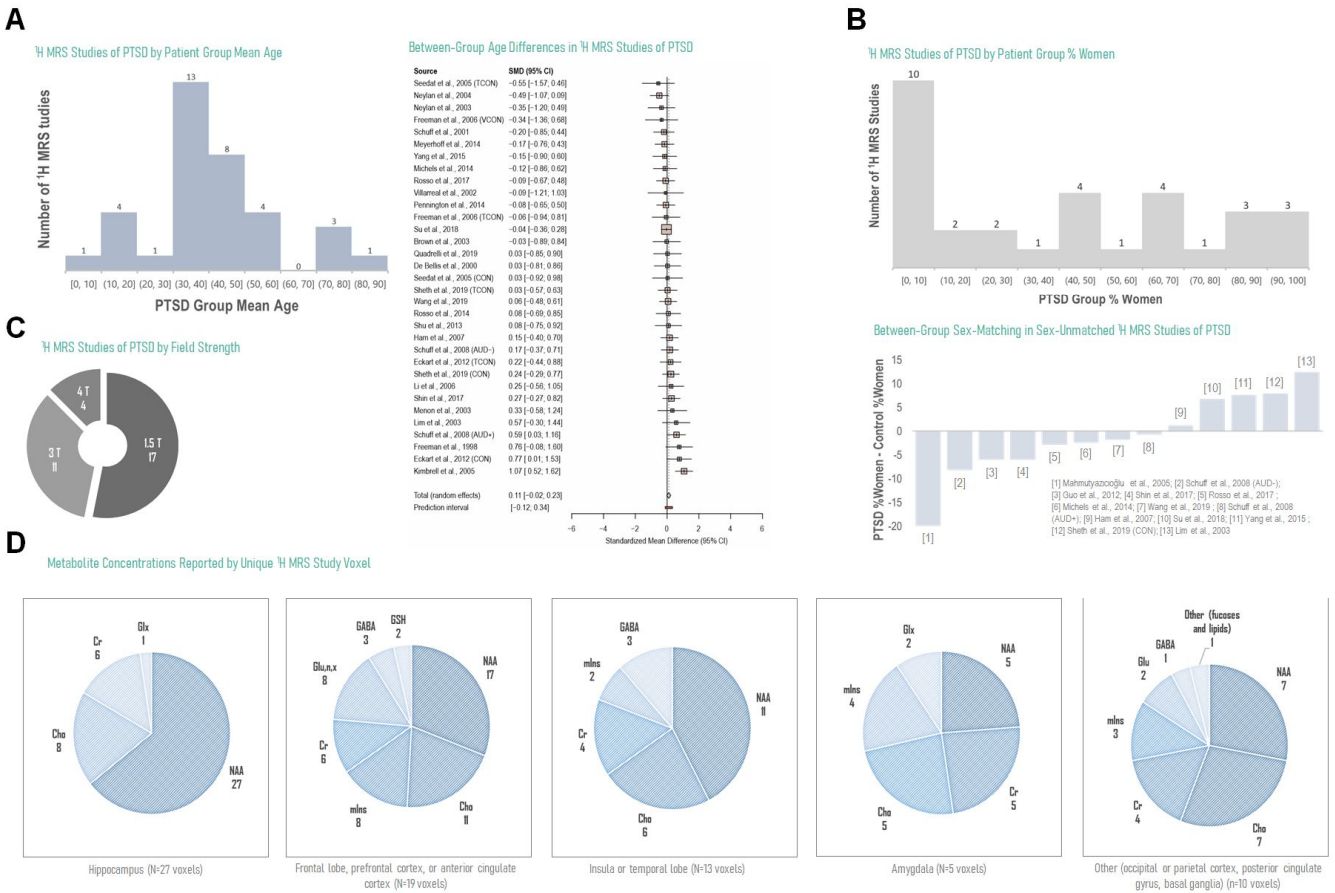

Figure 5.3. Overview of current literature on ¹H MRS in post-traumatic stress disorder (PTSD) by study design, hardware, and reported significant or null findings by metabolite and brain region. Currently published reports on ¹H MRS in PTSD cover a broad range of patient ages, with a smaller relative number of investigations into pediatric or geriatric participants, and generally demonstrate small disparities in age between groups under study for analyses reporting experimental group ages (random-effects standardized mean difference SMD 0.11, range -0.02-0.23; N = 33 comparisons from 27 studies) (A). The number of ¹H MRS analyses examining male-only participants is higher than the reverse, with a slight skew toward more male control groups in the few studies that demonstrated uneven between-group sex-matching (B). The great majority of existing ¹H-MRS investigations of PTSD have been conducted at 1.5 and 3 T, field strengths that do not typically enable the straightforward separation of signals from neurotransmitter glutamate from those of its metabolic byproduct glutamine (C). Especially in hippocampus, for which voxel placement and size may contribute to challenging spectral quantification of lower-signal metabolites, the ¹H-MRS literature on PTSD is currently dominated by N-acetyl aspartate (NAA), free cholines (Cho), creatine (Cr), and myoinositol (mIns), with only a few investigations on neurotransmitters glutamate (Glu) and GABA or endogenous antioxidant glutathione (GSH) despite putative roles in excitatory/inhibitory imbalance and neurodegeneration potentially important to regional anatomical and functional alterations previously observed in PTSD (D). Gln: glutamine; Glx: glutamate + glutamine.

glutamate correlated positively with anterior cingulate creatine and NAA in PTSD [611]. By contrast, anterior cingulate cortex glutamine has exhibited decreases [602] (HC) or null results [602] (TEC). Glu/Gln has exhibited no abnormality [600] (TEC).

GABA/Cr has exhibited increases [600] (TEC) or no abnormality [606] (HC). GABA has exhibited decreases [602] (HC) or no abnormality [602, 611, 613] (TEC). Individuals with both PTSD and AUD demonstrated GABA increases in anterior cingulate cortex relative to PTSD control [613]. Anterior cingulate cortex GABA exhibited a tendency to negative correlation with Insomnia Severity Index (ISI) in PTSD [611] as well as negative correlations with composite CAPS sleep symptom scores in PTSD [602]. GSH/Cr has exhibited increases [600] (TEC).

Basal Ganglia. The basal ganglia are a cluster of subcortical grey-matter nuclei comprising the striatum (caudate and putamen, with overlapping nucleus accumbens) and the globus pallidus. One previous study has targeted this region due to its proximity to the temporal lobes, also associated with a number of PTSD-associated metabolic abnormalities (below) while maintaining greater separation from the hippocampus enabling larger voxel size without partial-volume contamination from this other grey-matter region, as well as for its putative vulnerability to hypoxic damage and exposure to toxic metals [601].

In left basal ganglia of individuals with PTSD relative to control, NAA/Cr has exhibited decreases [601] (HC). Cho/Cr has exhibited no abnormality [601] (HC).

Occipital Cortex. The occipital cortex is a large posterior cortical region thought to predominantly comprise circuitry responsible for visual processing. While PTSD-specific hypotheses regarding this brain area are sparse and it has therefore served as a control region for hypothesis-driven

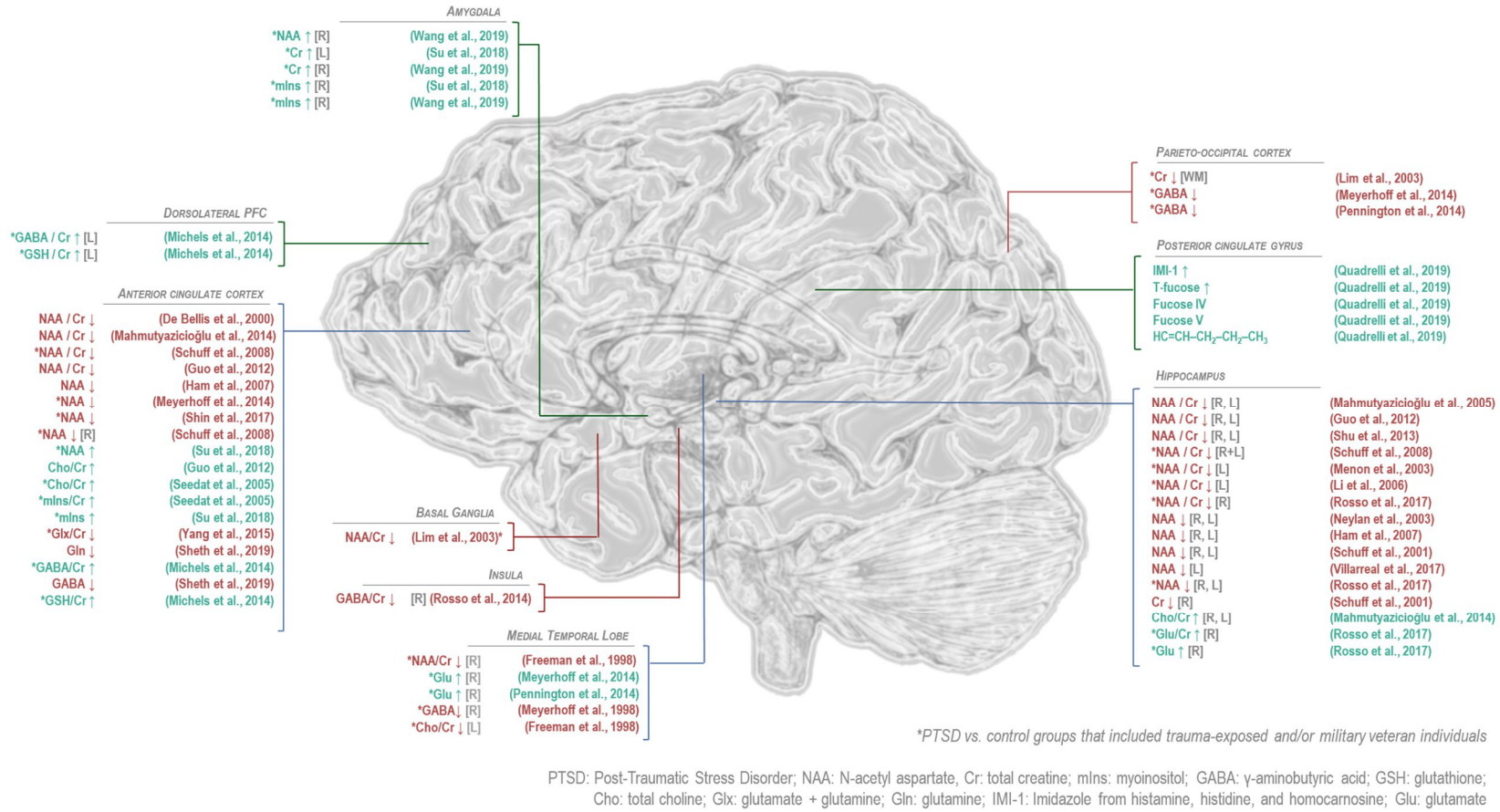

Figure 5.4. Findings of significant difference from control in ^{1}H-MRS-visible brain metabolites for patients with post-traumatic stress disorder (PTSD). General decreases in N-acetyl aspartate (NAA) in PTSD relative to trauma-exposed or -unmatched control groups have been observed predominantly in anterior cingulate cortex and hippocampus, while NAA increases in the amygdala have also been reported by one study. Differences from control in choline (Cho), when observed, have tended to be positive, also in anterior cingulate cortex and hippocampus, while decreases in choline have been observed in the medial temporal lobe. Regional effects of PTSD on common quantification reference metabolite creatine (Cr) have varied by region, with decreases reported in hippocampus and parieto-occipital cortex and increases in amygdala. Myoinositol (mIns) has been reported to increase in both anterior cingulate cortex and amygdala. Only a few studies have examined excitatory neurotransmitter glutamate to show increases in medial temporal lobe and hippocampus but decreases in both glutamate + glutamine (Glx) and glutamine (Gln) in anterior cingulate cortex. Reported alterations in GABA have similarly varied by region, with decreases reported in insula, medial temporal lobe, and parieto-occipital cortex; increases in dorsolateral prefrontal cortex; and mixed findings in anterior cingulate cortex. Only two published findings have been reported for GSH, both increases, in dorsolateral prefrontal and anterior cingulate cortices. Studies of additional metabolites, such as sugars and lipids measurable by 2D *J*-resolved proton spectroscopy reported in [614], have been limited.

research [607, 615], metabolite concentration abnormalities in parieto-occipital regions have been reportedly observed in anxiety and mood disorders, also impelling their targeted exploration in PTSD [611, 613]. In addition, the occipital cortex tends to lie close to radiofrequency receive coils and does not exhibit the steep transitions in magnetic susceptibility between tissue and air cavities that can influence data acquired from temporal and especially frontal regions, justifying the examination of this region for methodological convenience.

In the occipital cortex of individuals with PTSD relative to control, NAA/Cr has exhibited no abnormality [607] (HC) [607] (TEC). In the occipital or parieto-occipital cortex maximizing either grey or white matter, NAA referenced otherwise has exhibited no abnormality [615] (HC) [611, 613] (TEC). Individuals with both PTSD and AUD demonstrated no NAA changes in parieto-occipital grey matter relative to PTSD control [613].

In parieto-occipital grey matter creatine has exhibited no abnormality [611, 613] (TEC), while in bilateral white matter it has exhibited decreases [615] (HC). Individuals with PTSD and AUD demonstrated no creatine changes in parieto-occipital cortex relative to PTSD control [613]. Parieto-occipital creatine has correlated negatively with CAPS intrusion scores in PTSD [613].

Cho/Cr in left occipital grey matter demonstrated no abnormality [607] (HC) [607] (TEC). Parieto-occipital grey or occipital white matter choline has similarly demonstrated no abnormality [615] (HC) [611, 613] (TEC). Individuals with both PTSD and AUD demonstrated no choline changes in parieto-occipital cortex relative to PTSD control [613]. Parieto-occipital choline correlated positively with Insomnia Severity Index in PTSD [613].

mIns/Cr in left occipital grey matter has demonstrated no abnormality [607] (HC) [607] (TEC). In parieto-occipital grey matter myoinositol otherwise referenced has demonstrated no abnormality [611, 613] (TEC). Individuals with both PTSD and AUD demonstrated no

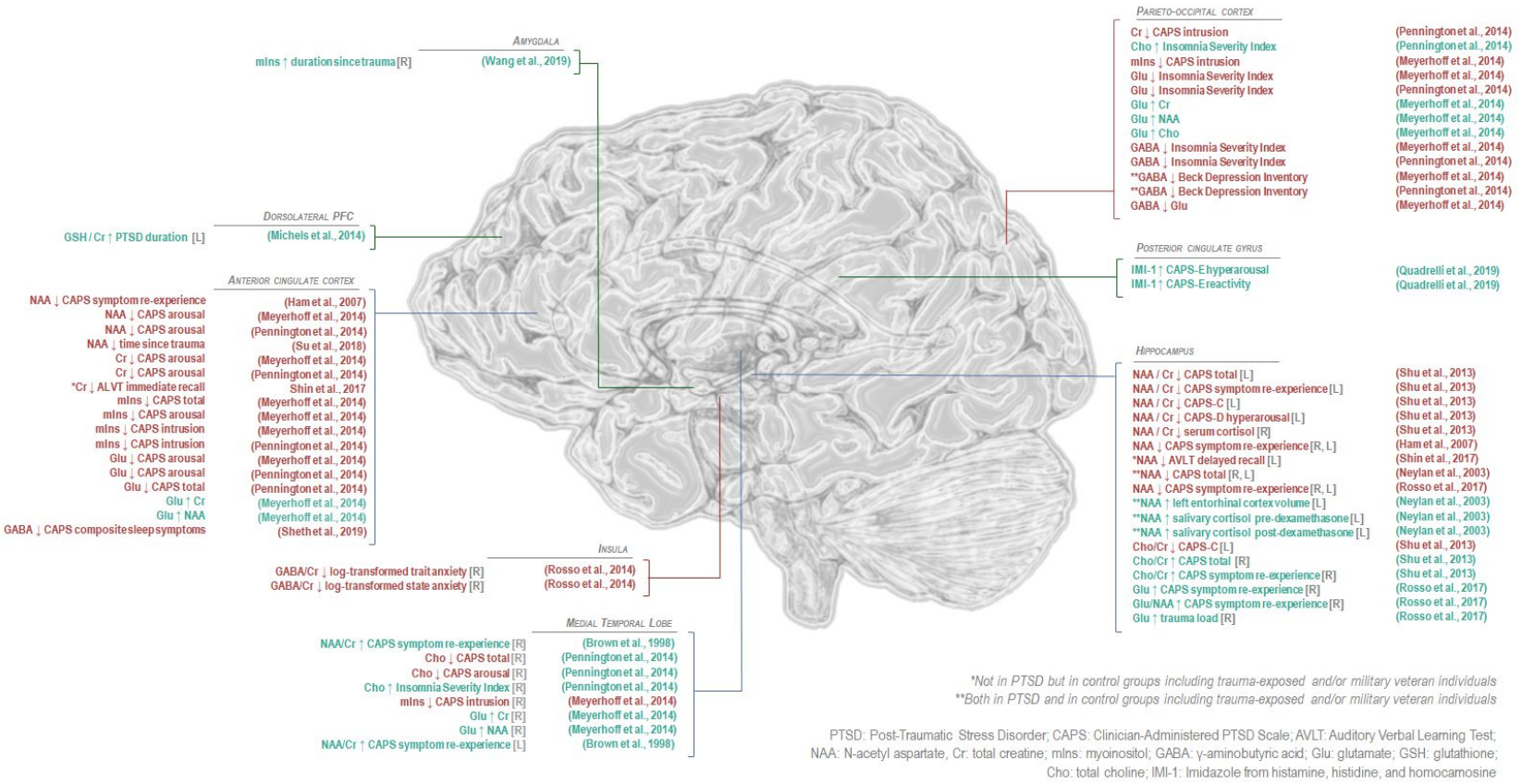

Figure 5.5. Findings of significant correlation, regression coefficient, or bivariate association between ^{1}H-MRS-measured brain metabolites with each other or other measures in post-traumatic stress disorder (PTSD) and/or control groups. Because proton magnetic resonance spectroscopy (^{1}H MRS) experiments measure multi-functional small molecules in large (>1 cm^{3}) heterogeneous voxels containing many different types of tissue, cell, and associated functional circuitry, correlations between measured metabolite concentrations and anatomical or cognitive measures or clinically relevant variables like symptom reports are useful for interpreting putative metabolite findings in ^{1}H-MRS studies of disease. The majority of such reported correlations have pertained to clinician-administered PTSD scale (CAPS) indices like arousal, intrusion, symptom re-experience, or total score. Other correlates have included self-reported insomnia indices, magnetic resonance imaging (MRI)-measured brain region volumes, memory performance, and other metabolites, though the latter may also sometimes indicate relationships introduced by quantification method rather than findings of biological significance. AVLT: Auditory Verbal Learning Test; NAA: N-acetyl aspartate, Cr: total creatine; mIns: myoinositol; GABA: γ-aminobutyric acid; Glu: glutamate; GSH: glutathione; Cho: total choline; IMI-1: Imidazole from histamine, histidine, and homocarnosine.

myoinositol alterations in parieto-occipital cortex relative to PTSD control [613]. Parieto-occipital grey-matter myoinositol correlated negatively with CAPS intrusion scores in PTSD [611].

Parieto-occipital grey-matter glutamate has demonstrated no abnormality [611, 613] (TEC). Individuals with both PTSD and AUD demonstrated no glutamate changes in parieto-occipital cortex relative to PTSD control [613]. Parieto-occipital grey-matter glutamate correlated negatively with Insomnia Severity Index in PTSD [611, 613]. It also correlated positively with corresponding creatine and NAA in PTSD and with choline in PTSD and combined PTSD + trauma-exposed control groups [611].

Parieto-occipital GABA has demonstrated decreases [611, 613] (TEC). Individuals with both PTSD and AUD demonstrated no GABA changes in parieto-occipital cortex relative to PTSD control [613]. Parieto-occipital GABA correlated negatively with Insomnia Severity Index in PTSD and with Beck Depression Inventory score in both PTSD and trauma-exposed control groups [611, 613]. GABA was also negatively correlated with parieto-occipital glutamate in PTSD [611].

Parietal Cortex. While, like the occipital cortex, the parietal cortex has been implicated in a minimum of hypothesis-driven ^{1}H-MRS research into PTSD, it has been involved in one study of periventricular white matter [601]. It also houses the posterior cingulate gyrus, the preferred first target of 2D COrrelated SpectroscopY (COSY) for its proximity to the radiofrequency receive hardware employed [614].

In right parietal periventricular white matter of individuals with PTSD relative to control, NAA/Cr has exhibited no abnormality [601] (HC).

Parietal Cho/Cr has also exhibited no abnormality [601] (HC).

In posterior cingulate gyrus PTSD patients have demonstrated increases in the imidazole moiety visible on histamine, histidine, and homocarnosine (IMI-1); fucosylated glycans including t-fucose, fucose IV, and fucose VI; and lipid HC=CH–CH_2–CH_2–CH_3 [614] (HC). Posterior cingulate gyrus IMI-1 positively correlated with CAPS-E hyperarousal and reactivity scores [614].

Insula (right). The insula correspond to Brodmann Areas 13 through 16, each located deep in the bilateral Sylvian fissures beneath the corresponding opercula, and are reportedly connected with several brain regions demonstrating associations with PTSD, including the prefrontal cortex, anterior cingulate gyrus, hippocampus, and amygdala [616]. They are also thought to be involved in emotional recall and have, among other regions, demonstrated regional cerebral blood flow signals correlating positively with severity of PTSD-associated flashbacks [617], justifying their exploration by ^{1}H MRS [589].

In the right insula of individuals with PTSD relative to control, NAA/Cr has exhibited no abnormality [589] (HC) [589, 606] (TEC). NAA has also exhibited no abnormality [589] (HC) [589] (TEC).

Creatine has exhibited no abnormality [589] (HC) [589] (TEC).

GABA/Cr has exhibited decreases [606] (HC). GABA/Cr correlated negatively with both log-transformed trait anxiety and state anxiety [606].

In the left insula, NAA/Cr has exhibited no abnormality [589] (HC) [589] (TEC). NAA has also exhibited no abnormality [589] (HC) [589] (TEC).

Similarly to reports on the right insula, left insula creatine has exhibited no abnormality [589] (HC) [589] (TEC).

Temporal lobe (right). The temporal lobe is the seat of both the hippocampus and the amygdala, subcortical structures that have both demonstrated a number of structural and functional abnormalities in PTSD. The subcortical hippocampus within the medial temporal lobe has generally been the target of proton spectroscopy voxels located in the temporal lobe, including within one group choosing the nomenclature "temporal cortex" instead [611, 613].

In the right medial temporal lobe of individuals with PTSD relative to control, NAA/Cr has exhibited decreases [618] (versus veteran control, VC) or no abnormality [619] (VC) [620] (TEC). In the right temporal cortex, NAA has exhibited no abnormality [611, 613] (TEC). Individuals with PTSD and AUD demonstrated NAA reductions in this region relative to PTSD control [613]. Right medial temporal lobe NAA/Cr correlated positively with CAPS symptom re-experience scores in PTSD but not control subjects [620].

In right temporal cortex creatine has exhibited no abnormality [611, 613] (TEC). Individuals with PTSD and AUD demonstrated no creatine changes in right temporal cortex relative to PTSD control [613].

Cho/Cr has demonstrated no abnormality [618] (VC) [620] (TEC). Choline has demonstrated no abnormality [611, 613] (TEC). Individuals with PTSD and AUD demonstrated choline decreases in right temporal cortex relative to PTSD control [613]. Right temporal cortex choline correlated negatively with CAPS total score and CAPS arousal score as well as positively with Insomnia Severity Index in PTSD [613].

mIns/Cr has demonstrated no abnormality [620] (TEC). Myoinositol has demonstrated no abnormality [611, 613] (TEC). Individuals with both PTSD and AUD demonstrated a trend to myoinositol reductions in right temporal cortex relative to PTSD control [613]. Right lateral temporal cortex grey-matter myoinositol correlated negatively with CAPS intrusion scores in

PTSD [611].

Right temporal cortex glutamate has demonstrated increases [611, 613] (TEC). Individuals with both PTSD and AUD demonstrated glutamate reductions in right temporal cortex relative to PTSD control [613]. Right temporal grey-matter glutamate also correlated positively with corresponding creatine and NAA in PTSD [611].

Right temporal cortex GABA has demonstrated decreases [611] (TEC) or null results [613] (TEC). Individuals with both PTSD and AUD demonstrated no GABA changes in right temporal cortex relative to PTSD control [613].

Temporal lobe (left). In left medial temporal lobe, NAA/Cr has exhibited a trend to decrease [620] (TEC) or no abnormality [618, 619] (VC). Left medial temporal lobe NAA/Cr correlated positively with CAPS symptom re-experience scores in PTSD but not control subjects [620].

Cho/Cr has demonstrated decreases [618] (VC) or no abnormality [620] (TEC).

mIns/Cr has demonstrated no abnormality [620] (TEC).

Hippocampus (right). The hippocampus is a subcortical structure implicated in the encoding of spatial information as well as long-term episodic memories [621]. In PTSD patients it has demonstrated altered white-matter integrity [563] and volumetric decreases [556], the latter across both non-dissociative and dissociative symptomatic presentations of disease [533] and possibly associated with either PTSD predisposition [527, 557] and/or development [558]. PTSD has also been linked with reduced bilateral hippocampal $GABA_A$ benzodiazepine receptor binding [567] but fMRI- or PET-visible functional abnormalities of inconsistent polarity [525] depending on task and statistical details [585]. Abnormalities in hippocampal function, with those also seen in the

medial prefrontal cortex, are thought to underlie degradations of fear extinction in PTSD symptomology [603].

In the right hippocampus of individuals with PTSD relative to control, NAA/Cr has exhibited decreases [597, 599, 622] (HC) [623] (TEC) or no abnormality [589] (HC) [624, 625] (VC) [589, 624, 626] (TEC). NAA has exhibited decreases [610, 627, 628] (HC) [623] (TEC) or no abnormality [589, 615] (HC) [589] (TEC). Right hippocampal NAA/Cr correlated negatively with serum cortisol in PTSD [622]. Similarly, right hippocampus NAA correlated negatively with CAPS symptom re-experience scores in PTSD [610, 623]. It also exhibited a bivariate association negative with CAPS total score and a trend to positive association with left entorhinal cortex volume in combined PTSD + control cohorts [628].

Creatine has exhibited decreases [627] (HC) or no abnormality [589, 610] [615] (HC) [589] (TEC).

Cho/Cr has demonstrated increases [599] (HC) or no abnormality [597, 622] (HC) [624] (VC) [624] (TEC). Choline has demonstrated no abnormality [610, 627] [615] (HC). Right hippocampal Cho/Cr has correlated positively with CAPS total score and with CAPS-B symptom re-experience scores in PTSD [622].

Myoinositol has demonstrated no abnormality [610] (HC).

Glu/Cr has demonstrated increases [623] (TEC). Glutamate has also demonstrated increases [623] (TEC). Right hippocampal glutamate and Glu/NAA but not Glu/Cr correlated positively with CAPS symptom re-experiencing score in PTSD [623]. Right hippocampal Glu/NAA also correlated positively with trauma load in PTSD but not trauma-exposed controls [623].

Hippocampus (left). In the left hippocampus of individuals with PTSD relative to control, NAA/Cr has exhibited decreases [597, 599, 622] (HC) [625] (VC) [626] (TEC) or no abnormality [589] (HC) [624] (VC) [589, 623, 624, 627] (TEC). NAA has exhibited decreases [610, 615, 628] (HC) [623] (TEC) or no abnormality [589] (HC) [589, 612] (TEC). It has also correlated negatively with CAPS total score, with CAPS-b symptom re-experiencing score, CAPS-C score, and CAPS-D hyperarousal score in PTSD [622]. Similarly, left hippocampus NAA associated negatively with CAPS symptom re-experience scores in PTSD [610, 623]. It has also exhibited a significant negative regression coefficient with auditory verbal learning test-delayed recall scores in trauma-exposed controls but not PTSD patients [612]. Additionally, NAA exhibited a bivariate association negative with CAPS total score, positive with left entorhinal cortex volume, and positive with salivary levels pre- and post- dexamethasone administration in combined PTSD + control cohorts [628].

Left hippocampal creatine has exhibited a trend to decrease [615] (HC) or no abnormality [589, 610, 627] (HC) [589] (TEC).

Left hippocampal Cho/Cr has demonstrated increases [599] (HC) or no abnormality [597, 622] (HC) [624] (VC) [624] (TEC). Choline has demonstrated no abnormality [610, 627] [615] (HC). Left hippocampal Cho/Cr has been showed separately to negatively correlate with CAPS-C score [622].

Left hippocampal myoinositol has demonstrated no abnormality [610] (HC).

Left hippocampal Glx has demonstrated no abnormality [612] (TEC). Glu/Cr has demonstrated no abnormality [623] (TEC). Glutamate has also demonstrated no abnormality [612, 623] (TEC).

Hippocampus (bilateral). In hippocampus taken bilaterally NAA/Cr has exhibited either decreases [605] (TEC+HC) or no abnormality [629] (VC). NAA has exhibited no abnormality [605] (TEC+HC) [629] (VC).

Amygdala. The amygdala comprises two almond-shaped subcortical structures located in the bilateral medial temporal lobes and is implicated in the integration of sensory information, predicted threats, and ensuing emotional and behavioral responses. As such, the amygdalae exhibit connections with the hippocampus and multiple regions in the prefrontal cortex, with which they are thought to regulate the learning and memory of fear [533]. PTSD has been associated with both volumetric increases [561] and decreases [560] in the amygdala or its various nuclei [562]. Reductions in amygdalar grey-matter volume have also been observed in PTSD precipitated by either single or prolonged trauma [556]. Reduced binding of both 5HT transporter [565] as well as $5HT_{1B}R$ [566] has also been observed in PTSD, as has differential response from control to injection of hydrocortisone in both the laterality of dorsal amygdala glucose consumption and subsequent working memory performance [574]. Functional studies tend to demonstrate amygdalar hyperactivity [525, 583] in concert with ventromedial prefrontal cortex hypoactivity [533] during fear acquisition or presentation of both trauma-related and unrelated stimuli in PTSD, with the polarity of alterations possibly flipped in patients demonstrating a dissociative subtype of disease [533, 584] as well as possibly different activation during fear conditioning in ventral anterior amygdala (hyperactivity) versus dorsal posterior amygdala (hypoactivity) in PTSD compared to other anxiety disorders [575].

In the amygdala of individuals with PTSD relative to control, NAA has exhibited increases on the right side only [630] (TEC) or no abnormality [609] (TEC) [598] (controls with borderline

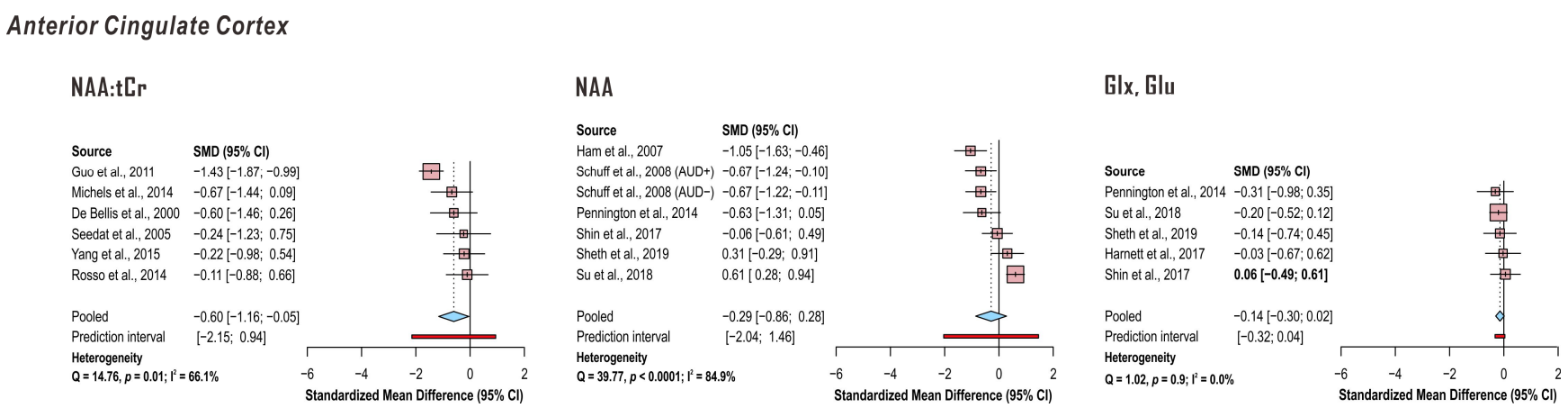

Figure 5.6. Random-effects model of group differences between post-traumatic stress disorder (PTSD) and control in ^{1}H-MRS-measured anterior cingulate cortex metabolite concentrations examined by five or more independent published investigations. Random-effects models across the listed studies demonstrated significantly lower anterior cingulate cortex N-acetyl aspartate (NAA) in PTSD when referenced to total creatine (tCr) (pooled standardized mean difference -0.60, 95% CI -1.16 to -0.05, p=0.04) but not otherwise. No significant effect of PTSD was discerned for anterior cingulate cortex glutamate (Glu) or glutamate + glutamine (Glx). Between-study heterogeneities were higher for NAA reports than those for Glx or Glu findings regardless of quantification reference. Because study pools from [611] and [613] exhibited overlap, only values from [613] were reported here. When PTSD groups were compared with both trauma-unmatched and trauma-exposed or veteran controls in the same study, only comparisons with trauma-exposed or veteran controls were included in this analysis.

personality disorder BPD). A trend to positive correlation between left amygdalar NAA and age was found in pediatric PTSD patients [630].

Amygdalar creatine has exhibited increases on left side only [609] (TEC), increases on right side only [630] (TEC), or no abnormality (left side) [598] (controls with BPD).

Amygdalar choline has demonstrated increases on right side only [630] (TEC) or no abnormality bilaterally [609] (HC) or on the left side [598] (controls with BPD).

Amygdalar myoinositol has demonstrated increases on right side only [609, 630] (TEC). Right amygdalar myoinositol correlated positively with duration since trauma in pediatric PTSD patients [630].

Bilateral amygdalar Glx has demonstrated no abnormality [609] (TEC).

Meta-analysis of anterior cingulate cortex and bilateral hippocampus metabolite findings. We conducted meta-analyses for all regions and metabolites for which at least five previously published cross-sectional comparisons were present, which included NAA (seven), NAA/Cr (six), and Glx (five) in the anterior cingulate cortex as well as NAA (seven, six) or NAA/Cr (seven, six) in the left and right hippocampus, respectively.

Random-effects models demonstrated significantly lower anterior cingulate cortex NAA in PTSD when referenced to creatine (k=6 studies; pooled standardized mean difference -0.60, 95% CI -1.16 to -0.05, p=0.04) but not otherwise (k=7 studies). No significant effect of PTSD was discerned for anterior cingulate cortex glutamate (k=5 studies). Between-study heterogeneities appeared to be higher for NAA (NAA Q=14.76, p=0.01, I^2=66.1%; NAA/Cr Q=39.77, p<0.0001, I^2=84.96%) reports than those for Glx or Glu findings (Q=1.02, p=0.9, I^2<0.01%) regardless of quantification reference. Because study pools from [611] and [613] exhibited overlap, only values

Left Hippocampus

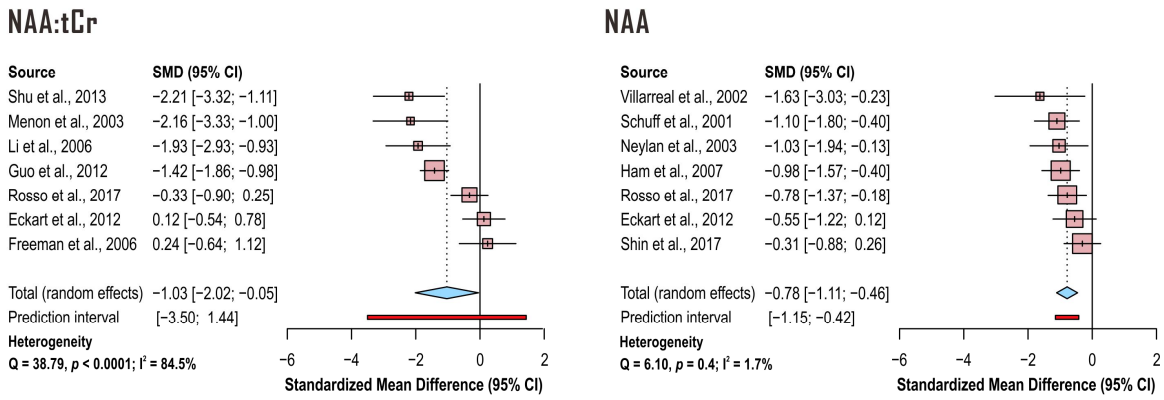

Right Hippocampus

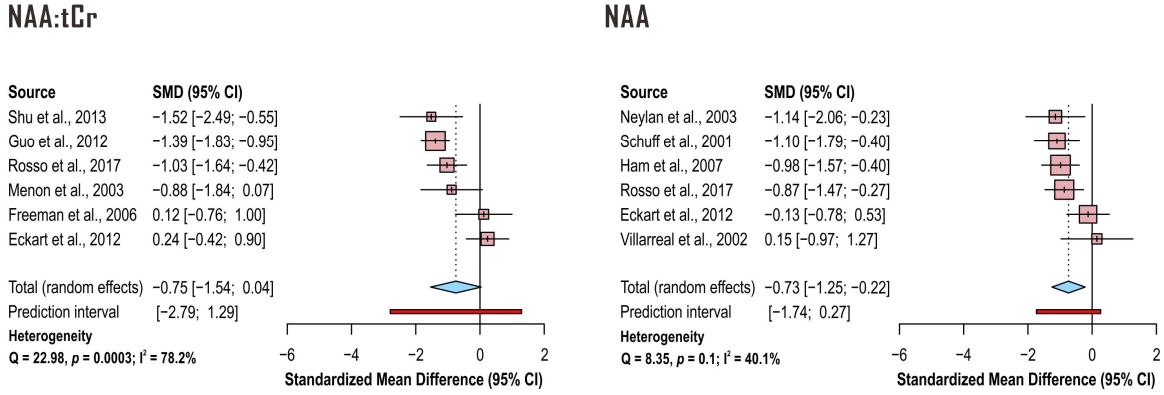

Figure 5.7. Random-effects model of group differences between post-traumatic stress disorder (PTSD) and control in ^{1}H-MRS-measured hippocampal metabolite concentrations examined by five or more independent published investigations. Random-effects models across the listed studies demonstrated significantly lower left but not right hippocampus N-acetyl aspartate (NAA) in PTSD when referenced to total creatine (tCr) (pooled standardized mean difference -1.03, 95% CI -2.02 to -0.05, p=0.04), while NAA referenced otherwise demonstrates significant effect for both left (pooled standardized mean difference -0.78, 95% CI -1.11 to -0.46, p=0.001) and right (pooled standardized mean difference -0.73, 95% CI -1.25 to -0.22, p=0.01) hippocampus. Between-study heterogeneities were higher for studies of hippocampal NAA when creatine was used as a reference than when it was not. When PTSD groups were compared with both trauma-unmatched and trauma-exposed or veteran controls in the same study, only comparisons with trauma-exposed or veteran controls were included in this analysis.

from [613] were reported here (Figure 5.6).

In addition, random-effects models demonstrated significantly lower left but not right hippocampus N-acetyl aspartate (NAA) in PTSD when referenced to creatine (left k=7 studies; pooled standardized mean difference -1.03, 95% CI -2.02 to -0.05, p=0.04; right k=6 studies), while NAA referenced otherwise demonstrated significant effect for both left (k=7 studies; pooled standardized mean difference -0.78, 95% CI -1.11 to -0.46, p=0.001) and right (k=6 studies; pooled standardized mean difference -0.73, 95% CI -1.25 to -0.22, p=0.01) hippocampus. Between-study heterogeneities appeared to be higher for studies of hippocampal NAA when creatine was used as a reference (left hippocampus NAA/Cr Q=38.79, p<0.00011, I^2=84.5%; right hippocampus NAA/Cr Q=22.98, p=0.0003, I^2=78.2%) than when it was not (left hippocampus NAA Q=6.10, p=0.4, I^2=1.7%; right hippocampus NAA Q=8.35, p=0.1, I^2=40.1%) (Figure 5.7).

5.1.4. Discussion

Here we have reviewed the proton magnetic resonance spectroscopy literature targeted to comparisons of individuals with PTSD and either trauma-exposed or trauma-unmatched controls to find N=32 publications, including 31 cross-sectional studies and one case report included for methodological considerations, fitting our inclusion criteria.

While the current PTSD ^{1}H MRS literature exhibits age- and sex-matching between experimental and control groups increased relative to the currently available ^{1}H MRS literature of at least one other disease [24], the distribution of ages previously studied is not uniform (Figure 5.3A), and the distribution of sex previously studied is heavily skewed toward male participants (Figure 5.3B) despite a lifetime prevalence in women potentially double that of men as previously reported [518, 519]. In addition, hardware fields employed by reviewed ^{1}H MRS analyses of PTSD

do not exceed 4 Tesla (Figure 5.3C), which may contribute to the relative skew of reported metabolite comparisons toward traditionally high-SNR singlets like NAA, creatine, and choline as detailed below.

Meta-analyses for all regions and metabolites for which at least five previously published cross-sectional comparisons were present included NAA and NAA/Cr in the anterior cingulate cortex and bilateral hippocampus as well as Glx in the anterior cingulate cortex; no other metabolites in any other region passed this k=5 threshold of published studies.

As concluded for a recent similar review of the literature on multiple sclerosis [24], regional decreases in N-acetyl aspartate are potentially too nonspecific and insensitive to serve as a biomarker for PTSD vulnerability, development, or treatment response. Abnormal decreases in anterior cingulate NAA or NAA/Cr have also been reported by meta-analysis of studies on first-episode psychosis [631] and autism spectrum disorders [632]; reductions in hippocampal NAA or NAA/Cr have additionally been observed in meta-analyses on schizophrenia [631], fibromyalgia [633], obstructive sleep apnea [634], mild cognitive impairment [635], and Alzheimer's disease [636]. The heavy focus of currently published ^{1}H MRS literature in PTSD on N-acetyl aspartate therefore in principle limits the application of its findings to the development of ^{1}H-MRS-based regional single-molecule biomarkers for the disease, calling for further targeted research into a more diverse range of metabolites measurable by the method, especially at higher field strengths and using acquisition, processing, and analysis pipelines that minimize both imprecision and inaccuracy in metabolite concentration estimates.

Meta-analysis of available studies demonstrated decreased anterior cingulate cortex NAA in PTSD only when creatine was used as a reference, decreased left hippocampus NAA regardless of whether creatine was used as a reference, and decreased right hippocampus NAA only when

creatine was not used as a reference. These findings further support the conclusions of a previous systematic review observing that decreases in hippocampal and anterior cingulate cortex NAA stood among the most consistent findings across the ^{1}H MRS literature on PTSD [105]. In particular, our findings in anterior cingulate cortex also extend previously published meta-analytic findings of decreased anterior cingulate NAA/Cr in PTSD relative to healthy controls and update three previously reviewed comparisons [605, 610] underlying a significant effect of NAA in anterior cingulate cortex [104] with four more [602, 609, 612, 613] that bring this metabolite result to non-significance. Similarly, findings in left hippocampal decreases of both NAA/Cr and NAA extend previously significant meta-analytic findings in both indices [104]. Our finding of significant right hippocampal NAA decreases in PTSD extends to a mixed-control cohort a previous meta-analytic result that was significant relative to trauma-unmatched controls only [104], while our own meta-analysis of right hippocampal NAA/Cr did not replicate a previous significant result, potentially because of our choice to exclude three previously incorporated studies that either did not report at least one group standard deviation or reported a voxel in the medial temporal lobe but not specifically the hippocampus [599, 605, 620].

Conflicting meta-analytic results between NAA and NAA/Cr in anterior cingulate cortex and right hippocampus may be suggestive of systematic heterogeneities between studies choosing to employ either referencing technique, i.e., groups choosing either creatine or non-creatine references may differ in other methodological details that themselves influence reported metabolite effect size. Indeed, very few groups included in our meta-analyses reported both values, making this a feasible explanation for the differences observed here. NAA results that differ by concentration reference may also suggest the differential influence of the reference itself either as an unwanted source of error or, on the other hand, as more sensitive to actual biological differences

among the participants of each study. For example, referencing to water may increase the probability of Type II error by exacerbating inter-subject variability attributable to uncertainties surrounding segmentation and relaxivity measures often employed to inform concentration estimates for water but not creatine. At the same time, referencing to water may also increase the probability of Type I error as water-referenced metabolite concentrations are in principle more sensitive to influence by biological phenomena like edema that may comprise a systematic aspect of some disease conditions under study as separate from zero-centered uncertainties equally influencing all study participants, even if their influence on resultant metabolite concentrations may be spurious. It is important to note that these two directions of influence are not necessarily mutually exclusive and may lead to different outcomes in different brain regions, as we observed here for PTSD-associated reductions in anterior cingulate NAA that were significant only when referenced to total creatine but right hippocampus NAA significant only when not referenced to total creatine. It is of potential note that increased cross-study heterogeneity was observed among reports of left and right hippocampal NAA/Cr relative to NAA, which when combined with the lower number of included studies targeting right than left hippocampal NAA/Cr may have contributed to the lack of significance in the former statistic, especially considering the previously mentioned published significant meta-analytic finding in the same region [104].

Meta-analysis of anterior cingulate glutamate or Glx, not previously attempted by the above reference [104], demonstrated no significant effect of PTSD. So far only one significant effect of PTSD on anterior cingulate cortex Glu or Glx, referenced to total creatine, has been published [608], though significant negative correlations with CAPS arousal [611, 613] and total scores [613] have been previously observed. In one model of PTSD pathogenesis, regional glutamate excitotoxicity can result from increases in the ratio of extrasynaptic to synaptic

glutamate due to glutamate "spillover," a consequence of inadequate astrocytic clearance of extrasynaptic glutamate, and attendant stimulation of presynaptic mGluR-2/3 inhibiting the release of synaptic glutamate [592]. It is important to note that while ^{1}H MRS may provide clues regarding the biochemical composition over a whole voxel, e.g. the possible cross-voxel density of metabolically healthy neurons [610] or glial cells [609] as loosely inferred from N-acetyl aspartate and myoinositol or choline concentrations, respectively, or the presence of excitotoxicity thought to be mediated not only by glial dysfunction but also activated macrophages and microglia as similarly inferred from abnormal white-matter glutamate increases in a large-scale study of multiple sclerosis [237], the proposed mechanism of regional excitotoxic damage in PTSD does not necessitate cross-voxel changes in glutamate concentration large enough to be detected by ^{1}H MRS. It remains therefore important to note that the mechanistic reasons behind disease-related metabolic abnormalities visible to ^{1}H MRS are often themselves unknown, complicating the use of ^{1}H MRS for conclusive hypothesis testing regarding pathophysiological mechanisms at the cellular or molecular scales.

The small size of this literature also limits the significance of further meta-analysis evaluating the use of ^{1}H MRS as a source of biomarkers for PTSD risk, effect, or both via parsing effect sizes by control group type (trauma-exposed or trauma-unmatched), though such bifurcations have been previously reported [104]. Even the most well studied metabolite (NAA) in the most widely studied regions (anterior cingulate cortex and left hippocampus) represents a maximum of four published analyses of either trauma-exposed or trauma-unmatched controls, each with group sizes well under N=100.

Taken together, these findings suggest a small (N=32 studies) literature employing ^{1}H MRS in the analysis of PTSD that is skewed in terms of participant ages (with a trend to older

PTSD than control groups), sex (with more than three times as many all-male than all-female studies), employed hardware (largely lacking field strengths at 4 Tesla and above), regional targets (focused heavily on only a few brain areas including the anterior cingulate cortex and hippocampus) and metabolic targets (heavily centered on N-acetyl aspartate regardless of region and, in anterior cingulate cortex only, glutamate or Glx). Regardless, a number of notable findings have been reported, including in brain areas like dorsolateral prefrontal cortex, anterior cingulate cortex, amygdala, and hippocampus previously shown to exhibit abnormalities relative to either trauma-unmatched or exposed controls in anatomy, receptor densities, and/or function (Figure 5.4), as well as a number of significant correlations between metabolites in these regions with clinically relevant variables like CAPS scores or other measures of symptom experience (Figure 5.5). As such, the potential for ^{1}H MRS to forge new ground in the understanding of PTSD, as well as play a role in the development of biomarkers for risk, diagnosis, and/or treatment monitoring, is not only as-yet largely untried but has also yielded meaningfully interpretable information where it has been, therefore remaining a needed piece of the puzzle.

5.2 Single-variable analysis of prefrontal cortex metabolic abnormality in post-traumatic stress disorder and comorbid major depressive disorder

5.2.1. Motivation

As introduced in Section 1, post-traumatic stress disorder (PTSD) is an anxiety condition precipitated by a traumatic stressor and manifest by a range of debilitating emotional and cognitive dysfunctions for at least one month following trauma exposure including intrusive thoughts, altered cognition, mood, and arousal; and avoidance of trauma-related triggers [516]. With an estimated incidence of 1 in 12 within some communities [101], post-traumatic stress disorder has

been estimated to develop in 0.1-19% of individuals exposed to traumatic stress, with varying conditional risk depending on the stressor [523].

It has been hypothesized that PTSD symptoms are influenced by exaggerated response of auto-inhibitory glucocorticoid receptors in the hypothalamic pituitary adrenal (HPA) axis resulting in constitutively low systemic cortisol [525]. Against this endocrine environment a number of brain regions demonstrate anatomical and functional abnormalities in PTSD, among them circuitry across the ventromedial and dorsolateral prefrontal cortex, amygdala, and hippocampus that is implicated in fear conditioning [533]. It has been postulated that in this network glutamatergic neurotransmission is not properly modulated due in part to both HPA and possibly glial dysfunction, leading to increases in the ratio of extrasynaptic to intrasynaptic glutamate and resultant excitotoxic damage to neurons [592, 603] that contribute to observed losses of prefrontal grey matter volume [556] and white matter integrity [533, 563] as well as ultimately abnormal regional functional responses to various trauma-related or -unrelated stimuli as measured by fMRI or PET[516, 575].

Despite the ability of proton magnetic resonance spectroscopy (^{1}H-MRS) to measure local concentrations of glutamate and related metabolites like inhibitory neurotransmitter GABA and antioxidant glutathione (GSH) in living humans, ^{1}H-MRS investigations of PTSD in humans are sparse and, as already presented in detail in Section 1, do not appear to involve any conducted at 7-Tesla field strength for separation of the glutamate signal from its structurally similar metabolic precursor and byproduct glutamine, which is controversial at field strengths <4 Tesla [450].

Motivated by the above hypothesis of prefrontal glutamatergic dysfunction engendering regional excitotoxicity in PTSD as well as the current dearth of published 7 T ^{1}H-MRS investigations of PTSD, we examined at 7 Tesla prefrontal cortex metabolite concentrations

including glutamate, glutamine, and GABA in individuals with and without PTSD. Because major depressive disorder (MDD) is comorbid with PTSD in an estimated 50% of cases [586] and is itself associated with alterations in ^{1}H-MRS-visible prefrontal glutamate concentration [637, 638], we included in both our PTSD and control cohorts individuals with comorbid MDD to tease out the potential influence of this variable on our findings.

5.2.2. Methods

Participants. We examined N=11 individuals with PTSD ($PTSD_{MDD+}$ 1F/5M; mean 39 ± S.D. 8 y.o.; $PTSD_{MDD-}$ 2F/3M; 37±16 y.o.) and N=27 trauma-unmatched healthy controls (HC_{MDD+} 2F/7M; 35±15 y.o.; HC_{MDD-} 5F/13M; 34±8 y.o.) with and without MDD. Unlike in Chapter 4, not only spectral processing and analysis but also spectral acquisition were conducted in a masked fashion wherein group identification was known only to our clinical collaborators until the statistical analysis step. All participants provided written informed consent prior to scanning according to the Declaration of Helsinki, and experimentation was conducted in accordance with guidelines approved by the Yale School of Medicine Human Investigation Committee.

Experimental setup. Spectroscopy data were obtained according to a procedure similar to that outlined in Chapter 4, on a 7-Tesla head-only magnetic resonance system (Agilent, Santa Clara, CA, USA) at the Yale School of Medicine Magnetic Resonance Research Center (MRRC) using a previously described acquisition protocol [106] for improved spectral dispersion and detection sensitivity. *J*-difference editing (MEGA) of semi-LASER (echo time T_E 72 ms; repetition time T_R 3 s) sequences for acquisition of glutathione or GABA and low-echo-time macromolecule-suppressed STEAM (T_E 10 ms, mixing time T_M 50 ms, T_R 3 s) for acquisition of glutamate,

glutamine, total N-acetyl aspartate (N-acetyl aspartate and N-acetyl aspartylglutamate), total choline (choline, phosphocholine, and glycerophosphocholine), and myoinositol were employed in a single 8-cc (STEAM) or 27-cc (sLASER) cubic voxel at the longitudinal fissure of the medial prefrontal cortex (Figure 5.8).

Spectral acquisition. An eight-channel phased-array radiofrequency coil was used for spin handling and signal reception [425]. Voxel placement was guided by T_1-weighted imaging. B_1 phase shimming was achieved through in-house software (IMAGO). B_0 shimming was performed with customized software (B0DETOX) [426] and comprised zero- through third-order spherical harmonics shapes.

Glutathione (2.95-ppm cysteine $^{7'}CH_2$ resonance; editing on the 4.56-ppm cysteine ^{7}CH resonance) and GABA (3.01-ppm $^{4}CH_2$ resonance; editing on the 1.89-ppm $^{3}CH_2$ resonance) were measured with single-voxel *J*-difference editing based on a MEGA semi-localized by adiabatic selective refocusing (sLASER) [427] sequence as previously applied in vivo [19, 422]. Water suppression was achieved using the CHEmical Shift Selective (CHESS) technique [428], and inversion recovery was applied to the GABA sequence for additional macromolecule nullification as detailed in Chapter 4.

Glutamate and several other metabolites, including total creatine (creatine and phosphocreatine), total choline (choline, phosphocholine, and glycerophosphocholine), total N-acetyl aspartate (N-acetyl aspartate and N-acetyl aspartylglutamate), glutamine, and myoinositol were measured using short echo-time stimulated echo acquisition mode (STEAM) [430]. Water suppression was based on CHESS as in Chapter 4, and complementary outer-volume suppression

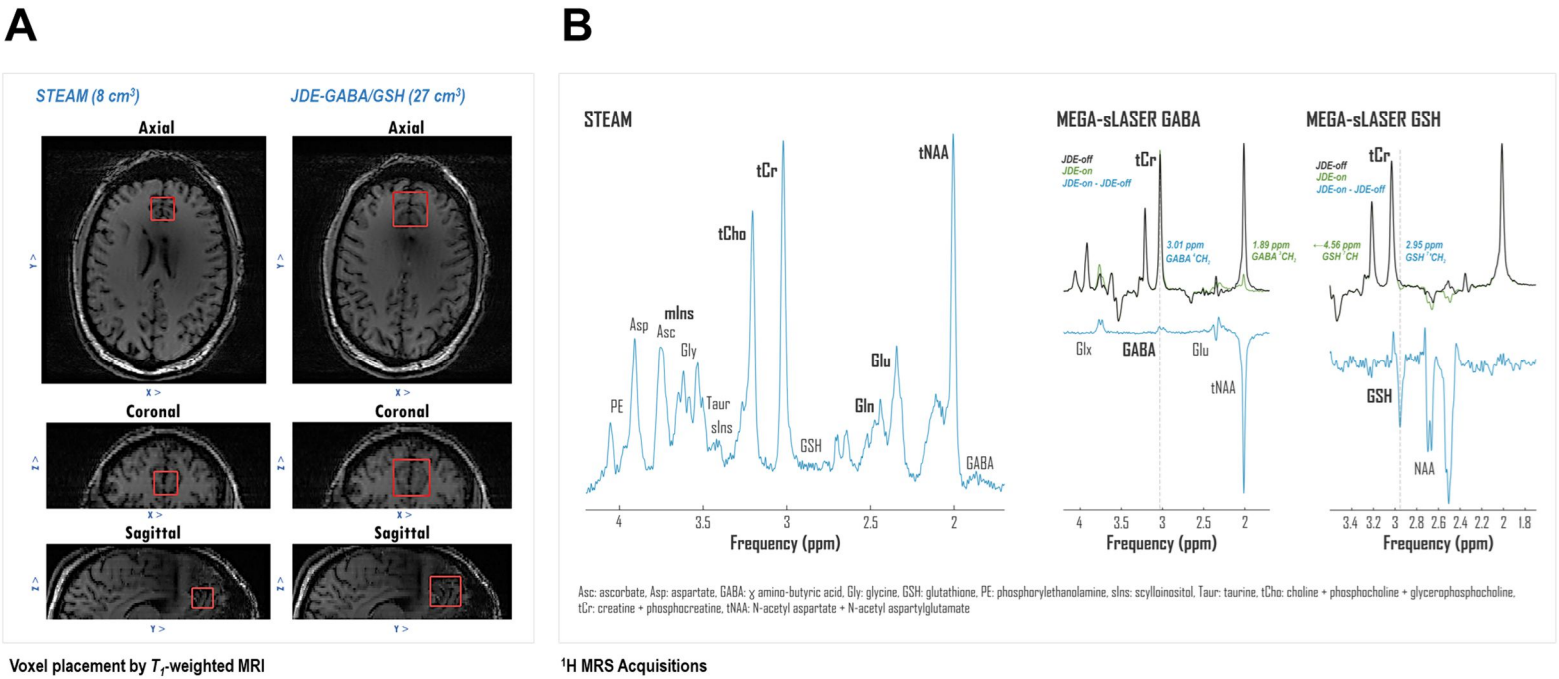

Figure 5.8. Medial prefrontal cortex (mPFC) metabolites were measured using ^{1}H MRS at 7 Tesla in individuals with (N=11) and without (N = 27) post-traumatic stress disorder (PTSD) and/or comorbid major depressive disorder (MDD). T_1-weighted imaging was employed to localize 8 cm^3 (STEAM) or 27 cm^3 (semi-LASER) cubic voxels in the medical prefrontal cortex (A) in a one-hour MR scan including STEAM (T_E 10 ms, T_M 50 ms, T_R 3000 ms, N_R 32 x 4-5) for detection of glutamate and semi-LASER (T_E 72 ms, T_R 3000 ms, N_R 60 x 2-6) with MEGA *J*-difference editing for either GABA or GSH. Depicted is the voxel placement for a 47-year-old male subject with neither PTSD nor MDD. ppm: parts per million.

was used to improve localization specificity [431]. STEAM acquisition was also preceded by an inversion-recovery preparation to minimize macromolecule signals (inversion time T_I 320 ms). Water-unsuppressed signals from each experiment were acquired for later use in eddy current correction.

Spectra were acquired as series of 4096 complex points in blocks of 32 traces (STEAM) or 64 traces (sLASER with JDE for GSH or GABA) each preceded by two dummy scans.

Spectral processing and quantification. Spectral processing was performed in INSPECTOR. Briefly, signals from individual receive channels were corrected for eddy currents using water-unsuppressed references [118], phase- and frequency-aligned, and averaged with weighting by receive channel sensitivities [119]. Summed metabolite spectra were zero-order phased but not truncated, zero-filled, or line-broadened before direct quantification or alignment between summed editing conditions for difference spectrum calculation, as applicable.

Spectral quantification was achieved by linear combination modeling with the same basis spectra density-matrix simulated in SpinWizard [117] as in Chapter 4. Basis sets included aspartate, choline, creatine, GABA, glycerophosphocholine, glutathione, glutamate, glutamine, glycine, myoinositol, N-acetyl aspartate, N-acetyl aspartylglutamate, phosphocholine, phosphocreatine, phosphorylethanolamine, scylloinositol, and taurine. GSH *J*-difference spectral basis sets included glutathione and N-acetyl aspartate, while GABA *J*-difference spectra employed GABA, N-acetyl aspartate, glutamate, and glutamine (Figure 5.9). Spectral quantification was performed in LCModel according to the processing parameters optimized and described in Chapter 4. Absolute quantification estimates of total N-acetyl aspartate (N-acetyl aspartate plus N-acetyl aspartylglutamate), total choline (choline, phosphocholine, and glycerophosphocholine),

Figure 5.9. Medial prefrontal cortex (mPFC) metabolite concentrations quantified via linear combination modeling were employed to assess the metabolic signatures of post-traumatic stress disorder (PTSD) with or without comorbid major depressive disorder (MDD). Linear combination modeling with a regularized cubic spline baseline was conducted in LCModel using density-matrix-simulated basis functions for the metabolites shown. Metabolite concentrations were referenced to total creatine signal (defined at 10 mM) from the corresponding acquisition type. ppm: parts per million.

glutamate, glutamine, myoinositol, GSH, and GABA were achieved by predefining the voxel concentration of total creatine (creatine and phosphocreatine) as 10 mM. Metabolite concentrations were corrected as needed using significant linear regression betas on subject age, calculated from the control cohort as detailed in Chapter 4.

Single-variable statistical analysis of between-group metabolite differences. Metabolite concentrations were estimated relative to 10 mM total creatine (tCr); all statistics were calculated in R (v. 4.0.5) [639] and reported as mean ± S.D with $\alpha = 0.05$. One-way ANOVA with fixed factor PTSD as well as two-way ANOVA with an additional MDD x PTSD interaction term tested PTSD effect with and without consideration of comorbid MDD, respectively. Shapiro-Wilk test $p>0.05$ confirmed normality on ANOVA residuals before resort to nonparametric testing. Spearman correlations assessed mPFC metabolite relationships to PTSD or MDD severity indices in those with either diagnosis.

5.2.3. Results

Spectral quality enabled quantification of glutamate, GABA, and glutathione for a majority of participants. Quantifiable STEAM spectra were acquired for all cases; GABA-JDE, N=37/38, and GSH-JDE, N=29/38 (3.03-ppm creatine full-width at half-maximum FWHM 10.7±1.3 Hz, 12.6±2.4 Hz, and 12.9±2.5 Hz). Clinician-administered PTSD Score (CAPS) did not differ in $PTSD_{MDD+}$ versus $PTSD_{MDD-}$ groups or correlate with Montgomery-Åsberg Depression Rating Scale (MADRS) in $PTSD_{MDD+}$ ($p>0.1$).

Major depressive disorder effects on glutamine concentrations and ratios replace those of post-

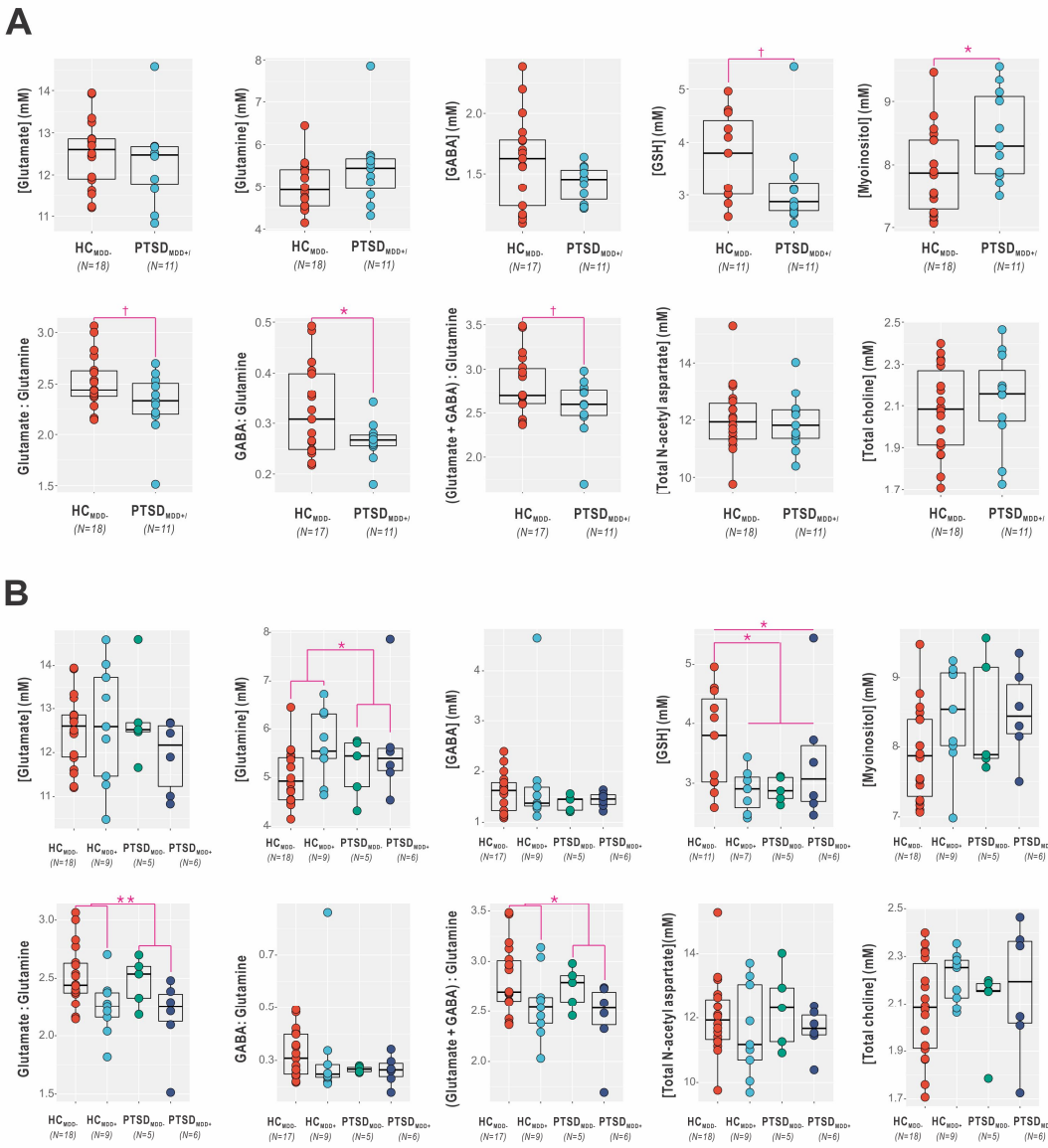

Figure 5.10. Individuals with post-traumatic stress disorder (PTSD) with or without major depressive disorder (MDD) exhibited higher glutamine : glutamate ratios as well as higher myoinositol than controls without PTSD or MDD. mPFC glutamate : glutamine and (GABA + glutamate) : glutamine demonstrated trends to decrease in PTSD relative to HC_{MDD-} when comorbid MDD was not considered (A) that became significant effects of MDD in glutamine ($F_{1,34}$=5.723 , p=0.02; mean difference 95% CI 0.08 to 1.05 mM, p=0.02), glutamate : glutamine ($F_{1,34}$=9.801 , p=0.004; mean difference 95% CI -0.45 to -0.091 mM, p=0.004) and (GABA + glutamate) : glutamine ($F_{1,34}$=5.737 , p=0.02; mean difference 95% CI -0.49 to -0.035 mM, p=0.02) when comorbid MDD was considered (B). Additionally, glutathione exhibited an interaction between MDD and PTSD ($F_{1,25}$=5.477, p=0.03) that manifest as a general decrease with either or both disease statuses w.r.t. HC_{MDD-} (Wilcoxon W = 146, p=0.04). Disease-related alterations were not seen in total N-acetyl aspartate, total choline, or GABA, suggesting that these effects on glutamine and GSH are not driven by disease-related changes in the total creatine reference. HC: Non-PTSD control; one-way ANOVA effect of fixed factor PTSD *p<0.05 †p<0.1 (A); two-way ANOVA effect of fixed factor MDD *p<0.05 **p<0.01 except GSH with PTSD x MDD *p<0.05 (B).

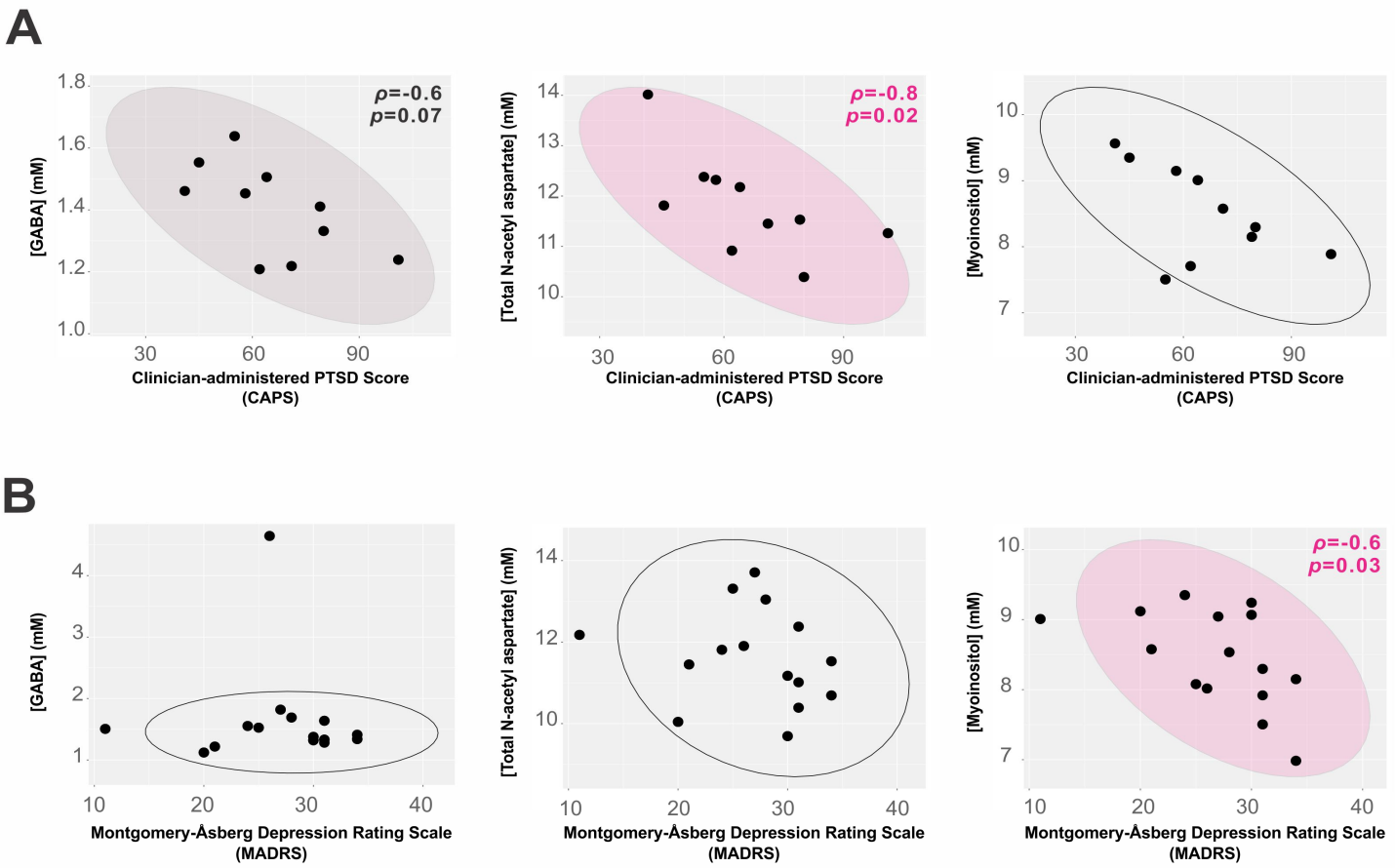

Figure 5.11. Non-glutamate medial prefrontal cortex (mPFC) metabolites correlate negatively with either post-traumatic stress disorder (PTSD) or major depressive disorder (MDD) symptoms but not both. Total N-acetyl aspartate correlated negatively, and GABA showed a trend to negative correlation, with Clinician-administered PTSD Score (CAPS) but not with Montgomery-Åsberg Depression Rating Scale (MADRS) (A), while myoinositol correlated negatively with MADR but not CAPS. Notably, CAPS and MADRS did not exhibit significant Spearman correlations with each other in individuals diagnosed with both PTSD and comorbid MDD (N=6; p>0.1).

traumatic stress disorder when this comorbidity is considered. mPFC glutamate : glutamine ($F_{1,27}$=3.95, p=0.06) and (glutamate + GABA) : glutamine ($F_{1,27}$=3.914, p=0.06) demonstrated a trend to decrease in PTSD relative to HC_{MDD-} (Figure 5.10A) that manifest as MDD effects on glutamine ($F_{1,34}$=5.723, p=0.02; mean difference M.D. 0.56±0.24 mM, p=0.02), glutamate : glutamine ($F_{1,34}$=9.801, p=0.004; M.D. -0.27±0.09 mM, p=0.004), and (glutamate + GABA) : glutamine ($F_{1,34}$=5.737, p=0.02; M.D. -0.26±0.11 mM, p=0.02) once comorbid MDD was considered (Figure 5.10B). Additionally, glutathione demonstrated an MDD x PSTD interaction ($F_{1,25}$=5.477, p=0.03) with decrease over all disease groups relative to HC_{MDD-} (Wilcoxon W=146, p=0.04) (Figure 5.10B).

^{1}H-MRS-visible metabolite concentrations correlate with reported symptom severity in either post-traumatic stress disorder or major depression but not both. Total N-acetyl aspartate (tNAA) correlated negatively (Spearman's ρ=-0.8, p=0.02; N=10), and GABA showed a trend to negative correlation (Spearman's ρ=-0.6, p=0.07; N=10), with CAPS but not MADRS; myoinositol, with MADRS (Spearman's ρ=-0.6, p=0.03; N=15) but not CAPS (Figure 5.11).

5.2.4. Discussion

In this section we have applied for the first time 7-Tesla ^{1}H-MRS investigation of brain tissue in individuals with and without post-traumatic stress disorder and/or comorbid or primary major depressive disorder. In a cross-sectional analysis of ^{1}H-MRS findings in a medial prefrontal cortex voxel, we have shown that apparent PTSD-associated ^{1}H-MRS-visible glutamatergic abnormalities in mPFC appear to be driven by MDD status when this comorbidity is considered. Glutamine is the metabolic byproduct of perisynaptic glutamate uptaken by nearby glia [640].

Altered mPFC concentrations of glutamine, as well as decreased GABA to glutamine and GABA + glutamate to glutamine seen with MDD either by itself or comorbid with PTSD, may therefore be consistent with alterations in glutamatergic neurotransmission and its interplay with local GABAergic networks, as well as attendant changes in metabolic burden on glial support. The MDD effect on apparent MRS-visible glutamatergic dysfunction appeared to be stronger than that of PTSD for this cohort, for whom the latter was only marginally significant and disappeared once MDD comorbidity was considered.

In addition to a negative relationship between mPFC myoinositol concentration, itself also potentially associated with but not fully explained by compensatory gliosis [641], and MDD symptom severity, we have also reported a significant negative correlation between total N-acetyl aspartate and PTSD severity, replicating for the first time at 7-Tesla field strength multiple previous findings of PTSD-associated abnormality in this metabolite [104, 105].

Taken together, our findings are consistent with the postulated role of mPFC metabolic dysfunction in PTSD pathophysiology and underline the importance of considering the overlapping role of depressive symptomology in glutamatergic involvement thereof, as well as the utility of ^{1}H MRS at 7-Tesla field strength for continued work in this domain.

As in Chapter 4, even these statistically significant single-metabolite ^{1}H-MRS findings would not individually support the sensitive and specific separation from control of individuals with either PTSD or MDD diagnoses. We therefore attempted to generalized the machine-learning pipeline developed in Chapter 4 to the present cohort, as described in the next section.

5.3 Binary classification of post-traumatic stress disorder and/or major depressive disorder status by supervised machine learning on multivariate metabolic signatures from prefrontal

cortex

5.3.1. Motivation

Post-traumatic stress disorder (PTSD) is a condition wherein experience of a traumatic event induces chronic emotional dysregulation that can disrupt functional participation in society. The 2012 economic toll of PTSD care was estimated at $300 million within the United States Department of Defense alone [100], a figure not considering its many comorbidities, including increased risk of suicide and of cardiorespiratory, gastrointestinal, immune, and additional psychiatric diagnoses [101]. Though the lifetime prevalence of PTSD in some communities is estimated up to 1 in 12 [101], diagnosis, and related treatment, continues to rely on the subjective and potentially slow evaluation of symptoms that must persist over several weeks [102].

The continued reliance on symptom-based diagnosis of PTSD is due in part to an incomplete understanding of its neurobiological manifestations, particularly the metabolic changes in central nervous system pathways affected by the condition [103]. The only method currently available for safely and noninvasively researching these changes by measuring local tissue metabolism in living humans is in vivo proton magnetic resonance spectroscopy (^{1}H-MRS). Preliminary ^{1}H-MRS research indicates that the pattern of cortical metabolic abnormalities in PTSD is subtle and complex [104], as also shown in Section 1, and therefore best negotiated using data-driven multivariate techniques like machine learning. Few applications of such approaches to interpreting the complexity of brain metabolic changes in PTSD have, however, been published, in part due to the dearth of studies simultaneously assessing a broad range of disease-relevant metabolites in the same participants.

^{1}H-MRS methods described in Chapter 4 have enabled for the first time the accurate and reproducible simultaneous in vivo measurement of three small molecules implicated in PTSD

pathophysiology: excitatory neurotransmitter glutamate, inhibitory neurotransmitter γ-amino-butyric acid (GABA), and antioxidant glutathione (GSH) [106]. Coupled with the measurement of five other small molecules (choline, creatine, myoinositol, N-acetyl aspartate, and glutamine) each also implicated in various neurological conditions [107], these ^{1}H-MRS data acquisitions are thus unique in enabling data-driven metabolomics-level analyses like machine learning in the effort toward more efficient and objective diagnosis of PTSD.

We hypothesize that the local metabolic alterations in brain tissue associated with PTSD can be exploited to enable the cost-efficient and accurate diagnosis of this disease. The aim of this section is the generalization from Chapter 4 of such a model for supporting the rapid and accurate diagnosis of PTSD using data-driven machine-learning techniques that distinguish patients from control using solely brain metabolite concentrations obtainable by clinical magnetic resonance (MR) scan. Because of association between MDD status and the PTSD-linked metabolite findings demonstrated in Section 2 as well as the low number of PTSD patients in the currently available data set, this goal was broadened to also include, as proof of concept, the diagnosis of major depressive disorder as either primary or comorbid to PSTD.

5.3.2. Methods

Participant demographics and spectroscopy acquisition, processing, and analysis methods are as described in Section 2. All participants in this analysis had full STEAM data sets; one control participant was missing GABA concentrations and nine participants (seven HC_{MDD-} and two non-HC_{MDD-} individuals) were missing GSH concentrations that were imputed as the average of their respective classes prior to analysis.

Classification pipelines were implemented in Python (v. 3.6.13) based on methods

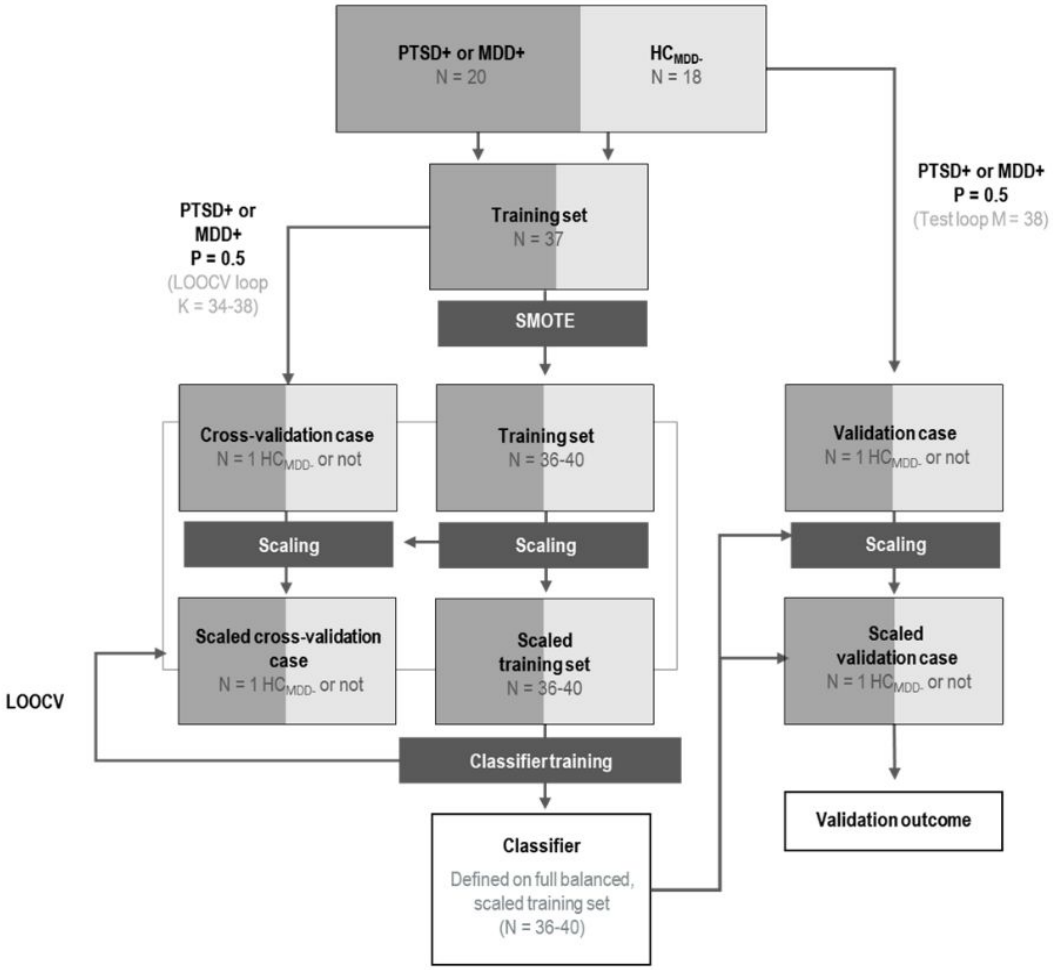

Figure 5.12. Medial prefrontal cortex (mPFC) metabolite concentrations quantified via linear combination modeling were employed for supervised classification of post-traumatic stress disorder (PTSD) and/or comorbid major depressive disorder (MDD). Linear combination modeling with a regularized cubic spline baseline was conducted in LCModel using density-matrix-simulated basis functions generated in SpinWizard for the metabolites shown in Figure 5.9. Metabolite concentrations were referenced to total creatine signal (defined at 10 mM) from the corresponding acquisition type. mPFC metabolite concentrations were employed as the sole features in a supervised learning pipeline applying support vector machine (SVM), k-nearest neighbors (KNN), and quadratic discriminant analysis (QDA) classifiers for identifying brain pathology (PTSD and/or MDD) from feature sets comprising only mPFC glutamate, glutamine, GABA, glutathione, total N-acetyl aspartate, total choline, and myoinositol concentrations, based on the previously reported approach for successful classification of multiple sclerosis subtypes in Chapter 4. LOOCV: Leave-one-out cross-validation; PTSD: post-traumatic stress disorder; MDD: major depressive disorder.

previously reported [642] and constitute one binary classification between individuals with and without PTSD. Support vector machines (SVM), k-nearest neighbors (KNN), and quadratic discriminant analysis (QDA) were employed based on the superior held-out validation accuracies of these algorithms in the relapsing versus progressive multiple sclerosis classification detailed in Chapter 4. All techniques were implemented in Sci-Kit Learn [94].

Briefly, as before, data were split into training and validation sets by removing one data set at a time for use as a held-out validation set, yielding a total of N_1 x 2 runs for data with smaller group size N_1. Model training was performed on only members of each training set. Leave-one-out cross validation (LOOCV) statistics were calculated for each training set for aggregate use in feature selection; notably, training hyperparameters were not re-optimized in order to re-test the values already optimized on entirely different training data for binary classification of multiple sclerosis as presented in Chapter 4. Undersampling proceeded similarly for cross-validation as for held-out validation in that each of the training cases was removed once for use as a cross-validation set for that training run, with a total of N_2 x 2 cross-validations for data with the smaller training group size N_2 to ensure class balancing in the population of cross-validation sets used for each training run. Class sizes were then balanced after removal of the aforementioned held-out validation and cross-validation sets using the Synthetic Minority Over-Sampling Technique (SMOTE) [78].

Each training set was scaled using a matrix calculated over that training set only, after which the same scaling was transferred to the held-out validation case, as in Chapter 4. Dimensionality reduction on the already small feature set of seven metabolites was also similarly not performed to avoid reduction in model interpretability. Model performance was averaged across all runs for each algorithm (Figure 5.12).

5.3.3. Results

mPFC metabolites alone supported supervised classification of non-HC_{MDD-} disease status with sensitivity and specificity either exceeding (support vector machines held-out validation sensitivity 83% and specificity 83%; Figure 5.13; k-nearest neighbors sensitivity 83% and specificity 83%) or approaching (quadratic discriminant analysis sensitivity 72% and specificity 83%) 80%.

Glutamine exhibited the highest permutation importance (0.17) for classification by support vector machines, followed by glutathione (0.15), myoinositol (0.10), total choline (0.05), glutamate (0.042), and total N-acetyl aspartate (0.04). Glutathione exhibited the highest permutation importance (0.17) for classification by k-nearest neighbors, followed by myoinositol (0.16) and glutamine (0.07). Finally, glutathione also exhibited the highest permutation importance (0.14) for classification by quadratic discriminant analysis, followed by glutamine (0.12), total choline (0.10), total N-acetyl aspartate (0.09), GABA (0.07), and myoinositol (0.06).

5.3.4. Discussion

In this work we extend to a new cluster of diagnoses in a new cohort the findings of Chapter 4 that the progressive multiple sclerosis subtype can be distinguished with substantial sensitivity and specificity from either control or relapsing-remitting multiple sclerosis on the sole basis of seven creatine-referenced frontal cortex metabolites measured by ^{1}H MRS at 7 Tesla: glutamate, glutamine, GABA glutathione, total N-acetyl aspartate, total choline, and myoinositol. Employing an entirely new 7-Tesla ^{1}H-MR spectral data set from different volunteers acquired, processed, quantified, and analyzed in identical fashion to the data presented in Chapter 4, we have shown that mPFC metabolite abnormalities alone, the most important being glutamine, also

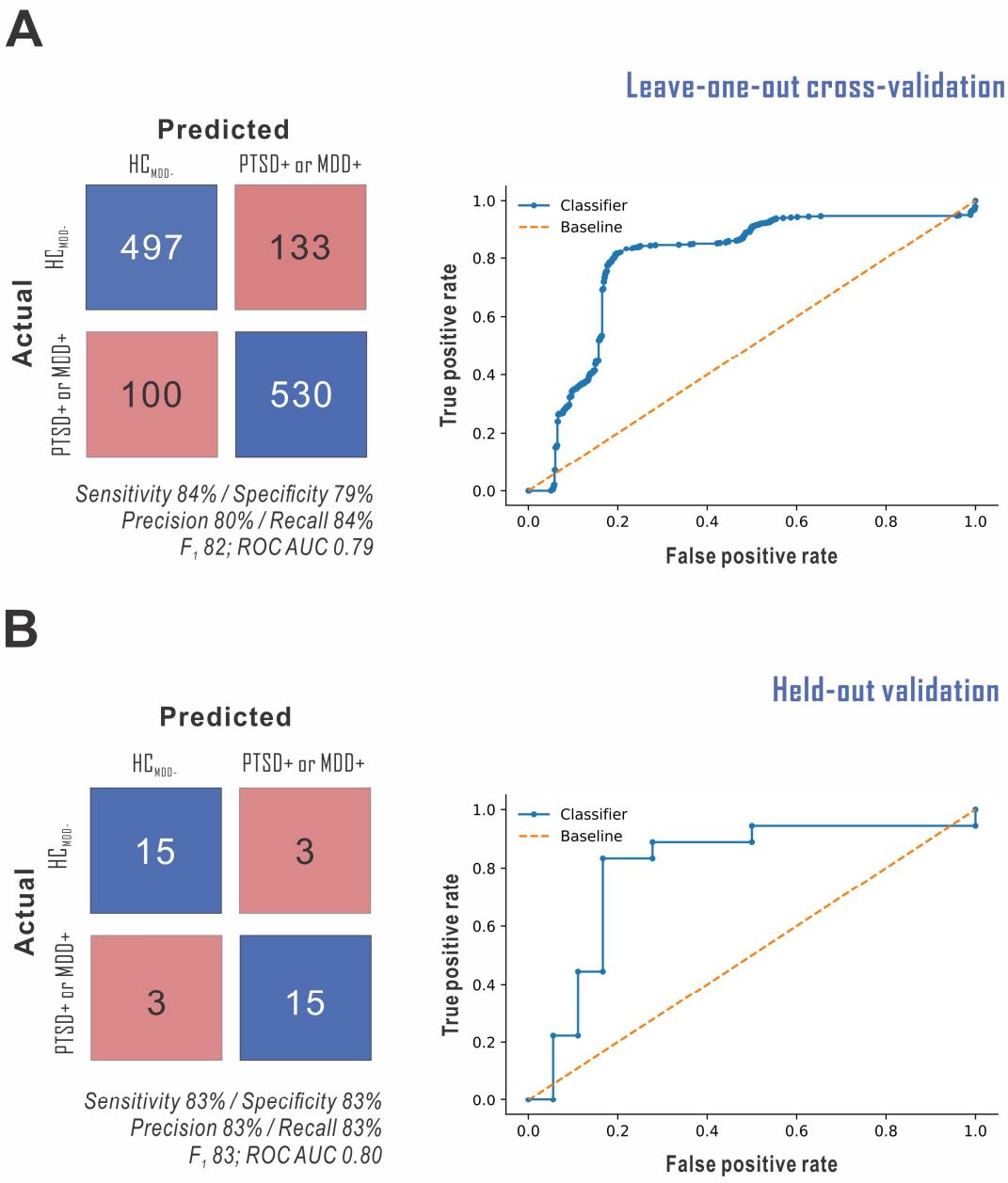

Figure 5.13. Medial prefrontal cortex (mPFC) metabolites separate post-traumatic stress disorder (PTSD) or major depressive disorder (MDD) from control. Support vector machines identified PTSD/MDD via mPFC metabolites alone. Low permutation importance (PI) features dropped against leave-one-out cross validation (LOOCV) performance left glutamine (PI 0.17), glutathione (0.15), myoinositol (0.1), total choline (0.05), glutamate (0.042), and total N-acetyl aspartate (0.04). LOOCV (A) and validation (B) had high accuracy (left) and convex ROC curves (right). ROC AUC: Receiver operating characteristic area under the curve, or area under the ROC (AUROC).

supported identification of either MDD or PTSD with respect to healthy control at accuracies comparable to those seen for the classification of progressive multiple sclerosis demonstrated in Chapter 4. Indeed, performance of support vector machine models lay beyond the 80% sensitivity and specificity thresholds previously proposed for a novel diagnostic biomarker of, for example, Alzheimer's Disease [643].

Similarly to the findings demonstrated in Chapter 4, wherein uncommonly measured ^{1}H-MRS-visible metabolites glutamate as separate from glutamine, GABA, and glutathione demonstrated high permutation importance for ^{1}H-MRS-based classification of multiple sclerosis status (glutamate) or the progressive phenotype thereof (glutamine and glutathione), in this analysis we found that glutamine and glutathione were also of consistently high permutation importance for distinguishing MDD-/PTSD- control individuals from those with either MDD, PTSD, or both. This replicated finding emphasizes the potential of methodologically more advanced (involving field strengths at 4 T or above and/or spectral editing) investigations involving these and possibly other ^{1}H-MRS-visible metabolites other than, as shown in Chapters 1 and Chapter 5 Section 1, those most commonly assessed compounds with high-signal-to-noise singlets like total N-acetyl aspartate, total choline, total creatine, and (though lacking singlets) sometimes myoinositol.

Also as for the results presented in Chapter 4, several steps stand between this preliminary finding and the practical employment of ^{1}H-MRS as a clinically serviceable diagnostic tool. First, the highly specialized acquisition methods, particularly STEAM enabling very short (10 ms) echo time and inversion-recovery preparation for macromolecule suppression as well as MEGA-sLASER with *J*-difference editing for glutathione and GABA, notably also with inversion preparation for macromolecule nullification and editing pulse mirroring around macromolecule

resonances for additional macromolecule control, would need to be implemented on clinically serviceable 7-Tesla MR scan systems, which is a challenge tractable in principle but potentially substantial in practice. Second, the data processing and quantification methods employed in this chapter employed two tools (INSPECTOR and LCModel) that require large (INSPECTOR) or moderate (LCModel) degrees of manual adjustment by experienced personnel, though the INSPECTOR Batch tool developed, tested, and presented in Chapter 2 constitutes one more step toward user-friendly automatability employable by individuals with little or no spectroscopy experience. Third, beyond a clear need for replication of the work presented here with larger patient samples, an important shortcoming of the present analysis, as in Chapter 4, is the use of healthy (negative) controls only, as opposed to non-healthy (positive) controls with differential diagnoses more reflective of the populations to which such diagnostic would realistically be applied.

5.4 General summary and conclusions

In this chapter we sought to address the following question: Can lessons about spectral processing and quantification (Chapter 2), concentration referencing (Chapter 3), and univariate and/or multivariate statistical analysis (Chapter 4) previously applied to maximizing sensitivity to metabolite concentration differences from control in progressive and/or relapsing-remitting multiple sclerosis be generalized to identification of another diagnosis cluster, namely post-traumatic stress disorder and/or major depressive disorder?

Taken together, our findings suggest that an ^{1}H-MRS processing, quantification, referencing, and statistical analysis pipeline optimized for maximizing the sensitivity of frontal cortex metabolite concentration estimates to cross-sectional effects of multiple sclerosis, particularly the progressive phenotype, yields metabolite findings supporting comparable

classification performance when applied to the identification of either post-traumatic stress disorder or major depressive disorder using an entirely different data set, acquired via similar methods, from a completely separate group of participants.

Chapter 6: Conclusions, Limitations, and Outlook

6.1 Conclusions

This dissertation has designed and implemented analytic pipelines for and demonstrated evidence toward the following claims:

- Chapter 2: Novel toolkits for ^{1}H-MRS spectral data analysis pipeline validation via batch spectral simulation and linear combination modeling, transparent and flexible user-defined regularized spline baseline handling for spectral quantification by linear combination modeling, and Cramér-Rao Lower Bound calculation directly for polynomial and spline baseline shapes are designed, implemented, and integrated into spectroscopy processing freeware INSPECTOR. Using these new tools it is shown that proton magnetic resonance spectral quality measures full width at half maximum and signal-to-noise ratio influence zero-centered errors (precision) to estimate relative metabolite concentrations via in vivo proton magnetic resonance spectral quantification in the absence of a spectral baseline. In the presence of an in vivo-like baseline, however, these metrics of spectral quality influence not only spectral quantification precision but also accuracy. Even in short-T_E ^{1}H-MRS acquisitions in the frontal and occipital cortex at 3 Tesla wherein spectral baselines are expected to be heavily influenced by signals from macromolecules, baselines of simulated macromolecules do not necessarily outperform splines in either macromolecule or metabolite prediction accuracy, but at least for some commonly measured metabolites, quantification pipelines employing prior knowledge from metabolite-nulled acquisitions exhibit superior metabolite fit precision and accuracy among all baseline models tested. The spectral quantification validation pipeline designed here demonstrated the validity of not only metabolite amplitude Cramér-Rao Lower

Bound calculations but also the utility of those designed and presented herein for polynomial and spline baseline shapes to support more accurate estimates of spectral fit precision of relative metabolite concentration estimates. This is especially useful for circumstances wherein comparisons to a known ground truth (as for in vivo measurements) are not available.

- Chapter 3: Individuals with progressive multiple sclerosis exhibited increased frontal cortex water T_2 relative to control, a difference that impacts the absolute quantification step of metabolites measured using in vivo ^{1}H MRS if water is employed as an internal concentration reference in this cohort. This potential confound was associated with age-related changes in tissue composition that can be considered in corrections for metabolite concentration estimates referenced to internal water. We have previously shown that evidence-based T_2 corrections can significantly affect metabolite concentration estimates, especially those derived from measurements at long echo time. Correction for these findings of disease effect on water T_2 demonstrated similar influence on metabolite concentrations estimated via referencing to water.
- Chapter 4: Employing an evidence-based spectral processing and quantification pipeline with particular attention to baseline modeling and potential relaxation-based confounds on internal concentration referencing, it was shown that progressive but not relapsing-remitting multiple sclerosis is associated with disease-related decreases in frontal cortex glutamate, GABA, and possibly glutathione as measured by ^{1}H MRS at 7 Tesla. While even significant between-group differences in single metabolites are not sufficient to distinguish accurately among disease groups, by employing multivariate statistics or supervised learning techniques, progressive multiple sclerosis could be differentiated from

control or relapsing-remitting multiple sclerosis with nearly 80% sensitivity and specificity on the basis of ^{1}H-MRS measurable frontal cortex metabolites alone.

- Chapter 5: Spectral processing and quantification procedures optimized for the aforementioned cross-sectional analysis of multiple sclerosis generalized to a similar cross-sectional analysis of individuals with and without post-traumatic stress disorder and/or major depressive disorder, supporting finding of altered glutamine : neurotransmitter (namely, glutamate and GABA) ratios in post-traumatic stress disorder that became a significant effect of major depressive disorder on glutamine concentration and neurotransmitter ratios when this comorbidity was considered. Additionally, a trend to decreased glutathione was observed in post-traumatic stress disorder that became a significant effect of diagnosis with any disorder (either post-traumatic stress disorder and/or major depressive disorder) when comorbid major depression was considered. Similarly, the binary classifiers (quadratic discriminant analysis, k-nearest neighbors, and support vector machines trained within the bootstrapped cross-validation pipelines depicted in Figure 4.7) shown to distinguish between relapsing-remitting and progressive multiple sclerosis on the basis of seven ^{1}H MRS-visible frontal cortex metabolites alone, along with spectral processing and quantification parameters also optimized on those previous data, were able to be generalized to a similar ^{1}H MRS data set for comparably accurate (maximum 83% sensitivity and specificity) binary classification of post-traumatic stress disorder and control.

6.2 Limitations and Outlook

The goal of this dissertation was to characterize and broaden the sensitivity limits of in vivo

magnetic resonance spectroscopy (^{1}H MRS), a promising method for noninvasively measuring metabolite concentrations in the tissue of living humans, to effects of neurological and psychiatric diseases, namely relapsing-remitting and progressive multiple sclerosis, post-traumatic stress disorder, and/or major depressive disorder. In the service of this goal, this work has attempted to design, implement, and validate generalizable simulation and analysis pipelines for quantifying the precision and accuracy of in vivo proton spectroscopy linear combination model fits (Chapter 2), quantify the influences of internal water referencing on errors of metabolite estimates derived from 7-Tesla ^{1}H MRS in a population of individuals with relapsing-remitting, progressive, or no multiple sclerosis (Chapter 3), apply lessons from Chapters 2 and 3 regarding key influences on metabolite quantification, particularly spectral baseline modeling approaches and internal referencing scheme, to assess the influences of multiple sclerosis disease state on concentration estimates of 7-Tesla ^{1}H-MRS-visible metabolites and support supervised machine-learning classification of multiple sclerosis state and phenotype on the basis of these metabolite concentration estimates alone (Chapter 4), and generalize in its entirety this evidence-based processing, quantification, and statistical analysis pipeline optimized on the multiple sclerosis dataset to an entirely different cohort to support the characterization and binary classification of post-traumatic stress disorder and/or major depressive disorder versus non-PTSD, non-MDD individuals (Chapter 5).

As mentioned in each individual respective chapter, some important caveats exist to the broad practical utility of the conclusions drawn therein. First, while the spectral processing and linear combination modeling validation paradigms designed and implemented in Chapter 2 attempt to maximize generalizability of calculated metabolite estimate errors for a given processing and analysis scheme to similar in vivo datasets for which gold-standard true values are not known by

including simulated metabolite spectra with some measured in vivo features (either fit residuals resembling the non-metabolite baseline signatures of *J*-difference-edited glutathione spectra acquired from a MEGA-sLASER sequence in human frontal cortex at 7 Tesla or real measured short-echo time macromolecule acquisitions measured by a double-inversion-recovery short-echo-time sLASER sequence at low echo time (T_E < 30 ms) in human frontal or occipital cortex at 3 Tesla), these composite simulated-acquired spectra do not capture the broad variety of possible in vivo ^{1}H-MRS experimental data to which such pseudo-validated processing and analysis pipelines may be applied. Indeed the gold-standard in-vivo-like spectra engineered in Chapter 2 do not even themselves perfectly resemble any single realistic in vivo experiment: For the first, a fit residual from an imperfect first linear combination model fit to glutathione difference spectrum is itself expected to include some residual glutathione resonance left uncaptured by an insufficient model, or perhaps excessive subtraction thereof of an overzealous model; similarly, an "in-vivo-like baseline" for a simulated low-echo-time metabolite acquisition is expected to comprise macromolecule resonances of slightly different T_1 weighting from that of the equivalent double-inversion-recovery macromolecule-"only" acquisition, in addition, again, to potentially unscrubbed residual metabolite resonances, particularly from large-amplitude singlets like creatine, choline, and N-acetyl aspartate.

One route to bridging the disconnect between in vivo data for which the ground truth cannot be known and a validation scheme dependent on simulated data for which true values are engineered and which can only be "in-vivo-like" in part for confounds like those detailed above is the Cramér-Rao Lower Bound (CRLB), expected to represent the lower bound of metabolite concentration estimate error standard deviation in the presence of a perfect model and only pointwise Gaussian deviations thereof of the targeted spectral data. The linear relationships

between fit error standard deviations, calculable only for validation standards, and CRLB, calculable also on fits to in vivo data, demonstrated in the first part of this chapter for baseline-less and residual-baseline simulated data, as well as in in the latter part for macromolecule-baseline simulated data, in addition to the design, implementation, and validation of CRLB for model baseline shapes themselves serving to tighten the identity relationship between fit error and CRLB, serve as an important steps toward future extensions investigating the degree to which spectral processing and analysis approaches shown to yield the lowest errors against in-vivo-like simulated spectral gold standards according to the methods developed in Chapter 2 might then yield the lowest CRLB, and presumably therefore also the lowest actual errors for which CRLB serve as a proxy, in analogous in vivo spectral measurements lacking gold standard values. It bears strong emphasis, however, that while the spline baseline modeling tool developed, implemented, and validated in Chapter 2 for spectral processing and analysis toolkit INSPECTOR improves the flexibility of linear combination models to better represent a broader range of spectral data, it does not guarantee the standard of the "perfect" linear combination model necessary for equivocation of CRLB and metabolite estimate error standard deviation. It is important to note, however, that the extension of the Fisher information matrix underlying CRLB calculations to include terms for model baseline shapes, also developed, implemented, and validated in Chapter 2, does appear to, in spectra and therefore associated models involving in-vivo-like baselines, at least serve to improve this correspondence between calculated CRLB and standard deviation of metabolite fit error needed to, in practice, treat the former as a lower bound for the latter for in vivo datasets lacking a true known gold standard. That said, while CRLB calculated directly for amplitudes of regularized spline baseline shapes from the same model demonstrate linear relationships with the standard deviation of errors on true baseline shape coefficients, these relationships still deviate

significantly from identity in spectra employing piecewise spline baseline handling, suggesting a continued disconnect between CRLB and error standard deviations in this spectral data type. As explained in Chapter 3, this disconnect is to be expected due to constraints on the possible coefficients of a modeled piecewise function, and therefore the actual standard deviations of their errors relative to a true standard, inherent in their existence as part of a continuous and interdependent whole.

Further work in this realm is needed to continue characterizing the circumstances under which CRLB-error standard deviation correspondence is or is not good enough to justify the employment of the former as a valid endpoint for spectral processing and analysis procedures, as error standard deviations were in Chapter 2, when such true values are not available. Finally, and most damningly, even if a method were developed to skirt these disconnects between CRLB and error standard deviation there still exists no method to estimate systematic inaccuracy (even in hypothetical situations of zero error standard deviation) in metabolite concentration estimates in the absence of known true values, and as Chapter 2 demonstrates, consistent and systematic over- or under-estimations of particular metabolites in the presence of a particular baseline environment and resultant modeling scheme can underlie even larger deviations from the truth than simple variability across repeated attempts to fit the same data. The current work offers no solution to characterize this in an in vivo dataset, just a method for systematically quantifying it for spectra and linear combination modeling schemes that resemble those encountered and employed for experiments in vivo.

Putting aside for now this harder problem of systematic inaccuracy and focusing only on the more tractable one of precision, due to this decreased but still continued unreliability of CRLB as an estimate of even just the latter for in vivo spectra involving complicated baselines and

typically modeled by similarly complicated regularized splines, Chapter 4 employed from Chapter 2 predominantly the observation that baseline modeling scheme exerts substantial influence on fit error relative to other minutiae of spectral processing and quantification and therefore focused evidence-based methodological optimization efforts on competing quantification pipelines that differed predominantly on this aspect. Again due to the shortcoming of the CRLB for in vivo data with baselines and associated modeling, linear combination modeling schemes were optimized against the minimum control cohort between-subjects coefficients of variation in major creatine-referenced metabolite concentrations rather than the CRLB. One obvious shortcoming of this approach is the inherent caveat that if any influences underpinning between-subjects differences in the control group were to also underlie legitimate biologically relevant differences between groups, minimizing the former via a certain analysis procedure would also decrease this procedure's sensitivity to the latter, which is precisely counter to the aim of the present work.

Even if between-group differences were accordingly blunted by calculated optimization of linear combination modeling approach against minimization of control between-subject coefficient of variation in Chapter 4, however, the application of this approach to cross-sectional analysis of multiple sclerosis effects on 7-Tesla ^{1}H-MRS-visible prefrontal cortex metabolite concentrations yielded findings of significant reductions in glutamate and GABA and trends to reduction in glutathione in progressive multiple sclerosis relative to control and/or relapsing-remitting multiple sclerosis; the extension of these methods in Chapter 5 also yielded findings of alterations in glutamine and/or glutamine : neurotransmitter (GABA and/or glutamate) ratios in either post-traumatic stress disorder or major depression depending on whether the latter comorbidity was considered. Both sets of frontal cortex metabolite concentration estimates also supported, on the basis of those data alone, supervised binary classification of disease state near

(progressive multiple sclerosis relative to healthy control or relapsing-remitting multiple sclerosis) or exceeding (post-traumatic stress disorder and/or major depression relative to healthy control) 80% sensitivity and specificity. It is important to note that without the sanity check provided on the entirely new data set presented in Chapter 5, especially the machine-learning results of Chapter 4, employing models with hyperparameters optimized on many bootstrapped iterations of the same training data heavily overlapping in the aggregate with the population of held-out validation cases used for each iteration of the outer loop, would be vulnerable to valid criticisms of potential overfitting, despite the very low number of hyperparameters optimized for each model. The high, indeed superior, performance of the very same models hyperparameter-optimized on one data set and generalized to another helps to allay some of this criticism, but importantly feature selection (if not hyperparameter optimization, already locked in from the results of Chapter 4) proceeded in Chapter 5 in the same way as in Chapter 4 and still therefore serves as a mechanism for potential overfitting.

Notably, in part due to findings in Chapter 3 of multiple sclerosis disease effect on frontal cortex water T_2 necessitating the potentially variance-broadening employment of individually measured water T_2 or image segmentation-based corrections thereof to avoid introduction of spurious systematic errors into group metabolite concentration estimates based on internal referencing to water, all metabolite concentrations subsequently employed in this work have been referenced to total creatine. It is possible that the confounds observed in Chapter 3, and further explored in the related Discussion in Section 2 of Chapter 4, for water referencing in multiple sclerosis do not similarly apply to either post-traumatic stress disorder or to major depression, highlighting the extension of metabolite estimates to water-referenced values, and assessment of between-group statistics thereof, as an important ongoing investigation of this data set.

Finally, as emphasized at the end of Chapter 5, the diagnostic promise of 7-Tesla ^{1}H MRS implied by the machine-learning investigations of the present work awaits much further validation, particularly with larger experiments involving appropriate differentially diagnosed positive controls, as well as with the more mainstream implementation of key acquisition and quality assurance protocols in clinically available scanners in addition to user-friendly interfaces for automated implementation of the data processing strategies subsequently employed. While the batch simulation and linear combination modeling functionality developed and demonstrated in Chapter 2 for spectral processing and analysis toolkit INSPECTOR represents some progress in the latter domain, the former and other considerations remain to be addressed in continued efforts toward the development of ^{1}H MR spectroscopy as not only an efficacious but also an accessible and pragmatic diagnostic tool for brain disease.

References

[1] A. Andreychenko, D. W. Klomp, R. A. de Graaf, P. R. Luijten, and V. O. Boer, "In vivo GABA T_2 determination with *J*-refocused echo time extension at 7 T," *NMR Biomed,* vol. 26, no. 11, pp. 1596-601, Nov 2013, doi: 10.1002/nbm.2997.

[2] W. A. Little, *Conductivity and magnetism: The legacy of Felix Bloch: Proceedings of the symposium, 27-28 October 1989, Stanford, USA*. Singapore; Teaneck, NJ: World Scientific, 1990, pp. xi, 162 p.

[3] G. R. Cresshull ID, P.E. Hanley, D. Shaw, D.G. Gacian, G.K. Radda, P. Styles, "Localization of metabolites in animal and human tissues using 31P topical magnetic resonance " *Bulletin of Magnetic Resonance,* vol. 2, p. 426, 1981.

[4] W. T. Dixon, "Simple proton spectroscopic imaging," *Radiology,* vol. 153, no. 1, pp. 189-94, Oct 1984, doi: 10.1148/radiology.153.1.6089263.

[5] R. D. Oberhaensli, G. J. Galloway, D. J. Taylor, P. J. Bore, and G. K. Radda, "Assessment of human liver metabolism by phosphorus-31 magnetic resonance spectroscopy," *Br J Radiol,* vol. 59, no. 703, pp. 695-9, Jul 1986, doi: 10.1259/0007-1285-59-703-695.

[6] S. K. Hilal, A. A. Maudsley, J. B. Ra, H. E. Simon, P. Roschmann, S. Wittekoek, Z. H. Cho, and S. K. Mun, "In vivo NMR imaging of sodium-23 in the human head," *J Comput Assist Tomogr,* vol. 9, no. 1, pp. 1-7, Jan-Feb 1985. [Online]. Available: http://www.ncbi.nlm.nih.gov/pubmed/3968256.

[7] P. A. Bottomley, "Noninvasive study of high-energy phosphate metabolism in human heart by depth-resolved 31P NMR spectroscopy," *Science,* vol. 229, no. 4715, pp. 769-72, Aug 23 1985. [Online]. Available: http://www.ncbi.nlm.nih.gov/pubmed/4023711.

[8] P. E. Sijens, H. K. Wijrdeman, M. A. Moerland, C. J. Bakker, J. W. Vermeulen, and P. R. Luyten, "Human breast cancer in vivo: H-1 and P-31 MR spectroscopy at 1.5 T," *Radiology,* vol. 169, no. 3, pp. 615-20, Dec 1988, doi: 10.1148/radiology.169.3.2847230.

[9] B. R. Rosen, D. M. Fleming, D. C. Kushner, K. S. Zaner, R. B. Buxton, W. P. Bennet, G. L. Wismer, and T. J. Brady, "Hematologic bone marrow disorders: quantitative chemical shift MR imaging," *Radiology,* vol. 169, no. 3, pp. 799-804, Dec 1988, doi: 10.1148/radiology.169.3.3187003.

[10] K. J. Thomas MA, P. Jajodia, G. Karczmar, B. Hubesch, G.B. Matson, T.L. James, P. Narayan, and M.W. Weiner, "31Phosphorus MR spectroscopy of human prostate in vivo," *8th Annual Meeting of the Society of Magnetic Resonance in Medicine,* p. 297, 1989.

[11] M. D. Boska, D. J. Meyerhoff, D. B. Twieg, G. S. Karczmar, G. B. Matson, and M. W. Weiner, "Image-guided 31P magnetic resonance spectroscopy of normal and transplanted human kidneys," *Kidney Int,* vol. 38, no. 2, pp. 294-300, Aug 1990. [Online]. Available: http://www.ncbi.nlm.nih.gov/pubmed/2402121.

[12] B. Gomez-Anson, D. G. MacManus, G. J. Parker, C. A. Davie, G. J. Barker, I. F. Moseley, W. I. McDonald, and D. H. Miller, "In vivo 1H-magnetic resonance spectroscopy of the spinal cord in humans," *Neuroradiology,* vol. 42, no. 7, pp. 515-7, Jul 2000. [Online]. Available: http://www.ncbi.nlm.nih.gov/pubmed/10952184.

[13] R. A. De Graaf, *In vivo NMR spectroscopy : principles and techniques*, 2nd ed. Chichester, West Sussex, England ; Hoboken, NJ: John Wiley & Sons, 2007, pp. xxi, 570 p., 8 p. of plates.

[14] J. Valette, B. Tiret, and F. Boumezbeur, "Experimental strategies for in vivo(13)C NMR spectroscopy," *Anal Biochem,* vol. 529, pp. 216-228, Jul 15 2017, doi: 10.1016/j.ab.2016.08.003.

[15] I. Aetna. "Magnetic Resonance Spectroscopy (MRS)." http://www.aetna.com/cpb/medical/data/200_299/0202.html.

[16] USFDA. "Information for Industry: Manufacturers of MRI scanners." https://www.fda.gov/radiation-emitting-products/mri-magnetic-resonance-imaging/information-industry.

[17] USFDA, "FDA clears first 7T magnetic resonance imaging device," ed. 2017.

[18] N. Tubridy and C. S. McKinstry, "Neuroradiological history: Sir Joseph Larmor and the basis of MRI physics," *Neuroradiology,* vol. 42, no. 11, pp. 852-5, Nov 2000. [Online]. Available: http://www.ncbi.nlm.nih.gov/pubmed/11151696.

[19] D. L. Rothman, O. A. Petroff, K. L. Behar, and R. H. Mattson, "Localized 1H NMR measurements of gamma-aminobutyric acid in human brain in vivo," *Proceedings of the National Academy of Sciences of the United States of America,* vol. 90, no. 12, pp. 5662-6, Jun 15 1993. [Online].

[20] S. W. Provencher, "Estimation of Metabolite Concentrations from Localized in-Vivo Proton Nmr-Spectra," *Magnet Reson Med,* vol. 30, no. 6, pp. 672-679, Dec 1993. [Online]. Available: <Go to ISI>://WOS:A1993MK17500003.

[21] J. Near, "Spectral quantification and pitfalls in interpreting magnetic resonance spectroscopic data: What to look out for," in *Magnetic resonance spectroscopy: tools for neuroscience research and emerging clinical applications*, C. J. Stagg and D. L. Rothman, Eds. Amsterdam: Elsevier/Academic Press, 2014, p. 359 pages.

[22] L. Barantin, A. Le Pape, and S. Akoka, "A new method for absolute quantitation of MRS metabolites," *Magn Reson Med,* vol. 38, no. 2, pp. 179-82, Aug 1997. [Online]. Available: http://www.ncbi.nlm.nih.gov/pubmed/9256094.

[23] K. Mehr, B. John, D. Russell, and D. Avizonis, "Electronic referencing techniques for quantitative NMR: pitfalls and how to avoid them using amplitude-corrected referencing through signal injection," *Anal Chem,* vol. 80, no. 21, pp. 8320-3, Nov 1 2008, doi: 10.1021/ac800865c.

[24] K. M. Swanberg, K. Landheer, D. Pitt, and C. Juchem, "Quantifying the Metabolic Signature of Multiple Sclerosis by in vivo Proton Magnetic Resonance Spectroscopy: Current Challenges and Future Outlook in the Translation From Proton Signal to Diagnostic Biomarker," *Front Neurol,* vol. 10, p. 1173, 2019, doi: 10.3389/fneur.2019.01173.

[25] E. E. Brief, I. M. Vavasour, C. Laule, D. K. Li, and A. L. Mackay, "Proton MRS of large multiple sclerosis lesions reveals subtle changes in metabolite T(1) and area," *NMR Biomed,* vol. 23, no. 9, pp. 1033-7, Nov 2010, doi: 10.1002/nbm.1527.

[26] P. M. Matthews, G. Francis, J. Antel, and D. L. Arnold, "Proton magnetic resonance spectroscopy for metabolic characterization of plaques in multiple sclerosis," *Neurology,* vol. 41, no. 8, pp. 1251-6, Aug 1991. [Online]. Available: http://www.ncbi.nlm.nih.gov/pubmed/1650931.

[27] G. B. D. M. S. Collaborators, "Global, regional, and national burden of multiple sclerosis 1990-2016: a systematic analysis for the Global Burden of Disease Study 2016," *Lancet Neurol,* vol. 18, no. 3, pp. 269-285, Mar 2019, doi: 10.1016/S1474-4422(18)30443-5.

[28] M. Trisolini, A. Honeycutt, J. Wiener, and S. Lesesne, "Global Economic Impact of Multiple Sclerosis," 2010. [Online]. Available: https://www.msif.org/wp-content/uploads/2014/09/Global_economic_impact_of_MS.pdf

[29] P. Andlin-Sobocki, B. Jonsson, H. U. Wittchen, and J. Olesen, "Cost of disorders of the brain in Europe," *Eur J Neurol,* vol. 12 Suppl 1, pp. 1-27, Jun 2005, doi: 10.1111/j.1468-1331.2005.01202.x.

[30] A. J. Thompson, B. L. Banwell, F. Barkhof, W. M. Carroll, T. Coetzee, G. Comi, J. Correale, F. Fazekas, M. Filippi, M. S. Freedman, K. Fujihara, S. L. Galetta, H. P. Hartung, L. Kappos, F. D. Lublin, R. A. Marrie, A. E. Miller, D. H. Miller, X. Montalban, E. M. Mowry, P. S. Sorensen, M. Tintore, A. L. Traboulsee, M. Trojano, B. M. J. Uitdehaag, S. Vukusic, E. Waubant, B. G. Weinshenker, S. C. Reingold, and J. A. Cohen, "Diagnosis of multiple sclerosis: 2017 revisions of the McDonald criteria," *Lancet Neurology,* vol. 17, no. 2, pp. 162-173, Feb 2018. [Online]. Available: <Go to ISI>://WOS:000422828500014.

[31] R. J. Franklin and C. Ffrench-Constant, "Remyelination in the CNS: from biology to therapy," *Nat Rev Neurosci,* vol. 9, no. 11, pp. 839-55, Nov 2008, doi: 10.1038/nrn2480.

[32] M. J. Craner, J. Newcombe, J. A. Black, C. Hartle, M. L. Cuzner, and S. G. Waxman, "Molecular changes in neurons in multiple sclerosis: altered axonal expression of Nav1.2 and Nav1.6 sodium channels and Na+/Ca2+ exchanger," *Proceedings of the National Academy of Sciences of the United States of America,* vol. 101, no. 21, pp. 8168-73, May 25 2004, doi: 10.1073/pnas.0402765101.

[33] V. Tomassini, P. M. Matthews, A. J. Thompson, D. Fuglo, J. J. Geurts, H. Johansen-Berg, D. K. Jones, M. A. Rocca, R. G. Wise, F. Barkhof, and J. Palace, "Neuroplasticity

and functional recovery in multiple sclerosis," *Nat Rev Neurol,* vol. 8, no. 11, pp. 635-46, Nov 5 2012, doi: 10.1038/nrneurol.2012.179.

[34] J. Sastre-Garriga, G. T. Ingle, D. T. Chard, M. Cercignani, L. Ramio-Torrenta, D. H. Miller, and A. J. Thompson, "Grey and white matter volume changes in early primary progressive multiple sclerosis: a longitudinal study," *Brain,* vol. 128, no. Pt 6, pp. 1454-60, Jun 2005, doi: 10.1093/brain/awh498.

[35] J. Sepulcre, J. Sastre-Garriga, M. Cercignani, G. T. Ingle, D. H. Miller, and A. J. Thompson, "Regional gray matter atrophy in early primary progressive multiple sclerosis: a voxel-based morphometry study," *Arch Neurol,* vol. 63, no. 8, pp. 1175-80, Aug 2006, doi: 10.1001/archneur.63.8.1175.

[36] K. Ahrweiller, C. Rousseau, E. Le Page, E. Bajeux, E. Leray, L. Michel, G. Edan, and A. Kerbrat, "Decreasing impact of late relapses on disability worsening in secondary progressive multiple sclerosis," *Mult Scler,* p. 1352458519848090, May 16 2019, doi: 10.1177/1352458519848090.

[37] G. C. Ebers, "Natural history of primary progressive multiple sclerosis," *Mult Scler,* vol. 10 Suppl 1, pp. S8-13; discussion S13-5, Jun 2004. [Online]. Available: https://www.ncbi.nlm.nih.gov/pubmed/15218804.

[38] B. G. Weinshenker, B. Bass, G. P. Rice, J. Noseworthy, W. Carriere, J. Baskerville, and G. C. Ebers, "The natural history of multiple sclerosis: a geographically based study. I. Clinical course and disability," *Brain,* vol. 112 (Pt 1), pp. 133-46, Feb 1989, doi: 10.1093/brain/112.1.133.

[39] A. J. Thompson, S. E. Baranzini, J. Geurts, B. Hemmer, and O. Ciccarelli, "Multiple sclerosis," *Lancet,* vol. 391, no. 10130, pp. 1622-1636, Apr 21 2018, doi: 10.1016/S0140-6736(18)30481-1.

[40] A. Kutzelnigg, C. F. Lucchinetti, C. Stadelmann, W. Bruck, H. Rauschka, M. Bergmann, M. Schmidbauer, J. E. Parisi, and H. Lassmann, "Cortical demyelination and diffuse white matter injury in multiple sclerosis," *Brain,* vol. 128, no. Pt 11, pp. 2705-12, Nov 2005, doi: 10.1093/brain/awh641.

[41] L. Haider, C. Simeonidou, G. Steinberger, S. Hametner, N. Grigoriadis, G. Deretzi, G. G. Kovacs, A. Kutzelnigg, H. Lassmann, and J. M. Frischer, "Multiple sclerosis deep grey matter: the relation between demyelination, neurodegeneration, inflammation and iron," *J Neurol Neurosurg Psychiatry,* vol. 85, no. 12, pp. 1386-95, Dec 2014, doi: 10.1136/jnnp-2014-307712.

[42] J. M. Frischer, S. Bramow, A. Dal-Bianco, C. F. Lucchinetti, H. Rauschka, M. Schmidbauer, H. Laursen, P. S. Sorensen, and H. Lassmann, "The relation between inflammation and neurodegeneration in multiple sclerosis brains," *Brain,* vol. 132, no. Pt 5, pp. 1175-89, May 2009, doi: 10.1093/brain/awp070.

[43] M. T. Fischer, R. Sharma, J. L. Lim, L. Haider, J. M. Frischer, J. Drexhage, D. Mahad, M. Bradl, J. van Horssen, and H. Lassmann, "NADPH oxidase expression in active multiple sclerosis lesions in relation to oxidative tissue damage and mitochondrial injury," *Brain,* vol. 135, no. Pt 3, pp. 886-99, Mar 2012, doi: 10.1093/brain/aws012.

[44] G. P. Rice, M. Kremenchutzky, D. A. Cottrell, J. Baskerville, and G. C. Ebers, in *Topics in Neuroscience: Primary Progressive Multiple Sclerosis*, M. Filippi and G. Comi Eds.

Milano: Springer Verlag Italia, 2002, ch. Observations from the natural history cohort of London, Ontario, pp. 5-10.

[45] F. De Angelis, N. A. John, and W. J. Brownlee, "Disease-modifying therapies for multiple sclerosis," *BMJ,* vol. 363, p. k4674, Nov 27 2018, doi: 10.1136/bmj.k4674.

[46] T. Masterman, A. Ligers, T. Olsson, M. Andersson, O. Olerup, and J. Hillert, "HLA-DR15 is associated with lower age at onset in multiple sclerosis," *Ann Neurol,* vol. 48, no. 2, pp. 211-9, Aug 2000. [Online]. Available: https://www.ncbi.nlm.nih.gov/pubmed/10939572.

[47] T. Masterman and J. Hillert, "HLA-DR15 and age at onset in multiple sclerosis," *Eur J Neurol,* vol. 9, no. 2, pp. 179-80, Mar 2002. [Online]. Available: https://www.ncbi.nlm.nih.gov/pubmed/11882062.

[48] R. Magliozzi, O. Howell, A. Vora, B. Serafini, R. Nicholas, M. Puopolo, R. Reynolds, and F. Aloisi, "Meningeal B-cell follicles in secondary progressive multiple sclerosis associate with early onset of disease and severe cortical pathology," *Brain,* vol. 130, no. Pt 4, pp. 1089-104, Apr 2007, doi: 10.1093/brain/awm038.

[49] B. Serafini, B. Rosicarelli, R. Magliozzi, E. Stigliano, and F. Aloisi, "Detection of ectopic B-cell follicles with germinal centers in the meninges of patients with secondary progressive multiple sclerosis," *Brain Pathol,* vol. 14, no. 2, pp. 164-74, Apr 2004. [Online]. Available: https://www.ncbi.nlm.nih.gov/pubmed/15193029.

[50] S. R. Choi, O. W. Howell, D. Carassiti, R. Magliozzi, D. Gveric, P. A. Muraro, R. Nicholas, F. Roncaroli, and R. Reynolds, "Meningeal inflammation plays a role in the pathology of primary progressive multiple sclerosis," *Brain,* vol. 135, no. Pt 10, pp. 2925-37, Oct 2012, doi: 10.1093/brain/aws189.

[51] D. A. Cottrell, M. Kremenchutzky, G. P. Rice, W. J. Koopman, W. Hader, J. Baskerville, and G. C. Ebers, "The natural history of multiple sclerosis: a geographically based study. 5. The clinical features and natural history of primary progressive multiple sclerosis," *Brain,* vol. 122 (Pt 4), pp. 625-39, Apr 1999, doi: 10.1093/brain/122.4.625.

[52] M. Filippi, A. Campi, V. Martinelli, M. Rodegher, G. Scotti, N. Canal, and G. Comi, "A brain MRI study of different types of chronic-progressive multiple sclerosis," *Acta Neurol Scand,* vol. 91, no. 4, pp. 231-3, Apr 1995, doi: 10.1111/j.1600-0404.1995.tb06995.x.

[53] A. J. Thompson, A. G. Kermode, D. G. MacManus, B. E. Kendall, D. P. Kingsley, I. F. Moseley, and W. I. McDonald, "Patterns of disease activity in multiple sclerosis: clinical and magnetic resonance imaging study," *BMJ,* vol. 300, no. 6725, pp. 631-4, Mar 10 1990, doi: 10.1136/bmj.300.6725.631.

[54] A. J. Thompson, A. G. Kermode, D. Wicks, D. G. MacManus, B. E. Kendall, D. P. Kingsley, and W. I. McDonald, "Major differences in the dynamics of primary and secondary progressive multiple sclerosis," *Ann Neurol,* vol. 29, no. 1, pp. 53-62, Jan 1991, doi: 10.1002/ana.410290111.

[55] S. Bramow, J. M. Frischer, H. Lassmann, N. Koch-Henriksen, C. F. Lucchinetti, P. S. Sorensen, and H. Laursen, "Demyelination versus remyelination in progressive multiple sclerosis," *Brain,* vol. 133, no. 10, pp. 2983-98, Oct 2010, doi: 10.1093/brain/awq250.

[56] D. Kidd, A. J. Thompson, D. H. Miller, A. G. Kermode, D. G. MacManus, and W. I. McDonald, "MRI activity and disability in multiple sclerosis: A two-year study [Abstract]," *J Neurol Neurosurg Psychiatry,* vol. 55, p. 1213, 1992.

[57] O. Olerup, J. Hillert, S. Fredrikson, T. Olsson, S. Kam-Hansen, E. Moller, B. Carlsson, and J. Wallin, "Primarily chronic progressive and relapsing/remitting multiple sclerosis: two immunogenetically distinct disease entities," *Proceedings of the National Academy of Sciences of the United States of America,* vol. 86, no. 18, pp. 7113-7, Sep 1989, doi: 10.1073/pnas.86.18.7113.

[58] J. M. Greer and M. P. Pender, "The presence of glutamic acid at positions 71 or 74 in pocket 4 of the HLA-DRbeta1 chain is associated with the clinical course of multiple sclerosis," *J Neurol Neurosurg Psychiatry,* vol. 76, no. 5, pp. 656-62, May 2005, doi: 10.1136/jnnp.2004.042168.

[59] T. Revesz, D. Kidd, A. J. Thompson, R. O. Barnard, and W. I. McDonald, "A comparison of the pathology of primary and secondary progressive multiple sclerosis," *Brain,* vol. 117 (Pt 4), pp. 759-65, Aug 1994, doi: 10.1093/brain/117.4.759.

[60] D. Ontaneda, A. J. Thompson, R. J. Fox, and J. A. Cohen, "Progressive multiple sclerosis: prospects for disease therapy, repair, and restoration of function," *Lancet,* Nov 23 2016, doi: 10.1016/S0140-6736(16)31320-4.

[61] B. Hemmer, M. Kerschensteiner, and T. Korn, "Role of the innate and adaptive immune responses in the course of multiple sclerosis," *Lancet Neurol,* vol. 14, no. 4, pp. 406-19, Apr 2015, doi: 10.1016/S1474-4422(14)70305-9.

[62] I. Y. Choi, S. P. Lee, D. R. Denney, and S. G. Lynch, "Lower levels of glutathione in the brains of secondary progressive multiple sclerosis patients measured by 1H magnetic resonance chemical shift imaging at 3 T," *Mult Scler,* vol. 17, no. 3, pp. 289-96, Mar 2010. [Online].

[63] R. L. Zuvich, J. L. McCauley, M. A. Pericak-Vance, and J. L. Haines, "Genetics and pathogenesis of multiple sclerosis," *Semin Immunol,* vol. 21, no. 6, pp. 328-33, Dec 2009, doi: 10.1016/j.smim.2009.08.003.

[64] W. J. Brownlee, T. A. Hardy, F. Fazekas, and D. H. Miller, "Diagnosis of multiple sclerosis: progress and challenges," *Lancet,* Nov 23 2016, doi: 10.1016/S0140-6736(16)30959-X.

[65] A. J. Solomon, E. P. Klein, and D. Bourdette, ""Undiagnosing" multiple sclerosis: the challenge of misdiagnosis in MS," *Neurology,* vol. 78, no. 24, pp. 1986-91, Jun 12 2012, doi: 10.1212/WNL.0b013e318259e1b2.

[66] M. Pugliatti, "Multiple sclerosis: preventing progression and disability in MS-when to treat?," *Nat Rev Neurol,* vol. 9, no. 3, pp. 129-30, Mar 2013, doi: 10.1038/nrneurol.2013.28.

[67] I. K. Sand, S. Krieger, C. Farrell, and A. E. Miller, "Diagnostic uncertainty during the transition to secondary progressive multiple sclerosis," *Mult Scler J,* vol. 20, no. 12, pp. 1654-1657, Oct 2014. [Online]. Available: <Go to ISI>://WOS:000344136400016.

[68] F. Gobbin, A. Marangi, R. Orlandi, S. Monaco, M. D. Benedetti, and A. Gajofatto, "Sensitivity and specificity of 2017 McDonald criteria for multiple sclerosis in patients with clinically isolated syndrome," *Mult Scler J,* vol. 24, pp. 531-532, Oct 2018. [Online]. Available: <Go to ISI>://WOS:000446861401319.

[69] A. C. Santos, S. Narayanan, N. de Stefano, M. C. Tartaglia, S. J. Francis, R. Arnaoutelis, Z. Caramanos, J. P. Antel, G. B. Pike, and D. L. Arnold, "Magnetization transfer can predict clinical evolution in patients with multiple sclerosis," *J Neurol,* vol. 249, no. 6, pp. 662-668, Jun 2002. [Online]. Available: <Go to ISI>://WOS:000176407100002.

[70] Z. Khaleeli, D. R. Altmann, M. Cercignani, O. Ciccarelli, D. H. Miller, and A. J. Thompson, "Magnetization Transfer Ratio in Gray Matter A Potential Surrogate Marker for Progression in Early Primary Progressive Multiple Sclerosis," *Arch Neurol-Chicago,* vol. 65, no. 11, pp. 1454-1459, Nov 2008. [Online]. Available: <Go to ISI>://WOS:000260797200007.

[71] R. J. Fox, "Picturing Multiple Sclerosis: Conventional and Diffusion Tensor Imaging," *Semin Neurol,* vol. 28, no. 4, pp. 453-466, Sep 2008. [Online]. Available: <Go to ISI>://WOS:000260171100007.

[72] R. J. Fox, E. Beall, P. Bhattacharyya, J. T. Chen, and K. Sakaie, "Advanced MRI in Multiple Sclerosis: Current Status and Future Challenges," *Neurol Clin,* vol. 29, no. 2, pp. 357-+, May 2011. [Online]. Available: <Go to ISI>://WOS:000289815200011.

[73] G. Y. Wu, Q. Zhang, J. L. Wu, L. Jing, Y. Tan, T. C. Qiu, and J. Zhao, "Changes in cerebral metabolites in type 2 diabetes mellitus: A meta-analysis of proton magnetic resonance spectroscopy," *J Clin Neurosci,* vol. 45, pp. 9-13, Nov 2017, doi: 10.1016/j.jocn.2017.07.017.

[74] A. Zimny, M. Szmyrka-Kaczmarek, P. Szewczyk, J. Bladowska, A. Pokryszko-Dragan, E. Gruszka, P. Wiland, and M. Sasiadek, "In vivo evaluation of brain damage in the course of systemic lupus erythematosus using magnetic resonance spectroscopy, perfusion-weighted and diffusion-tensor imaging," *Lupus,* vol. 23, no. 1, pp. 10-9, 2014, doi: 10.1177/0961203313511556.

[75] D. Bairwa, V. Kumar, S. Vyas, B. K. Das, A. K. Srivastava, R. M. Pandey, S. K. Sharma, N. R. Jagannathan, and S. Sinha, "Case control study: magnetic resonance spectroscopy

of brain in HIV infected patients," *BMC Neurol,* vol. 16, p. 99, Jul 12 2016, doi: 10.1186/s12883-016-0628-x.

[76] A. Bizzi, A. M. Ulug, T. O. Crawford, T. Passe, M. Bugiani, R. N. Bryan, and P. B. Barker, "Quantitative proton MR spectroscopic imaging in acute disseminated encephalomyelitis," *AJNR Am J Neuroradiol,* vol. 22, no. 6, pp. 1125-30, Jun-Jul 2001. [Online]. Available: https://www.ncbi.nlm.nih.gov/pubmed/11415908.

[77] A. Nitkunan, R. A. Charlton, T. R. Barrick, D. J. McIntyre, F. A. Howe, and H. S. Markus, "Reduced N-acetylaspartate is consistent with axonal dysfunction in cerebral small vessel disease," *NMR Biomed,* vol. 22, no. 3, pp. 285-91, Apr 2009, doi: 10.1002/nbm.1322.

[78] N. De Stefano, Z. Caramanos, M. C. Preul, G. Francis, J. P. Antel, and D. L. Arnold, "In vivo differentiation of astrocytic brain tumors and isolated demyelinating lesions of the type seen in multiple sclerosis using 1H magnetic resonance spectroscopic imaging," *Ann Neurol,* vol. 44, no. 2, pp. 273-8, Aug 1998, doi: 10.1002/ana.410440222.

[79] Y. Duan, Z. Liu, Y. Liu, J. Huang, Z. Ren, Z. Sun, H. Chen, H. Dong, J. Ye, and K. Li, "Metabolic changes in normal-appearing white matter in patients with neuromyelitis optica and multiple sclerosis: a comparative magnetic resonance spectroscopy study," *Acta Radiol,* vol. 58, no. 9, pp. 1132-1137, Sep 2017, doi: 10.1177/0284185116683575.

[80] J. de Seze, F. Blanc, S. Kremer, N. Collongues, M. Fleury, C. Marcel, and I. J. Namer, "Magnetic resonance spectroscopy evaluation in patients with neuromyelitis optica," *J Neurol Neurosurg Psychiatry,* vol. 81, no. 4, pp. 409-11, Apr 2010, doi: 10.1136/jnnp.2008.168070.

[81] A. Tourbah, J. L. Stievenart, O. Gout, B. Fontaine, R. Liblau, C. Lubetzki, E. A. Cabanis, and O. Lyon-Caen, "Localized proton magnetic resonance spectroscopy in relapsing remitting versus secondary progressive multiple sclerosis," *Neurology,* vol. 53, no. 5, pp. 1091-1091, 1999, doi: 10.1212/wnl.53.5.1091.

[82] N. De Stefano, S. Narayanan, G. S. Francis, R. Arnaoutelis, M. C. Tartaglia, J. P. Antel, P. M. Matthews, and D. L. Arnold, "Evidence of axonal damage in the early stages of multiple sclerosis and its relevance to disability," *Arch Neurol-Chicago,* vol. 58, no. 1, pp. 65-70, Jan 2001, doi: DOI 10.1001/archneur.58.1.65.

[83] F. Aboul-Enein, M. Krssak, R. Hoftberger, D. Prayer, and W. Kristoferitsch, "Reduced NAA-levels in the NAWM of patients with MS is a feature of progression. A study with quantitative magnetic resonance spectroscopy at 3 Tesla," *PLoS One,* vol. 5, no. 7, p. e11625, Jul 20 2010, doi: 10.1371/journal.pone.0011625.

[84] P. Sarchielli, O. Presciutti, G. P. Pelliccioli, R. Tarducci, G. Gobbi, P. Chiarini, A. Alberti, E. Vicinanza, and V. Gallai, "Absolute quantification of brain metabolites by proton magnetic resonance spectroscopy in normal-appearing white matter of multiple sclerosis patients," *Brain,* vol. 122, pp. 513-521, Mar 1999. [Online]. Available: <Go to ISI>://WOS:000079340800012.

[85] M. C. Gustafsson, O. Dahlqvist, J. Jaworski, P. Lundberg, and A. M. Landtblom, "Low choline concentrations in normal-appearing white matter of patients with multiple sclerosis and normal MR imaging brain scans," *AJNR Am J Neuroradiol,* vol. 28, no. 7, pp. 1306-12, Aug 2007, doi: 10.3174/ajnr.A0580.

[86] *meta: An R package for meta-analysis*. (2007).

[87] Z. Caramanos, S. Narayanan, and D. L. Arnold, "1H-MRS quantification of tNA and tCr in patients with multiple sclerosis: a meta-analytic review," *Brain,* vol. 128, no. Pt 11, pp. 2483-506, Nov 2005, doi: 10.1093/brain/awh640.

[88] C. Choi, S. K. Ganji, R. J. DeBerardinis, K. J. Hatanpaa, D. Rakheja, Z. Kovacs, X. L. Yang, T. Mashimo, J. M. Raisanen, I. Marin-Valencia, J. M. Pascual, C. J. Madden, B. E. Mickey, C. R. Malloy, R. M. Bachoo, and E. A. Maher, "2-hydroxyglutarate detection by magnetic resonance spectroscopy in IDH-mutated patients with gliomas," *Nat Med,* vol. 18, no. 4, pp. 624-9, Jan 26 2012, doi: 10.1038/nm.2682.

[89] C. H. Suh, H. S. Kim, S. C. Jung, C. G. Choi, and S. J. Kim, "2-hydroxyglutarate MR Spectroscopy for Prediction of Isocitrate Dehydrogenase Mutant Glioma: A Systemic Review and Meta-analysis using Individual Patient Data," *Neuro Oncol,* Jul 18 2018, doi: 10.1093/neuonc/noy113.

[90] O. C. Andronesi, "Precision oncology in the era of radiogenomics: the case of D-2HG as an imaging biomarker for mutant IDH gliomas," *Neuro Oncol,* vol. 20, no. 7, pp. 865-867, Jun 18 2018, doi: 10.1093/neuonc/noy085.

[91] M. Wilson, O. Andronesi, P. B. Barker, R. Bartha, A. Bizzi, P. J. Bolan, K. M. Brindle, I. Y. Choi, C. Cudalbu, U. Dydak, U. E. Emir, R. G. Gonzalez, S. Gruber, R. Gruetter, R. K. Gupta, A. Heerschap, A. Henning, H. P. Hetherington, P. S. Huppi, R. E. Hurd, K. Kantarci, R. A. Kauppinen, D. W. J. Klomp, R. Kreis, M. J. Kruiskamp, M. O. Leach, A. P. Lin, P. R. Luijten, M. Marjanska, A. A. Maudsley, D. J. Meyerhoff, C. E. Mountford, P. G. Mullins, J. B. Murdoch, S. J. Nelson, R. Noeske, G. Oz, J. W. Pan, A. C. Peet, H. Poptani, S. Posse, E. M. Ratai, N. Salibi, T. W. J. Scheenen, I. C. P. Smith, B. J. Soher, I. Tkác, D. B. Vigneron, and F. A. Howe, "Methodological consensus on clinical proton

MRS of the brain: Review and recommendations," *Magn Reson Med,* vol. 82, no. 2, pp. 527-550, Aug 2019, doi: 10.1002/mrm.27742.

[92] V. Wottschel, D. C. Alexander, P. P. Kwok, D. T. Chard, M. L. Stromillo, N. De Stefano, A. J. Thompson, D. H. Miller, and O. Ciccarelli, "Predicting outcome in clinically isolated syndrome using machine learning," *Neuroimage Clin,* vol. 7, pp. 281-7, 2015, doi: 10.1016/j.nicl.2014.11.021.

[93] A. Ion-Margineanu, G. Kocevar, C. Stamile, D. M. Sima, F. Durand-Dubief, S. Van Huffel, and D. Sappey-Marinier, "Machine Learning Approach for Classifying Multiple Sclerosis Courses by Combining Clinical Data with Lesion Loads and Magnetic Resonance Metabolic Features," *Front Neurosci,* vol. 11, p. 398, 2017, doi: 10.3389/fnins.2017.00398.

[94] F. Pedregosa, G. Varoquaux, A. Gramfort, V. Michel, B. Thirion, O. Grisel, M. Blondel, P. Prettenhofer, R. Weiss, V. Dubourg, J. Vanderplas, A. Passos, D. Cournapeau, M. Brucher, M. Perrot, and E. Duchesnay, "Scikit-learn: Machine Learning in Python," *J Mach Learn Res,* vol. 12, pp. 2825-2830, Oct 2011. [Online]. Available: <Go to ISI>://WOS:000298103200003.

[95] A. Paszke, S. Gross, S. Chintala, G. Chanan, E. Yang, Z. DeVito, Z. Lin, A. Desmaison, L. Antiga, and A. Lerer, "Automatic differentiation in PyTorch," presented at the NIPS 2017 Workshop Autodiff, 2017.

[96] M. Abadi, A. Agarwal, P. Barham, E. Brevdo, Z. Chen, C. Citro, G. Corrado, A. Davis, J. Dean, M. Devin, S. Ghemawat, I. Goodfellow, A. Harp, G. Irving, M. Isard, R. Jozefowicz, Y. Jia, L. Kaiser, M. Kudlur, J. Levenberg, D. Mané, M. Schuster, R. Monga, S. Moore, D. Murray, C. Olah, J. Shlens, B. Steiner, I. Sutskever, K. Talwar, R.

Tucker, V. Vanhoucke, V. Vasudevan, F. Viégas, O. Vinyals, P. Warden, M. Wattenberg, M. Wicke, Y. Yu, and X. Zheng, "TensorFlow: Large-scale machine learning on heterogeneous systems," *Software available from tensorflow.org,* 2015.

[97] *R: A language and environment for statistical computing*. (2010). R Foundation for Statistical Computing, Vienna, Austria.

[98] A. V. Kurada, K. M. Swanberg, H. Prinsen, and C. Juchem, "Diagnosis of multiple sclerosis subtype through machine learning analysis of frontal cortex metabolite profiles," *Proc Int Soc Magn Reson Med,* no. 4871, 2019.

[99] C. Barbour, P. Kosa, M. Komori, M. Tanigawa, R. Masvekar, T. Wu, K. Johnson, P. Douvaras, V. Fossati, R. Herbst, Y. Wang, K. Tan, M. Greenwood, and B. Bielekova, "Molecular-based diagnosis of multiple sclerosis and its progressive stage," *Ann Neurol,* vol. 82, no. 5, pp. 795-812, Nov 2017, doi: 10.1002/ana.25083.

[100] Committee on the Assessment of Ongoing Efforts in the Treatment of Posttraumatic Stress Disorder; Board on the Health of Select Populations; Institute of Medicine. *Treatment for Posttraumatic Stress Disorder in Military and Veteran Populations: Final Assessment.* Washington (DC): National Academies Press (US), 2014.

[101] J. I. Bisson, S. Cosgrove, C. Lewis, and N. P. Robert, "Post-traumatic stress disorder," *BMJ,* vol. 351, p. h6161, Nov 26 2015, doi: 10.1136/bmj.h6161.

[102] X. R. Miao, Q. B. Chen, K. Wei, K. M. Tao, and Z. J. Lu, "Posttraumatic stress disorder: from diagnosis to prevention," *Mil Med Res,* vol. 5, no. 1, p. 32, Sep 28 2018, doi: 10.1186/s40779-018-0179-0.

[103] C. S. de Kloet, E. Vermetten, E. Geuze, A. Kavelaars, C. J. Heijnen, and H. G. Westenberg, "Assessment of HPA-axis function in posttraumatic stress disorder:

pharmacological and non-pharmacological challenge tests, a review," *J Psychiatr Res,* vol. 40, no. 6, pp. 550-67, Sep 2006, doi: 10.1016/j.jpsychires.2005.08.002.

[104] A. Karl and A. Werner, "The use of proton magnetic resonance spectroscopy in PTSD research--meta-analyses of findings and methodological review," *Neurosci Biobehav Rev,* vol. 34, no. 1, pp. 7-22, Jan 2010, doi: 10.1016/j.neubiorev.2009.06.008.

[105] S. Quadrelli, C. Mountford, and S. Ramadan, "Systematic review of in-vivo neuro magnetic resonance spectroscopy for the assessment of posttraumatic stress disorder," *Psychiatry Res Neuroimaging,* vol. 282, pp. 110-125, Dec 30 2018, doi: 10.1016/j.pscychresns.2018.07.001.

[106] H. Prinsen, R. A. de Graaf, G. F. Mason, D. Pelletier, and C. Juchem, "Reproducibility measurement of glutathione, GABA, and glutamate: Towards in vivo neurochemical profiling of multiple sclerosis with MR spectroscopy at 7T," *J Magn Reson Imaging,* vol. 45, no. 1, pp. 187-198, Jan 2017, doi: 10.1002/jmri.25356.

[107] G. Oz, J. R. Alger, P. B. Barker, R. Bartha, A. Bizzi, C. Boesch, P. J. Bolan, K. M. Brindle, C. Cudalbu, A. Dincer, U. Dydak, U. E. Emir, J. Frahm, R. G. Gonzalez, S. Gruber, R. Gruetter, R. K. Gupta, A. Heerschap, A. Henning, H. P. Hetherington, F. A. Howe, P. S. Huppi, R. E. Hurd, K. Kantarci, D. W. Klomp, R. Kreis, M. J. Kruiskamp, M. O. Leach, A. P. Lin, P. R. Luijten, M. Marjanska, A. A. Maudsley, D. J. Meyerhoff, C. E. Mountford, S. J. Nelson, M. N. Pamir, J. W. Pan, A. C. Peet, H. Poptani, S. Posse, P. J. Pouwels, E. M. Ratai, B. D. Ross, T. W. Scheenen, C. Schuster, I. C. Smith, B. J. Soher, I. Tkác, D. B. Vigneron, R. A. Kauppinen, and M. R. S. C. Group, "Clinical proton MR spectroscopy in central nervous system disorders," *Radiology,* vol. 270, no. 3, pp. 658-79, Mar 2014, doi: 10.1148/radiol.13130531.

[108] J. J. Geurts, I. E. Reuling, H. Vrenken, B. M. Uitdehaag, C. H. Polman, J. A. Castelijns, F. Barkhof, and P. J. Pouwels, "MR spectroscopic evidence for thalamic and hippocampal, but not cortical, damage in multiple sclerosis," *Magn Reson Med,* vol. 55, no. 3, pp. 478-83, Mar 2006, doi: 10.1002/mrm.20792.

[109] L. T. Lucato, M. C. Otaduy, E. R. Barbosa, A. A. Machado, A. McKinney, L. A. Bacheschi, M. Scaff, G. G. Cerri, and C. C. Leite, "Proton MR spectroscopy in Wilson disease: analysis of 36 cases," *AJNR Am J Neuroradiol,* vol. 26, no. 5, pp. 1066-71, May 2005. [Online]. Available: http://www.ncbi.nlm.nih.gov/pubmed/15891161.

[110] P. J. Pouwels, K. Brockmann, B. Kruse, B. Wilken, M. Wick, F. Hanefeld, and J. Frahm, "Regional age dependence of human brain metabolites from infancy to adulthood as detected by quantitative localized proton MRS," *Pediatr Res,* vol. 46, no. 4, pp. 474-85, Oct 1999, doi: 10.1203/00006450-199910000-00019.

[111] R. Bartha, "Effect of signal-to-noise ratio and spectral linewidth on metabolite quantification at 4 T," *NMR Biomed,* vol. 20, no. 5, pp. 512-21, Aug 2007, doi: 10.1002/nbm.1122.

[112] M. Kanowski, J. Kaufmann, J. Braun, J. Bernarding, and C. Tempelmann, "Quantitation of simulated short echo time 1H human brain spectra by LCModel and AMARES," *Magn Reson Med,* vol. 51, no. 5, pp. 904-12, May 2004, doi: 10.1002/mrm.20063.

[113] R. Kreis and C. Boesch, "Bad Spectra Can Be Better Than Good Spectra," *Proc. Intl. Soc. Mag. Reson. Med.,* vol. 11, 2003 2003.

[114] A. J. L. Cooper, "Role of astrocytes in maintaining cerebral glutathione homeostasis and in protecting in the brain against xenobiotics and oxidative stress," in *Glutathione in the Nervous System*, C. A. Shaw Ed. Washington, DC: CRC Press, 1998.

[115] R. Bhat, R. Axtell, A. Mitra, M. Miranda, C. Lock, R. W. Tsien, and L. Steinman, "Inhibitory role for GABA in autoimmune inflammation," *Proceedings of the National Academy of Sciences of the United States of America,* vol. 107, no. 6, pp. 2580-5, Feb 9 2010. [Online].

[116] K. M. Swanberg, H. Prinsen, D. Coman, R. A. de Graaf, and C. Juchem, "Quantification of glutathione transverse relaxation time T2 using echo time extension with variable refocusing selectivity and symmetry in the human brain at 7 Tesla," *J Magn Reson,* vol. 290, pp. 1-11, May 2018, doi: 10.1016/j.jmr.2018.02.017.

[117] R. A. de Graaf, G. M. Chowdhury, and K. L. Behar, "Quantification of high-resolution (1)H NMR spectra from rat brain extracts," *Anal Chem,* vol. 83, no. 1, pp. 216-24, Jan 1 2011, doi: 10.1021/ac102285c.

[118] U. Klose, "In vivo proton spectroscopy in presence of eddy currents," *Magn Reson Med,* vol. 14, no. 1, pp. 26-30, Apr 1990, doi: 10.1002/mrm.1910140104.

[119] S. M. Wright and L. L. Wald, "Theory and application of array coils in MR spectroscopy," *NMR Biomed,* vol. 10, no. 8, pp. 394-410, Dec 1997, doi: 10.1002/(sici)1099-1492(199712)10:8<394::aid-nbm494>3.0.co;2-0.

[120] M. Gajdošík, K. Landheer, K. M. Swanberg, and C. Juchem, "INSPECTOR: free software for magnetic resonance spectroscopy data inspection, processing, simulation and analysis," *Sci Rep,* vol. 11, no. 1, p. 2094, Jan 22 2021, doi: 10.1038/s41598-021-81193-9.

[121] S. Cavassila, S. Deval, C. Huegen, D. van Ormondt, and D. Graveron-Demilly, "Cramer-Rao bounds: an evaluation tool for quantitation," *NMR Biomed,* vol. 14, no. 4, pp. 278-83, Jun 2001, doi: 10.1002/nbm.701.

[122] K. M. Swanberg, H. Prinsen, and C. Juchem, "Spectral quality differentially affects apparent metabolite concentrations as estimated by linear combination modeling of in vivo magnetic resonance spectroscopy data at 7 Tesla," *Proc Int Soc Magn Reson Med,* no. 4237, 2019.

[123] C. Cudalbu, O. Beuf, and S. Cavassila, "In Vivo Short Echo Time Localized H-1 MRS of the Rat Brain at 7 T: Influence of Two Strategies of Background-accommodation on the Metabolite Concentration Estimation using QUEST," *J Signal Process Sys,* vol. 55, no. 1-3, pp. 25-34, Apr 2009, doi: 10.1007/s11265-008-0187-5.

[124] Y. Zhang and J. Shen, "Smoothness of In Vivo Spectral Baseline Determined by Mean-Square Error," *Magnet Reson Med,* vol. 72, no. 4, pp. 913-922, Oct 2014, doi: 10.1002/mrm.25013.

[125] F. Sanaei Nezhad, A. Anton, L. M. Parkes, B. Deakin, and S. R. Williams, "Quantification of glutathione in the human brain by MR spectroscopy at 3 Tesla: Comparison of PRESS and MEGA-PRESS," *Magn Reson Med,* vol. 78, no. 4, pp. 1257-1266, Oct 2017, doi: 10.1002/mrm.26532.

[126] R. Bartha, D. J. Drost, and P. C. Williamson, "Factors affecting the quantification of short echo in-vivo 1H MR spectra: prior knowledge, peak elimination, and filtering," *NMR Biomed,* vol. 12, no. 4, pp. 205-16, Jun 1999. [Online]. Available: https://www.ncbi.nlm.nih.gov/pubmed/10421912.

[127] I. A. Giapitzakis, T. Borbath, S. Murali-Manohar, N. Avdievich, and A. Henning, "Investigation of the influence of macromolecules and spline baseline in the fitting model of human brain spectra at 9.4T," *Magn Reson Med,* vol. 81, no. 2, pp. 746-758, Feb 2019, doi: 10.1002/mrm.27467.

[128] R. J. Larsen, M. Newman, and A. Nikolaidis, "Reduction of variance in measurements of average metabolite concentration in anatomically-defined brain regions," *J Magn Reson,* vol. 272, pp. 73-81, Nov 2016, doi: 10.1016/j.jmr.2016.09.005.

[129] A. A. Bhogal, R. R. Schur, L. C. Houtepen, B. van de Bank, V. O. Boer, A. Marsman, P. B. Barker, T. W. J. Scheenen, J. P. Wijnen, C. H. Vinkers, and D. W. J. Klomp, "(1) H-MRS processing parameters affect metabolite quantification: The urgent need for uniform and transparent standardization," *NMR Biomed,* vol. 30, no. 11, Nov 2017, doi: 10.1002/nbm.3804.

[130] C. Cudalbu, V. Mlynarik, and R. Gruetter, "Handling macromolecule signals in the quantification of the neurochemical profile," *J Alzheimers Dis,* vol. 31 Suppl 3, pp. S101-15, 2012, doi: 10.3233/JAD-2012-120100.

[131] K. Landheer, M. Gajdošík, M. Treacy, and C. Juchem, "Concentration and effective T2 relaxation times of macromolecules at 3T," *Magn Reson Med,* vol. 84, no. 5, pp. 2327-2337, Nov 2020, doi: 10.1002/mrm.28282.

[132] K. Landheer and C. Juchem, "Dephasing optimization through coherence order pathway selection (DOTCOPS) for improved crusher schemes in MR spectroscopy," *Magn Reson Med,* vol. 81, no. 4, pp. 2209-2222, Apr 2019, doi: 10.1002/mrm.27587.

[133] K. Landheer and C. Juchem, "Simultaneous optimization of crusher and phase cycling schemes for magnetic resonance spectroscopy: an extension of dephasing optimization through coherence order pathway selection," *Magn Reson Med,* vol. 83, no. 2, pp. 391-402, Feb 2020, doi: 10.1002/mrm.27952.

[134] K. Landheer, K. M. Swanberg, and C. Juchem, "Magnetic resonance Spectrum simulator (MARSS), a novel software package for fast and computationally efficient basis set simulation," *NMR Biomed,* p. e4129, Jul 17 2019, doi: 10.1002/nbm.4129.

[135] I. Y. Choi, O. C. Andronesi, P. Barker, W. Bogner, R. A. E. Edden, L. G. Kaiser, P. Lee, M. Marjanska, M. Terpstra, and R. A. de Graaf, "Spectral editing in (1) H magnetic resonance spectroscopy: Experts' consensus recommendations," *NMR Biomed,* p. e4411, Sep 18 2020, doi: 10.1002/nbm.4411.

[136] G. Oz, D. K. Deelchand, J. P. Wijnen, V. Mlynarik, L. Xin, R. Mekle, R. Noeske, T. W. J. Scheenen, I. Tkác, and H. M. Experts' Working Group on Advanced Single Voxel, "Advanced single voxel (1) H magnetic resonance spectroscopy techniques in humans: Experts' consensus recommendations," *NMR Biomed,* p. e4236, Jan 10 2020, doi: 10.1002/nbm.4236.

[137] J. Near, A. D. Harris, C. Juchem, R. Kreis, M. Marjanska, G. Oz, J. Slotboom, M. Wilson, and C. Gasparovic, "Preprocessing, analysis and quantification in single-voxel magnetic resonance spectroscopy: experts' consensus recommendations," *NMR Biomed,* p. e4257, Feb 21 2020, doi: 10.1002/nbm.4257.

[138] R. Kreis, V. Boer, I. Y. Choi, C. Cudalbu, R. A. de Graaf, C. Gasparovic, A. Heerschap, M. Krssak, B. Lanz, A. A. Maudsley, M. Meyerspeer, J. Near, G. Oz, S. Posse, J. Slotboom, M. Terpstra, I. Tkác, M. Wilson, W. Bogner, and M. R. S. Experts' Working Group on Terminology for, "Terminology and concepts for the characterization of in vivo MR spectroscopy methods and MR spectra: Background and experts' consensus recommendations," *NMR Biomed,* p. e4347, Aug 17 2020, doi: 10.1002/nbm.4347.

[139] S. W. Provencher, "Estimation of metabolite concentrations from localized in vivo proton NMR spectra," *Magn Reson Med,* vol. 30, no. 6, pp. 672-9, Dec 1993, doi: 10.1002/mrm.1910300604.

[140] S. Cavassila, S. Deval, C. Huegen, D. van Ormondt, and D. Graveron-Demilly, "Cramer-Rao bound expressions for parametric estimation of overlapping peaks: influence of prior knowledge," *J Magn Reson,* vol. 143, no. 2, pp. 311-20, Apr 2000, doi: 10.1006/jmre.1999.2002.

[141] H. Ratiney, S. Cavassila, D. van Ormondt, and D. Graveron-Demilly, "Extended Cramér-Rao Lower Bounds: Background Accommodation," *Proceedings of the International Society for Magnetic Resonance in Medicine,* vol. 11, 2004.

[142] H. Ratiney, Y. Coenradie, S. Cavassila, D. van Ormondt, and D. Graveron-Demilly, "Time-domain quantitation of 1H short echo-time signals: background accommodation," *MAGMA,* vol. 16, no. 6, pp. 284-96, May 2004, doi: 10.1007/s10334-004-0037-9.

[143] C. Elster, F. Schubert, A. Link, M. Walzel, F. Seifert, and H. Rinneberg, "Quantitative magnetic resonance spectroscopy: semi-parametric modeling and determination of uncertainties," *Magn Reson Med,* vol. 53, no. 6, pp. 1288-96, Jun 2005, doi: 10.1002/mrm.20500.

[144] Y. Zhang and J. Shen, "Smoothness of in vivo spectral baseline determined by mean-square error," *Magn Reson Med,* vol. 72, no. 4, pp. 913-22, Oct 2014, doi: 10.1002/mrm.25013.

[145] K. M. Swanberg, K. Landheer, M. Gajdošík, M. S. Treacy, and C. Juchem., "Hunting the perfect spline: Baseline handling for accurate macromolecule estimation and metabolite quantification by in vivo 1H MRS," *Proc Int Soc Magn Reson Med,* no. 2020, 2019.

[146] N. Cawley, B. S. Solanky, N. Muhlert, C. Tur, R. A. Edden, C. A. Wheeler-Kingshott, D. H. Miller, A. J. Thompson, and O. Ciccarelli, "Reduced gamma-aminobutyric acid concentration is associated with physical disability in progressive multiple sclerosis," *Brain,* vol. 138, no. Pt 9, pp. 2584-95, Sep 2015, doi: 10.1093/brain/awv209.

[147] S. W. Provencher, *LCModel and LCMgui2 User's Manual*. 2005.

[148] M. Wilson and G. Reynolds, *Tarquin User Guide Version 4.3.5*. 2015.

[149] R. Kumar, S. Delshad, M. A. Woo, P. M. Macey, and R. M. Harper, "Age-related regional brain T2-relaxation changes in healthy adults," *J Magn Reson Imaging,* vol. 35, no. 2, pp. 300-8, Feb 2012, doi: 10.1002/jmri.22831.

[150] T. Usenius, J. P. Usenius, M. Tenhunen, P. Vainio, R. Johansson, S. Soimakallio, and R. Kauppinen, "Radiation-induced changes in human brain metabolites as studied by 1H nuclear magnetic resonance spectroscopy in vivo," *Int J Radiat Oncol Biol Phys,* vol. 33, no. 3, pp. 719-24, Oct 15 1995, doi: 10.1016/0360-3016(95)02011-Y.

[151] F. Jiru, A. Skoch, D. Wagnerova, M. Dezortova, J. Viskova, O. Profant, J. Syka, and M. Hajek, "The age dependence of T2 relaxation times of N-acetyl aspartate, creatine and choline in the human brain at 3 and 4T," *NMR Biomed,* vol. 29, no. 3, pp. 284-92, Mar 2016, doi: 10.1002/nbm.3456.

[152] T. Ernst, R. Kreis, and B. D. Ross, "Absolute quantitation of water and metabolites in the human brain. I. Compartments and water," *Journal of Magnetic Resonance,* vol. 102, no. 1, pp. 1-8, 1993.

[153] S. M. Smith, "Fast robust automated brain extraction," *Hum Brain Mapp,* vol. 17, no. 3, pp. 143-55, Nov 2002, doi: 10.1002/hbm.10062.

[154] D. W. Shattuck and R. M. Leahy, "BrainSuite: an automated cortical surface identification tool," *Med Image Anal,* vol. 6, no. 2, pp. 129-42, Jun 2002. [Online]. Available: https://www.ncbi.nlm.nih.gov/pubmed/12045000.

[155] M. Marjanska, J. R. McCarten, J. Hodges, L. S. Hemmy, A. Grant, D. K. Deelchand, and M. Terpstra, "Region-specific aging of the human brain as evidenced by neurochemical profiles measured noninvasively in the posterior cingulate cortex and the occipital lobe using (1)H magnetic resonance spectroscopy at 7 T," *Neuroscience,* vol. 354, pp. 168-177, Jun 23 2017, doi: 10.1016/j.neuroscience.2017.04.035.

[156] C. D. Browne P, Angood C, Tremlett H, Baker C, Taylor BV, Thompson AJ. , "Atlas of Multiple Sclerosis 2013: A growing global problem with widespread inequity," *Neurology,* vol. 83, no. 11, pp. 1022-24, 2013.

[157] O. Ciccarelli, F. Barkhof, B. Bodini, N. De Stefano, X. Golay, K. Nicolay, D. Pelletier, P. J. Pouwels, S. A. Smith, C. A. Wheeler-Kingshott, B. Stankoff, T. Yousry, and D. H. Miller, "Pathogenesis of multiple sclerosis: insights from molecular and metabolic imaging," *Lancet Neurol,* vol. 13, no. 8, pp. 807-22, Aug 2014, doi: 10.1016/S1474-4422(14)70101-2.

[158] K. K. Farh, A. Marson, J. Zhu, M. Kleinewietfeld, W. J. Housley, S. Beik, N. Shoresh, H. Whitton, R. J. Ryan, A. A. Shishkin, M. Hatan, M. J. Carrasco-Alfonso, D. Mayer, C. J. Luckey, N. A. Patsopoulos, P. L. De Jager, V. K. Kuchroo, C. B. Epstein, M. J. Daly, D. A. Hafler, and B. E. Bernstein, "Genetic and epigenetic fine mapping of causal autoimmune disease variants," *Nature,* vol. 518, no. 7539, pp. 337-43, Feb 19 2015, doi: 10.1038/nature13835.

[159] A. Ascherio, K. L. Munger, and J. D. Lunemann, "The initiation and prevention of multiple sclerosis," *Nat Rev Neurol,* vol. 8, no. 11, pp. 602-12, Nov 05 2012, doi: 10.1038/nrneurol.2012.198.

[160] C. Lucchinetti, W. Bruck, J. Parisi, B. Scheithauer, M. Rodriguez, and H. Lassmann, "Heterogeneity of multiple sclerosis lesions: implications for the pathogenesis of demyelination," *Ann Neurol,* vol. 47, no. 6, pp. 707-17, Jun 2000. [Online].

[161] G. Disanto, A. J. Berlanga, A. E. Handel, A. E. Para, A. M. Burrell, A. Fries, L. Handunnetthi, G. C. De Luca, and J. M. Morahan, "Heterogeneity in multiple sclerosis: scratching the surface of a complex disease," *Autoimmune Dis,* vol. 2011, p. 932351, Dec 09 2010, doi: 10.4061/2011/932351.

[162] C. A. Dendrou, L. Fugger, and M. A. Friese, "Immunopathology of multiple sclerosis," *Nat Rev Immunol,* vol. 15, no. 9, pp. 545-58, Sep 15 2015, doi: 10.1038/nri3871.

[163] C. J. Stagg and D. L. Rothman, *Magnetic resonance spectroscopy: tools for neuroscience research and emerging clinical applications*. Amsterdam: Elsevier/Academic Press, 2014, p. 359 pages.

[164] M. A. A. van Walderveen, F. Barkhof, P. J. W. Pouwels, R. A. van Schijndel, C. H. Polman, and J. A. Castelijns, "Neuronal damage in T1-hypointense multiple sclerosis lesions demonstrated in vivo using proton magnetic resonance spectroscopy," *Annals of Neurology,* vol. 46, no. 1, pp. 79-87, Jul 1999, doi: Doi 10.1002/1531-8249(199907)46:1<79::Aid-Ana12>3.3.Co;2-0.

[165] W. Roser, G. Hagberg, I. Mader, H. Brunnschweiler, E. W. Radue, J. Seelig, and L. Kappos, "Proton MRS of gadolinium-enhancing MS plaques and metabolic changes in

normal-appearing white matter," *Magn Reson Med,* vol. 33, no. 6, pp. 811-7, Jun 1995. [Online]. Available: https://www.ncbi.nlm.nih.gov/pubmed/7651118.

[166] C. A. Davie, C. P. Hawkins, G. J. Barker, A. Brennan, P. S. Tofts, D. H. Miller, and W. I. McDonald, "Serial proton magnetic resonance spectroscopy in acute multiple sclerosis lesions," *Brain,* vol. 117 (Pt 1), pp. 49-58, Feb 1994. [Online]. Available: https://www.ncbi.nlm.nih.gov/pubmed/8149214.

[167] M. C. Tartaglia, S. Narayanan, N. De Stefano, R. Arnaoutelis, S. B. Antel, S. J. Francis, A. C. Santos, Y. Lapierre, and D. L. Arnold, "Choline is increased in pre-lesional normal appearing white matter in multiple sclerosis," *J Neurol,* vol. 249, no. 10, pp. 1382-90, Oct 2002, doi: 10.1007/s00415-002-0846-6.

[168] D. L. Arnold, G. T. Riess, P. M. Matthews, G. S. Francis, D. L. Collins, C. Wolfson, and J. P. Antel, "Use of proton magnetic resonance spectroscopy for monitoring disease progression in multiple sclerosis," *Ann Neurol,* vol. 36, no. 1, pp. 76-82, Jul 1994, doi: 10.1002/ana.410360115.

[169] I. Mader, W. Roser, L. Kappos, G. Hagberg, J. Seelig, E. W. Radue, and W. Steinbrich, "Serial proton MR spectroscopy of contrast-enhancing multiple sclerosis plaques: Absolute metabolic values over 2 years during a clinical pharmacological study," *Am J Neuroradiol,* vol. 21, no. 7, pp. 1220-1227, Aug 2000. [Online]. Available: <Go to ISI>://WOS:000165054800011.

[170] H. Vafaeyan, S. A. Ebrahimzadeh, N. Rahimian, S. K. Alavijeh, A. Madadi, F. Faeghi, M. H. Harirchian, and H. S. Rad, "Quantification of diagnostic biomarkers to detect multiple sclerosis lesions employing (1)H-MRSI at 3T," *Australas Phys Eng Sci Med,* vol. 38, no. 4, pp. 611-8, Dec 2015, doi: 10.1007/s13246-015-0390-1.

[171] B. Bellenberg, M. Busch, N. Trampe, R. Gold, A. Chan, and C. Lukas, "1H-magnetic resonance spectroscopy in diffuse and focal cervical cord lesions in multiple sclerosis," *Eur Radiol,* vol. 23, no. 12, pp. 3379-92, Dec 2013, doi: 10.1007/s00330-013-2942-7.

[172] C. A. Husted, D. S. Goodin, J. W. Hugg, A. A. Maudsley, J. S. Tsuruda, S. H. de Bie, G. Fein, G. B. Matson, and M. W. Weiner, "Biochemical alterations in multiple sclerosis lesions and normal-appearing white matter detected by in vivo 31P and 1H spectroscopic imaging," *Ann Neurol,* vol. 36, no. 2, pp. 157-65, Aug 1994, doi: 10.1002/ana.410360207.

[173] D. H. Miller, S. J. Austin, A. Connelly, B. D. Youl, D. G. Gadian, and W. I. McDonald, "Proton magnetic resonance spectroscopy of an acute and chronic lesion in multiple sclerosis," *Lancet,* vol. 337, no. 8732, pp. 58-9, Jan 5 1991. [Online]. Available: http://www.ncbi.nlm.nih.gov/pubmed/1670684.

[174] H. Kimura, R. I. Grossman, R. E. Lenkinski, and F. Gonzalez-Scarano, "Proton MR spectroscopy and magnetization transfer ratio in multiple sclerosis: correlative findings of active versus irreversible plaque disease," *AJNR Am J Neuroradiol,* vol. 17, no. 8, pp. 1539-47, Sep 1996. [Online]. Available: https://www.ncbi.nlm.nih.gov/pubmed/8883654.

[175] P. Vanhecke, G. Marchal, K. Johannik, P. Demaerel, G. Wilms, H. Carton, and A. L. Baert, "Human Brain Proton Localized Nmr-Spectroscopy in Multiple-Sclerosis," *Magnet Reson Med,* vol. 18, no. 1, pp. 199-206, Mar 1991. [Online]. Available: <Go to ISI>://WOS:A1991EZ54700019.

[176] G. Tedeschi, S. Bonavita, H. F. McFarland, N. Richert, J. H. Duyn, and J. A. Frank, "Proton MR spectroscopic imaging in multiple sclerosis," *Neuroradiology,* vol. 44, no. 1,

pp. 37-42, Jan 2002. [Online]. Available: https://www.ncbi.nlm.nih.gov/pubmed/11942498.

[177] A. M. Landtblom, K. A. Thuomas, L. Sjodqvist, U. Flodin, F. H. Nyland, and B. Soderfeldt, "Hypointensity in T2-weighted images of the basal ganglia in solvent-exposed patients with multiple sclerosis: clinical, MRI and CSF characteristics," *Neurol Sci,* vol. 24, no. 1, pp. 2-9, Apr 2003, doi: 10.1007/s100720300014.

[178] W. D. Rooney, D. E. Goodkin, N. Schuff, D. J. Meyerhoff, D. Norman, and M. W. Weiner, "1H MRSI of normal appearing white matter in multiple sclerosis," *Mult Scler,* vol. 3, no. 4, pp. 231-7, Aug 1997, doi: 10.1177/135245859700300403.

[179] E. T. Wood, I. Ronen, A. Techawiboonwong, C. K. Jones, P. B. Barker, P. Calabresi, D. Harrison, and D. S. Reich, "Investigating axonal damage in multiple sclerosis by diffusion tensor spectroscopy," *J Neurosci,* vol. 32, no. 19, pp. 6665-9, May 9 2012, doi: 10.1523/JNEUROSCI.0044-12.2012.

[180] C. Steen, M. D'Haeseleer, J. M. Hoogduin, Y. Fierens, M. Cambron, J. P. Mostert, D. J. Heersema, M. W. Koch, and J. De Keyser, "Cerebral white matter blood flow and energy metabolism in multiple sclerosis," *Mult Scler,* vol. 19, no. 10, pp. 1282-9, Sep 2013, doi: 10.1177/1352458513477228.

[181] A. Tourbah, J. L. Stievenart, M. T. Iba-Zizen, G. Zannoli, O. Lyon-Caen, and E. A. Cabanis, "In vivo localized NMR proton spectroscopy of normal appearing white matter in patients with multiple sclerosis," *J Neuroradiol,* vol. 23, no. 2, pp. 49-55, Sep 1996. [Online]. Available: http://www.ncbi.nlm.nih.gov/pubmed/8948157.

[182] Y. Anik, A. Demirci, H. Efendi, S. S. Bulut, I. Celebi, and S. Komsuoglu, "Evaluation of normal appearing white matter in multiple sclerosis: comparison of diffusion magnetic

resonance, magnetization transfer imaging and multivoxel magnetic resonance spectroscopy findings with expanded disability status scale," *Clin Neuroradiol,* vol. 21, no. 4, pp. 207-15, Nov 2011, doi: 10.1007/s00062-011-0091-4.

[183] M. D'Haeseleer, C. Steen, J. M. Hoogduin, M. J. van Osch, Y. Fierens, M. Cambron, M. W. Koch, and J. De Keyser, "Performance on Paced Auditory Serial Addition Test and cerebral blood flow in multiple sclerosis," *Acta Neurol Scand,* vol. 128, no. 5, pp. e26-9, Nov 2013, doi: 10.1111/ane.12129.

[184] S. D. Brass, S. Narayanan, J. P. Antel, Y. Lapierre, L. Collins, and D. L. Arnold, "Axonal damage in multiple sclerosis patients with high versus low expanded disability status scale score," *Can J Neurol Sci,* vol. 31, no. 2, pp. 225-8, May 2004. [Online]. Available: http://www.ncbi.nlm.nih.gov/pubmed/15198448.

[185] M. Siger-Zajdel and K. W. Selmaj, "Proton magnetic resonance spectroscopy of normal appearing white matter in familial and sporadic multiple sclerosis," *J Neurol,* vol. 252, no. 7, pp. 830-2, Jul 2005, doi: 10.1007/s00415-005-0754-7.

[186] J. Oh, R. G. Henry, C. Genain, S. J. Nelson, and D. Pelletier, "Mechanisms of normal appearing corpus callosum injury related to pericallosal T1 lesions in multiple sclerosis using directional diffusion tensor and 1H MRS imaging," *J Neurol Neurosurg Psychiatry,* vol. 75, no. 9, pp. 1281-6, Sep 2004, doi: 10.1136/jnnp.2004.039032.

[187] A. Tourbah, J. L. Stievenart, A. Abanou, M. T. Iba-Zizen, H. Hamard, O. Lyon-Caen, and E. A. Cabanis, "Normal-appearing white matter in optic neuritis and multiple sclerosis: a comparative proton spectroscopy study," *Neuroradiology,* vol. 41, no. 10, pp. 738-43, Oct 1999. [Online]. Available: https://www.ncbi.nlm.nih.gov/pubmed/10552024.

[188] D. L. Arnold, P. M. Matthews, G. Francis, and J. Antel, "Proton magnetic resonance spectroscopy of human brain in vivo in the evaluation of multiple sclerosis: assessment of the load of disease," *Magn Reson Med,* vol. 14, no. 1, pp. 154-9, Apr 1990. [Online]. Available: http://www.ncbi.nlm.nih.gov/pubmed/2161982.

[189] L. K. Vingara, H. J. Yu, M. E. Wagshul, D. Serafin, C. Christodoulou, I. Pelczer, L. B. Krupp, and M. Maletic-Savatic, "Metabolomic approach to human brain spectroscopy identifies associations between clinical features and the frontal lobe metabolome in multiple sclerosis," *Neuroimage,* vol. 82, pp. 586-94, Nov 15 2013, doi: 10.1016/j.neuroimage.2013.05.125.

[190] A. F. Marliani, V. Clementi, L. Albini Riccioli, R. Agati, M. Carpenzano, F. Salvi, and M. Leonardi, "Quantitative cervical spinal cord 3T proton MR spectroscopy in multiple sclerosis," *AJNR Am J Neuroradiol,* vol. 31, no. 1, pp. 180-4, Jan 2010, doi: 10.3174/ajnr.A1738.

[191] J. Suhy, W. D. Rooney, D. E. Goodkin, A. A. Capizzano, B. J. Soher, A. A. Maudsley, E. Waubant, P. B. Andersson, and M. W. Weiner, "1H MRSI comparison of white matter and lesions in primary progressive and relapsing-remitting MS," *Mult Scler,* vol. 6, no. 3, pp. 148-55, Jun 2000, doi: 10.1177/135245850000600303.

[192] C. Takeuchi, K. Ota, Y. Ono, and M. Iwata, "Interferon Beta-1b may reverse axonal dysfunction in multiple sclerosis," *Neuroradiol J,* vol. 20, no. 5, pp. 531-40, Oct 31 2007, doi: 10.1177/197140090702000510.

[193] L. Fu, C. Wolfson, K. J. Worsley, N. DeStefano, D. L. Collins, S. Narayanan, and D. L. Arnold, "Statistics for investigation of multimodal MR imaging data and an application to

multiple sclerosis patients," *Nmr in Biomedicine,* vol. 9, no. 8, pp. 339-&, Dec 1996, doi: Doi 10.1002/(Sici)1099-1492(199612)9:8<339::Aid-Nbm422>3.0.Co;2-X.

[194] P. Sarchielli, O. Presciutti, R. Tarducci, G. Gobbi, A. Alberti, G. P. Pelliccioli, A. Orlacchio, and V. Gallai, "H-1-MRS in patients with multiple sclerosis undergoing treatment with interferon beta-1a: results of a preliminary study," *J Neurol Neurosur Ps,* vol. 64, no. 2, pp. 204-212, Feb 1998, doi: DOI 10.1136/jnnp.64.2.204.

[195] J. W. Pan, H. P. Hetherington, J. T. Vaughan, G. Mitchell, G. M. Pohost, and J. N. Whitaker, "Evaluation of multiple sclerosis by 1H spectroscopic imaging at 4.1 T," *Magn Reson Med,* vol. 36, no. 1, pp. 72-7, Jul 1996. [Online]. Available: https://www.ncbi.nlm.nih.gov/pubmed/8795023.

[196] M. F. Yetkin, M. Mirza, and H. Donmez, "Monitoring interferon beta treatment response with magnetic resonance spectroscopy in relapsing remitting multiple sclerosis," *Medicine (Baltimore),* vol. 95, no. 36, p. e4782, Sep 2016, doi: 10.1097/MD.0000000000004782.

[197] W. H. Zaini, F. Giuliani, C. Beaulieu, S. Kalra, and C. Hanstock, "Fatigue in Multiple Sclerosis: Assessing Pontine Involvement Using Proton MR Spectroscopic Imaging," *PLoS One,* vol. 11, no. 2, p. e0149622, 2016, doi: 10.1371/journal.pone.0149622.

[198] W. Staffen, H. Zauner, A. Mair, A. Kutzelnigg, P. Kapeller, H. Stangl, E. Raffer, H. Niederhofer, and G. Ladurner, "Magnetic resonance spectroscopy of memory and frontal brain region in early multiple sclerosis," *J Neuropsychiatry Clin Neurosci,* vol. 17, no. 3, pp. 357-63, Summer 2005, doi: 10.1176/jnp.17.3.357.

[199] H. Reddy, S. Narayanan, P. M. Matthews, R. D. Hoge, G. B. Pike, P. Duquette, J. Antel, and D. L. Arnold, "Relating axonal injury to functional recovery in MS," *Neurology,* vol.

54, no. 1, pp. 236-239, Jan 11 2000. [Online]. Available: <Go to ISI>://WOS:000084727900044.

[200] L. Fu, P. M. Matthews, N. De Stefano, K. J. Worsley, S. Narayanan, G. S. Francis, J. P. Antel, C. Wolfson, and D. L. Arnold, "Imaging axonal damage of normal-appearing white matter in multiple sclerosis," *Brain,* vol. 121 (Pt 1), pp. 103-13, Jan 1998. [Online]. Available: https://www.ncbi.nlm.nih.gov/pubmed/9549491.

[201] N. De Stefano, S. Narayanan, S. J. Francis, S. Smith, M. Mortilla, M. C. Tartaglia, M. L. Bartolozzi, L. Guidi, A. Federico, and D. L. Arnold, "Diffuse axonal and tissue injury in patients with multiple sclerosis with low cerebral lesion load and no disability," *Arch Neurol,* vol. 59, no. 10, pp. 1565-71, Oct 2002. [Online]. Available: https://www.ncbi.nlm.nih.gov/pubmed/12374493.

[202] S. Hannoun, M. Bagory, F. Durand-Dubief, D. Ibarrola, J. C. Comte, C. Confavreux, F. Cotton, and D. Sappey-Marinier, "Correlation of diffusion and metabolic alterations in different clinical forms of multiple sclerosis," *PLoS One,* vol. 7, no. 3, p. e32525, 2012, doi: 10.1371/journal.pone.0032525.

[203] A. Pokryszko-Dragan, J. Bladowska, A. Zimny, K. Slotwinski, M. Zagrajek, E. Gruszka, M. Bilinska, M. Sasiadek, and R. Podemski, "Magnetic resonance spectroscopy findings as related to fatigue and cognitive performance in multiple sclerosis patients with mild disability," *J Neurol Sci,* vol. 339, no. 1-2, pp. 35-40, Apr 15 2014, doi: 10.1016/j.jns.2014.01.013.

[204] J. Bellmann-Strobl, H. Stiepani, J. Wuerfel, G. Bohner, F. Paul, C. Warmuth, O. Aktas, K. P. Wandinger, F. Zipp, and R. Klingebiel, "MR spectroscopy (MRS) and magnetisation transfer imaging (MTI), lesion load and clinical scores in early relapsing

remitting multiple sclerosis: a combined cross-sectional and longitudinal study," *Eur Radiol,* vol. 19, no. 8, pp. 2066-74, Aug 2009, doi: 10.1007/s00330-009-1364-z.

[205] J. Oh, D. Pelletier, and S. J. Nelson, "Corpus callosum axonal injury in multiple sclerosis measured by proton magnetic resonance spectroscopic imaging," *Arch Neurol,* vol. 61, no. 7, pp. 1081-6, Jul 2004, doi: 10.1001/archneur.61.7.1081.

[206] M. P. Wattjes, M. Harzheim, G. G. Lutterbey, L. Klotz, H. H. Schild, and F. Traber, "Axonal damage but no increased glial cell activity in the normal-appearing white matter of patients with clinically isolated syndromes suggestive of multiple sclerosis using high-field magnetic resonance spectroscopy," *AJNR Am J Neuroradiol,* vol. 28, no. 8, pp. 1517-22, Sep 2007, doi: 10.3174/ajnr.A0594.

[207] J. Sun, H. Song, Y. Yang, K. Zhang, X. Gao, X. Li, L. Ni, P. Lin, and C. Niu, "Metabolic changes in normal appearing white matter in multiple sclerosis patients using multivoxel magnetic resonance spectroscopy imaging," *Medicine (Baltimore),* vol. 96, no. 14, p. e6534, Apr 2017, doi: 10.1097/MD.0000000000006534.

[208] H. Vrenken, F. Barkhof, B. M. Uitdehaag, J. A. Castelijns, C. H. Polman, and P. J. Pouwels, "MR spectroscopic evidence for glial increase but not for neuro-axonal damage in MS normal-appearing white matter," *Magn Reson Med,* vol. 53, no. 2, pp. 256-66, Feb 2005, doi: 10.1002/mrm.20366.

[209] M. Wylezinska, A. Cifelli, P. Jezzard, J. Palace, M. Alecci, and P. M. Matthews, "Thalamic neurodegeneration in relapsing-remitting multiple sclerosis," *Neurology,* vol. 60, no. 12, pp. 1949-54, Jun 24 2003. [Online]. Available: https://www.ncbi.nlm.nih.gov/pubmed/12821738.

[210] P. M. Matthews, E. Pioro, S. Narayanan, N. De Stefano, L. Fu, G. Francis, J. Antel, C. Wolfson, and D. L. Arnold, "Assessment of lesion pathology in multiple sclerosis using quantitative MRI morphometry and magnetic resonance spectroscopy," *Brain,* vol. 119 (Pt 3), pp. 715-22, Jun 1996. [Online]. Available: https://www.ncbi.nlm.nih.gov/pubmed/8673485.

[211] N. De Stefano, G. Iannucci, M. P. Sormani, L. Guidi, M. L. Bartolozzi, G. Comi, A. Federico, and M. Filippi, "MR correlates of cerebral atrophy in patients with multiple sclerosis," *J Neurol,* vol. 249, no. 8, pp. 1072-7, Aug 2002, doi: 10.1007/s00415-002-0790-5.

[212] S. Narayanan, L. Fu, E. Pioro, N. De Stefano, D. L. Collins, G. S. Francis, J. P. Antel, P. M. Matthews, and D. L. Arnold, "Imaging of axonal damage in multiple sclerosis: spatial distribution of magnetic resonance imaging lesions," *Ann Neurol,* vol. 41, no. 3, pp. 385-91, Mar 1997, doi: 10.1002/ana.410410314.

[213] A. Parry, R. Corkill, A. M. Blamire, J. Palace, S. Narayanan, D. Arnold, P. Styles, and P. M. Matthews, "Beta-Interferon treatment does not always slow the progression of axonal injury in multiple sclerosis," *J Neurol,* vol. 250, no. 2, pp. 171-8, Feb 2003, doi: 10.1007/s00415-003-0965-8.

[214] N. Tellez, J. Alonso, J. Rio, M. Tintore, C. Nos, X. Montalban, and A. Rovira, "The basal ganglia: a substrate for fatigue in multiple sclerosis," *Neuroradiology,* vol. 50, no. 1, pp. 17-23, Jan 2008, doi: 10.1007/s00234-007-0304-3.

[215] M. Maffei, A. F. Marliani, F. Salvi, V. Clementi, R. Agati, and M. Leonardi, "Metabolite Changes in Normal Appearing Cervical Spinal Cord in Two Patients with Multiple

Sclerosis. A Proton MR Spectroscopic Analysis," *Neuroradiol J,* vol. 21, no. 2, pp. 228-35, Apr 7 2008, doi: 10.1177/197140090802100212.

[216] A. Falini, G. Calabrese, M. Filippi, D. Origgi, S. Lipari, B. Colombo, G. Comi, and G. Scotti, "Benign versus secondary-progressive multiple sclerosis: the potential role of proton MR spectroscopy in defining the nature of disability," *AJNR Am J Neuroradiol,* vol. 19, no. 2, pp. 223-9, Feb 1998. [Online]. Available: https://www.ncbi.nlm.nih.gov/pubmed/9504469.

[217] M. G. Cucurella, A. Rovira, J. Rio, S. Pedraza, M. M. Tintore, X. Montalban, and J. Alonso, "Proton magnetic resonance spectroscopy in primary and secondary progressive multiple sclerosis," *NMR Biomed,* vol. 13, no. 2, pp. 57-63, Apr 2000. [Online]. Available: https://www.ncbi.nlm.nih.gov/pubmed/10797633.

[218] C. Steen, N. Wilczak, J. M. Hoogduin, M. Koch, and J. De Keyser, "Reduced creatine kinase B activity in multiple sclerosis normal appearing white matter," *PLoS One,* vol. 5, no. 5, p. e10811, May 25 2010, doi: 10.1371/journal.pone.0010811.

[219] S. M. Leary, C. A. Davie, G. J. Parker, V. L. Stevenson, L. Wang, G. J. Barker, D. H. Miller, and A. J. Thompson, "1H magnetic resonance spectroscopy of normal appearing white matter in primary progressive multiple sclerosis," *J Neurol,* vol. 246, no. 11, pp. 1023-6, Nov 1999. [Online]. Available: https://www.ncbi.nlm.nih.gov/pubmed/10631633.

[220] Z. Caramanos, S. DiMaio, S. Narayanan, Y. Lapierre, and D. L. Arnold, "(1)H-MRSI evidence for cortical gray matter pathology that is independent of cerebral white matter lesion load in patients with secondary progressive multiple sclerosis," *J Neurol Sci,* vol. 282, no. 1-2, pp. 72-9, Jul 15 2009, doi: 10.1016/j.jns.2009.01.015.

[221] M. Bagory, F. Durand-Dubief, D. Ibarrola, J. C. Comte, F. Cotton, C. Confavreux, and D. Sappey-Marinier, "Implementation of an absolute brain 1H-MRS quantification method to assess different tissue alterations in multiple sclerosis," *IEEE Trans Biomed Eng,* vol. 59, no. 10, pp. 2687-94, Oct 2012, doi: 10.1109/TBME.2011.2161609.

[222] D. Pelletier, S. J. Nelson, D. Grenier, Y. Lu, C. Genain, and D. E. Goodkin, "3-D echo planar (1)HMRS imaging in MS: metabolite comparison from supratentorial vs. central brain," *Magn Reson Imaging,* vol. 20, no. 8, pp. 599-606, Oct 2002. [Online]. Available: https://www.ncbi.nlm.nih.gov/pubmed/12467867.

[223] N. De Stefano, P. M. Matthews, S. Narayanan, G. S. Francis, J. P. Antel, and D. L. Arnold, "Axonal dysfunction and disability in a relapse of multiple sclerosis: longitudinal study of a patient," *Neurology,* vol. 49, no. 4, pp. 1138-41, Oct 1997. [Online]. Available: https://www.ncbi.nlm.nih.gov/pubmed/9339704.

[224] P. A. Narayana, J. S. Wolinsky, S. B. Rao, R. J. He, M. Mehta, and P. T. M. Grp, "Multicentre proton magnetic resonance spectroscopy imaging of primary progressive multiple sclerosis," *Mult Scler J,* vol. 10, pp. S73-S78, Jun 2004, doi: 10.1191/1352458504ms1035oa.

[225] P. Sarchielli, O. Presciutti, R. Tarducci, G. Gobbi, A. Alberti, G. P. Pelliccioli, P. Chiarini, and V. Gallai, "Localized (1)H magnetic resonance spectroscopy in mainly cortical gray matter of patients with multiple sclerosis," *J Neurol,* vol. 249, no. 7, pp. 902-10, Jul 2002, doi: 10.1007/s00415-002-0758-5.

[226] D. Pelletier, S. J. Nelson, J. Oh, J. P. Antel, M. Kita, S. S. Zamvil, and D. E. Goodkin, "MRI lesion volume heterogeneity in primary progressive MS in relation with axonal

damage and brain atrophy," *J Neurol Neurosur Ps,* vol. 74, no. 7, pp. 950-952, Jul 2003. [Online]. Available: <Go to ISI>://WOS:000183543800029.

[227] A. Bitsch, H. Bruhn, V. Vougioukas, A. Stringaris, H. Lassmann, J. Frahm, and W. Bruck, "Inflammatory CNS demyelination: histopathologic correlation with in vivo quantitative proton MR spectroscopy," *AJNR Am J Neuroradiol,* vol. 20, no. 9, pp. 1619-27, Oct 1999. [Online]. Available: http://www.ncbi.nlm.nih.gov/pubmed/10543631.

[228] C. Schiepers, P. Van Hecke, R. Vandenberghe, S. Van Oostende, P. Dupont, P. Demaerel, G. Bormans, and H. Carton, "Positron emission tomography, magnetic resonance imaging and proton NMR spectroscopy of white matter in multiple sclerosis," *Mult Scler,* vol. 3, no. 1, pp. 8-17, Feb 1997, doi: 10.1177/135245859700300102.

[229] R. Srinivasan, N. Sailasuta, R. Hurd, S. Nelson, and D. Pelletier, "Evidence of elevated glutamate in multiple sclerosis using magnetic resonance spectroscopy at 3 T," *Brain,* vol. 128, no. Pt 5, pp. 1016-25, May 2005, doi: 10.1093/brain/awh467.

[230] P. A. Narayana, T. J. Doyle, D. Lai, and J. S. Wolinsky, "Serial proton magnetic resonance spectroscopic imaging, contrast-enhanced magnetic resonance imaging, and quantitative lesion volumetry in multiple sclerosis," *Ann Neurol,* vol. 43, no. 1, pp. 56-71, Jan 1998, doi: 10.1002/ana.410430112.

[231] P. E. Sijens, J. P. Mostert, R. Irwan, J. H. Potze, M. Oudkerk, and J. De Keyser, "Impact of fluoxetine on the human brain in multiple sclerosis as quantified by proton magnetic resonance spectroscopy and diffusion tensor imaging," *Psychiatry Res,* vol. 164, no. 3, pp. 274-82, Dec 30 2008, doi: 10.1016/j.pscychresns.2007.12.014.

[232] U. Seeger, U. Klose, I. Mader, W. Grodd, and T. Nagele, "Parameterized evaluation of macromolecules and lipids in proton MR spectroscopy of brain diseases," *Magn Reson Med,* vol. 49, no. 1, pp. 19-28, Jan 2003, doi: 10.1002/mrm.10332.

[233] C. A. Davie, N. C. Silver, G. J. Barker, P. S. Tofts, A. J. Thompson, W. I. McDonald, and D. H. Miller, "Does the extent of axonal loss and demyelination from chronic lesions in multiple sclerosis correlate with the clinical subgroup?," *J Neurol Neurosurg Psychiatry,* vol. 67, no. 6, pp. 710-5, Dec 1999. [Online]. Available: http://www.ncbi.nlm.nih.gov/pubmed/10567484.

[234] M. A. Lee, A. M. Blamire, S. Pendlebury, K. H. Ho, K. R. Mills, P. Styles, J. Palace, and P. M. Matthews, "Axonal injury or loss in the internal capsule and motor impairment in multiple sclerosis," *Arch Neurol,* vol. 57, no. 1, pp. 65-70, Jan 2000. [Online]. Available: http://www.ncbi.nlm.nih.gov/pubmed/10634450.

[235] C. A. Davie, G. J. Barker, S. Webb, P. S. Tofts, A. J. Thompson, A. E. Harding, W. I. McDonald, and D. H. Miller, "Persistent functional deficit in multiple sclerosis and autosomal dominant cerebellar ataxia is associated with axon loss," *Brain,* vol. 118 (Pt 6), pp. 1583-92, Dec 1995. [Online]. Available: https://www.ncbi.nlm.nih.gov/pubmed/8595487.

[236] A. Tisell, O. D. Leinhard, J. B. Warntjes, A. Aalto, O. Smedby, A. M. Landtblom, and P. Lundberg, "Increased concentrations of glutamate and glutamine in normal-appearing white matter of patients with multiple sclerosis and normal MR imaging brain scans," *PLoS One,* vol. 8, no. 4, p. e61817, 2013, doi: 10.1371/journal.pone.0061817.

[237] C. J. Azevedo, J. Kornak, P. Chu, M. Sampat, D. T. Okuda, B. A. Cree, S. J. Nelson, S. L. Hauser, and D. Pelletier, "In vivo evidence of glutamate toxicity in multiple sclerosis," *Ann Neurol,* vol. 76, no. 2, pp. 269-78, Aug 2014, doi: 10.1002/ana.24202.

[238] J. Mellergard, A. Tisell, O. Dahlqvist Leinhard, I. Blystad, A. M. Landtblom, K. Blennow, B. Olsson, C. Dahle, J. Ernerudh, P. Lundberg, and M. Vrethem, "Association between change in normal appearing white matter metabolites and intrathecal inflammation in natalizumab-treated multiple sclerosis," *PLoS One,* vol. 7, no. 9, p. e44739, 2012, doi: 10.1371/journal.pone.0044739.

[239] S. Llufriu, J. Kornak, H. Ratiney, J. Oh, D. Brenneman, B. A. Cree, M. Sampat, S. L. Hauser, S. J. Nelson, and D. Pelletier, "Magnetic resonance spectroscopy markers of disease progression in multiple sclerosis," *JAMA Neurol,* vol. 71, no. 7, pp. 840-7, Jul 1 2014, doi: 10.1001/jamaneurol.2014.895.

[240] B. Bodini, F. Branzoli, E. Poirion, D. García-Lorenzo, M. Didier, E. Maillart, J. Socha, G. Bera, C. Lubetzki, I. Ronen, S. Lehericy, and B. Stankoff, "Dysregulation of energy metabolism in multiple sclerosis measured in vivo with diffusion-weighted spectroscopy," *Mult Scler J,* vol. 24, no. 3, pp. 313-321, 2017, doi: 10.1177/1352458517698249.

[241] R. Srinivasan, H. Ratiney, K. E. Hammond-Rosenbluth, D. Pelletier, and S. J. Nelson, "MR spectroscopic imaging of glutathione in the white and gray matter at 7 T with an application to multiple sclerosis," *Magn Reson Imaging,* vol. 28, no. 2, pp. 163-70, Feb 2010, doi: 10.1016/j.mri.2009.06.008.

[242] J. C. Nantes, S. Proulx, J. Zhong, S. A. Holmes, S. Narayanan, R. A. Brown, R. D. Hoge, and L. Koski, "GABA and glutamate levels correlate with MTR and clinical disability:

Insights from multiple sclerosis," *Neuroimage,* vol. 157, pp. 705-715, Aug 15 2017, doi: 10.1016/j.neuroimage.2017.01.033.

[243] S. T. Pendlebury, M. A. Lee, A. M. Blamire, P. Styles, and P. M. Matthews, "Correlating magnetic resonance imaging markers of axonal injury and demyelination in motor impairment secondary to stroke and multiple sclerosis," *Magnetic Resonance Imaging,* vol. 18, no. 4, pp. 369-378, May 2000, doi: Doi 10.1016/S0730-725x(00)00115-6.

[244] O. Ciccarelli, D. R. Altmann, M. A. McLean, C. A. Wheeler-Kingshott, K. Wimpey, D. H. Miller, and A. J. Thompson, "Spinal cord repair in MS: Does mitochondrial metabolism play a role?," *Neurology,* vol. 74, no. 9, pp. 721-727, Mar 2 2010, doi: 10.1212/WNL.0b013e3181d26968.

[245] A. M. Blamire, S. Cader, M. Lee, J. Palace, and P. M. Matthews, "Axonal damage in the spinal cord of multiple sclerosis patients detected by magnetic resonance spectroscopy," *Magn Reson Med,* vol. 58, no. 5, pp. 880-5, Nov 2007, doi: 10.1002/mrm.21382.

[246] O. Ciccarelli, A. T. Toosy, N. De Stefano, C. A. M. Wheeler-Kingshott, D. H. Miller, and A. J. Thompson, "Assessing Neuronal Metabolism In Vivo by Modeling Imaging Measures," *Journal of Neuroscience,* vol. 30, no. 45, pp. 15030-15033, Nov 10 2010, doi: 10.1523/Jneurosci.3330-10.2010.

[247] O. Ciccarelli, C. A. Wheeler-Kingshott, M. A. McLean, M. Cercignani, K. Wimpey, D. H. Miller, and A. J. Thompson, "Spinal cord spectroscopy and diffusion-based tractography to assess acute disability in multiple sclerosis," *Brain,* vol. 130, pp. 2220-2231, Aug 2007, doi: 10.1093/brain/awm152.

[248] D. J. Rigotti, A. Gass, L. Achtnichts, M. Inglese, J. S. Babb, Y. Naegelin, J. Hirsch, M. Amann, L. Kappos, and O. Gonen, "Multiple Sclerosis Severity Scale and whole-brain N-

acetylaspartate concentration for patients' assessment," *Mult Scler,* vol. 18, no. 1, pp. 98-107, Jan 2012, doi: 10.1177/1352458511415142.

[249] L. Achtnichts, O. Gonen, D. J. Rigotti, J. S. Babb, Y. Naegelin, I. K. Penner, K. Bendfeldt, J. Hirsch, M. Amann, L. Kappos, and A. Gass, "Global N-acetylaspartate concentration in benign and non-benign multiple sclerosis patients of long disease duration," *Eur J Radiol,* vol. 82, no. 12, pp. e848-52, Dec 2013, doi: 10.1016/j.ejrad.2013.08.037.

[250] P. Kapeller, M. A. McLean, C. M. Griffin, D. Chard, G. J. Parker, G. J. Barker, A. J. Thompson, and D. H. Miller, "Preliminary evidence for neuronal damage in cortical grey matter and normal appearing white matter in short duration relapsing-remitting multiple sclerosis: a quantitative MR spectroscopic imaging study," *J Neurol,* vol. 248, no. 2, pp. 131-8, Feb 2001. [Online]. Available: https://www.ncbi.nlm.nih.gov/pubmed/11284131.

[251] G. Helms, "Volume correction for edema in single-volume proton MR spectroscopy of contrast-enhancing multiple sclerosis lesions," *Magn Reson Med,* vol. 46, no. 2, pp. 256-63, Aug 2001. [Online]. Available: https://www.ncbi.nlm.nih.gov/pubmed/11477628.

[252] O. T. Wiebenga, A. M. Klauser, M. M. Schoonheim, G. J. Nagtegaal, M. D. Steenwijk, J. A. van Rossum, C. H. Polman, F. Barkhof, P. J. Pouwels, and J. J. Geurts, "Enhanced axonal metabolism during early natalizumab treatment in relapsing-remitting multiple sclerosis," *AJNR Am J Neuroradiol,* vol. 36, no. 6, pp. 1116-23, Jun 2015, doi: 10.3174/ajnr.A4252.

[253] M. Tiberio, D. T. Chard, D. R. Altmann, G. Davies, C. M. Griffin, M. A. McLean, W. Rashid, J. Sastre-Garriga, A. J. Thompson, and D. H. Miller, "Metabolite changes in

early relapsing-remitting multiple sclerosis. A two year follow-up study," *J Neurol,* vol. 253, no. 2, pp. 224-30, Feb 2006, doi: 10.1007/s00415-005-0964-z.

[254] D. T. Chard, C. M. Griffin, M. A. McLean, P. Kapeller, R. Kapoor, A. J. Thompson, and D. H. Miller, "Brain metabolite changes in cortical grey and normal-appearing white matter in clinically early relapsing-remitting multiple sclerosis," *Brain,* vol. 125, no. Pt 10, pp. 2342-52, Oct 2002. [Online]. Available: https://www.ncbi.nlm.nih.gov/pubmed/12244090.

[255] E. Adalsteinsson, A. Langer-Gould, R. J. Homer, A. Rao, E. V. Sullivan, C. A. Lima, A. Pfefferbaum, and S. W. Atlas, "Gray matter N-acetyl aspartate deficits in secondary progressive but not relapsing-remitting multiple sclerosis," *AJNR Am J Neuroradiol,* vol. 24, no. 10, pp. 1941-5, Nov-Dec 2003. [Online]. Available: https://www.ncbi.nlm.nih.gov/pubmed/14625214.

[256] M. Inglese, S. Liu, J. S. Babb, L. J. Mannon, R. I. Grossman, and O. Gonen, "Three-dimensional proton spectroscopy of deep gray matter nuclei in relapsing-remitting MS," *Neurology,* vol. 63, no. 1, pp. 170-2, Jul 13 2004. [Online]. Available: https://www.ncbi.nlm.nih.gov/pubmed/15249633.

[257] M. Inglese, B. S. Li, H. Rusinek, J. S. Babb, R. I. Grossman, and O. Gonen, "Diffusely elevated cerebral choline and creatine in relapsing-remitting multiple sclerosis," *Magn Reson Med,* vol. 50, no. 1, pp. 190-5, Jul 2003, doi: 10.1002/mrm.10481.

[258] M. Donadieu, Y. Le Fur, A. Lecocq, A. A. Maudsley, S. Gherib, E. Soulier, S. Confort-Gouny, F. Pariollaud, M. P. Ranjeva, J. Pelletier, M. Guye, W. Zaaraoui, B. Audoin, and J. P. Ranjeva, "Metabolic voxel-based analysis of the complete human brain using fast

3D-MRSI: Proof of concept in multiple sclerosis," *J Magn Reson Imaging,* vol. 44, no. 2, pp. 411-9, Aug 2016, doi: 10.1002/jmri.25139.

[259] M. Inglese, Y. Ge, M. Filippi, A. Falini, R. I. Grossman, and O. Gonen, "Indirect evidence for early widespread gray matter involvement in relapsing–remitting multiple sclerosis," *NeuroImage,* vol. 21, no. 4, pp. 1825-1829, 2004, doi: 10.1016/j.neuroimage.2003.12.008.

[260] A. Pulizzi, M. Rovaris, E. Judica, M. P. Sormani, V. Martinelli, G. Comi, and M. Filippi, "Determinants of disability in multiple sclerosis at various disease stages: a multiparametric magnetic resonance study," *Arch Neurol,* vol. 64, no. 8, pp. 1163-8, Aug 2007, doi: 10.1001/archneur.64.8.1163.

[261] O. Gonen, I. Catalaa, J. S. Babb, Y. Ge, L. J. Mannon, D. L. Kolson, and R. I. Grossman, "Total brain N-acetylaspartate - A new measure of disease load in MS," *Neurology,* vol. 54, no. 1, pp. 15-19, Jan 11 2000, doi: Doi 10.1212/Wnl.54.1.15.

[262] D. J. Rigotti, M. Inglese, I. I. Kirov, E. Gorynski, N. N. Perry, J. S. Babb, J. Herbert, R. I. Grossman, and O. Gonen, "Two-year serial whole-brain N-acetyl-L-aspartate in patients with relapsing-remitting multiple sclerosis," *Neurology,* vol. 78, no. 18, pp. 1383-1389, May 2012. [Online]. Available: <Go to ISI>://WOS:000303498000007.

[263] C. A. Davie, G. J. Barker, A. J. Thompson, P. S. Tofts, W. I. McDonald, and D. H. Miller, "1H magnetic resonance spectroscopy of chronic cerebral white matter lesions and normal appearing white matter in multiple sclerosis," *J Neurol Neurosurg Psychiatry,* vol. 63, no. 6, pp. 736-42, Dec 1997. [Online]. Available: https://www.ncbi.nlm.nih.gov/pubmed/9416807.

[264] P. E. Sijens, J. P. Mostert, M. Oudkerk, and J. De Keyser, "(1)H MR spectroscopy of the brain in multiple sclerosis subtypes with analysis of the metabolite concentrations in gray and white matter: initial findings," *Eur Radiol,* vol. 16, no. 2, pp. 489-95, Feb 2006, doi: 10.1007/s00330-005-2839-1.

[265] J. Sastre-Garriga, G. T. Ingle, D. T. Chard, L. Ramio-Torrenta, M. A. McLean, D. H. Miller, and A. J. Thompson, "Metabolite changes in normal-appearing gray and white matter are linked with disability in early primary progressive multiple sclerosis," *Arch Neurol,* vol. 62, no. 4, pp. 569-73, Apr 2005, doi: 10.1001/archneur.62.4.569.

[266] A. Cifelli, M. Arridge, P. Jezzard, M. M. Esiri, J. Palace, and P. M. Matthews, "Thalamic neurodegeneration in multiple sclerosis," *Ann Neurol,* vol. 52, no. 5, pp. 650-3, Nov 2002, doi: 10.1002/ana.10326.

[267] P. E. Sijens, R. Irwan, J. H. Potze, J. P. Mostert, J. De Keyser, and M. Oudkerk, "Analysis of the human brain in primary progressive multiple sclerosis with mapping of the spatial distributions using 1H MR spectroscopy and diffusion tensor imaging," *Eur Radiol,* vol. 15, no. 8, pp. 1686-93, Aug 2005, doi: 10.1007/s00330-005-2775-0.

[268] J. W. Pan, D. B. Twieg, and H. P. Hetherington, "Quantitative spectroscopic imaging of the human brain," *Magn Reson Med,* vol. 40, no. 3, pp. 363-9, Sep 1998. [Online]. Available: https://www.ncbi.nlm.nih.gov/pubmed/9727938.

[269] K. Abdel-Aziz, T. Schneider, B. S. Solanky, M. C. Yiannakas, D. R. Altmann, C. A. Wheeler-Kingshott, A. L. Peters, B. L. Day, A. J. Thompson, and O. Ciccarelli, "Evidence for early neurodegeneration in the cervical cord of patients with primary progressive multiple sclerosis," *Brain,* vol. 138, no. Pt 6, pp. 1568-82, Jun 2015, doi: 10.1093/brain/awv086.

[270] J. He, M. Inglese, B. S. Li, J. S. Babb, R. I. Grossman, and O. Gonen, "Relapsing-remitting multiple sclerosis: metabolic abnormality in nonenhancing lesions and normal-appearing white matter at MR imaging: initial experience," *Radiology,* vol. 234, no. 1, pp. 211-7, Jan 2005, doi: 10.1148/radiol.2341031895.

[271] R. A. Koopmans, D. K. Li, G. Zhu, P. S. Allen, A. Penn, and D. W. Paty, "Magnetic resonance spectroscopy of multiple sclerosis: in-vivo detection of myelin breakdown products," *Lancet,* vol. 341, no. 8845, pp. 631-2, Mar 6 1993. [Online]. Available: http://www.ncbi.nlm.nih.gov/pubmed/8094855.

[272] L. Rozewicz, D. W. Langdon, C. A. Davie, A. J. Thompson, and M. Ron, "Resolution of left hemisphere cognitive dysfunction in multiple sclerosis with magnetic resonance correlates: a case report," *Cogn Neuropsychiatry,* vol. 1, no. 1, pp. 17-26, Feb 1 1996, doi: 10.1080/135468096396677.

[273] G. Kocevar, C. Stamile, S. Hannoun, J. A. Roch, F. Durand-Dubief, S. Vukusic, F. Cotton, and D. Sappey-Marinier, "Weekly follow up of acute lesions in three early multiple sclerosis patients using MR spectroscopy and diffusion," *J Neuroradiol,* vol. 45, no. 2, pp. 108-113, Mar 2018, doi: 10.1016/j.neurad.2017.06.010.

[274] A. M. Pascual, M. C. Martinez-Bisbal, I. Bosca, C. Valero, F. Coret, B. Martinez-Granados, L. Marti-Bonmati, A. Mir, B. Celda, and B. Casanova, "Axonal loss is progressive and partly dissociated from lesion load in early multiple sclerosis," *Neurology,* vol. 69, no. 1, pp. 63-7, Jul 3 2007, doi: 10.1212/01.wnl.0000265054.08610.12.

[275] L. Albini Riccioli, A. F. Marliani, V. Clementi, I. Bartolomei, R. Agati, and M. Leonardi, "Evolutive study of relapsing-remitting multiple sclerosis with cervical proton magnetic

resonance spectroscopy. A case report," *Neuroradiol J,* vol. 21, no. 4, pp. 511-7, Oct 1 2008, doi: 10.1177/197140090802100407.

[276] J. L. Ruiz-Pena, P. Pinero, G. Sellers, J. Argente, A. Casado, J. Foronda, A. Ucles, and G. Izquierdo, "Magnetic resonance spectroscopy of normal appearing white matter in early relapsing-remitting multiple sclerosis: correlations between disability and spectroscopy," *BMC Neurol,* vol. 4, p. 8, Jun 10 2004, doi: 10.1186/1471-2377-4-8.

[277] H. K. Mathiesen, T. Tscherning, P. S. Sorensen, H. B. Larsson, E. Rostrup, O. B. Paulson, and L. G. Hanson, "Multi-slice echo-planar spectroscopic MR imaging provides both global and local metabolite measures in multiple sclerosis," *Magn Reson Med,* vol. 53, no. 4, pp. 750-9, Apr 2005, doi: 10.1002/mrm.20407.

[278] X. Wu, L. G. Hanson, A. Skimminge, P. S. Sorensen, O. B. Paulson, H. K. Mathiesen, and M. Blinkenberg, "Cortical N-acetyl aspartate is a predictor of long-term clinical disability in multiple sclerosis," *Neurol Res,* vol. 36, no. 8, pp. 701-8, Aug 2014, doi: 10.1179/1743132813Y.0000000312.

[279] R. Sharma, "Serial amino-neurochemicals analysis in progressive lesion analysis of multiple sclerosis by magnetic resonance imaging and proton magnetic resonance spectroscopic imaging," *Magn Reson Med Sci,* vol. 1, no. 3, pp. 169-73, Nov 1 2002. [Online]. Available: https://www.ncbi.nlm.nih.gov/pubmed/16082140.

[280] C. A. Davie, C. P. Hawkins, G. J. Barker, A. Brennan, P. S. Tofts, D. H. Miller, and W. I. McDonald, "Detection of myelin breakdown products by proton magnetic resonance spectroscopy," *Lancet,* vol. 341, no. 8845, pp. 630-1, Mar 6 1993. [Online]. Available: http://www.ncbi.nlm.nih.gov/pubmed/8094854.

[281] K. K. Oguz, A. Kurne, A. O. Aksu, E. Karabulut, A. Serdaroglu, S. Teber, S. Haspolat, N. Senbil, S. Kurul, and B. Anlar, "Assessment of citrullinated myelin by 1H-MR spectroscopy in early-onset multiple sclerosis," *AJNR Am J Neuroradiol,* vol. 30, no. 4, pp. 716-21, Apr 2009, doi: 10.3174/ajnr.A1425.

[282] W. Zaaraoui, A. Rico, B. Audoin, F. Reuter, I. Malikova, E. Soulier, P. Viout, Y. Le Fur, S. Confort-Gouny, P. J. Cozzone, J. Pelletier, and J. P. Ranjeva, "Unfolding the long-term pathophysiological processes following an acute inflammatory demyelinating lesion of multiple sclerosis," *Magn Reson Imaging,* vol. 28, no. 4, pp. 477-86, May 2010, doi: 10.1016/j.mri.2009.12.011.

[283] T. Zeis, I. Allaman, M. Gentner, K. Schroder, J. Tschopp, P. J. Magistretti, and N. Schaeren-Wiemers, "Metabolic gene expression changes in astrocytes in Multiple Sclerosis cerebral cortex are indicative of immune-mediated signaling," *Brain Behav Immun,* vol. 48, pp. 313-25, Aug 2015, doi: 10.1016/j.bbi.2015.04.013.

[284] R. Dutta, A. Chang, M. K. Doud, G. J. Kidd, M. V. Ribaudo, E. A. Young, R. J. Fox, S. M. Staugaitis, and B. D. Trapp, "Demyelination causes synaptic alterations in hippocampi from multiple sclerosis patients," *Ann Neurol,* vol. 69, no. 3, pp. 445-54, Mar 2011, doi: 10.1002/ana.22337.

[285] M. Vercellino, A. Merola, C. Piacentino, B. Votta, E. Capello, G. L. Mancardi, R. Mutani, M. T. Giordana, and P. Cavalla, "Altered glutamate reuptake in relapsing-remitting and secondary progressive multiple sclerosis cortex: correlation with microglia infiltration, demyelination, and neuronal and synaptic damage," *J Neuropathol Exp Neurol,* vol. 66, no. 8, pp. 732-9, Aug 2007, doi: 10.1097/nen.0b013e31812571b0.

[286] A. Vallejo-Illarramendi, M. Domercq, F. Perez-Cerda, R. Ravid, and C. Matute, "Increased expression and function of glutamate transporters in multiple sclerosis," *Neurobiol Dis,* vol. 21, no. 1, pp. 154-64, Jan 2006, doi: 10.1016/j.nbd.2005.06.017.

[287] O. Pampliega, M. Domercq, F. N. Soria, P. Villoslada, A. Rodriguez-Antiguedad, and C. Matute, "Increased expression of cystine/glutamate antiporter in multiple sclerosis," *J Neuroinflammation,* vol. 8, p. 63, Jun 03 2011, doi: 10.1186/1742-2094-8-63.

[288] E. Merckx, G. Albertini, M. Paterka, C. Jensen, P. Albrecht, M. Dietrich, J. Van Liefferinge, E. Bentea, L. Verbruggen, T. Demuyser, L. Deneyer, J. Lewerenz, G. van Loo, J. De Keyser, H. Sato, P. Maher, A. Methner, and A. Massie, "Absence of system xc- on immune cells invading the central nervous system alleviates experimental autoimmune encephalitis," *J Neuroinflammation,* vol. 14, no. 1, p. 9, Jan 13 2017, doi: 10.1186/s12974-016-0787-0.

[289] D. Pitt, I. E. Nagelmeier, H. C. Wilson, and C. S. Raine, "Glutamate uptake by oligodendrocytes: Implications for excitotoxicity in multiple sclerosis," *Neurology,* vol. 61, no. 8, pp. 1113-20, Oct 28 2003. [Online].

[290] S. E. Baranzini, R. Srinivasan, P. Khankhanian, D. T. Okuda, S. J. Nelson, P. M. Matthews, S. L. Hauser, J. R. Oksenberg, and D. Pelletier, "Genetic variation influences glutamate concentrations in brains of patients with multiple sclerosis," *Brain,* vol. 133, no. 9, pp. 2603-2611, 2010, doi: 10.1093/brain/awq192.

[291] R. Mazzoli and E. Pessione, "The Neuro-endocrinological Role of Microbial Glutamate and GABA Signaling," *Front Microbiol,* vol. 7, p. 1934, 2016, doi: 10.3389/fmicb.2016.01934.

[292] J. Lewerenz, S. J. Hewett, Y. Huang, M. Lambros, P. W. Gout, P. W. Kalivas, A. Massie, I. Smolders, A. Methner, M. Pergande, S. B. Smith, V. Ganapathy, and P. Maher, "The cystine/glutamate antiporter system x(c)(-) in health and disease: from molecular mechanisms to novel therapeutic opportunities," *Antioxid Redox Signal,* vol. 18, no. 5, pp. 522-55, Feb 10 2013, doi: 10.1089/ars.2011.4391.

[293] J. Frade, S. Pope, M. Schmidt, R. Dringen, R. Barbosa, J. Pocock, J. Laranjinha, and S. Heales, "Glutamate induces release of glutathione from cultured rat astrocytes--a possible neuroprotective mechanism?," *Journal of neurochemistry,* vol. 105, no. 4, pp. 1144-52, May 2008. [Online].

[294] N. Muhlert, M. Atzori, E. De Vita, D. L. Thomas, R. S. Samson, C. A. Wheeler-Kingshott, J. J. Geurts, D. H. Miller, A. J. Thompson, and O. Ciccarelli, "Memory in multiple sclerosis is linked to glutamate concentration in grey matter regions," *J Neurol Neurosurg Psychiatry,* vol. 85, no. 8, pp. 833-9, Aug 2014, doi: 10.1136/jnnp-2013-306662.

[295] A. Mohamed, A. Shoker, F. Bendjelloul, A. Mare, M. Alzrigh, H. Benghuzzi, and T. Desin, "Improvement of experimental allergic encephalomyelitis (EAE) by thymoquinone; an oxidative stress inhibitor," *Biomedical sciences instrumentation,* vol. 39, pp. 440-5, 2003. [Online].

[296] G. Cao, R. A. E. Edden, F. Gao, H. Li, T. Gong, W. Chen, X. Liu, G. Wang, and B. Zhao, "Reduced GABA levels correlate with cognitive impairment in patients with relapsing-remitting multiple sclerosis," *Eur Radiol,* vol. 28, no. 3, pp. 1140-1148, Mar 2018, doi: 10.1007/s00330-017-5064-9.

[297] P. K. Bhattacharyya, M. D. Phillips, L. A. Stone, R. A. Bermel, and M. J. Lowe, "Sensorimotor cortex gamma-aminobutyric acid concentration correlates with impaired performance in patients with MS," *AJNR Am J Neuroradiol,* vol. 34, no. 9, pp. 1733-9, Sep 2013, doi: 10.3174/ajnr.A3483.

[298] R. Dutta, J. McDonough, X. Yin, J. Peterson, A. Chang, T. Torres, T. Gudz, W. B. Macklin, D. A. Lewis, R. J. Fox, R. Rudick, K. Mirnics, and B. D. Trapp, "Mitochondrial dysfunction as a cause of axonal degeneration in multiple sclerosis patients," *Ann Neurol,* vol. 59, no. 3, pp. 478-89, Mar 2006, doi: 10.1002/ana.20736.

[299] L. Steinman, "No quiet surrender: molecular guardians in multiple sclerosis brain," *J Clin Invest,* vol. 125, no. 4, pp. 1371-8, Apr 2015, doi: 10.1172/JCI74255.

[300] I. Y. Choi, S. P. Lee, D. R. Denney, and S. G. Lynch, "Lower levels of glutathione in the brains of secondary progressive multiple sclerosis patients measured by 1H magnetic resonance chemical shift imaging at 3 T," *Mult Scler,* vol. 17, no. 3, pp. 289-96, Mar 2011, doi: 10.1177/1352458510384010.

[301] L. Hofmann, J. Slotboom, C. Boesch, and R. Kreis, "Characterization of the macromolecule baseline in localized (1)H-MR spectra of human brain," *Magn Reson Med,* vol. 46, no. 5, pp. 855-63, Nov 2001. [Online].

[302] I. Y. Choi, P. Lee, A. J. Hughes, D. R. Denney, and S. G. Lynch, "Longitudinal changes of cerebral glutathione (GSH) levels associated with the clinical course of disease progression in patients with secondary progressive multiple sclerosis," *Mult Scler,* vol. 23, no. 7, pp. 956-962, Jun 2017, doi: 10.1177/1352458516669441.

[303] F. D. Lublin, T. Coetzee, J. A. Cohen, R. A. Marrie, A. J. Thompson, and M. S. International Advisory Committee on Clinical Trials in, "The 2013 clinical course

descriptors for multiple sclerosis: A clarification," *Neurology,* vol. 94, no. 24, pp. 1088-1092, Jun 16 2020, doi: 10.1212/WNL.0000000000009636.

[304] H. Lassmann and M. Bradl, "Multiple sclerosis: experimental models and reality," *Acta Neuropathol,* vol. 133, no. 2, pp. 223-244, Feb 2017, doi: 10.1007/s00401-016-1631-4.

[305] A. Scalfari, C. Lederer, M. Daumer, R. Nicholas, G. C. Ebers, and P. A. Muraro, "The relationship of age with the clinical phenotype in multiple sclerosis," *Mult Scler,* vol. 22, no. 13, pp. 1750-1758, Nov 2016, doi: 10.1177/1352458516630396.

[306] H. Lassmann, "Pathogenic Mechanisms Associated With Different Clinical Courses of Multiple Sclerosis," *Front Immunol,* vol. 9, p. 3116, 2018, doi: 10.3389/fimmu.2018.03116.

[307] M. Kremenchutzky, G. P. Rice, J. Baskerville, D. M. Wingerchuk, and G. C. Ebers, "The natural history of multiple sclerosis: a geographically based study 9: observations on the progressive phase of the disease," *Brain,* vol. 129, no. Pt 3, pp. 584-94, Mar 2006, doi: 10.1093/brain/awh721.

[308] M. Trojano, M. Liguori, G. Bosco Zimatore, R. Bugarini, C. Avolio, D. Paolicelli, F. Giuliani, F. De Robertis, M. G. Marrosu, and P. Livrea, "Age-related disability in multiple sclerosis," *Ann Neurol,* vol. 51, no. 4, pp. 475-80, Apr 2002. [Online]. Available: https://www.ncbi.nlm.nih.gov/pubmed/11921053.

[309] S. A. Shields, J. M. Gilson, W. F. Blakemore, and R. J. Franklin, "Remyelination occurs as extensively but more slowly in old rats compared to young rats following gliotoxin-induced CNS demyelination," *Glia,* vol. 28, no. 1, pp. 77-83, Oct 1999. [Online]. Available: https://www.ncbi.nlm.nih.gov/pubmed/10498825.

[310] W. W. Li, J. Penderis, C. Zhao, M. Schumacher, and R. J. Franklin, "Females remyelinate more efficiently than males following demyelination in the aged but not young adult CNS," *Exp Neurol,* vol. 202, no. 1, pp. 250-4, Nov 2006, doi: 10.1016/j.expneurol.2006.05.012.

[311] K. A. Irvine and W. F. Blakemore, "Age increases axon loss associated with primary demyelination in cuprizone-induced demyelination in C57BL/6 mice," *J Neuroimmunol,* vol. 175, no. 1-2, pp. 69-76, Jun 2006, doi: 10.1016/j.jneuroim.2006.03.002.

[312] M. E. Smith, N. L. Eller, H. F. McFarland, M. K. Racke, and C. S. Raine, "Age dependence of clinical and pathological manifestations of autoimmune demyelination. Implications for multiple sclerosis," *Am J Pathol,* vol. 155, no. 4, pp. 1147-61, Oct 1999, doi: 10.1016/S0002-9440(10)65218-2.

[313] M. Filippi, J. S. Wolinsky, M. P. Sormani, G. Comi, and G. European/Canadian Glatiramer Acetate Study, "Enhancement frequency decreases with increasing age in relapsing-remitting multiple sclerosis," *Neurology,* vol. 56, no. 3, pp. 422-3, Feb 13 2001, doi: 10.1212/wnl.56.3.422.

[314] J. S. Wolinsky, P. A. Narayana, J. H. Noseworthy, F. D. Lublin, J. N. Whitaker, A. Linde, P. Gjorstrup, and H. C. Sullivan, "Linomide in relapsing and secondary progressive MS: part II: MRI results. MRI Analysis Center of the University of Texas-Houston, Health Science Center, and the North American Linomide Investigators," *Neurology,* vol. 54, no. 9, pp. 1734-41, May 9 2000, doi: 10.1212/wnl.54.9.1734.

[315] D. Baroncini, P. Annovazzi, N. De Rossi, G. Mallucci, V. T. Clerici, S. Tonietti, V. Mantero, M. T. Ferro, M. J. Messina, V. Barcella, L. La Mantia, M. Ronzoni, C. Barrila, R. Clerici, E. Susani, M. L. Fusco, L. Chiveri, L. Abate, O. Ferraro, R. Capra, E.

Colombo, P. Confalonieri, M. Zaffaroni, and R. S. L. N. M. Ctr, "What is the impact of natural menopause on multiple sclerosis? An Italian, multicentre, retrospective, observational study," *Mult Scler J,* vol. 24, pp. 147-148, Oct 2018. [Online]. Available: <Go to ISI>://WOS:000446861400225.

[316] A. Scalfari, A. Neuhaus, M. Daumer, P. A. Muraro, and G. C. Ebers, "Onset of secondary progressive phase and long-term evolution of multiple sclerosis," *J Neurol Neurosurg Psychiatry,* vol. 85, no. 1, pp. 67-75, Jan 2014, doi: 10.1136/jnnp-2012-304333.

[317] A. Scalfari, A. Neuhaus, A. Degenhardt, G. P. Rice, P. A. Muraro, M. Daumer, and G. C. Ebers, "The natural history of multiple sclerosis: a geographically based study 10: relapses and long-term disability," *Brain,* vol. 133, no. Pt 7, pp. 1914-29, Jul 2010, doi: 10.1093/brain/awq118.

[318] C. Confavreux, S. Vukusic, T. Moreau, and P. Adeleine, "Relapses and progression of disability in multiple sclerosis," *N Engl J Med,* vol. 343, no. 20, pp. 1430-8, Nov 16 2000, doi: 10.1056/NEJM200011163432001.

[319] C. Confavreux, S. Vukusic, and P. Adeleine, "Early clinical predictors and progression of irreversible disability in multiple sclerosis: an amnesic process," *Brain,* vol. 126, no. Pt 4, pp. 770-82, Apr 2003, doi: 10.1093/brain/awg081.

[320] S. J. Pittock, W. T. Mayr, R. L. McClelland, N. W. Jorgensen, S. D. Weigand, J. H. Noseworthy, and M. Rodriguez, "Disability profile of MS did not change over 10 years in a population-based prevalence cohort," *Neurology,* vol. 62, no. 4, pp. 601-6, Feb 24 2004, doi: 10.1212/wnl.62.4.601.

[321] B. D. Trapp and P. K. Stys, "Virtual hypoxia and chronic necrosis of demyelinated axons in multiple sclerosis," *Lancet Neurol,* vol. 8, no. 3, pp. 280-91, Mar 2009, doi: 10.1016/S1474-4422(09)70043-2.

[322] D. H. Mahad, B. D. Trapp, and H. Lassmann, "Progressive multiple sclerosis 1 Pathological mechanisms in progressive multiple sclerosis," *Lancet Neurology,* vol. 14, no. 2, pp. 183-193, Feb 2015, doi: Doi 10.1016/S1474-4422(14)70256-X.

[323] C. Bjartmar, J. R. Wujek, and B. D. Trapp, "Axonal loss in the pathology of MS: consequences for understanding the progressive phase of the disease," *J Neurol Sci,* vol. 206, no. 2, pp. 165-71, Feb 15 2003, doi: 10.1016/s0022-510x(02)00069-2.

[324] S. G. Waxman, "Ions, energy and axonal injury: towards a molecular neurology of multiple sclerosis," *Trends Mol Med,* vol. 12, no. 5, pp. 192-5, May 2006, doi: 10.1016/j.molmed.2006.03.001.

[325] P. K. Stys, "Axonal degeneration in multiple sclerosis: is it time for neuroprotective strategies?," *Ann Neurol,* vol. 55, no. 5, pp. 601-3, May 2004, doi: 10.1002/ana.20082.

[326] H. E. Andrews, P. P. Nichols, D. Bates, and D. M. Turnbull, "Mitochondrial dysfunction plays a key role in progressive axonal loss in Multiple Sclerosis," *Med Hypotheses,* vol. 64, no. 4, pp. 669-77, 2005, doi: 10.1016/j.mehy.2004.09.001.

[327] P. K. Stys, S. G. Waxman, and B. R. Ransom, "Ionic mechanisms of anoxic injury in mammalian CNS white matter: role of Na+ channels and Na(+)-Ca2+ exchanger," *J Neurosci,* vol. 12, no. 2, pp. 430-9, Feb 1992. [Online]. Available: https://www.ncbi.nlm.nih.gov/pubmed/1311030.

[328] D. C. Shields, K. E. Schaecher, T. C. Saido, and N. L. Banik, "A putative mechanism of demyelination in multiple sclerosis by a proteolytic enzyme, calpain," *Proceedings of the*

National Academy of Sciences of the United States of America, vol. 96, no. 20, pp. 11486-91, Sep 28 1999, doi: 10.1073/pnas.96.20.11486.

[329] L. Schirmer, J. P. Antel, W. Bruck, and C. Stadelmann, "Axonal loss and neurofilament phosphorylation changes accompany lesion development and clinical progression in multiple sclerosis," *Brain Pathol,* vol. 21, no. 4, pp. 428-40, Jul 2011, doi: 10.1111/j.1750-3639.2010.00466.x.

[330] C. Moll, C. Mourre, M. Lazdunski, and J. Ulrich, "Increase of sodium channels in demyelinated lesions of multiple sclerosis," *Brain Res,* vol. 556, no. 2, pp. 311-6, Aug 16 1991, doi: 10.1016/0006-8993(91)90321-l.

[331] E. A. Young, C. D. Fowler, G. J. Kidd, A. Chang, R. Rudick, E. Fisher, and B. D. Trapp, "Imaging correlates of decreased axonal Na+/K+ ATPase in chronic multiple sclerosis lesions," *Ann Neurol,* vol. 63, no. 4, pp. 428-35, Apr 2008, doi: 10.1002/ana.21381.

[332] J. van Horssen, M. E. Witte, G. Schreibelt, and H. E. de Vries, "Radical changes in multiple sclerosis pathogenesis," *Biochim Biophys Acta,* vol. 1812, no. 2, pp. 141-50, Feb 2011, doi: 10.1016/j.bbadis.2010.06.011.

[333] P. Mecocci, U. MacGarvey, A. E. Kaufman, D. Koontz, J. M. Shoffner, D. C. Wallace, and M. F. Beal, "Oxidative damage to mitochondrial DNA shows marked age-dependent increases in human brain," *Ann Neurol,* vol. 34, no. 4, pp. 609-16, Oct 1993, doi: 10.1002/ana.410340416.

[334] J. van Horssen, G. Schreibelt, J. Drexhage, T. Hazes, C. D. Dijkstra, P. van der Valk, and H. E. de Vries, "Severe oxidative damage in multiple sclerosis lesions coincides with enhanced antioxidant enzyme expression," *Free Radic Biol Med,* vol. 45, no. 12, pp. 1729-37, Dec 15 2008, doi: 10.1016/j.freeradbiomed.2008.09.023.

[335] A. H. Cross, P. T. Manning, R. M. Keeling, R. E. Schmidt, and T. P. Misko, "Peroxynitrite formation within the central nervous system in active multiple sclerosis," *J Neuroimmunol,* vol. 88, no. 1-2, pp. 45-56, Aug 1 1998, doi: 10.1016/s0165-5728(98)00078-2.

[336] O. A. Bizzozero, G. DeJesus, H. A. Bixler, and A. Pastuszyn, "Evidence of nitrosative damage in the brain white matter of patients with multiple sclerosis," *Neurochem Res,* vol. 30, no. 1, pp. 139-49, Jan 2005, doi: 10.1007/s11064-004-9695-2.

[337] J. van Horssen, J. A. Drexhage, T. Flor, W. Gerritsen, P. van der Valk, and H. E. de Vries, "Nrf2 and DJ1 are consistently upregulated in inflammatory multiple sclerosis lesions," *Free Radic Biol Med,* vol. 49, no. 8, pp. 1283-9, Nov 1 2010, doi: 10.1016/j.freeradbiomed.2010.07.013.

[338] S. Hametner, I. Wimmer, L. Haider, S. Pfeifenbring, W. Bruck, and H. Lassmann, "Iron and neurodegeneration in the multiple sclerosis brain," *Ann Neurol,* vol. 74, no. 6, pp. 848-61, Dec 2013, doi: 10.1002/ana.23974.

[339] M. P. Murphy, "How mitochondria produce reactive oxygen species," *Biochem J,* vol. 417, no. 1, pp. 1-13, Jan 1 2009, doi: 10.1042/BJ20081386.

[340] G. R. Campbell, I. Ziabreva, A. K. Reeve, K. J. Krishnan, R. Reynolds, O. Howell, H. Lassmann, D. M. Turnbull, and D. J. Mahad, "Mitochondrial DNA deletions and neurodegeneration in multiple sclerosis," *Ann Neurol,* vol. 69, no. 3, pp. 481-92, Mar 2011, doi: 10.1002/ana.22109.

[341] D. J. Mahad, I. Ziabreva, G. Campbell, N. Lax, K. White, P. S. Hanson, H. Lassmann, and D. M. Turnbull, "Mitochondrial changes within axons in multiple sclerosis," *Brain,* vol. 132, no. Pt 5, pp. 1161-74, May 2009, doi: 10.1093/brain/awp046.

[342] A. Blokhin, T. Vyshkina, S. Komoly, and B. Kalman, "Variations in mitochondrial DNA copy numbers in MS brains," *J Mol Neurosci,* vol. 35, no. 3, pp. 283-7, Jul 2008, doi: 10.1007/s12031-008-9115-1.

[343] I. Griffiths, M. Klugmann, T. Anderson, D. Yool, C. Thomson, M. H. Schwab, A. Schneider, F. Zimmermann, M. McCulloch, N. Nadon, and K. A. Nave, "Axonal swellings and degeneration in mice lacking the major proteolipid of myelin," *Science,* vol. 280, no. 5369, pp. 1610-3, Jun 5 1998, doi: 10.1126/science.280.5369.1610.

[344] C. Lappe-Siefke, S. Goebbels, M. Gravel, E. Nicksch, J. Lee, P. E. Braun, I. R. Griffiths, and K. A. Nave, "Disruption of Cnp1 uncouples oligodendroglial functions in axonal support and myelination," *Nat Genet,* vol. 33, no. 3, pp. 366-74, Mar 2003, doi: 10.1038/ng1095.

[345] K. A. Nave and B. D. Trapp, "Axon-glial signaling and the glial support of axon function," *Annu Rev Neurosci,* vol. 31, pp. 535-61, 2008, doi: 10.1146/annurev.neuro.30.051606.094309.

[346] N. Manrique-Hoyos, T. Jurgens, M. Gronborg, M. Kreutzfeldt, M. Schedensack, T. Kuhlmann, C. Schrick, W. Bruck, H. Urlaub, M. Simons, and D. Merkler, "Late motor decline after accomplished remyelination: impact for progressive multiple sclerosis," *Ann Neurol,* vol. 71, no. 2, pp. 227-44, Feb 2012, doi: 10.1002/ana.22681.

[347] J. Penderis, S. A. Shields, and R. J. Franklin, "Impaired remyelination and depletion of oligodendrocyte progenitors does not occur following repeated episodes of focal demyelination in the rat central nervous system," *Brain,* vol. 126, no. Pt 6, pp. 1382-91, Jun 2003, doi: 10.1093/brain/awg126.

[348] S. K. Ludwin, "Chronic demyelination inhibits remyelination in the central nervous system. An analysis of contributing factors," *Lab Invest,* vol. 43, no. 4, pp. 382-7, Oct 1980. [Online]. Available: https://www.ncbi.nlm.nih.gov/pubmed/7442125.

[349] J. L. Mason, A. Toews, J. D. Hostettler, P. Morell, K. Suzuki, J. E. Goldman, and G. K. Matsushima, "Oligodendrocytes and progenitors become progressively depleted within chronically demyelinated lesions," *Am J Pathol,* vol. 164, no. 5, pp. 1673-82, May 2004, doi: 10.1016/S0002-9440(10)63726-1.

[350] H. M. French, M. Reid, P. Mamontov, R. A. Simmons, and J. B. Grinspan, "Oxidative stress disrupts oligodendrocyte maturation," *J Neurosci Res,* vol. 87, no. 14, pp. 3076-87, Nov 1 2009, doi: 10.1002/jnr.22139.

[351] I. Ziabreva, G. Campbell, J. Rist, J. Zambonin, J. Rorbach, M. M. Wydro, H. Lassmann, R. J. Franklin, and D. Mahad, "Injury and differentiation following inhibition of mitochondrial respiratory chain complex IV in rat oligodendrocytes," *Glia,* vol. 58, no. 15, pp. 1827-37, Nov 15 2010, doi: 10.1002/glia.21052.

[352] R. Sharma, M. T. Fischer, J. Bauer, P. A. Felts, K. J. Smith, T. Misu, K. Fujihara, M. Bradl, and H. Lassmann, "Inflammation induced by innate immunity in the central nervous system leads to primary astrocyte dysfunction followed by demyelination," *Acta Neuropathol,* vol. 120, no. 2, pp. 223-36, Aug 2010, doi: 10.1007/s00401-010-0704-z.

[353] G. Mallucci, L. Peruzzotti-Jametti, J. D. Bernstock, and S. Pluchino, "The role of immune cells, glia and neurons in white and gray matter pathology in multiple sclerosis," *Prog Neurobiol,* vol. 127-128, pp. 1-22, Apr 2015, doi: 10.1016/j.pneurobio.2015.02.003.

[354] B. Ferguson, M. K. Matyszak, M. M. Esiri, and V. H. Perry, "Axonal damage in acute multiple sclerosis lesions," *Brain,* vol. 120 (Pt 3), pp. 393-9, Mar 1997, doi: 10.1093/brain/120.3.393.

[355] A. Bitsch, J. Schuchardt, S. Bunkowski, T. Kuhlmann, and W. Bruck, "Acute axonal injury in multiple sclerosis. Correlation with demyelination and inflammation," *Brain,* vol. 123 (Pt 6), pp. 1174-83, Jun 2000, doi: 10.1093/brain/123.6.1174.

[356] T. Kuhlmann, G. Lingfeld, A. Bitsch, J. Schuchardt, and W. Bruck, "Acute axonal damage in multiple sclerosis is most extensive in early disease stages and decreases over time," *Brain,* vol. 125, no. Pt 10, pp. 2202-12, Oct 2002, doi: 10.1093/brain/awf235.

[357] B. D. Trapp, J. Peterson, R. M. Ransohoff, R. Rudick, S. Mork, and L. Bo, "Axonal transection in the lesions of multiple sclerosis," *N Engl J Med,* vol. 338, no. 5, pp. 278-85, Jan 29 1998, doi: 10.1056/NEJM199801293380502.

[358] D. T. Chard, C. M. Griffin, G. J. Parker, R. Kapoor, A. J. Thompson, and D. H. Miller, "Brain atrophy in clinically early relapsing-remitting multiple sclerosis," *Brain,* vol. 125, no. Pt 2, pp. 327-37, Feb 2002, doi: 10.1093/brain/awf025.

[359] P. A. Brex, R. Jenkins, N. C. Fox, W. R. Crum, J. I. O'Riordan, G. T. Plant, and D. H. Miller, "Detection of ventricular enlargement in patients at the earliest clinical stage of MS," *Neurology,* vol. 54, no. 8, pp. 1689-91, Apr 25 2000, doi: 10.1212/wnl.54.8.1689.

[360] N. De Stefano, P. M. Matthews, M. Filippi, F. Agosta, M. De Luca, M. L. Bartolozzi, L. Guidi, A. Ghezzi, E. Montanari, A. Cifelli, A. Federico, and S. M. Smith, "Evidence of early cortical atrophy in MS: relevance to white matter changes and disability," *Neurology,* vol. 60, no. 7, pp. 1157-62, Apr 8 2003, doi: 10.1212/01.wnl.0000055926.69643.03.

[361] M. A. Rocca, G. Iannucci, M. Rovaris, G. Comi, and M. Filippi, "Occult tissue damage in patients with primary progressive multiple sclerosis is independent of T2-visible lesions--a diffusion tensor MR study," *J Neurol,* vol. 250, no. 4, pp. 456-60, Apr 2003, doi: 10.1007/s00415-003-1024-1.

[362] I. Duran, E. M. Martinez-Caceres, J. Rio, N. Barbera, M. E. Marzo, and X. Montalban, "Immunological profile of patients with primary progressive multiple sclerosis. Expression of adhesion molecules," *Brain,* vol. 122 (Pt 12), pp. 2297-307, Dec 1999, doi: 10.1093/brain/122.12.2297.

[363] D. Chard and D. Miller, "Grey matter pathology in clinically early multiple sclerosis: evidence from magnetic resonance imaging," *J Neurol Sci,* vol. 282, no. 1-2, pp. 5-11, Jul 15 2009, doi: 10.1016/j.jns.2009.01.012.

[364] D. T. Chard, P. A. Brex, O. Ciccarelli, C. M. Griffin, G. J. Parker, C. Dalton, D. R. Altmann, A. J. Thompson, and D. H. Miller, "The longitudinal relation between brain lesion load and atrophy in multiple sclerosis: a 14 year follow up study," *J Neurol Neurosurg Psychiatry,* vol. 74, no. 11, pp. 1551-4, Nov 2003, doi: 10.1136/jnnp.74.11.1551.

[365] E. Fisher, J. C. Lee, K. Nakamura, and R. A. Rudick, "Gray matter atrophy in multiple sclerosis: a longitudinal study," *Ann Neurol,* vol. 64, no. 3, pp. 255-65, Sep 2008, doi: 10.1002/ana.21436.

[366] N. C. Fox, R. Jenkins, S. M. Leary, V. L. Stevenson, N. A. Losseff, W. R. Crum, R. J. Harvey, M. N. Rossor, D. H. Miller, and A. J. Thompson, "Progressive cerebral atrophy in MS: a serial study using registered, volumetric MRI," *Neurology,* vol. 54, no. 4, pp. 807-12, Feb 22 2000, doi: 10.1212/wnl.54.4.807.

[367] Y. Ge, R. I. Grossman, J. K. Udupa, L. Wei, L. J. Mannon, M. Polansky, and D. L. Kolson, "Brain atrophy in relapsing-remitting multiple sclerosis and secondary progressive multiple sclerosis: longitudinal quantitative analysis," *Radiology,* vol. 214, no. 3, pp. 665-70, Mar 2000, doi: 10.1148/radiology.214.3.r00mr30665.

[368] N. F. Kalkers, N. Ameziane, J. C. J. Bot, A. Minneboo, C. H. Polman, and F. Barkhof, "Longitudinal brain volume measurement in multiple sclerosis - Rate of brain atrophy is independent of the disease subtype," *Arch Neurol-Chicago,* vol. 59, no. 10, pp. 1572-1576, Oct 2002, doi: DOI 10.1001/archneur.59.10.1572.

[369] C. M. Dalton, D. T. Chard, G. R. Davies, K. A. Miszkiel, D. R. Altmann, K. Fernando, G. T. Plant, A. J. Thompson, and D. H. Miller, "Early development of multiple sclerosis is associated with progressive grey matter atrophy in patients presenting with clinically isolated syndromes," *Brain,* vol. 127, no. Pt 5, pp. 1101-7, May 2004, doi: 10.1093/brain/awh126.

[370] M. Tiberio, D. T. Chard, D. R. Altmann, G. Davies, C. M. Griffin, W. Rashid, J. Sastre-Garriga, A. J. Thompson, and D. H. Miller, "Gray and white matter volume changes in early RRMS: a 2-year longitudinal study," *Neurology,* vol. 64, no. 6, pp. 1001-7, Mar 22 2005, doi: 10.1212/01.WNL.0000154526.22878.30.

[371] S. E. Schutzer, T. E. Angel, T. Liu, A. A. Schepmoes, F. Xie, J. Bergquist, L. Vecsei, D. Zadori, D. G. Camp, 2nd, B. K. Holland, R. D. Smith, and P. K. Coyle, "Gray matter is targeted in first-attack multiple sclerosis," *PLoS One,* vol. 8, no. 9, p. e66117, 2013, doi: 10.1371/journal.pone.0066117.

[372] J. J. Geurts, M. Calabrese, E. Fisher, and R. A. Rudick, "Measurement and clinical effect of grey matter pathology in multiple sclerosis," *Lancet Neurol,* vol. 11, no. 12, pp. 1082-92, Dec 2012, doi: 10.1016/S1474-4422(12)70230-2.

[373] S. D. Roosendaal, K. Bendfeldt, H. Vrenken, C. H. Polman, S. Borgwardt, E. W. Radue, L. Kappos, D. Pelletier, S. L. Hauser, P. M. Matthews, F. Barkhof, and J. J. Geurts, "Grey matter volume in a large cohort of MS patients: relation to MRI parameters and disability," *Mult Scler,* vol. 17, no. 9, pp. 1098-106, Sep 2011, doi: 10.1177/1352458511404916.

[374] L. Bo, C. A. Vedeler, H. I. Nyland, B. D. Trapp, and S. J. Mork, "Subpial demyelination in the cerebral cortex of multiple sclerosis patients," *J Neuropathol Exp Neurol,* vol. 62, no. 7, pp. 723-32, Jul 2003, doi: 10.1093/jnen/62.7.723.

[375] L. Bo, J. J. Geurts, P. van der Valk, C. Polman, and F. Barkhof, "Lack of correlation between cortical demyelination and white matter pathologic changes in multiple sclerosis," *Arch Neurol,* vol. 64, no. 1, pp. 76-80, Jan 2007, doi: 10.1001/archneur.64.1.76.

[376] R. Magliozzi, O. W. Howell, R. Nicholas, C. Cruciani, M. Castellaro, C. Romualdi, S. Rossi, M. Pitteri, M. D. Benedetti, A. Gajofatto, F. B. Pizzini, S. Montemezzi, S. Rasia, R. Capra, A. Bertoldo, F. Facchiano, S. Monaco, R. Reynolds, and M. Calabrese, "Inflammatory intrathecal profiles and cortical damage in multiple sclerosis," *Annals of Neurology,* vol. 83, no. 4, pp. 739-755, Apr 2018, doi: 10.1002/ana.25197.

[377] O. W. Howell, C. A. Reeves, R. Nicholas, D. Carassiti, B. Radotra, S. M. Gentleman, B. Serafini, F. Aloisi, F. Roncaroli, R. Magliozzi, and R. Reynolds, "Meningeal

inflammation is widespread and linked to cortical pathology in multiple sclerosis," *Brain,* vol. 134, no. Pt 9, pp. 2755-71, Sep 2011, doi: 10.1093/brain/awr182.

[378] C. W. Hollen, M. M. Paz Soldan, J. R. Rinker, 2nd, and R. I. Spain, "The Future of Progressive Multiple Sclerosis Therapies," *Fed Pract,* vol. 37, no. Suppl 1, pp. S43-S49, Apr 2020. [Online]. Available: http://www.ncbi.nlm.nih.gov/pubmed/32341636.

[379] U. S. F. a. D. Administration, "FDA approves new oral treatment for multiple sclerosis," ed, 2019.

[380] S. M. Leary and A. J. Thompson, "Interferon beta-1a in primary progressive multiple sclerosis," *J Neurol Sci,* vol. 206, no. 2, pp. 215-6, Feb 15 2003, doi: 10.1016/s0022-510x(02)00350-7.

[381] J. S. Wolinsky, P. A. Narayana, P. O'Connor, P. K. Coyle, C. Ford, K. Johnson, A. Miller, L. Pardo, S. Kadosh, D. Ladkani, and P. R. T. S. Group, "Glatiramer acetate in primary progressive multiple sclerosis: results of a multinational, multicenter, double-blind, placebo-controlled trial," *Ann Neurol,* vol. 61, no. 1, pp. 14-24, Jan 2007, doi: 10.1002/ana.21079.

[382] K. Hawker, P. O'Connor, M. S. Freedman, P. A. Calabresi, J. Antel, J. Simon, S. Hauser, E. Waubant, T. Vollmer, H. Panitch, J. Zhang, P. Chin, C. H. Smith, and O. t. group, "Rituximab in patients with primary progressive multiple sclerosis: results of a randomized double-blind placebo-controlled multicenter trial," *Ann Neurol,* vol. 66, no. 4, pp. 460-71, Oct 2009, doi: 10.1002/ana.21867.

[383] "Placebo-controlled multicentre randomised trial of interferon beta-1b in treatment of secondary progressive multiple sclerosis. European Study Group on interferon beta-1b in

secondary progressive MS," *Lancet,* vol. 352, no. 9139, pp. 1491-7, Nov 7 1998. [Online]. Available: https://www.ncbi.nlm.nih.gov/pubmed/9820296.

[384] H. Panitch, A. Miller, D. Paty, B. Weinshenker, and M. S. North American Study Group on Interferon beta-1b in Secondary Progressive, "Interferon beta-1b in secondary progressive MS: results from a 3-year controlled study," *Neurology,* vol. 63, no. 10, pp. 1788-95, Nov 23 2004, doi: 10.1212/01.wnl.0000146958.77317.3e.

[385] L. Kappos, B. Weinshenker, C. Pozzilli, A. J. Thompson, F. Dahlke, K. Beckmann, C. Polman, H. McFarland, C. European Interferon beta-1b in Secondary Progressive Multiple Sclerosis Trial Steering, B. Independent Advisory, C. North American Interferon beta-1b in Secondary Progressive Multiple Sclerosis Trial Steering, and B. Independent Advisory, "Interferon beta-1b in secondary progressive MS: a combined analysis of the two trials," *Neurology,* vol. 63, no. 10, pp. 1779-87, Nov 23 2004, doi: 10.1212/01.wnl.0000145561.08973.4f.

[386] M. P. Sormani, P. A. Muraro, I. Schiavetti, A. Signori, A. Laroni, R. Saccardi, and G. L. Mancardi, "Autologous hematopoietic stem cell transplantation in multiple sclerosis: A meta-analysis," *Neurology,* vol. 88, no. 22, pp. 2115-2122, May 30 2017, doi: 10.1212/WNL.0000000000003987.

[387] F. Ge, H. Lin, Z. Li, and T. Chang, "Efficacy and safety of autologous hematopoietic stem-cell transplantation in multiple sclerosis: a systematic review and meta-analysis," *Neurol Sci,* vol. 40, no. 3, pp. 479-487, Mar 2019, doi: 10.1007/s10072-018-3670-1.

[388] M. Gavriilaki, I. Sakellari, E. Gavriilaki, V. K. Kimiskidis, and A. Anagnostopoulos, "Autologous Hematopoietic Cell Transplantation in Multiple Sclerosis: Changing

Paradigms in the Era of Novel Agents," *Stem Cells Int,* vol. 2019, p. 5840286, 2019, doi: 10.1155/2019/5840286.

[389] F. X. Cuascut and G. J. Hutton, "Stem Cell-Based Therapies for Multiple Sclerosis: Current Perspectives," *Biomedicines,* vol. 7, no. 2, Mar 30 2019, doi: 10.3390/biomedicines7020026.

[390] V. K. Harris, J. Stark, T. Vyshkina, L. Blackshear, G. Joo, V. Stefanova, G. Sara, and S. A. Sadiq, "Phase I Trial of Intrathecal Mesenchymal Stem Cell-derived Neural Progenitors in Progressive Multiple Sclerosis," *EBioMedicine,* vol. 29, pp. 23-30, Mar 2018, doi: 10.1016/j.ebiom.2018.02.002.

[391] J. Romme Christensen, R. Ratzer, L. Bornsen, M. Lyksborg, E. Garde, T. B. Dyrby, H. R. Siebner, P. S. Sorensen, and F. Sellebjerg, "Natalizumab in progressive MS: results of an open-label, phase 2A, proof-of-concept trial," *Neurology,* vol. 82, no. 17, pp. 1499-507, Apr 29 2014, doi: 10.1212/WNL.0000000000000361.

[392] R. Kapoor, P. R. Ho, N. Campbell, I. Chang, A. Deykin, F. Forrestal, N. Lucas, B. Yu, D. L. Arnold, M. S. Freedman, M. D. Goldman, H. P. Hartung, E. K. Havrdova, D. Jeffery, A. Miller, F. Sellebjerg, D. Cadavid, D. Mikol, D. Steiner, and A. investigators, "Effect of natalizumab on disease progression in secondary progressive multiple sclerosis (ASCEND): a phase 3, randomised, double-blind, placebo-controlled trial with an open-label extension," *Lancet Neurol,* vol. 17, no. 5, pp. 405-415, May 2018, doi: 10.1016/S1474-4422(18)30069-3.

[393] L. Kappos, A. Bar-Or, B. A. C. Cree, R. J. Fox, G. Giovannoni, R. Gold, P. Vermersch, D. L. Arnold, S. Arnould, T. Scherz, C. Wolf, E. Wallstrom, F. Dahlke, and E. C. Investigators, "Siponimod versus placebo in secondary progressive multiple sclerosis

(EXPAND): a double-blind, randomised, phase 3 study," *Lancet,* vol. 391, no. 10127, pp. 1263-1273, Mar 31 2018, doi: 10.1016/S0140-6736(18)30475-6.

[394] B. A. C. Cree, J. Mares, and H. P. Hartung, "Current therapeutic landscape in multiple sclerosis: an evolving treatment paradigm," *Curr Opin Neurol,* vol. 32, no. 3, pp. 365-377, Jun 2019, doi: 10.1097/WCO.0000000000000700.

[395] R. J. Fox, C. S. Coffey, R. Conwit, M. E. Cudkowicz, T. Gleason, A. Goodman, E. C. Klawiter, K. Matsuda, M. McGovern, R. T. Naismith, A. Ashokkumar, J. Barnes, D. Ecklund, E. Klingner, M. Koepp, J. D. Long, S. Natarajan, B. Thornell, J. Yankey, R. A. Bermel, J. P. Debbins, X. Huang, P. Jagodnik, M. J. Lowe, K. Nakamura, S. Narayanan, K. E. Sakaie, B. Thoomukuntla, X. Zhou, S. Krieger, E. Alvarez, M. Apperson, K. Bashir, B. A. Cohen, P. K. Coyle, S. Delgado, L. D. Dewitt, A. Flores, B. S. Giesser, M. D. Goldman, B. Jubelt, N. Lava, S. G. Lynch, H. Moses, D. Ontaneda, J. S. Perumal, M. Racke, P. Repovic, C. S. Riley, C. Severson, S. Shinnar, V. Suski, B. Weinstock-Guttman, V. Yadav, A. Zabeti, and N. S.-M. T. Investigators, "Phase 2 Trial of Ibudilast in Progressive Multiple Sclerosis," *N Engl J Med,* vol. 379, no. 9, pp. 846-855, Aug 30 2018, doi: 10.1056/NEJMoa1803583.

[396] G. Giovannoni, V. Knappertz, J. R. Steinerman, A. P. Tansy, T. Li, S. Krieger, A. Uccelli, B. M. J. Uitdehaag, X. Montalban, H. P. Hartung, M. P. Sormani, B. A. C. Cree, F. Lublin, and F. Barkhof, "A randomized, placebo-controlled phase 2 trial of laquinimod in primary progressive multiple sclerosis," *Neurology,* Jul 10 2020, doi: 10.1212/WNL.0000000000010284.

[397] R. Kapoor, J. Furby, T. Hayton, K. J. Smith, D. R. Altmann, R. Brenner, J. Chataway, R. A. Hughes, and D. H. Miller, "Lamotrigine for neuroprotection in secondary progressive

multiple sclerosis: a randomised, double-blind, placebo-controlled, parallel-group trial," *Lancet Neurol,* vol. 9, no. 7, pp. 681-8, Jul 2010, doi: 10.1016/S1474-4422(10)70131-9.

[398] G. P. Rice, M. Filippi, and G. Comi, "Cladribine and progressive MS: clinical and MRI outcomes of a multicenter controlled trial. Cladribine MRI Study Group," *Neurology,* vol. 54, no. 5, pp. 1145-55, Mar 14 2000, doi: 10.1212/wnl.54.5.1145.

[399] J. H. Noseworthy, P. O'Brien, B. J. Erickson, D. Lee, D. Sneve, G. C. Ebers, G. P. Rice, A. Auty, W. J. Hader, A. Kirk, P. Duquette, J. Carter, G. Francis, L. Metz, and E. Shuster, "The Mayo Clinic-Canadian Cooperative trial of sulfasalazine in active multiple sclerosis," *Neurology,* vol. 51, no. 5, pp. 1342-52, Nov 1998, doi: 10.1212/wnl.51.5.1342.

[400] M. B. Bornstein, A. Miller, S. Slagle, M. Weitzman, E. Drexler, M. Keilson, V. Spada, W. Weiss, S. Appel, L. Rolak, and et al., "A placebo-controlled, double-blind, randomized, two-center, pilot trial of Cop 1 in chronic progressive multiple sclerosis," *Neurology,* vol. 41, no. 4, pp. 533-9, Apr 1991, doi: 10.1212/wnl.41.4.533.

[401] X. Montalban, S. L. Hauser, L. Kappos, D. L. Arnold, A. Bar-Or, G. Comi, J. de Seze, G. Giovannoni, H. P. Hartung, B. Hemmer, F. Lublin, K. W. Rammohan, K. Selmaj, A. Traboulsee, A. Sauter, D. Masterman, P. Fontoura, S. Belachew, H. Garren, N. Mairon, P. Chin, J. S. Wolinsky, and O. C. Investigators, "Ocrelizumab versus Placebo in Primary Progressive Multiple Sclerosis," *N Engl J Med,* vol. 376, no. 3, pp. 209-220, Jan 19 2017, doi: 10.1056/NEJMoa1606468.

[402] X. Montalban, B. Hemmer, K. Rammohan, G. Giovannoni, J. De Seze, A. Bar-Or, D. Arnold, A. Sauter, D. Masterman, P. Fontoura, H. Garren, P. Chin, and J. Wolinsky, "Efficacy and Safety of Ocrelizumab in Primary Progressive Multiple Sclerosis: Results

of the Phase III Double-Blind, Placebo-Controlled ORATORIO Study (S49.001)," *Neurology,* vol. 86, 2016-04-05 00:00:00 2016.

[403] A. J. Coles, M. G. Wing, P. Molyneux, A. Paolillo, C. M. Davie, G. Hale, D. Miller, H. Waldmann, and A. Compston, "Monoclonal antibody treatment exposes three mechanisms underlying the clinical course of multiple sclerosis," *Ann Neurol,* vol. 46, no. 3, pp. 296-304, Sep 1999, doi: 10.1002/1531-8249(199909)46:3<296::aid-ana4>3.0.co;2-#.

[404] F. Sedel, C. Papeix, A. Bellanger, V. Touitou, C. Lebrun-Frenay, D. Galanaud, O. Gout, O. Lyon-Caen, and A. Tourbah, "High doses of biotin in chronic progressive multiple sclerosis: a pilot study," *Mult Scler Relat Disord,* vol. 4, no. 2, pp. 159-69, Mar 2015, doi: 10.1016/j.msard.2015.01.005.

[405] A. Tourbah, C. Lebrun-Frenay, G. Edan, M. Clanet, C. Papeix, S. Vukusic, J. De Seze, M. Debouverie, O. Gout, P. Clavelou, G. Defer, D. A. Laplaud, T. Moreau, P. Labauge, B. Brochet, F. Sedel, J. Pelletier, and M.-S. s. group, "MD1003 (high-dose biotin) for the treatment of progressive multiple sclerosis: A randomised, double-blind, placebo-controlled study," *Mult Scler,* vol. 22, no. 13, pp. 1719-1731, Nov 2016, doi: 10.1177/1352458516667568.

[406] A. Tourbah, O. Gout, A. Vighetto, V. Deburghgraeve, J. Pelletier, C. Papeix, C. Lebrun-Frenay, P. Labauge, D. Brassat, A. Toosy, D. A. Laplaud, O. Outteryck, T. Moreau, M. Debouverie, P. Clavelou, O. Heinzlef, J. De Seze, G. Defer, F. Sedel, and C. Arndt, "MD1003 (High-Dose Pharmaceutical-Grade Biotin) for the Treatment of Chronic Visual Loss Related to Optic Neuritis in Multiple Sclerosis: A Randomized, Double-Blind,

Placebo-Controlled Study," *CNS Drugs,* vol. 32, no. 7, pp. 661-672, Jul 2018, doi: 10.1007/s40263-018-0528-2.

[407] E. T. Granella F., E. Siena, E. Curti., "Breakthrough disease under high-dose biotin treatment in progressive multiple sclerosis," presented at the Joint Meeting of the European Committee for Treatment and Research in Multiple Sclerosis (ECTRIMS) and the Americas Committee for Treatment and Research in Multiple Sclerosis, 2017.

[408] A. Ben-Nun, H. Wekerle, and I. R. Cohen, "The rapid isolation of clonable antigen-specific T lymphocyte lines capable of mediating autoimmune encephalomyelitis," *Eur J Immunol,* vol. 11, no. 3, pp. 195-9, Mar 1981, doi: 10.1002/eji.1830110307.

[409] C. Linington, M. Bradl, H. Lassmann, C. Brunner, and K. Vass, "Augmentation of demyelination in rat acute allergic encephalomyelitis by circulating mouse monoclonal antibodies directed against a myelin/oligodendrocyte glycoprotein," *Am J Pathol,* vol. 130, no. 3, pp. 443-54, Mar 1988. [Online]. Available: https://www.ncbi.nlm.nih.gov/pubmed/2450462.

[410] J. Goverman, A. Woods, L. Larson, L. P. Weiner, L. Hood, and D. M. Zaller, "Transgenic mice that express a myelin basic protein-specific T cell receptor develop spontaneous autoimmunity," *Cell,* vol. 72, no. 4, pp. 551-60, Feb 26 1993, doi: 10.1016/0092-8674(93)90074-z.

[411] R. P. Lisak and B. Zweiman, "In vitro cell-mediated immunity of cerebrospinal-fluid lymphocytes to myelin basic protein in primary demyelinating diseases," *N Engl J Med,* vol. 297, no. 16, pp. 850-3, Oct 20 1977, doi: 10.1056/NEJM197710202971602.

[412] V. Lampasona, D. Franciotta, R. Furlan, S. Zanaboni, R. Fazio, E. Bonifacio, G. Comi, and G. Martino, "Similar low frequency of anti-MOG IgG and IgM in MS patients and

healthy subjects," *Neurology,* vol. 62, no. 11, pp. 2092-4, Jun 8 2004, doi: 10.1212/01.wnl.0000127615.15768.ae.

[413] E. T. Lim, T. Berger, M. Reindl, C. M. Dalton, K. Fernando, G. Keir, E. J. Thompson, D. H. Miller, and G. Giovannoni, "Anti-myelin antibodies do not allow earlier diagnosis of multiple sclerosis," *Mult Scler,* vol. 11, no. 4, pp. 492-4, Aug 2005, doi: 10.1191/1352458505ms1187sr.

[414] K. C. O'Connor, K. A. McLaughlin, P. L. De Jager, T. Chitnis, E. Bettelli, C. Xu, W. H. Robinson, S. V. Cherry, A. Bar-Or, B. Banwell, H. Fukaura, T. Fukazawa, S. Tenembaum, S. J. Wong, N. P. Tavakoli, Z. Idrissova, V. Viglietta, K. Rostasy, D. Pohl, R. C. Dale, M. Freedman, L. Steinman, G. J. Buckle, V. K. Kuchroo, D. A. Hafler, and K. W. Wucherpfennig, "Self-antigen tetramers discriminate between myelin autoantibodies to native or denatured protein," *Nat Med,* vol. 13, no. 2, pp. 211-7, Feb 2007, doi: 10.1038/nm1488.

[415] M. K. Storch, J. Bauer, C. Linington, T. Olsson, R. Weissert, and H. Lassmann, "Cortical demyelination can be modeled in specific rat models of autoimmune encephalomyelitis and is major histocompatability complex (MHC) haplotype-related," *J Neuropath Exp Neur,* vol. 65, no. 12, pp. 1137-1142, Dec 2006, doi: DOI 10.1097/01.jnen.0000248547.13176.9d.

[416] I. M. Pomeroy, P. M. Matthews, J. A. Frank, E. K. Jordan, and M. M. Esiri, "Demyelinated neocortical lesions in marmoset autoimmune encephalomyelitis mimic those in multiple sclerosis," *Brain,* vol. 128, no. Pt 11, pp. 2713-21, Nov 2005, doi: 10.1093/brain/awh626.

[417] H. Levy, Y. Assaf, and D. Frenkel, "Characterization of brain lesions in a mouse model of progressive multiple sclerosis," *Experimental Neurology,* vol. 226, no. 1, pp. 148-158, Nov 2010, doi: 10.1016/j.expneurol.2010.08.017.

[418] A. Peters, L. A. Pitcher, J. M. Sullivan, M. Mitsdoerffer, S. E. Acton, B. Franz, K. Wucherpfennig, S. Turley, M. C. Carroll, R. A. Sobel, E. Bettelli, and V. K. Kuchroo, "Th17 Cells Induce Ectopic Lymphoid Follicles in Central Nervous System Tissue Inflammation," *Immunity,* vol. 35, no. 6, pp. 986-996, Dec 23 2011, doi: 10.1016/j.immuni.2011.10.015.

[419] C. Schuh, I. Wimmer, S. Hametner, L. Haider, A. M. Van Dam, R. S. Liblau, K. J. Smith, L. Probert, C. J. Binder, J. Bauer, M. Bradl, D. Mahad, and H. Lassmann, "Oxidative tissue injury in multiple sclerosis is only partly reflected in experimental disease models," *Acta Neuropathologica,* vol. 128, no. 2, pp. 247-266, Aug 2014, doi: 10.1007/s00401-014-1263-5.

[420] M. Calabrese, M. Filippi, and P. Gallo, "Cortical lesions in multiple sclerosis," *Nature Reviews Neurology,* vol. 6, no. 8, pp. 438-444, Aug 2010. [Online]. Available: <Go to ISI>://WOS:000280667100010.

[421] J. Newcombe, C. P. Hawkins, C. L. Henderson, H. A. Patel, M. N. Woodroofe, G. M. Hayes, M. L. Cuzner, D. Macmanus, E. P. G. H. Duboulay, and W. I. Mcdonald, "Histopathology of Multiple-Sclerosis Lesions Detected by Magnetic-Resonance-Imaging in Unfixed Postmortem Central-Nervous-System Tissue," *Brain,* vol. 114, pp. 1013-1023, Apr 1991. [Online]. Available: <Go to ISI>://WOS:A1991FQ67500022.

[422] M. Terpstra, P. G. Henry, and R. Gruetter, "Measurement of reduced glutathione (GSH) in human brain using LCModel analysis of difference-edited spectra," *Magn Reson Med,* vol. 50, no. 1, pp. 19-23, Jul 2003. [Online].

[423] P. G. Henry, C. Dautry, P. Hantraye, and G. Bloch, "Brain GABA editing without macromolecule contamination," *Magn Reson Med,* vol. 45, no. 3, pp. 517-20, Mar 2001. [Online]. Available: https://www.ncbi.nlm.nih.gov/pubmed/11241712.

[424] Z. Caramanos, S. Narayanan, and D. L. Arnold, "H-1-MRS quantification of tNA and tCr in patients with multiple sclerosis: a meta-analytic review," *Brain,* vol. 128, pp. 2483-2506, Nov 2005, doi: 10.1093/brain/awh640.

[425] N. I. Avdievich and H. P. Hetherington, "High-field head radiofrequency volume coils using transverse electromagnetic (TEM) and phased array technologies," *NMR Biomed,* vol. 22, no. 9, pp. 960-74, Nov 2009. [Online].

[426] C. Juchem, S. Umesh Rudrapatna, T. W. Nixon, and R. A. de Graaf, "Dynamic multi-coil technique (DYNAMITE) shimming for echo-planar imaging of the human brain at 7 Tesla," *Neuroimage,* vol. 105, pp. 462-72, Jan 15 2015. [Online].

[427] T. W. Scheenen, D. W. Klomp, J. P. Wijnen, and A. Heerschap, "Short echo time 1H-MRSI of the human brain at 3T with minimal chemical shift displacement errors using adiabatic refocusing pulses," *Magn Reson Med,* vol. 59, no. 1, pp. 1-6, Jan 2008. [Online].

[428] A. Haase, J. Frahm, W. Hanicke, and D. Matthaei, "1H NMR chemical shift selective (CHESS) imaging," *Physics in medicine and biology,* vol. 30, no. 4, pp. 341-4, Apr 1985. [Online].

[429] K. L. Behar, D. L. Rothman, D. D. Spencer, and O. A. Petroff, "Analysis of macromolecule resonances in 1H NMR spectra of human brain," *Magn Reson Med,* vol. 32, no. 3, pp. 294-302, Sep 1994. [Online].

[430] J. Frahm, H. Bruhn, M. L. Gyngell, K. D. Merboldt, W. Hanicke, and R. Sauter, "Localized high-resolution proton NMR spectroscopy using stimulated echoes: initial applications to human brain in vivo," *Magn Reson Med,* vol. 9, no. 1, pp. 79-93, Jan 1989. [Online].

[431] C. Juchem, N. K. Logothetis, and J. Pfeuffer, "1H-MRS of the macaque monkey primary visual cortex at 7 T: strategies and pitfalls of shimming at the brain surface," *Magn Reson Imaging,* vol. 25, no. 6, pp. 902-12, Jul 2007, doi: 10.1016/j.mri.2007.03.008.

[432] I. Mader, U. Seeger, R. Weissert, U. Klose, T. Naegele, A. Melms, and W. Grodd, "Proton MR spectroscopy with metabolite-nulling reveals elevated macromolecules in acute multiple sclerosis," *Brain,* vol. 124, no. Pt 5, pp. 953-61, May 2001. [Online]. Available: https://www.ncbi.nlm.nih.gov/pubmed/11335697.

[433] R. A. de Graaf, P. B. Brown, S. McIntyre, T. W. Nixon, K. L. Behar, and D. L. Rothman, "High magnetic field water and metabolite proton T1 and T2 relaxation in rat brain in vivo," *Magn Reson Med,* vol. 56, no. 2, pp. 386-94, Aug 2006. [Online].

[434] C. Juchem. "INSPECTOR - Magnetic Resonance Spectroscopy Software." Columbia TechVenture (CTV). http://innovation.columbia.edu/technologies/cu17130_inspector (accessed.

[435] R. A. de Graaf, G. M. I. Chowdhury, and K. L. Behar, "Quantification of High-Resolution H-1 NMR Spectra from Rat Brain Extracts," *Analytical Chemistry,* vol. 83, no. 1, pp. 216-224, Jan 1 2011, doi: 10.1021/ac102285c.

[436] V. Govindaraju, K. Young, and A. A. Maudsley, "Proton NMR chemical shifts and coupling constants for brain metabolites," *NMR Biomed,* vol. 13, no. 3, pp. 129-53, May 2000. [Online].

[437] V. Govind, K. Young, and A. A. Maudsley, "Corrigendum: proton NMR chemical shifts and coupling constants for brain metabolites. Govindaraju V, Young K, Maudsley AA, NMR Biomed. 2000; 13: 129-153," *NMR Biomed,* vol. 28, no. 7, pp. 923-4, Jul 2015, doi: 10.1002/nbm.3336.

[438] C. Juchem, N. K. Logothetis, and J. Pfeuffer, "High-resolution (1)H chemical shift imaging in the monkey visual cortex," *Magn Reson Med,* vol. 54, no. 6, pp. 1541-1546, Dec 2005. [Online].

[439] S. Cavassila, S. Deval, C. Huegen, D. Van Ormondt, and D. Graveron-Demilly, "Cramer-Rao Bound Expressions for Parametric Estimation of Overlapping Peaks: Influence of Prior Knowledge," *J Magn Reson,* vol. 143, pp. 311-320, 2000. [Online].

[440] K. M. Swanberg, H. Prinsen, A. V. Kurada, R. K. Fulbright, D. Pitt, K. Destefano, M. Bailey, and C. Juchem, "Towards in vivo neurochemical profiling of multiple sclerosis with MR spectroscopy at 7 Tesla: Apparent increase in frontal cortex water T2 in aged individuals with progressive multiple sclerosis stabilizes in biexponential model constrained by tissue partial volumes," *Proc Int Soc Magn Reson Med* vol. 0161, 2018.

[441] S. Michaeli, M. Garwood, X. H. Zhu, L. DelaBarre, P. Andersen, G. Adriany, H. Merkle, K. Ugurbil, and W. Chen, "Proton T2 relaxation study of water, N-acetylaspartate, and creatine in human brain using Hahn and Carr-Purcell spin echoes at 4T and 7T," *Magn Reson Med,* vol. 47, no. 4, pp. 629-33, Apr 2002, doi: 10.1002/mrm.10135.

[442] M. Garwood and L. DelaBarre, "The return of the frequency sweep: designing adiabatic pulses for contemporary NMR," *J Magn Reson,* vol. 153, no. 2, pp. 155-77, Dec 2001, doi: 10.1006/jmre.2001.2340.

[443] S. Posse, C. A. Cuenod, R. Risinger, D. Le Bihan, and R. S. Balaban, "Anomalous transverse relaxation in 1H spectroscopy in human brain at 4 Tesla," *Magn Reson Med,* vol. 33, no. 2, pp. 246-52, Feb 1995, doi: 10.1002/mrm.1910330215.

[444] D. K. Deelchand, P. F. Van de Moortele, G. Adriany, I. Iltis, P. Andersen, J. P. Strupp, J. T. Vaughan, K. Ugurbil, and P. G. Henry, "In vivo 1H NMR spectroscopy of the human brain at 9.4 T: initial results," *J Magn Reson,* vol. 206, no. 1, pp. 74-80, Sep 2010, doi: 10.1016/j.jmr.2010.06.006.

[445] K. Landheer, R. F. Schulte, M. S. Treacy, K. M. Swanberg, and C. Juchem, "Theoretical description of modern (1) H in Vivo magnetic resonance spectroscopic pulse sequences," *J Magn Reson Imaging,* vol. 51, no. 4, pp. 1008-1029, Apr 2020, doi: 10.1002/jmri.26846.

[446] S. Provencher, "LCModel and LCMgui User's Manual.," 2009. [Online]. Available: http://s-provencher.com/pub/LCModel/manual/manual.pdf.

[447] T. Ernst, R. Kreis, and B. Ross, "Absolute quantitation of water and metabolites in the human brain. Compartments and water," *Journal of Magnetic Resonance, Series B,* vol. 102, pp. 1-8, 1993.

[448] J. Dukart, M. L. Schroeter, K. Mueller, and A. D. Neuroimaging, "Age Correction in Dementia - Matching to a Healthy Brain," *Plos One,* vol. 6, no. 7, Jul 29 2011, doi: ARTN e2219310.1371/journal.pone.0022193.

[449] D. Pitt, P. Werner, and C. S. Raine, "Glutamate excitotoxicity in a model of multiple sclerosis," *Nat Med,* vol. 6, no. 1, pp. 67-70, Jan 2000, doi: 10.1038/71555.

[450] I. Tkác, G. Oz, G. Adriany, K. Ugurbil, and R. Gruetter, "In Vivo H-1 NMR Spectroscopy of the Human Brain at High Magnetic Fields: Metabolite Quantification at 4T vs. 7T," *Magnet Reson Med,* vol. 62, no. 4, pp. 868-879, Oct 2009, doi: 10.1002/mrm.22086.

[451] E. L. MacMillan, R. Tam, Y. Zhao, I. M. Vavasour, D. K. B. Li, J. Oger, M. S. Freedman, S. H. Kolind, and A. L. Traboulsee, "Progressive multiple sclerosis exhibits decreasing glutamate and glutamine over two years," *Mult Scler J,* vol. 22, no. 1, pp. 112-116, Jan 2016. [Online]. Available: <Go to ISI>://WOS:000367252500017.

[452] V. Calabrese, R. Raffaele, E. Cosentino, and V. Rizza, "Changes in cerebrospinal fluid levels of malondialdehyde and glutathione reductase activity in multiple sclerosis," *International journal of clinical pharmacology research,* vol. 14, no. 4, pp. 119-23, 1994. [Online]. Available: http://www.ncbi.nlm.nih.gov/entrez/query.fcgi?cmd=Retrieve&db=PubMed&dopt=Citation&list_uids=7607784

[453] C. L. Mann, M. B. Davies, M. D. Boggild, J. Alldersea, A. A. Fryer, P. W. Jones, C. Ko Ko, C. Young, R. C. Strange, and C. P. Hawkins, "Glutathione S-transferase polymorphisms in MS: their relationship to disability," *Neurology,* vol. 54, no. 3, pp. 552-7, Feb 8 2000. [Online].

[454] I. Y. Choi, P. Lee, P. Adany, A. J. Hughes, S. Belliston, D. R. Denney, and S. G. Lynch, "In vivo evidence of oxidative stress in brains of patients with progressive multiple

sclerosis," *Mult Scler,* vol. 24, no. 8, pp. 1029-1038, Jul 2018, doi: 10.1177/1352458517711568.

[455] D. T. Chard, C. M. Griffin, W. Rashid, G. R. Davies, D. R. Altmann, R. Kapoor, G. J. Barker, A. J. Thompson, and D. H. Miller, "Progressive grey matter atrophy in clinically early relapsing-remitting multiple sclerosis," *Mult Scler,* vol. 10, no. 4, pp. 387-91, Aug 2004, doi: 10.1191/1352458504ms1050oa.

[456] M. Battaglini, M. Jenkinson, and N. De Stefano, "Evaluating and reducing the impact of white matter lesions on brain volume measurements," *Hum Brain Mapp,* vol. 33, no. 9, pp. 2062-71, Sep 2012, doi: 10.1002/hbm.21344.

[457] A. Kutzelnigg, C. F. Lucchinetti, C. Stadelmann, W. Bruck, H. Rauschka, M. Bergmann, M. Schmidbauer, J. E. Parisi, and H. Lassmann, "Cortical demyelination and diffuse white matter injury in multiple sclerosis," *Brain,* vol. 128, pp. 2705-2712, Nov 2005. [Online]. Available: <Go to ISI>://WOS:000233044600020.

[458] L. Bo, C. A. Vedeler, H. I. Nyland, B. D. Trapp, and S. J. Mork, "Subpial demyelination in the cerebral cortex of multiple sclerosis patients," *J Neuropath Exp Neur,* vol. 62, no. 7, pp. 723-732, Jul 2003. [Online]. Available: <Go to ISI>://WOS:000184177300003.

[459] N. De Stefano, S. Narayanan, G. S. Francis, R. Arnaoutelis, M. C. Tartaglia, J. P. Antel, P. M. Matthews, and D. L. Arnold, "Evidence of axonal damage in the early stages of multiple sclerosis and its relevance to disability," *Arch Neurol,* vol. 58, no. 1, pp. 65-70, Jan 2001, doi: 10.1001/archneur.58.1.65.

[460] F. Aboul-Enein, M. Krssak, R. Hoftberger, D. Prayer, and W. Kristoferitsch, "Reduced NAA-Levels in the NAWM of Patients with MS Is a Feature of Progression. A Study

with Quantitative Magnetic Resonance Spectroscopy at 3 Tesla," *Plos One,* vol. 5, no. 7, Jul 20 2010. [Online]. Available: <Go to ISI>://WOS:000280109700001.

[461] M. C. Gustafsson, O. Dahlqvist, J. Jaworski, P. Lundberg, and A. M. E. Landtblom, "Low choline concentrations in normal-appearing white matter of patients with multiple sclerosis and normal MR imaging brain scans," *Am J Neuroradiol,* vol. 28, no. 7, pp. 1306-1312, Aug 2007. [Online]. Available: <Go to ISI>://WOS:000249278700021.

[462] S. Hannoun, M. Bagory, F. Durand-Dubief, D. Ibarrola, J. C. Comte, C. Confavreux, F. Cotton, and D. Sappey-Marinier, "Correlation of Diffusion and Metabolic Alterations in Different Clinical Forms of Multiple Sclerosis," *Plos One,* vol. 7, no. 3, Mar 30 2012. [Online]. Available: <Go to ISI>://WOS:000305339100013.

[463] Z. Caramanos, S. DiMaio, S. Narayanan, Y. Lapierre, and D. L. Arnold, "H-1-MRSI evidence for cortical gray matter pathology that is independent of cerebral white matter lesion load in patients with secondary progressive multiple sclerosis," *Journal of the Neurological Sciences,* vol. 282, no. 1-2, pp. 72-79, Jul 15 2009. [Online]. Available: <Go to ISI>://WOS:000267499200012.

[464] J. J. G. Geurts, I. E. W. Reuling, H. Vrenken, B. M. J. Uitdehaag, C. H. Polman, J. A. Castelijns, F. Barkhof, and P. J. W. Pouwels, "MR spectroscopic evidence for thalamic and hippocampal, but not cortical, damage in multiple sclerosis," *Magnet Reson Med,* vol. 55, no. 3, pp. 478-483, Mar 2006. [Online]. Available: <Go to ISI>://WOS:000235858400003.

[465] N. Schaffler, S. Kopke, L. Winkler, S. Schippling, M. Inglese, K. Fischer, and C. Heesen, "Accuracy of diagnostic tests in multiple sclerosis - a systematic review," *Acta*

Neurologica Scandinavica, vol. 124, no. 3, pp. 151-164, Sep 2011. [Online]. Available: <Go to ISI>://WOS:000293650400001.

[466] The Ronald and Nancy Reagan Research Institute of the Alzheimer's Association and the National Institute on Aging Working Group, "Consensus report of the working group on molecular and biochemical markers of Alzheimer's Disease," *Neurobiol Aging,* vol. 19, no. 3, pp. 285-285, May-Jun 1998. [Online]. Available: <Go to ISI>://WOS:000074451400015.

[467] S. Bang, D. Yoo, S. J. Kim, S. Jhang, S. Cho, and H. Kim, "Establishment and evaluation of prediction model for multiple disease classification based on gut microbial data," *Sci Rep-Uk,* vol. 9, Jul 15 2019. [Online]. Available: <Go to ISI>://WOS:000475467800032.

[468] M. Goyal, D. Khanna, P. S. Rana, T. Khaibullin, E. Martynova, A. A. Rizvanov, S. F. Khaiboullina, and M. Baranwal, "Computational Intelligence Technique for Prediction of Multiple Sclerosis Based on Serum Cytokines," *Frontiers in Neurology,* vol. 10, Jul 18 2019. [Online]. Available: <Go to ISI>://WOS:000475925300002.

[469] G. Kocevar, C. Stamile, S. Hannoun, F. Cotton, S. Vukusic, F. Durand-Dubief, and D. Sappey-Marinier, "Graph Theory-Based Brain Connectivity for Automatic Classification of Multiple Sclerosis Clinical Courses," *Front Neurosci,* vol. 10, p. 478, 2016, doi: 10.3389/fnins.2016.00478.

[470] A. Torabi, M. R. Daliri, and S. H. Sabzposhan, "Diagnosis of multiple sclerosis from EEG signals using nonlinear methods," *Australas Phys Eng Sci Med,* vol. 40, no. 4, pp. 785-797, Dec 2017, doi: 10.1007/s13246-017-0584-9.

[471] S. C. Reitz, S. M. Hof, V. Fleischer, A. Brodski, A. Groger, R. M. Gracien, A. Droby, H. Steinmetz, U. Ziemann, F. Zipp, R. Deichmann, and J. C. Klein, "Multi-parametric

quantitative MRI of normal appearing white matter in multiple sclerosis, and the effect of disease activity on T2," *Brain Imaging Behav,* vol. 11, no. 3, pp. 744-753, Jun 2017, doi: 10.1007/s11682-016-9550-5.

[472] P. Kontschieder, J. F. Dorn, C. Morrison, R. Corish, D. Zikic, A. Sellen, M. D'Souza, C. P. Kamm, J. Burggraaff, P. Tewarie, T. Vogel, M. Azzarito, B. Glocker, P. Chin, F. Dahlke, C. Polman, L. Kappos, B. Uitdehaag, and A. Criminisi, "Quantifying progression of multiple sclerosis via classification of depth videos," *Med Image Comput Comput Assist Interv,* vol. 17, no. Pt 2, pp. 429-37, 2014, doi: 10.1007/978-3-319-10470-6_54.

[473] M. Weygandt, K. Hackmack, C. Pfuller, J. Bellmann-Strobl, F. Paul, F. Zipp, and J. D. Haynes, "MRI pattern recognition in multiple sclerosis normal-appearing brain areas," *PLoS One,* vol. 6, no. 6, p. e21138, 2011, doi: 10.1371/journal.pone.0021138.

[474] M. Zurita, C. Montalba, T. Labbe, J. P. Cruz, J. Dalboni da Rocha, C. Tejos, E. Ciampi, C. Carcamo, R. Sitaram, and S. Uribe, "Characterization of relapsing-remitting multiple sclerosis patients using support vector machine classifications of functional and diffusion MRI data," *Neuroimage Clin,* vol. 20, pp. 724-730, 2018, doi: 10.1016/j.nicl.2018.09.002.

[475] V. Sacca, A. Sarica, F. Novellino, S. Barone, T. Tallarico, E. Filippelli, A. Granata, C. Chiriaco, R. Bruno Bossio, P. Valentino, and A. Quattrone, "Evaluation of machine learning algorithms performance for the prediction of early multiple sclerosis from resting-state FMRI connectivity data," *Brain Imaging Behav,* vol. 13, no. 4, pp. 1103-1114, Aug 2019, doi: 10.1007/s11682-018-9926-9.

[476] A. Perez Del Palomar, J. Cegonino, A. Montolio, E. Orduna, E. Vilades, B. Sebastian, L. E. Pablo, and E. Garcia-Martin, "Swept source optical coherence tomography to early

detect multiple sclerosis disease. The use of machine learning techniques," *PLoS One,* vol. 14, no. 5, p. e0216410, 2019, doi: 10.1371/journal.pone.0216410.

[477] S. Fiorini, A. Verri, A. Tacchino, M. Ponzio, G. Brichetto, and A. Barla, "A machine learning pipeline for multiple sclerosis course detection from clinical scales and patient reported outcomes," *Conf Proc IEEE Eng Med Biol Soc,* vol. 2015, pp. 4443-6, Aug 2015, doi: 10.1109/EMBC.2015.7319381.

[478] B. Taschler, T. Ge, K. Bendfeldt, N. Muller-Lenke, T. D. Johnson, and T. E. Nichols, "Spatial modeling of multiple sclerosis for disease subtype prediction," *Med Image Comput Comput Assist Interv,* vol. 17, no. Pt 2, pp. 797-804, 2014, doi: 10.1007/978-3-319-10470-6_99.

[479] P. Guo, Q. Zhang, Z. Zhu, Z. Huang, and K. Li, "Mining gene expression data of multiple sclerosis," *PLoS One,* vol. 9, no. 6, p. e100052, 2014, doi: 10.1371/journal.pone.0100052.

[480] A. Eshaghi, V. Wottschel, R. Cortese, M. Calabrese, M. A. Sahraian, A. J. Thompson, D. C. Alexander, and O. Ciccarelli, "Gray matter MRI differentiates neuromyelitis optica from multiple sclerosis using random forest," *Neurology,* vol. 87, no. 23, pp. 2463-2470, Dec 6 2016. [Online]. Available: <Go to ISI>://WOS:000392241900017.

[481] J. Richiardi, M. Gschwind, S. Simioni, J. M. Annoni, B. Greco, P. Hagmann, M. Schluep, P. Vuilleumier, and D. Van De Ville, "Classifying minimally disabled multiple sclerosis patients from resting state functional connectivity," *Neuroimage,* vol. 62, no. 3, pp. 2021-33, Sep 2012, doi: 10.1016/j.neuroimage.2012.05.078.

[482] Y. Yoo, L. Y. W. Tang, T. Brosch, D. K. B. Li, S. Kolind, I. Vavasour, A. Rauscher, A. L. MacKay, A. Traboulsee, and R. C. Tam, "Deep learning of joint myelin and T1w MRI

features in normal-appearing brain tissue to distinguish between multiple sclerosis patients and healthy controls," *Neuroimage Clin,* vol. 17, pp. 169-178, 2018, doi: 10.1016/j.nicl.2017.10.015.

[483] S. L. Andersen, F. B. S. Briggs, J. H. Winnike, Y. Natanzon, S. Maichle, K. J. Knagge, L. K. Newby, and S. G. Gregory, "Metabolome-based signature of disease pathology in MS," *Mult Scler Relat Disord,* vol. 31, pp. 12-21, Jun 2019, doi: 10.1016/j.msard.2019.03.006.

[484] F. Eitel, E. Soehler, J. Bellmann-Strobl, A. U. Brandt, K. Ruprecht, R. M. Giess, J. Kuchling, S. Asseyer, M. Weygandt, J. D. Haynes, M. Scheel, F. Paul, and K. Ritter, "Uncovering convolutional neural network decisions for diagnosing multiple sclerosis on conventional MRI using layer-wise relevance propagation," *Neuroimage Clin,* vol. 24, p. 102003, 2019, doi: 10.1016/j.nicl.2019.102003.

[485] J. Lotsch, M. Thrun, F. Lerch, R. Brunkhorst, S. Schiffmann, D. Thomas, I. Tegder, G. Geisslinger, and A. Ultsch, "Machine-Learned Data Structures of Lipid Marker Serum Concentrations in Multiple Sclerosis Patients Differ from Those in Healthy Subjects," *Int J Mol Sci,* vol. 18, no. 6, Jun 7 2017, doi: 10.3390/ijms18061217.

[486] M. Alaqtash, T. Sarkodie-Gyan, H. Yu, O. Fuentes, R. Brower, and A. Abdelgawad, "Automatic classification of pathological gait patterns using ground reaction forces and machine learning algorithms," *Conf Proc IEEE Eng Med Biol Soc,* vol. 2011, pp. 453-7, 2011, doi: 10.1109/IEMBS.2011.6090063.

[487] J. Zhang, L. Tong, L. Wang, and N. Li, "Texture analysis of multiple sclerosis: a comparative study," *Magn Reson Imaging,* vol. 26, no. 8, pp. 1160-6, Oct 2008, doi: 10.1016/j.mri.2008.01.016.

[488] A. Ahmadi, S. Davoudi, and M. R. Daliri, "Computer Aided Diagnosis System for multiple sclerosis disease based on phase to amplitude coupling in covert visual attention," *Comput Meth Prog Bio,* vol. 169, pp. 9-18, Feb 2019. [Online]. Available: <Go to ISI>://WOS:000455473300002.

[489] D. Ohanian, A. Brown, M. Sunnquist, J. Furst, L. Nicholson, L. Klebek, and L. A. Jason, "Identifying Key Symptoms Differentiating Myalgic Encephalomyelitis and Chronic Fatigue Syndrome from Multiple Sclerosis," *Neurology (ECronicon),* vol. 4, no. 2, pp. 41-45, 2016. [Online]. Available: https://www.ncbi.nlm.nih.gov/pubmed/28066845.

[490] J. Ostmeyer, S. Christley, W. H. Rounds, I. Toby, B. M. Greenberg, N. L. Monson, and L. G. Cowell, "Statistical classifiers for diagnosing disease from immune repertoires: a case study using multiple sclerosis," *BMC Bioinformatics,* vol. 18, no. 1, p. 401, Sep 7 2017, doi: 10.1186/s12859-017-1814-6.

[491] J. C. Corvol, D. Pelletier, R. G. Henry, S. J. Caillier, J. Wang, D. Pappas, S. Casazza, D. T. Okuda, S. L. Hauser, J. R. Oksenberg, and S. E. Baranzini, "Abrogation of T cell quiescence characterizes patients at high risk for multiple sclerosis after the initial neurological event," *Proceedings of the National Academy of Sciences of the United States of America,* vol. 105, no. 33, pp. 11839-11844, Aug 19 2008. [Online]. Available: <Go to ISI>://WOS:000258723800047.

[492] T. Flauzino, A. N. C. Simao, W. L. D. J. Pereira, D. F. Alfieri, S. R. Oliveira, A. P. Kallaur, M. A. B. Lozovoy, D. R. Kaimen-Maciel, M. Maes, and E. M. V. Reiche, "Disability in multiple sclerosis is associated with age and inflammatory, metabolic and oxidative/nitrosative stress biomarkers: results of multivariate and machine learning

procedures," *Metab Brain Dis,* vol. 34, no. 5, pp. 1401-1413, Oct 2019. [Online]. Available: <Go to ISI>://WOS:000485925900015.

[493] K. C. Jackson, K. Sun, C. Barbour, D. Hernandez, P. Kosa, M. Tanigawa, A. M. Weideman, and B. Bielekova, "Genetic model of MS severity predicts future accumulation of disability," *Ann Hum Genet,* Aug 8 2019. [Online]. Available: <Go to ISI>://WOS:000481031600001.

[494] S. Mesaros, M. A. Rocca, K. Kacar, J. Kostic, M. Copetti, T. Stosic-Opincal, P. Preziosa, S. Sala, G. Riccitelli, M. A. Horsfield, J. Drulovic, G. Comi, and M. Filippi, "Diffusion tensor MRI tractography and cognitive impairment in multiple sclerosis," *Neurology,* vol. 78, no. 13, pp. 969-975, Mar 2012. [Online]. Available: <Go to ISI>://WOS:000302125600011.

[495] A. Crimi, O. Commowick, A. Maarouf, J. C. Ferre, E. Bannier, A. Tourbah, I. Berry, J. P. Ranjeva, G. Edan, and C. Barillot, "Predictive Value of Imaging Markers at Multiple Sclerosis Disease Onset Based on Gadolinium- and USPIO-Enhanced MRI and Machine Learning," *Plos One,* vol. 9, no. 4, Apr 1 2014. [Online]. Available: <Go to ISI>://WOS:000334101100039.

[496] K. Bendfeldt, S. Kloppel, T. E. Nichols, R. Smieskova, P. Kuster, S. Traud, N. Mueller-Lenke, Y. Naegelin, L. Kappos, E. W. Radue, and S. J. Borgwardt, "Multivariate pattern classification of gray matter pathology in multiple sclerosis," *Neuroimage,* vol. 60, no. 1, pp. 400-408, Mar 2012. [Online]. Available: <Go to ISI>://WOS:000301218700041.

[497] H. Kiiski, L. Jollans, S. O. Donnchadha, H. Nolan, R. Lonergan, S. Kelly, M. C. O'Brien, K. Kinsella, J. Bramham, T. Burke, M. Hutchinson, N. Tubridy, R. B. Reilly, and R. Whelan, "Machine Learning EEG to Predict Cognitive Functioning and Processing Speed

Over a 2-Year Period in Multiple Sclerosis Patients and Controls," *Brain Topogr,* vol. 31, no. 3, pp. 346-363, May 2018, doi: 10.1007/s10548-018-0620-4.

[498] A. Tacchella, S. Romano, M. Ferraldeschi, M. Salvetti, A. Zaccaria, A. Crisanti, and F. Grassi, "Collaboration between a human group and artificial intelligence can improve prediction of multiple sclerosis course: a proof-of-principle study," *F1000Res,* vol. 6, p. 2172, 2017, doi: 10.12688/f1000research.13114.2.

[499] T. Brosch, Y. Yoo, D. K. Li, A. Traboulsee, and R. Tam, "Modeling the variability in brain morphology and lesion distribution in multiple sclerosis by deep learning," *Med Image Comput Comput Assist Interv,* vol. 17, no. Pt 2, pp. 462-9, 2014, doi: 10.1007/978-3-319-10470-6_58.

[500] P. Fagone, E. Mazzon, S. Mammana, R. Di Marco, F. Spinasanta, M. S. Basile, M. C. Petralia, P. Bramanti, F. Nicoletti, and K. Mangano, "Identification of CD4(+) T cell biomarkers for predicting the response of patients with relapsing-remitting multiple sclerosis to natalizumab treatment," *Mol Med Rep,* vol. 20, no. 1, pp. 678-684, Jul 2019. [Online]. Available: <Go to ISI>://WOS:000474876100072.

[501] T. Lyu, E. F. Lock, and L. E. Eberly, "Discriminating sample groups with multi-way data," *Biostatistics,* vol. 18, no. 3, pp. 434-450, Jul 2017. [Online]. Available: <Go to ISI>://WOS:000407269200008.

[502] M. F. Ghalwash, D. Ramljak, and Z. Obradovic, "Patient-specific early classification of multivariate observations," *Int J Data Min Bioin,* vol. 11, no. 4, pp. 392-411, 2015. [Online]. Available: <Go to ISI>://WOS:000352842000002.

[503] S. E. Baranzini, L. R. Madireddy, A. Cromer, M. D'Antonio, L. Lehr, M. Beelke, P. Farmer, M. Battaglini, S. J. Caillier, M. L. Stromillo, N. De Stefano, E. Monnet, and B.

A. C. Cree, "Prognostic biomarkers of IFNb therapy in multiple sclerosis patients," *Mult Scler J,* vol. 21, no. 7, pp. 894-904, Jun 2015. [Online]. Available: <Go to ISI>://WOS:000355414500009.

[504] X. Llado, A. Oliver, M. Cabezas, J. Freixenet, J. C. Vilanova, A. Quiles, L. Valls, L. Ramio-Torrenta, and A. Rovira, "Segmentation of multiple sclerosis lesions in brain MRI: A review of automated approaches," *Inform Sciences,* vol. 186, no. 1, pp. 164-185, Mar 1 2012. [Online]. Available: <Go to ISI>://WOS:000298460300011.

[505] C. T. Ventures, "INSPECTOR." [Online]. Available: http://innovation.columbia.edu/technologies/cu17130_inspector-magnetic-resonance-spectroscopy-software-for-optimized-data-extraction/licensing

[506] *4.2. Permutation feature importance*. https://scikit-learn.org/stable/modules/permutation_importance.html.

[507] S. A. Glantz, *Primer of biostatistics*, 5th ed. New York: McGraw-Hill Medical, 2002.

[508] K. M. Swanberg, H. Prinsen, K. DeStefano, M. Bailey, A. V. Kurada, D. Pitt, R. K. Fulbright, and C. Juchem, "In vivo evidence of differential frontal cortex metabolic abnormalities in progressive and relapsing-remitting multiple sclerosis," *NMR in Biomedicine,* p. e4590.

[509] W. I. McDonald, A. Compston, G. Edan, D. Goodkin, H. P. Hartung, F. D. Lublin, H. F. McFarland, D. W. Paty, C. H. Polman, S. C. Reingold, M. Sandberg-Wollheim, W. Sibley, A. J. Thompson, S. van den Noort, B. Y. Weinshenker, and J. S. Wolinsky, "Recommended diagnostic criteria for multiple sclerosis: Guidelines from the International Panel on the Diagnosis of Multiple Sclerosis," *Annals of Neurology,* vol. 50, no. 1, pp. 121-127, Jul 2001. [Online]. Available: <Go to ISI>://WOS:000169561300017.

[510] C. M. Dalton, P. A. Brex, K. A. Miszkiel, S. J. Hickman, D. G. MacManus, G. T. Plant, A. J. Thompson, and D. H. Miller, "Application of the new McDonald criteria to patients with clinically isolated syndromes suggestive of multiple sclerosis," *Annals of Neurology,* vol. 52, no. 1, pp. 47-53, Jul 2002. [Online]. Available: <Go to ISI>://WOS:000176451800008.

[511] P. Whiting, R. Harbord, C. Main, J. J. Deeks, G. Filippini, M. Egger, and J. A. C. Sterne, "Accuracy of magnetic resonance imaging for the diagnosis of multiple sclerosis: systematic review," *Bmj-Brit Med J,* vol. 332, no. 7546, pp. 875-878, Apr 15 2006. [Online]. Available: <Go to ISI>://WOS:000237132100013.

[512] K. Sakai and K. Yamada, "Machine learning studies on major brain diseases: 5-year trends of 2014-2018," *Jpn J Radiol,* vol. 37, no. 1, pp. 34-72, Jan 2019. [Online]. Available: <Go to ISI>://WOS:000454911500004.

[513] I. Tkác, G. Oz, G. Adriany, K. Ugurbil, and R. Gruetter, "In vivo 1H NMR spectroscopy of the human brain at high magnetic fields: metabolite quantification at 4T vs. 7T," *Magn Reson Med,* vol. 62, no. 4, pp. 868-79, Oct 2009, doi: 10.1002/mrm.22086.

[514] American Psychiatric Association. Task Force on Nomenclature and Statistics. and American Psychiatric Association. Committee on Nomenclature and Statistics., *Diagnostic and statistical manual of mental disorders*, 3d ed. Washington, D.C.: American Psychiatric Association, 1980, p. 494.

[515] C. W. Hoge, L. A. Riviere, J. E. Wilk, R. K. Herrell, and F. W. Weathers, "The prevalence of post-traumatic stress disorder (PTSD) in US combat soldiers: a head-to-head comparison of DSM-5 versus DSM-IV-TR symptom criteria with the PTSD

checklist," *Lancet Psychiatry,* vol. 1, no. 4, pp. 269-77, Sep 2014, doi: 10.1016/S2215-0366(14)70235-4.

[516] R. Yehuda, C. W. Hoge, A. C. McFarlane, E. Vermetten, R. A. Lanius, C. M. Nievergelt, S. E. Hobfoll, K. C. Koenen, T. C. Neylan, and S. E. Hyman, "Post-traumatic stress disorder," *Nat Rev Dis Primers,* vol. 1, p. 15057, Oct 8 2015, doi: 10.1038/nrdp.2015.57.

[517] American Psychiatric Association and DSM-5 Task Force, *Diagnostic and statistical manual of mental disorders: DSM-5*, 5th ed. Washington, D.C.: American Psychiatric Association, 2013, pp. xliv, 947 p.

[518] M. Perrin, C. L. Vandeleur, E. Castelao, S. Rothen, J. Glaus, P. Vollenweider, and M. Preisig, "Determinants of the development of post-traumatic stress disorder, in the general population," *Soc Psychiatry Psychiatr Epidemiol,* vol. 49, no. 3, pp. 447-57, Mar 2014, doi: 10.1007/s00127-013-0762-3.

[519] M. L. A. Duckers and M. Olff, "Does the Vulnerability Paradox in PTSD Apply to Women and Men? An Exploratory Study," *J Trauma Stress,* vol. 30, no. 2, pp. 200-204, Apr 2017, doi: 10.1002/jts.22173.

[520] D. F. Tolin and E. B. Foa, "Sex differences in trauma and posttraumatic stress disorder: a quantitative review of 25 years of research," *Psychol Bull,* vol. 132, no. 6, pp. 959-92, Nov 2006, doi: 10.1037/0033-2909.132.6.959.

[521] L. M. Cortina and S. P. Kubiak, "Gender and posttraumatic stress: Sexual violence as an explanation for women's increased risk," *J Abnorm Psychol,* vol. 115, no. 4, pp. 753-759, Nov 2006, doi: 10.1037/0021-843x.115.4.753.

[522] L. E. Duncan, B. N. Cooper, and H. Shen, "Robust Findings From 25 Years of PTSD Genetics Research," *Curr Psychiatry Rep,* vol. 20, no. 12, p. 115, Oct 23 2018, doi: 10.1007/s11920-018-0980-1.

[523] R. C. Kessler, S. Aguilar-Gaxiola, J. Alonso, C. Benjet, E. J. Bromet, G. Cardoso, L. Degenhardt, G. de Girolamo, R. V. Dinolova, F. Ferry, S. Florescu, O. Gureje, J. M. Haro, Y. Huang, E. G. Karam, N. Kawakami, S. Lee, J. P. Lepine, D. Levinson, F. Navarro-Mateu, B. E. Pennell, M. Piazza, J. Posada-Villa, K. M. Scott, D. J. Stein, M. Ten Have, Y. Torres, M. C. Viana, M. V. Petukhova, N. A. Sampson, A. M. Zaslavsky, and K. C. Koenen, "Trauma and PTSD in the WHO World Mental Health Surveys," *Eur J Psychotraumatol,* vol. 8, no. sup5, p. 1353383, 2017, doi: 10.1080/20008198.2017.1353383.

[524] N. Breslau and J. C. Anthony, "Gender differences in the sensitivity to posttraumatic stress disorder: An epidemiological study of urban young adults," *J Abnorm Psychol,* vol. 116, no. 3, pp. 607-11, Aug 2007, doi: 10.1037/0021-843X.116.3.607.

[525] R. K. Pitman, A. M. Rasmusson, K. C. Koenen, L. M. Shin, S. P. Orr, M. W. Gilbertson, M. R. Milad, and I. Liberzon, "Biological studies of post-traumatic stress disorder," *Nat Rev Neurosci,* vol. 13, no. 11, pp. 769-87, Nov 2012, doi: 10.1038/nrn3339.

[526] M. W. Gilbertson, M. E. Shenton, A. Ciszewski, K. Kasai, N. B. Lasko, S. P. Orr, and R. K. Pitman, "Smaller hippocampal volume predicts pathologic vulnerability to psychological trauma," *Nat Neurosci,* vol. 5, no. 11, pp. 1242-7, Nov 2002, doi: 10.1038/nn958.

[527] S. J. van Rooij, M. Kennis, R. Sjouwerman, M. P. van den Heuvel, R. S. Kahn, and E. Geuze, "Smaller hippocampal volume as a vulnerability factor for the persistence of post-

traumatic stress disorder," *Psychol Med,* vol. 45, no. 13, pp. 2737-46, Oct 2015, doi: 10.1017/S0033291715000707.

[528] M. R. Milad, S. P. Orr, N. B. Lasko, Y. Chang, S. L. Rauch, and R. K. Pitman, "Presence and acquired origin of reduced recall for fear extinction in PTSD: results of a twin study," *J Psychiatr Res,* vol. 42, no. 7, pp. 515-20, Jun 2008, doi: 10.1016/j.jpsychires.2008.01.017.

[529] F. L. Woon, S. Sood, and D. W. Hedges, "Hippocampal volume deficits associated with exposure to psychological trauma and posttraumatic stress disorder in adults: a meta-analysis," *Prog Neuropsychopharmacol Biol Psychiatry,* vol. 34, no. 7, pp. 1181-8, Oct 1 2010, doi: 10.1016/j.pnpbp.2010.06.016.

[530] E. Brivio, J. P. Lopez, and A. Chen, "Sex differences: Transcriptional signatures of stress exposure in male and female brains," *Genes Brain Behav,* vol. 19, no. 3, p. e12643, Mar 2020, doi: 10.1111/gbb.12643.

[531] J. M. Cisler and R. J. Herringa, "Posttraumatic Stress Disorder and the Developing Adolescent Brain," *Biol Psychiatry,* vol. 89, no. 2, pp. 144-151, Jan 15 2021, doi: 10.1016/j.biopsych.2020.06.001.

[532] N. Malikowska-Racia and K. Salat, "Recent advances in the neurobiology of posttraumatic stress disorder: A review of possible mechanisms underlying an effective pharmacotherapy," *Pharmacol Res,* vol. 142, pp. 30-49, Apr 2019, doi: 10.1016/j.phrs.2019.02.001.

[533] N. G. Harnett, A. M. Goodman, and D. C. Knight, "PTSD-related neuroimaging abnormalities in brain function, structure, and biochemistry," *Exp Neurol,* vol. 330, p. 113331, Aug 2020, doi: 10.1016/j.expneurol.2020.113331.

[534] R. H. Segman, N. Shefi, T. Goltser-Dubner, N. Friedman, N. Kaminski, and A. Y. Shalev, "Peripheral blood mononuclear cell gene expression profiles identify emergent post-traumatic stress disorder among trauma survivors," *Mol Psychiatry,* vol. 10, no. 5, pp. 500-13, 425, May 2005, doi: 10.1038/sj.mp.4001636.

[535] S. Wuchty, A. J. Myers, M. Ramirez-Restrepo, M. Huentelman, R. Richolt, F. Gould, P. D. Harvey, V. Michopolous, J. S. Steven, A. P. Wingo, A. Lori, J. L. Maples-Keller, A. O. Rothbaum, T. Jovanovic, B. O. Rothbaum, K. J. Ressler, and C. B. Nemeroff, "Integration of peripheral transcriptomics, genomics, and interactomics following trauma identifies causal genes for symptoms of post-traumatic stress and major depression," *Mol Psychiatry,* May 7 2021, doi: 10.1038/s41380-021-01084-3.

[536] A. K. Smith, A. Ratanatharathorn, A. X. Maihofer, R. K. Naviaux, A. E. Aiello, A. B. Amstadter, A. E. Ashley-Koch, D. G. Baker, J. C. Beckham, M. P. Boks, E. Bromet, M. Dennis, S. Galea, M. E. Garrett, E. Geuze, G. Guffanti, M. A. Hauser, S. Katrinli, V. Kilaru, R. C. Kessler, N. A. Kimbrel, K. C. Koenen, P. F. Kuan, K. Li, M. W. Logue, A. Lori, B. J. Luft, M. W. Miller, J. C. Naviaux, N. R. Nugent, X. Qin, K. J. Ressler, V. B. Risbrough, B. P. F. Rutten, M. B. Stein, R. J. Ursano, E. Vermetten, C. H. Vinkers, L. Wang, N. A. Youssef, I. N. C. Consortium, V. A. M.-A. M. Workgroup, P. P. E. Workgroup, M. Uddin, and C. M. Nievergelt, "Epigenome-wide meta-analysis of PTSD across 10 military and civilian cohorts identifies methylation changes in AHRR," *Nat Commun,* vol. 11, no. 1, p. 5965, Nov 24 2020, doi: 10.1038/s41467-020-19615-x.

[537] M. Uddin, A. Ratanatharathorn, D. Armstrong, P. F. Kuan, A. E. Aiello, E. J. Bromet, S. Galea, K. C. Koenen, B. Luft, K. J. Ressler, D. E. Wildman, C. M. Nievergelt, and A. Smith, "Epigenetic meta-analysis across three civilian cohorts identifies NRG1 and HGS

as blood-based biomarkers for post-traumatic stress disorder," *Epigenomics,* vol. 10, no. 12, pp. 1585-1601, Dec 2018, doi: 10.2217/epi-2018-0049.

[538] S. P. Orr, L. J. Metzger, N. B. Lasko, M. L. Macklin, F. B. Hu, A. Y. Shalev, R. K. Pitman, and I. Harvard/Veterans Affairs Post-traumatic Stress Disorder Twin Study, "Physiologic responses to sudden, loud tones in monozygotic twins discordant for combat exposure: association with posttraumatic stress disorder," *Arch Gen Psychiatry,* vol. 60, no. 3, pp. 283-8, Mar 2003, doi: 10.1001/archpsyc.60.3.283.

[539] T. M. Keane, L. C. Kolb, D. G. Kaloupek, S. P. Orr, E. B. Blanchard, R. G. Thomas, F. Y. Hsieh, and P. W. Lavori, "Utility of psychophysiological measurement in the diagnosis of posttraumatic stress disorder: Results from a Department of Veterans Affairs Cooperative Study," *J Consult Clin Psychol,* vol. 66, no. 6, pp. 914-23, Dec 1998, doi: 10.1037//0022-006x.66.6.914.

[540] L. N. Miller, J. G. Simmons, S. Whittle, D. Forbes, and K. Felmingham, "The impact of posttraumatic stress disorder on event-related potentials in affective and non-affective paradigms: A systematic review with meta-analysis," *Neurosci Biobehav Rev,* vol. 122, pp. 120-142, Mar 2021, doi: 10.1016/j.neubiorev.2020.12.027.

[541] M. Atmaca, O. Ozer, S. Korkmaz, I. Taskent, and H. Yildirim, "Evidence for the changes of pituitary volumes in patients with post-traumatic stress disorder," *Psychiatry Res Neuroimaging,* vol. 260, pp. 49-52, Feb 28 2017, doi: 10.1016/j.pscychresns.2016.12.004.

[542] M. Olff, Y. Guzelcan, G. J. de Vries, J. Assies, and B. P. Gersons, "HPA- and HPT-axis alterations in chronic posttraumatic stress disorder," *Psychoneuroendocrinology,* vol. 31, no. 10, pp. 1220-30, Nov 2006, doi: 10.1016/j.psyneuen.2006.09.003.

[543] A. M. Rasmusson, R. L. Hauger, C. A. Morgan, J. D. Bremner, D. S. Charney, and S. M. Southwick, "Low baseline and yohimbine-stimulated plasma neuropeptide Y (NPY) levels in combat-related PTSD," *Biol Psychiatry,* vol. 47, no. 6, pp. 526-39, Mar 15 2000, doi: 10.1016/s0006-3223(99)00185-7.

[544] R. Sah, N. N. Ekhator, L. Jefferson-Wilson, P. S. Horn, and T. D. Geracioti, Jr., "Cerebrospinal fluid neuropeptide Y in combat veterans with and without posttraumatic stress disorder," *Psychoneuroendocrinology,* vol. 40, pp. 277-83, Feb 2014, doi: 10.1016/j.psyneuen.2013.10.017.

[545] C. S. de Kloet, E. Vermetten, A. R. Rademaker, E. Geuze, and H. G. Westenberg, "Neuroendocrine and immune responses to a cognitive stress challenge in veterans with and without PTSD," *Eur J Psychotraumatol,* vol. 3, 2012, doi: 10.3402/ejpt.v3i0.16206.

[546] A. Strohle, M. Scheel, S. Modell, and F. Holsboer, "Blunted ACTH response to dexamethasone suppression-CRH stimulation in posttraumatic stress disorder," *J Psychiatr Res,* vol. 42, no. 14, pp. 1185-8, Oct 2008, doi: 10.1016/j.jpsychires.2008.01.015.

[547] C. S. de Kloet, E. Vermetten, E. Geuze, V. M. Wiegant, and H. G. Westenberg, "Elevated plasma arginine vasopressin levels in veterans with posttraumatic stress disorder," *J Psychiatr Res,* vol. 42, no. 3, pp. 192-8, Feb 2008, doi: 10.1016/j.jpsychires.2006.11.009.

[548] G. I. Hockings, J. E. Grice, W. K. Ward, M. M. Walters, G. R. Jensen, and R. V. Jackson, "Hypersensitivity of the hypothalamic-pituitary-adrenal axis to naloxone in post-traumatic stress disorder," *Biol Psychiatry,* vol. 33, no. 8-9, pp. 585-93, Apr 15-May 1 1993, doi: 10.1016/0006-3223(93)90096-v.

[549] C. S. de Kloet, E. Vermetten, E. Geuze, E. G. Lentjes, C. J. Heijnen, G. K. Stalla, and H. G. Westenberg, "Elevated plasma corticotrophin-releasing hormone levels in veterans with posttraumatic stress disorder," *Prog Brain Res,* vol. 167, pp. 287-91, 2008, doi: 10.1016/S0079-6123(07)67025-3.

[550] T. D. Geracioti, Jr., D. G. Baker, J. W. Kasckow, J. R. Strawn, J. Jeffrey Mulchahey, B. A. Dashevsky, P. S. Horn, and N. N. Ekhator, "Effects of trauma-related audiovisual stimulation on cerebrospinal fluid norepinephrine and corticotropin-releasing hormone concentrations in post-traumatic stress disorder," *Psychoneuroendocrinology,* vol. 33, no. 4, pp. 416-24, May 2008, doi: 10.1016/j.psyneuen.2007.12.012.

[551] D. G. Baker, N. N. Ekhator, J. W. Kasckow, B. Dashevsky, P. S. Horn, L. Bednarik, and T. D. Geracioti, Jr., "Higher levels of basal serial CSF cortisol in combat veterans with posttraumatic stress disorder," *Am J Psychiatry,* vol. 162, no. 5, pp. 992-4, May 2005, doi: 10.1176/appi.ajp.162.5.992.

[552] R. Yehuda, M. T. Lowy, S. M. Southwick, D. Shaffer, and E. L. Giller, Jr., "Lymphocyte glucocorticoid receptor number in posttraumatic stress disorder," *Am J Psychiatry,* vol. 148, no. 4, pp. 499-504, Apr 1991, doi: 10.1176/ajp.148.4.499.

[553] M. Trousselard, B. Lefebvre, L. Caillet, Y. Andruetan, F. de Montleau, J. Denis, and F. Canini, "Is plasma GABA level a biomarker of Post-Traumatic Stress Disorder (PTSD) severity? A preliminary study," *Psychiatry Res,* vol. 241, pp. 273-9, Jul 30 2016, doi: 10.1016/j.psychres.2016.05.013.

[554] A. M. Rasmusson, G. Pinna, P. Paliwal, D. Weisman, C. Gottschalk, D. Charney, J. Krystal, and A. Guidotti, "Decreased cerebrospinal fluid allopregnanolone levels in

women with posttraumatic stress disorder," *Biol Psychiatry,* vol. 60, no. 7, pp. 704-13, Oct 1 2006, doi: 10.1016/j.biopsych.2006.03.026.

[555] J. R. Strawn, G. J. Pyne-Geithman, N. N. Ekhator, P. S. Horn, T. W. Uhde, L. A. Shutter, D. G. Baker, and T. D. Geracioti, Jr., "Low cerebrospinal fluid and plasma orexin-A (hypocretin-1) concentrations in combat-related posttraumatic stress disorder," *Psychoneuroendocrinology,* vol. 35, no. 7, pp. 1001-7, Aug 2010, doi: 10.1016/j.psyneuen.2010.01.001.

[556] L. Meng, J. Jiang, C. Jin, J. Liu, Y. Zhao, W. Wang, K. Li, and Q. Gong, "Trauma-specific Grey Matter Alterations in PTSD," *Sci Rep,* vol. 6, p. 33748, Sep 21 2016, doi: 10.1038/srep33748.

[557] M. W. Logue, S. J. H. van Rooij, E. L. Dennis, S. L. Davis, J. P. Hayes, J. S. Stevens, M. Densmore, C. C. Haswell, J. Ipser, S. B. J. Koch, M. Korgaonkar, L. A. M. Lebois, M. Peverill, J. T. Baker, P. S. W. Boedhoe, J. L. Frijling, S. A. Gruber, I. Harpaz-Rotem, N. Jahanshad, S. Koopowitz, I. Levy, L. Nawijn, L. O'Connor, M. Olff, D. H. Salat, M. A. Sheridan, J. M. Spielberg, M. van Zuiden, S. R. Winternitz, J. D. Wolff, E. J. Wolf, X. Wang, K. Wrocklage, C. G. Abdallah, R. A. Bryant, E. Geuze, T. Jovanovic, M. L. Kaufman, A. P. King, J. H. Krystal, J. Lagopoulos, M. Bennett, R. Lanius, I. Liberzon, R. E. McGlinchey, K. A. McLaughlin, W. P. Milberg, M. W. Miller, K. J. Ressler, D. J. Veltman, D. J. Stein, K. Thomaes, P. M. Thompson, and R. A. Morey, "Smaller Hippocampal Volume in Posttraumatic Stress Disorder: A Multisite ENIGMA-PGC Study: Subcortical Volumetry Results From Posttraumatic Stress Disorder Consortia," *Biol Psychiatry,* vol. 83, no. 3, pp. 244-253, Feb 1 2018, doi: 10.1016/j.biopsych.2017.09.006.

[558] K. Kasai, H. Yamasue, M. W. Gilbertson, M. E. Shenton, S. L. Rauch, and R. K. Pitman, "Evidence for acquired pregenual anterior cingulate gray matter loss from a twin study of combat-related posttraumatic stress disorder," *Biol Psychiatry,* vol. 63, no. 6, pp. 550-6, Mar 15 2008, doi: 10.1016/j.biopsych.2007.06.022.

[559] A. Sekiguchi, M. Sugiura, Y. Taki, Y. Kotozaki, R. Nouchi, H. Takeuchi, T. Araki, S. Hanawa, S. Nakagawa, C. M. Miyauchi, A. Sakuma, and R. Kawashima, "Brain structural changes as vulnerability factors and acquired signs of post-earthquake stress," *Mol Psychiatry,* vol. 18, no. 5, pp. 618-23, May 2013, doi: 10.1038/mp.2012.51.

[560] R. A. Morey, A. L. Gold, K. S. LaBar, S. K. Beall, V. M. Brown, C. C. Haswell, J. D. Nasser, H. R. Wagner, G. McCarthy, and M. W. Mid-Atlantic, "Amygdala volume changes in posttraumatic stress disorder in a large case-controlled veterans group," *Arch Gen Psychiatry,* vol. 69, no. 11, pp. 1169-78, Nov 2012, doi: 10.1001/archgenpsychiatry.2012.50.

[561] J. R. Kuo, D. G. Kaloupek, and S. H. Woodward, "Amygdala volume in combat-exposed veterans with and without posttraumatic stress disorder: a cross-sectional study," *Arch Gen Psychiatry,* vol. 69, no. 10, pp. 1080-6, Oct 2012, doi: 10.1001/archgenpsychiatry.2012.73.

[562] R. A. Morey, E. K. Clarke, C. C. Haswell, R. D. Phillips, A. N. Clausen, M. S. Mufford, Z. Saygin, V. A. M.-A. M. Workgroup, H. R. Wagner, and K. S. LaBar, "Amygdala Nuclei Volume and Shape in Military Veterans With Posttraumatic Stress Disorder," *Biol Psychiatry Cogn Neurosci Neuroimaging,* vol. 5, no. 3, pp. 281-290, Mar 2020, doi: 10.1016/j.bpsc.2019.11.016.

[563] J. K. Daniels, J. P. Lamke, M. Gaebler, H. Walter, and M. Scheel, "White matter integrity and its relationship to PTSD and childhood trauma--a systematic review and meta-analysis," *Depress Anxiety,* vol. 30, no. 3, pp. 207-16, Mar 2013, doi: 10.1002/da.22044.

[564] D. C. M. O'Doherty, W. Ryder, C. Paquola, A. Tickell, C. Chan, D. F. Hermens, M. R. Bennett, and J. Lagopoulos, "White matter integrity alterations in post-traumatic stress disorder," *Hum Brain Mapp,* vol. 39, no. 3, pp. 1327-1338, Mar 2018, doi: 10.1002/hbm.23920.

[565] J. W. Murrough, Y. Huang, J. Hu, S. Henry, W. Williams, J. D. Gallezot, C. R. Bailey, J. H. Krystal, R. E. Carson, and A. Neumeister, "Reduced amygdala serotonin transporter binding in posttraumatic stress disorder," *Biol Psychiatry,* vol. 70, no. 11, pp. 1033-8, Dec 1 2011, doi: 10.1016/j.biopsych.2011.07.003.

[566] J. W. Murrough, C. Czermak, S. Henry, N. Nabulsi, J. D. Gallezot, R. Gueorguieva, B. Planeta-Wilson, J. H. Krystal, J. F. Neumaier, Y. Huang, Y. S. Ding, R. E. Carson, and A. Neumeister, "The effect of early trauma exposure on serotonin type 1B receptor expression revealed by reduced selective radioligand binding," *Arch Gen Psychiatry,* vol. 68, no. 9, pp. 892-900, Sep 2011, doi: 10.1001/archgenpsychiatry.2011.91.

[567] E. Geuze, B. N. van Berckel, A. A. Lammertsma, R. Boellaard, C. S. de Kloet, E. Vermetten, and H. G. Westenberg, "Reduced GABAA benzodiazepine receptor binding in veterans with post-traumatic stress disorder," *Mol Psychiatry,* vol. 13, no. 1, pp. 74-83, 3, Jan 2008, doi: 10.1038/sj.mp.4002054.

[568] E. C. Nelson, A. Agrawal, M. L. Pergadia, M. T. Lynskey, A. A. Todorov, J. C. Wang, R. D. Todd, N. G. Martin, A. C. Heath, A. M. Goate, G. W. Montgomery, and P. A. Madden, "Association of childhood trauma exposure and GABRA2 polymorphisms with

risk of posttraumatic stress disorder in adults," *Mol Psychiatry,* vol. 14, no. 3, pp. 234-5, Mar 2009, doi: 10.1038/mp.2008.81.

[569] S. E. Holmes, M. J. Girgenti, M. T. Davis, R. H. Pietrzak, N. DellaGioia, N. Nabulsi, D. Matuskey, S. Southwick, R. S. Duman, R. E. Carson, J. H. Krystal, I. Esterlis, and G. Traumatic Stress Brain Study, "Altered metabotropic glutamate receptor 5 markers in PTSD: In vivo and postmortem evidence," *Proc Natl Acad Sci U S A,* vol. 114, no. 31, pp. 8390-8395, Aug 1 2017, doi: 10.1073/pnas.1701749114.

[570] I. Liberzon, S. F. Taylor, K. L. Phan, J. C. Britton, L. M. Fig, J. A. Bueller, R. A. Koeppe, and J. K. Zubieta, "Altered central micro-opioid receptor binding after psychological trauma," *Biol Psychiatry,* vol. 61, no. 9, pp. 1030-8, May 1 2007, doi: 10.1016/j.biopsych.2006.06.021.

[571] A. Neumeister, M. D. Normandin, R. H. Pietrzak, D. Piomelli, M. Q. Zheng, A. Gujarro-Anton, M. N. Potenza, C. R. Bailey, S. F. Lin, S. Najafzadeh, J. Ropchan, S. Henry, S. Corsi-Travali, R. E. Carson, and Y. Huang, "Elevated brain cannabinoid CB1 receptor availability in post-traumatic stress disorder: a positron emission tomography study," *Mol Psychiatry,* vol. 18, no. 9, pp. 1034-40, Sep 2013, doi: 10.1038/mp.2013.61.

[572] J. D. Bremner, R. B. Innis, C. K. Ng, L. H. Staib, R. M. Salomon, R. A. Bronen, J. Duncan, S. M. Southwick, J. H. Krystal, D. Rich, G. Zubal, H. Dey, R. Soufer, and D. S. Charney, "Positron emission tomography measurement of cerebral metabolic correlates of yohimbine administration in combat-related posttraumatic stress disorder," *Arch Gen Psychiatry,* vol. 54, no. 3, pp. 246-54, Mar 1997, doi: 10.1001/archpsyc.1997.01830150070011.

[573] S. M. Southwick, J. H. Krystal, J. D. Bremner, C. A. Morgan, 3rd, A. L. Nicolaou, L. M. Nagy, D. R. Johnson, G. R. Heninger, and D. S. Charney, "Noradrenergic and serotonergic function in posttraumatic stress disorder," *Arch Gen Psychiatry,* vol. 54, no. 8, pp. 749-58, Aug 1997, doi: 10.1001/archpsyc.1997.01830200083012.

[574] R. Yehuda, P. D. Harvey, J. A. Golier, R. E. Newmark, C. R. Bowie, J. J. Wohltmann, R. A. Grossman, J. Schmeidler, E. A. Hazlett, and M. S. Buchsbaum, "Changes in relative glucose metabolic rate following cortisol administration in aging veterans with posttraumatic stress disorder: an FDG-PET neuroimaging study," *J Neuropsychiatry Clin Neurosci,* vol. 21, no. 2, pp. 132-43, Spring 2009, doi: 10.1176/appi.neuropsych.21.2.132 10.1176/jnp.2009.21.2.132.

[575] A. Etkin and T. D. Wager, "Functional neuroimaging of anxiety: a meta-analysis of emotional processing in PTSD, social anxiety disorder, and specific phobia," *Am J Psychiatry,* vol. 164, no. 10, pp. 1476-88, Oct 2007, doi: 10.1176/appi.ajp.2007.07030504.

[576] R. A. Lanius, R. Bluhm, U. Lanius, and C. Pain, "A review of neuroimaging studies in PTSD: heterogeneity of response to symptom provocation," *J Psychiatr Res,* vol. 40, no. 8, pp. 709-29, Dec 2006, doi: 10.1016/j.jpsychires.2005.07.007.

[577] M. R. Milad, R. K. Pitman, C. B. Ellis, A. L. Gold, L. M. Shin, N. B. Lasko, M. A. Zeidan, K. Handwerger, S. P. Orr, and S. L. Rauch, "Neurobiological basis of failure to recall extinction memory in posttraumatic stress disorder," *Biol Psychiatry,* vol. 66, no. 12, pp. 1075-82, Dec 15 2009, doi: 10.1016/j.biopsych.2009.06.026.

[578] L. M. Williams, A. H. Kemp, K. Felmingham, M. Barton, G. Olivieri, A. Peduto, E. Gordon, and R. A. Bryant, "Trauma modulates amygdala and medial prefrontal responses

to consciously attended fear," *Neuroimage,* vol. 29, no. 2, pp. 347-57, Jan 15 2006, doi: 10.1016/j.neuroimage.2005.03.047.

[579] K. Felmingham, A. Kemp, L. Williams, P. Das, G. Hughes, A. Peduto, and R. Bryant, "Changes in anterior cingulate and amygdala after cognitive behavior therapy of posttraumatic stress disorder," *Psychol Sci,* vol. 18, no. 2, pp. 127-9, Feb 2007, doi: 10.1111/j.1467-9280.2007.01860.x.

[580] L. M. Shin, P. J. Whalen, R. K. Pitman, G. Bush, M. L. Macklin, N. B. Lasko, S. P. Orr, S. C. McInerney, and S. L. Rauch, "An fMRI study of anterior cingulate function in posttraumatic stress disorder," *Biol Psychiatry,* vol. 50, no. 12, pp. 932-42, Dec 15 2001, doi: 10.1016/s0006-3223(01)01215-x.

[581] L. M. Shin, S. P. Orr, M. A. Carson, S. L. Rauch, M. L. Macklin, N. B. Lasko, P. M. Peters, L. J. Metzger, D. D. Dougherty, P. A. Cannistraro, N. M. Alpert, A. J. Fischman, and R. K. Pitman, "Regional cerebral blood flow in the amygdala and medial prefrontal cortex during traumatic imagery in male and female Vietnam veterans with PTSD," *Arch Gen Psychiatry,* vol. 61, no. 2, pp. 168-76, Feb 2004, doi: 10.1001/archpsyc.61.2.168.

[582] A. Pissiota, O. Frans, M. Fernandez, L. von Knorring, H. Fischer, and M. Fredrikson, "Neurofunctional correlates of posttraumatic stress disorder: a PET symptom provocation study," *Eur Arch Psychiatry Clin Neurosci,* vol. 252, no. 2, pp. 68-75, Apr 2002, doi: 10.1007/s004060200014.

[583] J. D. Bremner, E. Vermetten, C. Schmahl, V. Vaccarino, M. Vythilingam, N. Afzal, C. Grillon, and D. S. Charney, "Positron emission tomographic imaging of neural correlates of a fear acquisition and extinction paradigm in women with childhood sexual-abuse-

related post-traumatic stress disorder," *Psychol Med,* vol. 35, no. 6, pp. 791-806, Jun 2005, doi: 10.1017/s0033291704003290.

[584] R. A. Lanius, E. Vermetten, R. J. Loewenstein, B. Brand, C. Schmahl, J. D. Bremner, and D. Spiegel, "Emotion modulation in PTSD: Clinical and neurobiological evidence for a dissociative subtype," *Am J Psychiatry,* vol. 167, no. 6, pp. 640-7, Jun 2010, doi: 10.1176/appi.ajp.2009.09081168.

[585] L. M. Shin and I. Liberzon, "The neurocircuitry of fear, stress, and anxiety disorders," *Neuropsychopharmacology,* vol. 35, no. 1, pp. 169-91, Jan 2010, doi: 10.1038/npp.2009.83.

[586] N. K. Rytwinski, M. D. Scur, N. C. Feeny, and E. A. Youngstrom, "The co-occurrence of major depressive disorder among individuals with posttraumatic stress disorder: a meta-analysis," *J Trauma Stress,* vol. 26, no. 3, pp. 299-309, Jun 2013, doi: 10.1002/jts.21814.

[587] I. Agartz, R. Momenan, R. R. Rawlings, M. J. Kerich, and D. W. Hommer, "Hippocampal volume in patients with alcohol dependence," *Arch Gen Psychiatry,* vol. 56, no. 4, pp. 356-63, Apr 1999, doi: 10.1001/archpsyc.56.4.356.

[588] M. Driessen, J. Herrmann, K. Stahl, M. Zwaan, S. Meier, A. Hill, M. Osterheider, and D. Petersen, "Magnetic resonance imaging volumes of the hippocampus and the amygdala in women with borderline personality disorder and early traumatization," *Arch Gen Psychiatry,* vol. 57, no. 12, pp. 1115-22, Dec 2000, doi: 10.1001/archpsyc.57.12.1115.

[589] C. Eckart, J. Kaufmann, M. Kanowski, C. Tempelmann, H. Hinrichs, T. Elbert, H. J. Heinze, and I. T. Kolassa, "Magnetic resonance volumetry and spectroscopy of hippocampus and insula in relation to severe exposure of traumatic stress,"

Psychophysiology, vol. 49, no. 2, pp. 261-70, Feb 2012, doi: 10.1111/j.1469-8986.2011.01303.x.

[590] S. H. Woodward, D. G. Kaloupek, C. C. Streeter, M. O. Kimble, A. L. Reiss, S. Eliez, L. L. Wald, P. F. Renshaw, B. B. Frederick, B. Lane, J. I. Sheikh, W. K. Stegman, C. J. Kutter, L. P. Stewart, R. S. Prestel, and N. J. Arsenault, "Hippocampal volume, PTSD, and alcoholism in combat veterans," *Am J Psychiatry,* vol. 163, no. 4, pp. 674-81, Apr 2006, doi: 10.1176/appi.ajp.163.4.674.

[591] G. de Moraes Costa, F. B. Zanatta, P. K. Ziegelmann, A. J. Soares Barros, and C. F. Mello, "Pharmacological treatments for adults with post-traumatic stress disorder: A network meta-analysis of comparative efficacy and acceptability," *J Psychiatr Res,* vol. 130, pp. 412-420, Nov 2020, doi: 10.1016/j.jpsychires.2020.07.046.

[592] L. A. Averill, P. Purohit, C. L. Averill, M. A. Boesl, J. H. Krystal, and C. G. Abdallah, "Glutamate dysregulation and glutamatergic therapeutics for PTSD: Evidence from human studies," *Neurosci Lett,* vol. 649, pp. 147-155, May 10 2017, doi: 10.1016/j.neulet.2016.11.064.

[593] A. Verbitsky, D. Dopfel, and N. Zhang, "Rodent models of post-traumatic stress disorder: behavioral assessment," *Transl Psychiatry,* vol. 10, no. 1, p. 132, May 6 2020, doi: 10.1038/s41398-020-0806-x.

[594] D. Knox, S. A. George, C. J. Fitzpatrick, C. A. Rabinak, S. Maren, and I. Liberzon, "Single prolonged stress disrupts retention of extinguished fear in rats," *Learn Mem,* vol. 19, no. 2, pp. 43-9, Feb 2012, doi: 10.1101/lm.024356.111.

[595] M. D. De Bellis, M. S. Keshavan, and K. A. Harenski, "Anterior cingulate N-acetylaspartate/creatine ratios during clonidine treatment in a maltreated child with

posttraumatic stress disorder," *J Child Adolesc Psychopharmacol,* vol. 11, no. 3, pp. 311-6, Fall 2001, doi: 10.1089/10445460152595649.

[596] S. G, "meta: an R package for meta-analysis," *R News,* no. 7, pp. 40–7, 2007.

[597] M. Guo, F. Chen, J.-C. Guo, C.-Z. Lu, X.-L. Jiang, T. Liu, M. Li, and W. Song, "Study of the hippocampus and the anterior cingulate gyrus by proton MR spectroscopy in patients with post–traumatic stress disorder," *Asian Pacific Journal of Tropical Medicine,* vol. 5, no. 2, pp. 162-164, 2012, doi: 10.1016/s1995-7645(12)60017-0.

[598] M. Hoerst, W. Weber-Fahr, N. Tunc-Skarka, M. Ruf, M. Bohus, C. Schmahl, and G. Ende, "Metabolic alterations in the amygdala in borderline personality disorder: a proton magnetic resonance spectroscopy study," *Biol Psychiatry,* vol. 67, no. 5, pp. 399-405, Mar 1 2010, doi: 10.1016/j.biopsych.2009.09.030.

[599] K. Mahmutyazicioglu, N. Konuk, H. Ozdemir, N. Atasoy, L. Atik, and S. Gundogdu, "Evaluation of the hippocampus and the anterior cingulate gyrus by proton MR spectroscopy in patients with post-traumatic stress disorder," *Diagn Interv Radiol,* vol. 11, no. 3, pp. 125-9, Sep 2005. [Online]. Available: http://www.ncbi.nlm.nih.gov/pubmed/16206051.

[600] L. Michels, T. Schulte-Vels, M. Schick, R. L. O'Gorman, T. Zeffiro, G. Hasler, and C. Mueller-Pfeiffer, "Prefrontal GABA and glutathione imbalance in posttraumatic stress disorder: preliminary findings," *Psychiatry Res,* vol. 224, no. 3, pp. 288-95, Dec 30 2014, doi: 10.1016/j.pscychresns.2014.09.007.

[601] M. K. Lim, C. H. Suh, H. J. Kim, S. T. Kim, J. S. Lee, M. H. Kang, J. H. Kim, and J. H. Lee, "Fire-related post-traumatic stress disorder: brain 1H-MR spectroscopic findings," *Korean J Radiol,* vol. 4, no. 2, pp. 79-84, Apr-Jun 2003, doi: 10.3348/kjr.2003.4.2.79.

[602] C. Sheth, A. P. Prescot, M. Legarreta, P. F. Renshaw, E. McGlade, and D. Yurgelun-Todd, "Reduced gamma-amino butyric acid (GABA) and glutamine in the anterior cingulate cortex (ACC) of veterans exposed to trauma," *J Affect Disord,* vol. 248, pp. 166-174, Apr 1 2019, doi: 10.1016/j.jad.2019.01.037.

[603] C. G. Abdallah, L. A. Averill, T. J. Akiki, M. Raza, C. L. Averill, H. Gomaa, A. Adikey, and J. H. Krystal, "The Neurobiology and Pharmacotherapy of Posttraumatic Stress Disorder," *Annu Rev Pharmacol Toxicol,* vol. 59, pp. 171-189, Jan 6 2019, doi: 10.1146/annurev-pharmtox-010818-021701.

[604] M. D. De Bellis, M. S. Keshavan, S. Spencer, and J. Hall, "N-Acetylaspartate concentration in the anterior cingulate of maltreated children and adolescents with PTSD," *Am J Psychiatry,* vol. 157, no. 7, pp. 1175-7, Jul 2000, doi: 10.1176/appi.ajp.157.7.1175.

[605] N. Schuff, T. C. Neylan, S. Fox-Bosetti, M. Lenoci, K. W. Samuelson, C. Studholme, J. Kornak, C. R. Marmar, and M. W. Weiner, "Abnormal N-acetylaspartate in hippocampus and anterior cingulate in posttraumatic stress disorder," *Psychiatry Res,* vol. 162, no. 2, pp. 147-57, Feb 28 2008, doi: 10.1016/j.pscychresns.2007.04.011.

[606] I. M. Rosso, M. R. Weiner, D. J. Crowley, M. M. Silveri, S. L. Rauch, and J. E. Jensen, "Insula and anterior cingulate GABA levels in posttraumatic stress disorder: preliminary findings using magnetic resonance spectroscopy," *Depress Anxiety,* vol. 31, no. 2, pp. 115-23, Feb 2014, doi: 10.1002/da.22155.

[607] S. Seedat, J. S. Videen, C. M. Kennedy, and M. B. Stein, "Single voxel proton magnetic resonance spectroscopy in women with and without intimate partner violence-related

posttraumatic stress disorder," *Psychiatry Res,* vol. 139, no. 3, pp. 249-58, Aug 30 2005, doi: 10.1016/j.pscychresns.2005.06.001.

[608] Z. Y. Yang, H. Quan, Z. L. Peng, Y. Zhong, Z. J. Tan, and Q. Y. Gong, "Proton magnetic resonance spectroscopy revealed differences in the glutamate + glutamine/creatine ratio of the anterior cingulate cortex between healthy and pediatric post-traumatic stress disorder patients diagnosed after 2008 Wenchuan earthquake," *Psychiatry Clin Neurosci,* vol. 69, no. 12, pp. 782-90, Dec 2015, doi: 10.1111/pcn.12332.

[609] X. Su, C. Xia, W. Wang, H. Sun, Q. Tan, S. Zhang, L. Li, G. J. Kemp, Q. Yue, and Q. Gong, "Abnormal metabolite concentrations and amygdala volume in patients with recent-onset posttraumatic stress disorder," *J Affect Disord,* vol. 241, pp. 539-545, Dec 1 2018, doi: 10.1016/j.jad.2018.08.018.

[610] B. J. Ham, J. Chey, S. J. Yoon, Y. Sung, D. U. Jeong, S. Ju Kim, M. E. Sim, N. Choi, I. G. Choi, P. F. Renshaw, and I. K. Lyoo, "Decreased N-acetyl-aspartate levels in anterior cingulate and hippocampus in subjects with post-traumatic stress disorder: a proton magnetic resonance spectroscopy study," *Eur J Neurosci,* vol. 25, no. 1, pp. 324-9, Jan 2007, doi: 10.1111/j.1460-9568.2006.05253.x.

[611] D. J. Meyerhoff, A. Mon, T. Metzler, and T. C. Neylan, "Cortical gamma-aminobutyric acid and glutamate in posttraumatic stress disorder and their relationships to self-reported sleep quality," *Sleep,* vol. 37, no. 5, pp. 893-900, May 1 2014, doi: 10.5665/sleep.3654.

[612] J. E. Shin, C. H. Choi, J. M. Lee, J. S. Kwon, S. H. Lee, H. C. Kim, N. Y. Han, S. H. Choi, and S. Y. Yoo, "Association between memory impairment and brain metabolite concentrations in North Korean refugees with posttraumatic stress disorder," *PLoS One,* vol. 12, no. 12, p. e0188953, 2017, doi: 10.1371/journal.pone.0188953.

[613] D. L. Pennington, C. Abe, S. L. Batki, and D. J. Meyerhoff, "A preliminary examination of cortical neurotransmitter levels associated with heavy drinking in posttraumatic stress disorder," *Psychiatry Res,* vol. 224, no. 3, pp. 281-7, Dec 30 2014, doi: 10.1016/j.pscychresns.2014.09.004.

[614] S. Quadrelli, N. Tosh, A. Urquhart, K. Trickey, R. Tremewan, G. Galloway, L. Rich, R. Lea, P. Malycha, and C. Mountford, "Post-traumatic stress disorder affects fucose-alpha(1-2)-glycans in the human brain: preliminary findings of neuro deregulation using in vivo two-dimensional neuro MR spectroscopy," *Transl Psychiatry,* vol. 9, no. 1, p. 27, Jan 18 2019, doi: 10.1038/s41398-018-0365-6.

[615] G. Villarreal, H. Petropoulos, D. A. Hamilton, L. M. Rowland, W. P. Horan, J. A. Griego, M. Moreshead, B. L. Hart, and W. M. Brooks, "Proton magnetic resonance spectroscopy of the hippocampus and occipital white matter in PTSD: preliminary results," *Can J Psychiatry,* vol. 47, no. 7, pp. 666-70, Sep 2002, doi: 10.1177/070674370204700709.

[616] J. R. Augustine, "Circuitry and functional aspects of the insular lobe in primates including humans," *Brain Res Brain Res Rev,* vol. 22, no. 3, pp. 229-44, Oct 1996, doi: 10.1016/s0165-0173(96)00011-2.

[617] E. A. Osuch, B. Benson, M. Geraci, D. Podell, P. Herscovitch, U. D. McCann, and R. M. Post, "Regional cerebral blood flow correlated with flashback intensity in patients with posttraumatic stress disorder," *Biol Psychiatry,* vol. 50, no. 4, pp. 246-53, Aug 15 2001, doi: 10.1016/s0006-3223(01)01107-6.

[618] T. W. Freeman, D. Cardwell, C. N. Karson, and R. A. Komoroski, "In vivo proton magnetic resonance spectroscopy of the medial temporal lobes of subjects with combat-

related posttraumatic stress disorder," *Magn Reson Med,* vol. 40, no. 1, pp. 66-71, Jul 1998, doi: 10.1002/mrm.1910400110.

[619] T. Kimbrell, C. Leulf, D. Cardwell, R. A. Komoroski, and T. W. Freeman, "Relationship of in vivo medial temporal lobe magnetic resonance spectroscopy to documented combat exposure in veterans with chronic posttraumatic stress disorder," *Psychiatry Res,* vol. 140, no. 1, pp. 91-4, Oct 30 2005, doi: 10.1016/j.pscychresns.2005.07.001.

[620] S. Brown, T. Freeman, T. Kimbrell, D. Cardwell, and R. Komoroski, "In vivo proton magnetic resonance spectroscopy of the medial temporal lobes of former prisoners of war with and without posttraumatic stress disorder," *J Neuropsychiatry Clin Neurosci,* vol. 15, no. 3, pp. 367-70, Summer 2003, doi: 10.1176/jnp.15.3.367.

[621] C. M. Bird and N. Burgess, "The hippocampus and memory: insights from spatial processing," *Nat Rev Neurosci,* vol. 9, no. 3, pp. 182-94, Mar 2008, doi: 10.1038/nrn2335.

[622] X. J. Shu, L. Xue, W. Liu, F. Y. Chen, C. Zhu, X. H. Sun, X. P. Wang, Z. C. Liu, and H. Zhao, "More vulnerability of left than right hippocampal damage in right-handed patients with post-traumatic stress disorder," *Psychiatry Res,* vol. 212, no. 3, pp. 237-44, Jun 30 2013, doi: 10.1016/j.pscychresns.2012.04.009.

[623] I. M. Rosso, D. J. Crowley, M. M. Silveri, S. L. Rauch, and J. E. Jensen, "Hippocampus Glutamate and N-Acetyl Aspartate Markers of Excitotoxic Neuronal Compromise in Posttraumatic Stress Disorder," *Neuropsychopharmacology,* vol. 42, no. 8, pp. 1698-1705, Jul 2017, doi: 10.1038/npp.2017.32.

[624] T. Freeman, T. Kimbrell, L. Booe, M. Myers, D. Cardwell, D. M. Lindquist, J. Hart, and R. A. Komoroski, "Evidence of resilience: neuroimaging in former prisoners of war,"

Psychiatry Res, vol. 146, no. 1, pp. 59-64, Jan 30 2006, doi: 10.1016/j.pscychresns.2005.07.007.

[625] P. Mohanakrishnan Menon, H. A. Nasrallah, J. A. Lyons, M. F. Scott, and V. Liberto, "Single-voxel proton MR spectroscopy of right versus left hippocampi in PTSD," *Psychiatry Research: Neuroimaging,* vol. 123, no. 2, pp. 101-108, 2003, doi: 10.1016/s0925-4927(03)00044-1.

[626] L. Li, S. Chen, J. Liu, J. Zhang, Z. He, and X. Lin, "Magnetic resonance imaging and magnetic resonance spectroscopy study of deficits in hippocampal structure in fire victims with recent-onset posttraumatic stress disorder," *Can J Psychiatry,* vol. 51, no. 7, pp. 431-7, Jun 2006, doi: 10.1177/070674370605100704.

[627] N. Schuff, T. C. Neylan, M. A. Lenoci, A. T. Du, D. S. Weiss, C. R. Marmar, and M. W. Weiner, "Decreased hippocampal N-acetylaspartate in the absence of atrophy in posttraumatic stress disorder," *Biol Psychiatry,* vol. 50, no. 12, pp. 952-9, Dec 15 2001, doi: 10.1016/s0006-3223(01)01245-8.

[628] T. C. Neylan, N. Schuff, M. Lenoci, R. Yehuda, M. W. Weiner, and C. R. Marmar, "Cortisol levels are positively correlated with hippocampal N-acetylaspartate," *Biological Psychiatry,* vol. 54, no. 10, pp. 1118-1121, 2003, doi: 10.1016/s0006-3223(02)01974-1.

[629] T. C. Neylan, M. Lenoci, J. Rothlind, T. J. Metzler, N. Schuff, A. T. Du, K. W. Franklin, D. S. Weiss, M. W. Weiner, and C. R. Marmar, "Attention, learning, and memory in posttraumatic stress disorder," *J Trauma Stress,* vol. 17, no. 1, pp. 41-6, Feb 2004, doi: 10.1023/B:JOTS.0000014675.75686.ee.

[630] W. Wang, H. Sun, X. Su, Q. Tan, S. Zhang, C. Xia, L. Li, G. J. Kemp, Q. Yue, and Q. Gong, "Increased right amygdala metabolite concentrations in the absence of atrophy in

children and adolescents with PTSD," *Eur Child Adolesc Psychiatry,* vol. 28, no. 6, pp. 807-817, Jun 2019, doi: 10.1007/s00787-018-1241-x.

[631] T. S. Whitehurst, M. Osugo, L. Townsend, E. Shatalina, R. Vava, E. C. Onwordi, and O. Howes, "Proton Magnetic Resonance Spectroscopy of N-acetyl Aspartate in Chronic Schizophrenia, First Episode of Psychosis and High-Risk of Psychosis: A Systematic Review and Meta-Analysis," *Neurosci Biobehav Rev,* vol. 119, pp. 255-267, Dec 2020, doi: 10.1016/j.neubiorev.2020.10.001.

[632] J. C. Ipser, S. Syal, J. Bentley, C. M. Adnams, B. Steyn, and D. J. Stein, "1H-MRS in autism spectrum disorders: a systematic meta-analysis," *Metab Brain Dis,* vol. 27, no. 3, pp. 275-87, Sep 2012, doi: 10.1007/s11011-012-9293-y.

[633] Y. Aoki, R. Inokuchi, and H. Suwa, "Reduced N-acetylaspartate in the hippocampus in patients with fibromyalgia: a meta-analysis," *Psychiatry Res,* vol. 213, no. 3, pp. 242-8, Sep 30 2013, doi: 10.1016/j.pscychresns.2013.03.008.

[634] Y. Xia, Y. Fu, H. Xu, J. Guan, H. Yi, and S. Yin, "Changes in cerebral metabolites in obstructive sleep apnea: a systemic review and meta-analysis," *Sci Rep,* vol. 6, p. 28712, Jun 28 2016, doi: 10.1038/srep28712.

[635] S. Tumati, S. Martens, and A. Aleman, "Magnetic resonance spectroscopy in mild cognitive impairment: systematic review and meta-analysis," *Neurosci Biobehav Rev,* vol. 37, no. 10 Pt 2, pp. 2571-86, Dec 2013, doi: 10.1016/j.neubiorev.2013.08.004.

[636] H. Wang, L. Tan, H. F. Wang, Y. Liu, R. H. Yin, W. Y. Wang, X. L. Chang, T. Jiang, and J. T. Yu, "Magnetic Resonance Spectroscopy in Alzheimer's Disease: Systematic Review and Meta-Analysis," *J Alzheimers Dis,* vol. 46, no. 4, pp. 1049-70, 2015, doi: 10.3233/JAD-143225.

[637] Y. Shirayama, M. Takahashi, F. Osone, A. Hara, and T. Okubo, "Myo-inositol, Glutamate, and Glutamine in the Prefrontal Cortex, Hippocampus, and Amygdala in Major Depression," *Biol Psychiatry Cogn Neurosci Neuroimaging,* vol. 2, no. 2, pp. 196-204, Mar 2017, doi: 10.1016/j.bpsc.2016.11.006.

[638] G. Hasler, J. W. van der Veen, T. Tumonis, N. Meyers, J. Shen, and W. C. Drevets, "Reduced prefrontal glutamate/glutamine and gamma-aminobutyric acid levels in major depression determined using proton magnetic resonance spectroscopy," *Arch Gen Psychiatry,* vol. 64, no. 2, pp. 193-200, Feb 2007, doi: 10.1001/archpsyc.64.2.193.

[639] R. C. Team, "R: A language and environment for statistical computing. R," *Foundation for Statistical Computing, Vienna, Austria. URL https://www.R-project.org/.* 2020.

[640] S. Broer and N. Brookes, "Transfer of glutamine between astrocytes and neurons," *J Neurochem,* vol. 77, no. 3, pp. 705-19, May 2001, doi: 10.1046/j.1471-4159.2001.00322.x.

[641] J. P. Kim, M. R. Lentz, S. V. Westmoreland, J. B. Greco, E. M. Ratai, E. Halpern, A. A. Lackner, E. Masliah, and R. G. Gonzalez, "Relationships between astrogliosis and 1H MR spectroscopic measures of brain choline/creatine and myo-inositol/creatine in a primate model," *AJNR Am J Neuroradiol,* vol. 26, no. 4, pp. 752-9, Apr 2005. [Online]. Available: https://www.ncbi.nlm.nih.gov/pubmed/15814917.

[642] A. V. Kurada, K. M. Swanberg, H. Prinsen, and C. Juchem., "Diagnosis of multiple sclerosis subtype through machine learning analysis of frontal cortex metabolite profiles," *Proc Int Soc Magn Reson Med* vol. 4871, 2019.

[643] "Consensus report of the Working Group on: "Molecular and Biochemical Markers of Alzheimer's Disease". The Ronald and Nancy Reagan Research Institute of the

Alzheimer's Association and the National Institute on Aging Working Group," *Neurobiol Aging,* vol. 19, no. 2, pp. 109-16, Mar-Apr 1998. [Online]. Available: https://www.ncbi.nlm.nih.gov/pubmed/9558143.